UNIVERSITÄT LEIPZIG

REPORT
Institute für Physik
The Physics Institutes

2006
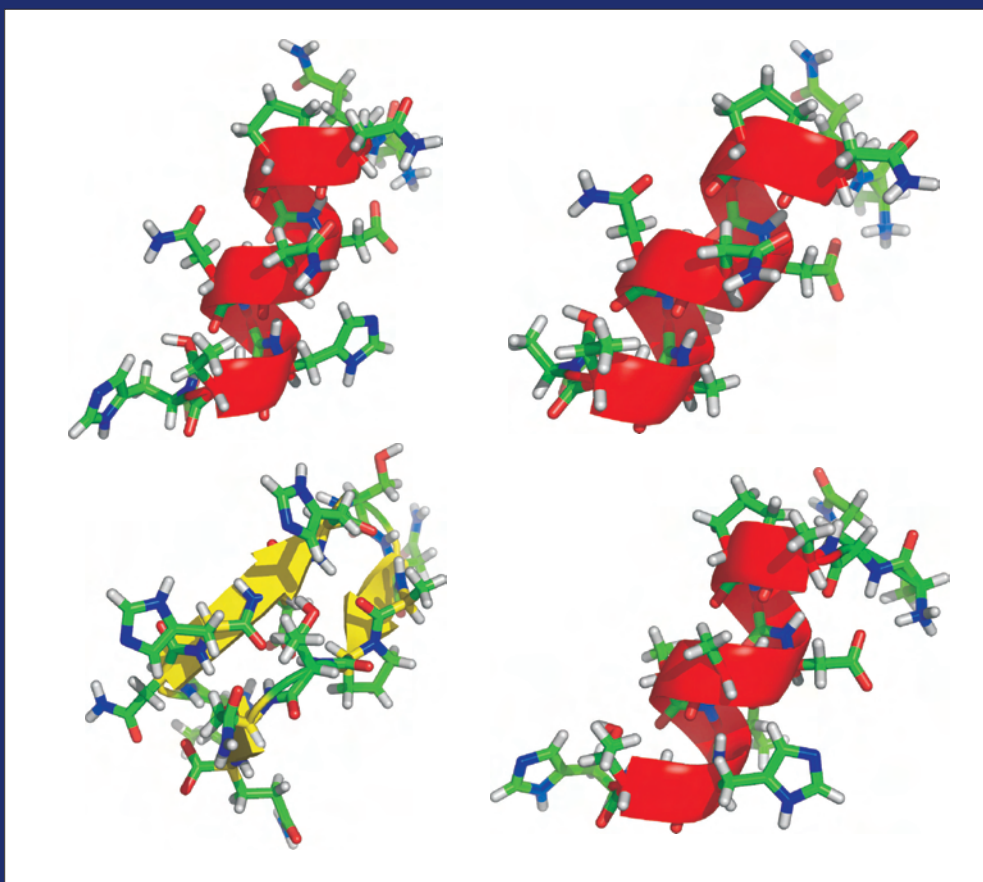
Front cover
Typical low-energy conformations exhibiting α-helical (*red*) and β-sheet (*yellow*) conformations for the peptide sequences: AQNPSDNNTHTH (*top left*), its double His→Ala mutant AQNPSDNNTATA (*top right*), a random permutation TNHDHSNAPTNQ (*bottom left*), and the triple Asn→Ala mutant AQAPSDAATHTH (*bottom right*). The capital letters "A", "Q", "N", etc. are the standard one-letter abbreviations for the 20 naturally occurring amino acids. Further information can be found in Sect. 9.10.

Back cover
Recent book publications.

Institut für Experimentelle Physik I
Institut für Experimentelle Physik II
Institut für Theoretische Physik

Fakultät für
Physik und Geowissenschaften

Universität Leipzig

Institute for Experimental Physics I
Institute for Experimental Physics II
Institute for Theoretical Physics

Faculty of Physics and Geosciences

Universität Leipzig

Report 2006

Addresses

Institute for Experimental Physics I

Linnéstraße 5
D-04103 Leipzig, Germany
Phone: +49 341 97-32551
Fax: +49 341 97-32599
WWW: http://www.uni-leipzig.de/~gasse/nysid_a/inst/exp_1.htm
Mailing
address: Postfach 100 920, D-04009 Leipzig, Germany

Institute for Experimental Physics II

Linnéstraße 5
D-04103 Leipzig, Germany
Phone: +49 341 97-32650
Fax: +49 341 97-32668
WWW: http://www.uni-leipzig.de/~exph2
Mailing
address: Postfach 100 920, D-04009 Leipzig, Germany

Institute for Theoretical Physics

Vor dem Hospitaltore 1
D-04103 Leipzig, Germany
Phone: +49 341 97-32420
Fax: +49 341 97-32548
WWW: http://www.physik.uni-leipzig.de
Mailing
address: Postfach 100 920, D-04009 Leipzig, Germany

Preface

Welcome to the 2006 Report of the Physics Institutes of Universität Leipzig. In the following we present our internal structure and document our scientific progress, sorted by the work groups. Many challenging scientific questions are worked on jointly by several groups, in cooperation with the local research institutes of Max-Planck-Gesellschaft and Leibniz-Gemeinschaft and of course with many colleagues worldwide. In the brief reports also the various sources of external funding, vital to our success, are gratefully acknowledged.

The Faculty of Physics and Geosciences of the University of Leipzig conferred the Honorary Doctorate upon Professor Sir Peter Mansfield in recognition of his extraordinary contributions to the field of nuclear magnetic resonance (NMR) spectroscopy, in particular to solid-state NMR and to magnetic resonance imaging (MRI). In 1996 the physicist Peter Mansfield invented the so-called "solid echo", a line-narrowing procedure for solid-state NMR. In 1972–1973 he realized that NMR could be used as a diffraction technique to determine the crystal structure, which proved to be the beginning of his most seminal contributions to the field of magnetic resonance imaging (MRI) for which he received the 2003 Nobel Prize in Medicine.

In the Institute for Experimental Physics I, the vacant position of our retired colleague Prof. Dr. Dieter Geschke was filled with our new colleague Prof. Dr. Frank Cichos, previously at TU Chemnitz. He is a leading expert in the field of single-molecule techniques and has started work in November 2006. He will set up and employ new experimental techniques of single molecule optical detection for the study and manipulation of nanomaterials ranging from quantum dots to biological systems. Dr. Ulrich F. Keyser who works in the group "Molecular Physics", has received an Emmy-Noether grant of the German Science Foundation (DFG), starting April 2007, for his achievements in experiments with nanometer-size holes and its applications in bio-physics. Dr. Anatoli Serghei was awarded for his Ph.D. thesis with the Young-Researcher Prize of the International Dielectrics Society (IDS). Under 160 participants from physics, chemistry, life sciences and material sciences, Dr. Rustem Valiullin was honored with the Giulio Cesare Borgia Award of the 8th "Bologna" Conference on Magnetic Resonance in Porous Media.

From the Institute for Theoretical Physics, Klaus Kroy, Gerd Rudolph, Manfred Salmhofer, Klaus Sibold and Rainer Verch are principal investigators of the proposal for the *Felix Klein Center for Mathematical Sciences and their Application*, which entered the final round of the nationwide Excellence Cluster competition.

In December 2006, the proposal for a DFG research unit *Functional Renormalization Group for Correlated Fermions* (FOR 723) was evaluated positively. This

research group is headed by Manfred Salmhofer from the Institute for Theoretical Physics and contains people from six universities in Germany. It has started its work by now, in spring 2007. The DFG research unit FOR 522 *Architecture of nano- and microdimensional building blocks* (Speaker: Marius Grundmann, Institute of Experimental Physics II) was evaluated very positively and will be funded for a second three year term until 2009.

Leipzig,   *M. Grundmann*
May 2007   *F. Kremer*
                                                                                           G. Rudolph
                                                                                            Directors

Contents

II Institute for Experimental Physics II 85

5 Nuclear Solid State Physics 87

6   Semiconductor Physics   **109**

1

Structure and Staff of the Institutes

1.1 Institute for Experimental Physics I

1.1.1 Office of the Director

Prof. Dr. Friedrich Kremer (director)
Prof. Dr. Jörg Kärger (vice director)

1.1.2 Molecular Nano-Physics, Molekulare Nanophysik [MON]

Prof. Dr. Frank Cichos

Technical staff

Christine Adolph
Dipl.-Phys. Uwe Weber

PhD candidates

Dipl.-Phys. Nicole Amecke
Dipl.-Phys. Romy Radünz
Dipl.-Phys. Rebecca Wagner

1.1.3 Physics of Anisotropic Fluids, Physik anisotroper Fluide [PAF]

Prof. Dr. F. Kremer

Secretary

Karin Girke

Technical staff

PTA Ines Grünwald
Dipl.-Ing. Jörg Reinmuth
Dipl.-Phys. Viktor Skokov

Academic staff

Dr. Gustavo Dominguez
Dr. Ulrich Keyser
Dr. Periklis Papadopoulos
Dr. Anatoli Serghei

PhD candidates

Dipl.-Phys. Christof Gutsche
Dipl.-Phys. Kati Kegler
Joshua Rume Sangoro, M.Sc.
Dipl.-Biochem. Mathias Salomo
Julius Tsuwi Kazungu, M.Sc.

1.1.4   Physics of Interfaces, Grenzflächenphysik [GFP]

Prof. Dr. Jörg Kärger

Secretary

Katrin Kunze

Technical staff

Dipl.-Ing. Bernd Knorr
Dipl.-Phys. Cordula Bärbel Krause
Lutz Moschkowitz
Dagmar Prager
Stefan Schlayer

Academic staff

PD Dr. Horst Ernst
Prof. Dr. Dieter Freude
Dr. Karen Friedemann
Dr. Petrik Galvosas
PD Dr. Farida Grinberg
Dr. Pavel Kortunov
Dr. Margarita Krutyeva

Prof. (i.R.) Dr. Dr. h.c. Harry Pfeifer
Dr. Andreas Schüring
Dr. habil. Frank Stallmach
PD Dr. Sergey Vasenkov
Dr. Rustem Valiullin

PhD candidates

Dr. Andreas Brzank
Dr. Johanna Kanellopoulos
Dipl.-Phys. Christian Chmelik
Dipl.-Phys. Muslim Dvoyashkin
Dipl.-Phys. Moisés Fernadez
Dipl.-Phys. Wadinga Fomba
Dipl.-Chem. Filipe Furtado
Dipl.-Phys. Lars Heinke
Dipl.-Phys. Aleksey Khokhlov
Dipl.-Phys. Sergej Naumov
Dipl.-Phys. Ekaterina Romanova
Dipl.-Phys. Oraphan Saengsawang
Dipl.-Phys. Denis Schneider
Dipl.-Geophys. Wiete Schönfelder
Dipl.-Ing. Despina Tzoulaki
Dipl.-Phys. Konstantin Ulrich
Dipl.-Phys. Markus Wehring

Students

Tomas Binder
Florian Hibbe
Carsten Horch
Clemens Gottert
Marcel Gratz
Mario Grossmann
Jakob Mauritz

1.1.5 Soft Matter Physics, Physik der weichen Materie [PWM]

Prof. Dr. Josef A. Käs

1.2   Institute for Experimental Physics II

1.2.1   Office of the Director

Prof. Dr. Marius Grundmann (director)
Prof. Dr. Tilman Butz (vice director)

1.2.2   Magnetic Resonance of Complex Quantum Solids, Magnetische Resonanz Komplexer Quantenfestkörper [MQF]

Prof. Dr. Jürgen Haase

1.2.3   Nuclear Solid State Physics, Nukleare Festkörperphysik [NFP]

Prof. Dr. Tilman Butz

Secretary

Teresa Nitsch

Technical staff

Dipl.-Ing. Bernd Krause
PTA Raimund Wipper

Academic staff

Dr. Thomas Agne
Dr. Tilo Reinert
Dr. Jürgen Vogt

PhD candidates

Dipl.-Biol. Anja Fiedler
Dipl.-Phys. Steffen Jankuhn
Dipl.-Phys. Christoph Meinecke
Dipl.-Phys. Frank Menzel
Charlotta Nilsson, M.Sc.
Dipl.-Phys. Daniel Spemann

Students

Nirav Barapatre
Martin Henze
Marcus Hohlweg
Silvio Petriconi

Martin Rothermel
Seung-Beak Ryu
Stephan Werner

1.2.4 Semiconductor Physics, Halbleiterphysik [HLP]

Prof. Dr. Marius Grundmann

Secretary

Anja Heck

SANDiE Network Office

Dr. Alexander Weber (Network Officer)
Birgit Wendisch (Secretary)

Technical staff

Dipl.-Phys. Gabriele Benndorf
Dipl.-Ing. Gisela Biehne
Christian Hanisch
Dipl.-Ing. Holger Hochmuth
Dipl.-Phys. Jörg Lenzner
Gabriele Ramm
Roswitha Riedel

Academic staff

Dr. Bingqiang Cao
Dr. Nilotpal Ghosh
Dr. Michael Lorenz
PD Dr. Rainer Pickenhain
Prof. Dr. Bernd Rheinländer
Dr. Heidemarie Schmidt
Dr. Alexander Weber
Dr. Qingyu Xu
Dr. Jesús Zúñiga Pérez

PhD candidates

Dipl.-Phys. Matthias Brandt
Dipl.-Phys. Christian Czekalla
Dipl.-Phys. Heiko Frenzel
Dipl.-Phys. Daniel Fritsch
Dipl.-Phys. Karsten Goede

Dipl.-Phys. Lars Hartmann
Susanne Heitsch, M.Sc.
Dipl.-Ing. Stefan Jaensch
Dipl.-Phys. Andreas Rahm
Dipl.-Phys. Matthias Schmidt
Dipl.-Phys. Rüdiger Schmidt-Grund
Dipl.-Phys. Chris Sturm
Mariana Ungureanu, M.Sc.
Dipl.-Phys. Holger von Wenckstern
Dipl.-Phys. Gregor Zimmermann

Students

Tsvetan Chavdarov
Christoph Henkel
Alexander Müller
Jan Sellmann
Robin Weirauch

1.2.5   Solid State Optics and Acoustics, Festkörperoptik und -akustik [FKO]

Prof. Dr. Wolfgang Grill

1.2.6   Superconductivity and Magnetism, Supraleitung und Magnetismus [SUM]

Prof. Dr. Pablo Esquinazi

Technical staff

Dr. Winfried Böhlmann
Klaus Grünwald
Dipl.-Krist. Annette Setzer
Monika Steinhardt

Academic staff

Dr. José Barzola
Dr. YuanFu Chen
Dr. Roland Höhne
Dr. Hans-Christoph Semmelhack
Dr. Detlef Spoddig
Dr. Jin-lei Yao
PD Dr. Michael Ziese

PhD candidates

Dipl.-Phys. Kristian Schindler

Students

Katharina Fritsch
Ingo Hilschenz
Norman Leps
Peter Rödiger
Roland Salzer
Thomas Scheller
Yashwant Verma

1.3 Institute for Theoretical Physics

1.3.1 Office of the Director

Prof. Dr. Gerd Rudolph (director)
Prof. Dr. Klaus Kroy (vice director)

Secretary

Gabriele Menge
Lea Voigt

1.3.2 Computational Quantum Field Theory, Computerorientierte Quantenfeldtheorie [CQT]

Prof. Dr. Wolfhard Janke

Academic staff

Dr. Michael Bachmann
Dr. Viktoria Blavatska
Dr. Elmar Bittner
Dr. Leszek Bogacz
Dr. Peter Crompton

PhD candidates

Dipl.-Phys. Rainer Bischof
Dipl.-Phys. Andreas Nußbaumer
Dipl.-Phys. Stefan Schnabel
Dipl.-Phys. Thomas Vogel
Dipl.-Phys. Bartłomiej Wacław
Sandro Wenzel, M.Sc.

Students

Mathias Aust
Frank Beyer
Thomas Haase
Christoph Junghans
Anna Kallias
Eric Lorenz
Monika Möddel
Jakob Schluttig
Micha Wiedenmann

1.3.3   Molecular Dynamics / Computer Simulation, Moleküldynamik / Computersimulation [MDC]

PD Dr. H.L. Vörtler (Speaker)
PD Dr. S. Fritzsche

Academic staff

Dr. Partha Biswas
Prof. Dr. Reinhold Haberlandt
Dr. Andreas Schüring

PhD candidates

Arthorn Loisruangsin, B.Sc.
Oraphan Saengsawang, M.Sc.
Somphop Thompho, M.Sc.

Students

Katja Schaefer

1.3.4   Quantum Field Theory and Gravity, Quantenfeldtheorie und Gravitation [QFG]

Prof. Dr. Gerd Rudolph (Speaker)
Prof. Dr. Rainer Verch

Academic staff

PD Dr. Michael Bordag
Dr. Daniel Grumiller
Prof. Dr. Johannes Huebschmann
Dr. Pjotr Marecki
Dr. Matthias Schmidt
Dr. Dmitri V. Vassilevich

Retired

Prof. em. Bodo Geyer
Prof. em. Armin Uhlmann
Prof. em. Wolfgang Weller (deceased in 2006)

Permanent Guests

Dr. Bernd Crell
Dr. Rainer Matthes

PhD candidates

Dipl.-Phys. Marcus Borris
Mgr. Szymon Charzynski
Dipl.-Phys. Alexander Hertsch
Dipl.-Phys. Jan Schlemmer

Students

Frank Bauer
Friederike Danneil
Stefan Funkner
Diana Kaminski
Michael Kath
René Meyer
Rainer Mühlhoff
Christoph Solveen
Gilbert Spiegel
Sandra Stephan
Sebastian Sturm

1.3.5   Statistical Physics, Statistische Physik [STP]

Prof. Dr. Manfred Salmhofer

Academic staff

Dr. Oliver Lauscher
Dipl.-Ing. Dr. Walter Pedra

PhD candidates

Dipl.-Phys. Christoph Husemann
Dipl.-Phys. Kay–Uwe Giering

1.3.6   Theory of Condensed Matter, Festkörpertheorie [TKM]

Prof. Dr. Ulrich Behn (Speaker)
Prof. Dr. Klaus Kroy

Prof. Dr. Dieter Ihle (retired)
Prof. Dr. Adolf Kühnel (retired)

PhD candidates

Dipl.-Phys. Dipl.-Math. Steffen Arnrich
Dipl.-Phys. Jens Glaser
Dipl.-Phys. Iren Juhász Junger
Dipl.-Phys. Micaela Krieger-Hauwede
Dipl.-Phys. Benedikt Obermayer
Dipl.-Phys. Daniel Rings
Dipl.-Phys. Holger Schmidtchen

Students

Philipp Altrock
Christian Brettschneider
Susanne Gütter
Sebastian Schöbl
Fabian Senf
Reinhard Vogel
Lucas Wetzel

1.3.7   Theory of Elementary Particles, Theorie der Elementarteilchen [TET]

Prof. Dr. Klaus Sibold

Academic staff

PD Dr. Roland Kirschner
PD Dr. Arwed Schiller

PhD candidates

Dipl.-Phys. Christoph Dehne

Students

Martin Bock

I

Institute for Experimental Physics I

2

Molecular Nano-Physics

The group of molecular nanophotonics has been established in November 2006 at the Institute of Experimental Physics I in Leipzig. Since then we were certainly not able to provide new experimental results for this short research summary, but we were at least industriously setting up our experimental equipment to contribute some results for the new year 2007. Let us thus fill this place with a short view on our experimental background and our future plans which are largely based on optical single molecule detection.

Single molecule detection just touches the ultimate limit of analytical chemistry, where just one molecule is observed at a time to give information on its own properties or even more excitingly, on the properties of its local surrounding. Applying these techniques in various flavors to problems in material science, molecular physics, biophysics, photonics and solid state physics is one of the central issues of our future work in Leipzig.

One of the limitations of single molecule detection is set by the probe molecule itself, which shall be fluorescent to be observed by optical microscopy. Part of our research is thus focused on the development of methods, which allow to image and to track single non-fluorescent objects in solution and other environment. For this purpose, we apply photothermal detection techniques, which rely on the conversion of light into heat at the absorbing nano-object and thus provide an alternative optical contrast mechanism (Fig. 2.1). The photothermal detection method is actually much more powerful than just detecting small non-fluorescent objects. The future research of the group in Leipzig will focus on the use of small nano-objects as local nano-heat sources to manipulate chemical reactions, single molecules and other nano-objects in solution. In combination with single molecule fluorescence detection, this will allow a completely new approach to study physical and biophysical processes in solution on just one single molecule.

Our efforts in the field of photonics are related to the study of semiconductor quantum dots and their aggregates. Small nanocrystals of semiconductor materials can be taylored in their optical properties just by tuning their size. They thus provide photonic building blocks, which allows us to obtain single or multiple photons on demand for the use in quantum information processing. Colloidal semiconductor quantum dots can be chemically functionalized to self-assemble into larger photonic units to take advance of their coupled electronic states. Quantum dots show a photoinduced switching between emissive and non-emissive states beeing related to a photoinduced charging mechanism. This mechanism shall provide the ability to control the emissive behavior
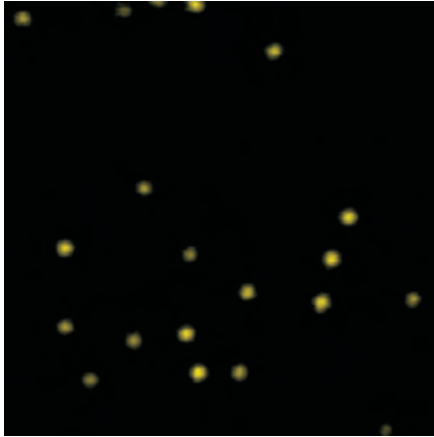
Figure 2.1: Photothermal microscopy image of single 10-nm gold nanoparticles in a polymer matrix. The image size is 8 μm × 8 μm.
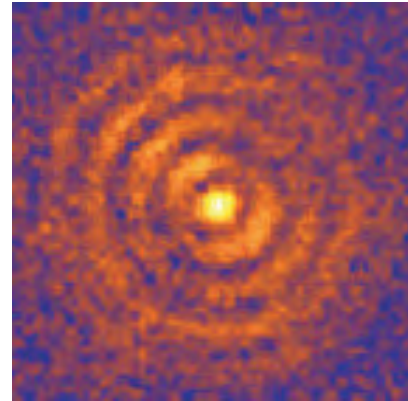
Figure 2.2: Defocused fluorescence image of a single quantum dot in a colloidal photonic crystal. The characteristic pattern tells about the light propagation inside the photonic crystal.

of these systems. Therefore a part of our research is focused on a technique, which will allow for a controlled charging of single quantum dots which hopefully turns out as an electrochemical single molecule detection technique. These are just two examples of a wide range of problems to be addressed and to be solved during the next years. Among other are the study of hydrodynamics boundary condition by single molecule tracking of ultrathin liquid films. Further we will light up photonic crystals with the help of single emitters (Fig. 2.2) to gain new insight into the way light is emitted and transported in these new type materials. The combination of single emitters and photonic crystals will in this way certainly raise new routes for a bending of light.

Frank Cichos

3

Physics of Anisotropic Fluids

3.1 Introduction

In 2006 we strengthened our activities in the traditional fields like Broadband Dielectric Spectroscopy (BDS), time-resolved Fourier-Transform Infrared Spectroscopy (FTIR) and especially experiments with Optical Tweezers (OT). As outlined in the publications list a variety of novel exiting results were obtained. Additionally our group widened its scope and with Ulrich Keyser a leading expert joined, well experienced in experiments with single molecules and nanopores. Furthermore Periklis Papadopoulos (who graduated with Prof. Dr. G. Floudas, Ioannina) started as Post-Doc. The biannual meeting of the International Dielectric Society (IDS) took place in Poznan, Poland. Anatoli Serghei was awarded by an international price committee with the Young Researcher Prize of IDS for his achievements in exploring the molecular dynamics in thin polymer films. This is a great encouraging acknowledgement.

Friedrich Kremer

3.2 Molecular Dynamics in Thin Films of Polymers with Different Macromolecular Architectures

A. Serghei, F. Kremer

The changes in the relaxation time distribution of the dynamic glass transition in thin films of polymers having different (linear, hyperbranched, star-branched and dendritic) macromolecular architectures is investigated. Based on measurements of the molecular dynamics by means of Broadband Dielectric Spectroscopy, the following issues are addressed:

- What role plays the macromolecular architecture in the dynamics of confined polymers [1]?
- Do different experimental techniques deliver similar results when applied to investigate the glassy dynamics of confined polymers?
- What is the molecular mechanism of the confinement effects, i.e. shifts and broadening of the dynamic glass transition in thin polymer films (Fig. 3.1) [2, 3]?
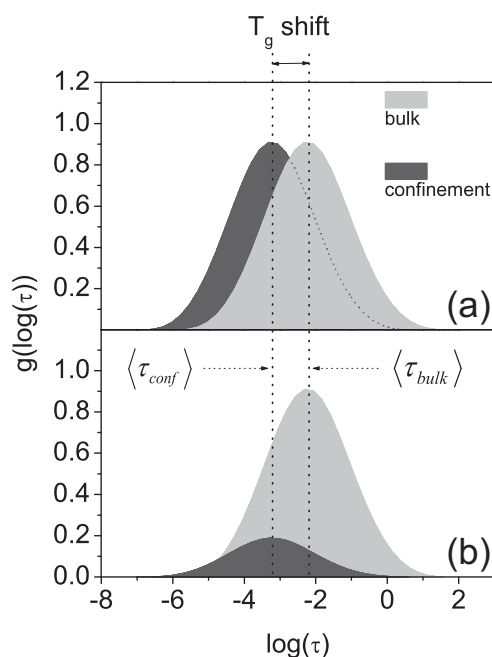
Figure 3.1: Schematic representation of two possible mechanisms leading to a shift of the mean relaxation time: (**a**) shifts of the relaxation time distribution as a whole due to the fact the polymer segments fluctuate faster in confinement than in the bulk, or (**b**) freezing-out of the slower relaxation modes.

- Does the presence of free interfaces influence the glassy dynamics of confined polymers?

[1] A. Serghei et al.: J. Polym. Sci. (B) **44**, 3006 (2006)
[2] A. Serghei et al.: Eur. Phys. J. E **17**, 199 (2005)
[3] A. Serghei et al.: Macromolecules **39**, 9385 (2006)

3.3   Novel Developments in the Preparation of Thin Polymer Films

A. Serghei, F. Kremer

In this work novel methods for the preparation of thin polymer films are developed [1]. One approach is schematically described in Fig. 3.2. Silica nano-colloids are used as spacers between two ultra-flat highly conductive silicon wafers. On one of the two wafers a thin polymer film was previously deposited by spin-coating from solution. This preparation procedure enables one – in contrast to conventional dielectric studies – the investigation of the dynamic glass transition in thin films having a free upper interface. This method avoids the evaporation of metal electrodes on thin organic layers (and the related drawbacks) and gives rise to a multitude of possible applications in soft matter physics: thin liquid layers, thin films of polyelectrolytes, biomolecules and liquid crystals, organic nano-colloids, dielectric studies on single (isolated) macromolecules.
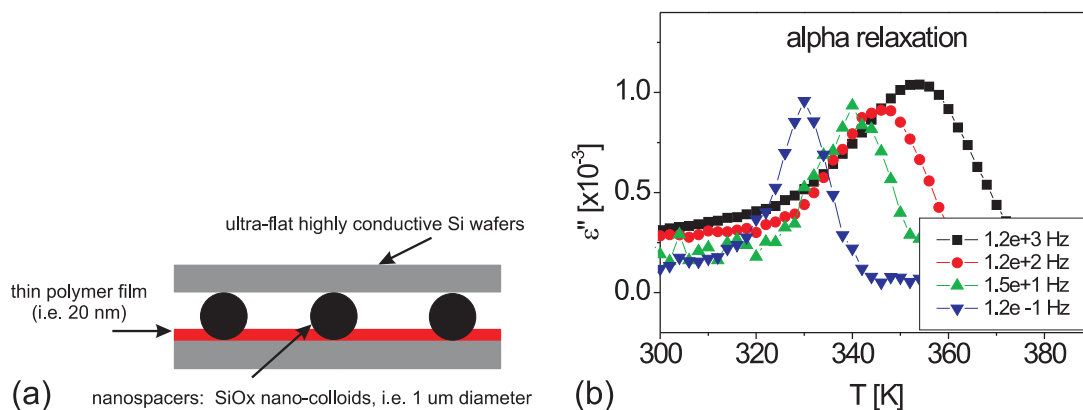
Figure 3.2: (**a**) Schematic representation of the sample preparation; (**b**) dielectric loss vs. temperature at different frequencies, as indicated, for a thin film of PMMA having a thickness of 7 nm and the upper interface free.

[1] A. Serghei, F. Kremer: Rev. Scient. Instrum. **77**, 116 108 (2006)

3.4   Study of the Receptor–Ligand Interactions by the Use of Optical Tweezers

M. Salomo, K. Kegler, M. Struhalla, J. Reinmuth, W. Skokow, F. Kremer

Receptor–ligand interactions are crucial for a manifold of biological processes like the transport of substances within cells or the exchange with their environment. They also have central impact on signal transduction by initializing signal cascades (e.g. in the synaptic gap or for endokrine reactions). Most studies have been performed with the reactants in solution. This does not reflect the general conditions that are relevant *in vivo* [1, 2].

By the use of optical tweezers we want to study the interactions between receptors and their ligands that are attached to the surface of microparticles. The measurements will be carried out with high resolution (≤ 0.1 pN, ≤ 1 nm) on a *single molecule* level. As a model system we want to utilize protein A which acts as an antigen for a wide variety of antibodies. At the moment we develop a procedure that will allow us to immobilize protein A on the surface of microparticles. Different types of antibodies will be attached to one end of a DNA linker which is immobilized at another particle (Fig. 3.3). The DNA acts as a spacer to avoid unspecific interactions between the surfaces of the particles. Using the optical tweezers contacts between antigens and antibodies will be established and than disrupted. This will enable us to unravel the static and dynamic properties of the receptor–ligand interaction.

[1] Stout L.: Biophys. J. **80**, 2976 (2001)
[2] Kienberger F. et al.: J. Mol. Biol. **347**, 597 (2005)
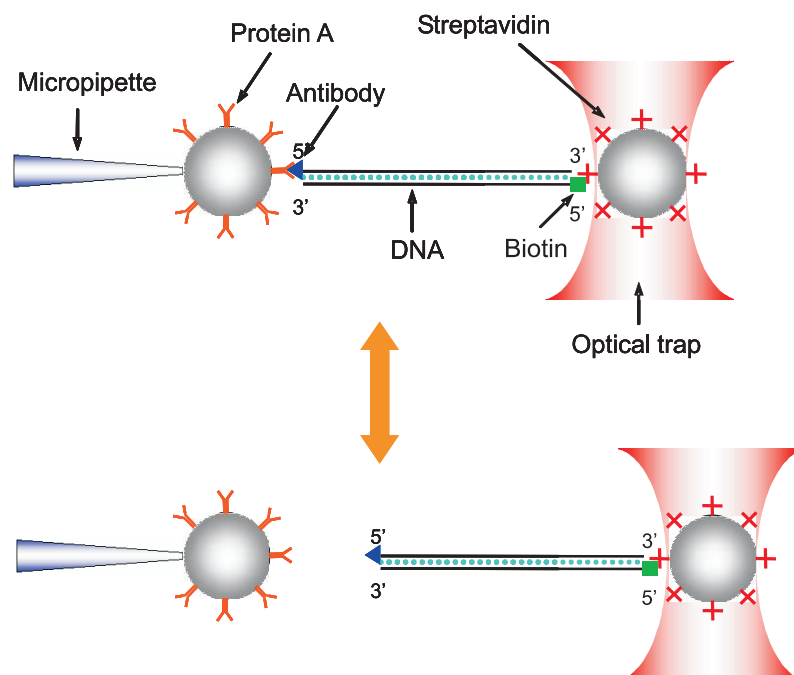
Figure 3.3: One particle with protein A on its surface is fixed at a micropipette by suction. The other one is held in the optical trap. Between them a single DNA strand is spanned. One end is immobilized on the particle in the photonic potential. The other end carries an antibody that interacts with the protein A (*top*). By pulling the colloids apart the junction breaks and the resulting forces can be measured directly (*bottom*).

3.5   Kinetics of TmHU Binding to DNA as Observed by Optical Tweezers

M. Salomo, K. Kegler, M. Struhalla, J. Reinmuth, W. Skokow, U.F. Keyser, F. Kremer

The kinetics of binding for the histone-like protein TmHU (from *Thermotoga maritima*) to DNA was analysed on a *single molecule level* by use of optical tweezers.

The histone-like protein TmHU from the hyperthermophilic eubacterium *Thermotoga maritima* belongs to the group of HU proteins that are small basic proteins occurring in all prokaryotes. Its major function consists in binding and compacting DNA into structures similar to eukaryotic chromatin. TmHU binds the DNA tightly (KD = 73 nM) without detectable sequence specificity. It bends the DNA ($\sim 160°$) and simultaneously increases its flexibility.

For our experiments we developed a special flow cell which enables us to immobilize a single DNA molecule between two functionalized polystyrene beads [1]. Further more it is possible to flush the cell with buffers or protein solution. After establishing a single DNA chain between two beads the sample cell was flushed with TmHU solution with different concentration ($0 - 250\,\mu g/ml$). If the protein bound to DNA a rapid decrease in the length of DNA chain was observed. For the reaction rate a pronounced concentration dependence was found with an "all or nothing" limit indicating towards a cooperative nature of the binding reaction. By analyzing the statistics of mechanically induced disruption events of TmHU from DNA multiple reaction sites are observed to become
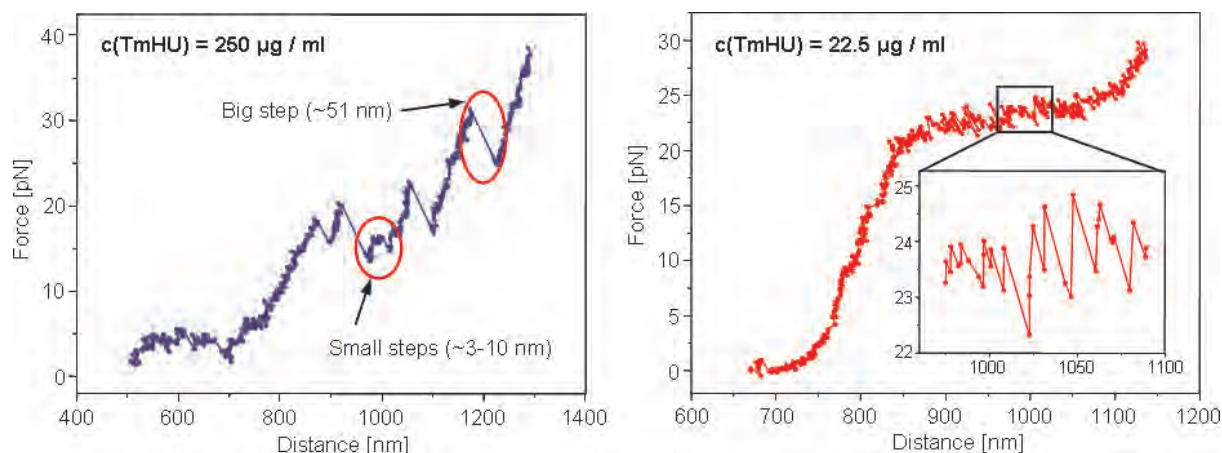
Figure 3.4: (**a**) Force–distance plot at a TmHU concentration of 250 µg/ml. (**b**) Force distance plot at a TmHU concentration of 22.5 µg/ml.

more likely with increasing TmHU concentration (Fig. 3.4). This is interpreted as a hint for a secondary organisational level of the TmHU/DNA complex. The reaction rate of TmHU is remarkably higher than that of the HU protein from *E. coli* [2, 3].

[1] M. Salomo et al.: Colloid Polym. Sci. **284**, 1325 (2006)
[2] M. Salomo et al.: J. Mol. Biol. **359**, 769 (2006)
[3] M. Salomo et al.: *Kinetics of TmHU binding to DNA as observed by optical tweezers*, Microsc. Res. Techn. (2006), in press

3.6   Dielectric Properties of Ionic Liquids

J. Rume, A. Serghei, F. Kremer

Salts characterized by low melting points, often below room temperature, have been developed and studied extensively during the last few years [1–3]. However, the quantitative understanding of the nature and impact of charge transport processes in such room temperature ionic liquids has been elusive. Due to Maxwell's equations the complex dielectric function $\varepsilon^*(\omega, T)$ is directly related to the complex conductivity $\sigma^*(\omega, T) = \text{ß}\omega\varepsilon_0\varepsilon^*(\omega, T)$, where ε_0 is the permitivity of free space . Broadband Dielectric Spectroscopy (BDS) is the natural experimental tool to measure these quantities. Special emphasis is given to the frequency and temperature dependence of $\varepsilon^*(\omega, T)$ but as well to non-linear effects with respect to the applied electric field (Fig. 3.5). This enables one to analyse in detail the mechanisms of charge transport (Fig. 3.6) in the materials under study and to determine the underlying molecular relaxation processes.

[1] A. Jarosik et al.: J. Mol. Liq. **123**, 43 (2006)
[2] F. Bordusa et al.: Angew. Chem. **6**, 1775 (1997)
[3] F. Bordusa: Chem. Rev. **102**, 4817 (2002)
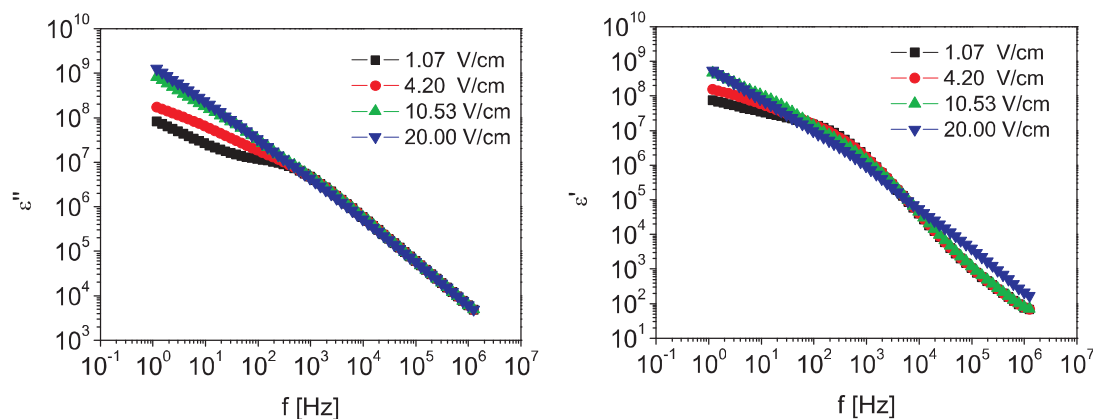
Figure 3.5: The complex dielectric function – real (*right*) and imaginary (*left*) part of the complex permittivity – vs. frequency at room temperature for tetraflouroborate (BF4) as measured for electric fields as indicated.
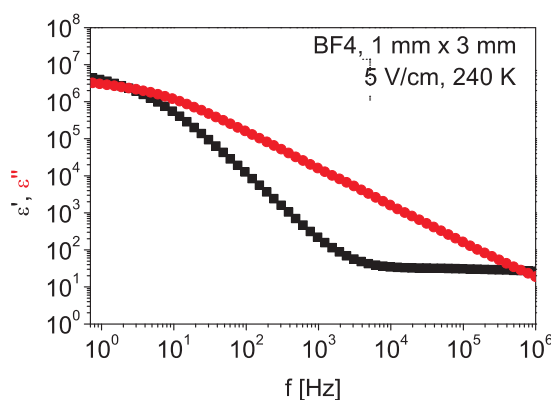
Figure 3.6: Scheme of the superposition of charge transport due to electronic and ionic charge carriers.

3.7 Rheo-FTIR on Spider Silk

J. Sölter, P. Papadopoulos, F. Kremer

Spider silk has unique mechanical properties which are currently not met by man-made materials [1]. To study the interrelationship between (microscopic) molecular structure and the (macroscopic) mechanical response a polarized time-resolved FTIR-spectrometer is combined with a custom-made setup to measure the complex mechanical modulus. For that a dense wire grid of single parallel arranged spider threads of *Araneus diadematus* is prepared (Fig. 3.7) and a step-like increase of the strain is applied while measuring the resulting stress. The specifity of the IR spectral range enables one to trace in detail the microscopic response of the different molcular moieties, i.e. the reorientation and the order parameter, the phase relation within the molecular system with respect to the mechanical excitations and possible memory effects. Comparison of silk FTIR spectra to the composition-weighted sum of all polyaminoacid spectra (Fig. 3.8a) can be very helpful in assigning the absorption bands to certain groups in the macromolecule. The two protein components of dragline silk, referred to as MaSp1 and MaSp2, consist mainly of repetitive sequences with polyalanine and glycine-rich
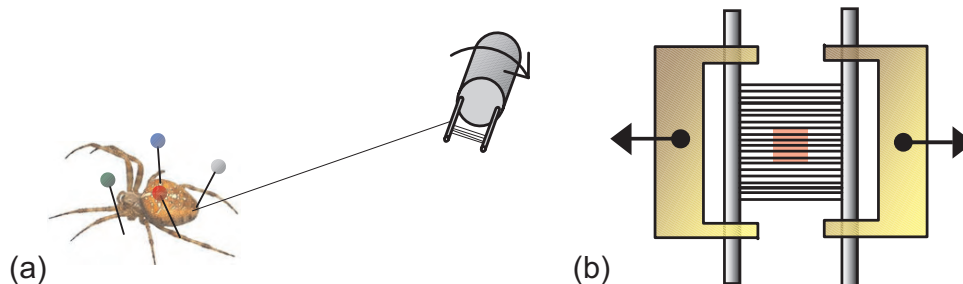
Figure 3.7: (**a**) Forced-milking setup. The spider is immobilized using pins between its legs, while the silk is wound around two metal rods whose rotation is controlled by a motor. Finally, the threads are glued to the rods and one of the layers is removed. (**b**) The wire grid of spider silk threads. The IR beam is focused on a $250 \times 250\,\mu m^2$ square (indicated in *red*).
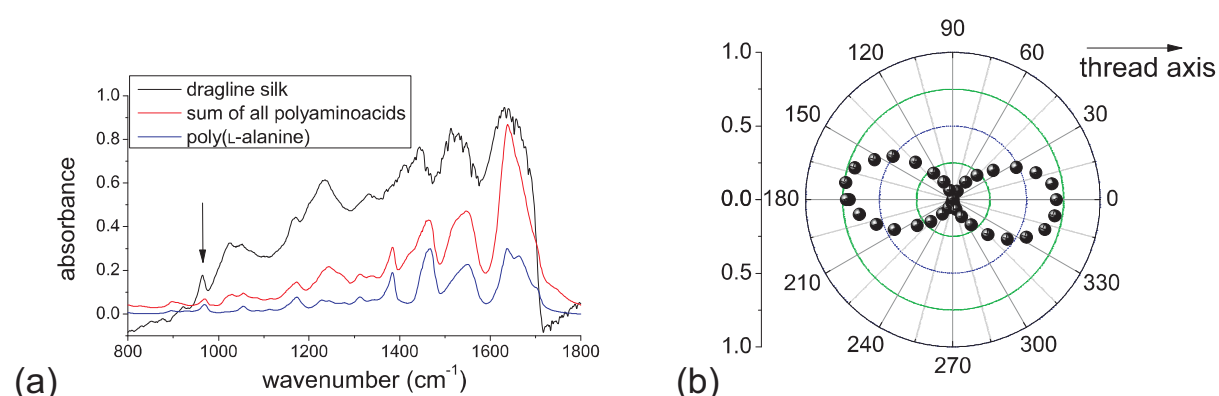
Figure 3.8: (**a**) FTIR spectra of dragline silk and poly(l-alanine) and composition-weighted sum of spectra of all polyaminoacids. (**b**) Polar plot of the absorbance at $960\,cm^{-1}$. Notice the almost perfect orientation of the transient moment along the thread axis.

motifs. A characteristic single peak at $\sim 960\,cm^{-1}$ corresponds to vibrations of polyalanine β-sheets. The latter are very well oriented along the fiber axis (Fig. 3.8b) [2].

[1] F. Vollrath, D. Porter: Soft Matter **2**, 377 (2006)
[2] J. Sölter et al.: *in preparation*

3.8 Forces of Interaction Between DNA-Grafted Colloids: An Optical Tweezers Measurement

K. Kegler, F. Kremer

Optical tweezers are employed to measure the forces of interaction between single DNA-grafted colloids. Parameters to be varied are the length of the DNA (1000 base pairs (bp) to 6000 bp), the grafting density (1.84×10^{-4} chains/nm^2 to 1.97×10^{-5} chains/nm^2) (Fig. 3.9a) and the ionic concentration (10^{-5} M to 10^{-2} M NaCl) of the surrounding medium (Fig. 3.9b). From the measured force-separation dependence an interaction length at a given force (2 pN) is deduced. It shows in the "mushroom"-regime (grafting densities $\leq 6.5 \times 10^{-5}$ chains/nm^2) a scaling with the grafting density
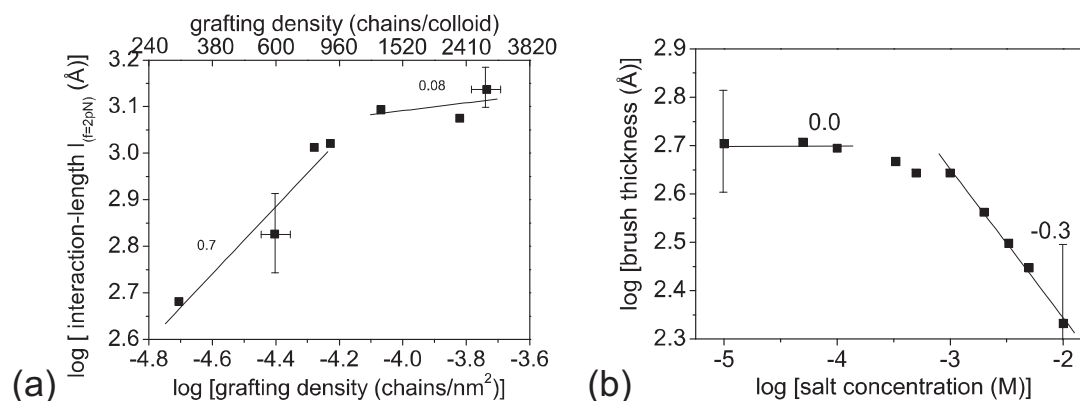
Figure 3.9: (**a**) Interaction length $l_{(f=2\,pN)}$ at a force of $2\,pN$ versus grafting density for DNA(1000 bp)-grafted colloids of varying grafting density in buffered ($10\,mM$ $C_4H_{11}NO_3$, pH 8.5) solution. (**b**) Brush thickness versus salt concentration for DNA(1000 bp)-grafted (8.25×10^{-5} chains/nm^2) colloids in buffered ($10\,mM$ $C_4H_{11}NO_3$, pH 8.5) solution of varying ionic strength. The scaling relationships are indicated by straight lines.

which levels off for "brushes" (grafting densities $\leq 6.5 \times 10^{-5}$ chains/nm^2). For the latter the transition from an "osmotic" to a "salted" brush can be traced in detail by varying the ionic concentration in accordance with meanfield theories. Further experiments are carried out to measure the influence of the valency of the added salt. Special emphasis is given to the interaction between one DNA-grafted and one blank colloid. The results are discussed with respect to the different brush regimes.

[1] K. Kegler et al.: Phys. Rev. Lett. **98**, 41 801 (2006)

3.9 Direct Force Measurements on DNA in Solid-State Nanopores

U.F. Keyser

Among the variety of roles for nanopores in biology, an important one is enabling polymer transport, for example in gene transfer between bacteria and transport of RNA through the nuclear membrane. Recently, this has inspired the use of protein and solid-state nanopores as single-molecule sensors for the detection and structural analysis of DNA and RNA by voltage-driven translocation. The magnitude of the force involved is of fundamental importance in understanding and exploiting this translocation mechanism, yet so far it has remained unknown. Recently, we demonstrated at the TU Delft the first measurements of the force on a single DNA molecule in a solid-state nanopore by combining optical tweezers with ionic-current detection [1]. The opposing force exerted by the optical tweezers can be used to slow down and even arrest the translocation of the DNA molecules. We obtain a value of $(0.24 \pm 0.02)\,pN/mV$ for the force on a single DNA molecule, independent of salt concentration from 0.02 to $1\,M$ KCl (Fig. 3.10). This force corresponds to an effective charge of 0.50 ± 0.05 electrons per base pair equivalent to a 75 % reduction of the bare DNA charge. We will establish a
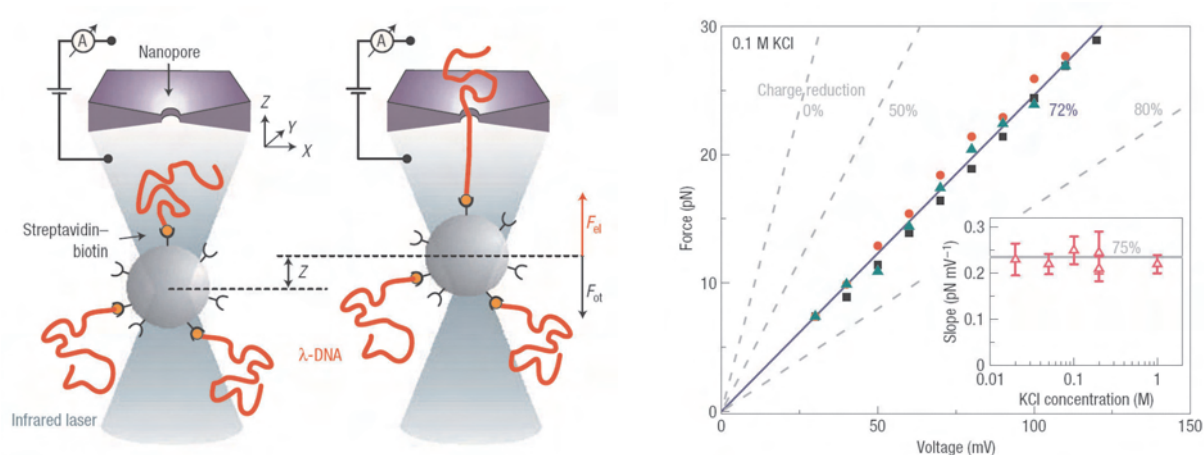
Figure 3.10: *Left*: Combining optical tweezers with a nanopore. A tightly focused laser beam is used to hold a colloid coated with DNA molecules. When DNA is pulled into the nanopore the force exerted by the field is measured and controlled by the optical trap [1]. *Right*: Force on a single DNA molecule as a function of applied voltage over a single nanopore. The inset shows the dependence on the salt solution [2].

research program combining optical tweezers and nanopores to learn more about the basic physical and chemical processes during voltage driven translocation of DNA. This may shed light on biological relevant processes like the above mentioned transfer of mRNA through the cell nucleus.

[1] U.F. Keyser et al.: Nature Phys. **2**, 473 (2006)
[2] U.F. Keyser et al.: Rev. Sci. Instrum. **77**, 105 105 (2006)

3.10   Nanobubbles in Nanopores

U.F. Keyser

Solid-state nanopores are promising as future components for lab-on-a-chip technology because of the possibility to use nanopores as molecular coulter counters for detecting nucleic acids like DNA [1]. Understanding the properties of these nanopores is important to develop better nanopores with lower noise and higher sensitivity. From conductance and noise studies, we infer that nanometer-sized gaseous bubbles (nanobubbles) are the dominant noise source in solid-state nanopores. We study the ionic conductance through solid-state nanopores as they are moved through the focus of an infrared laser beam (Fig. 3.11). In the resulting conductance profiles show strong variations in both the magnitude of the conductance and in the low-frequency noise when a single nanopore is measured multiple times. Differences up to 5 orders of magnitude are found in the current power spectral density. In addition, we measure an unexpected double-peak ionic conductance profile. A simple model of a cylindrical nanopore that contains a nanobubble explains the measured profile and accounts for the observed variations in the magnitude of the conductance [2]. These effects will be studied at the University of Leipzig during the next years.
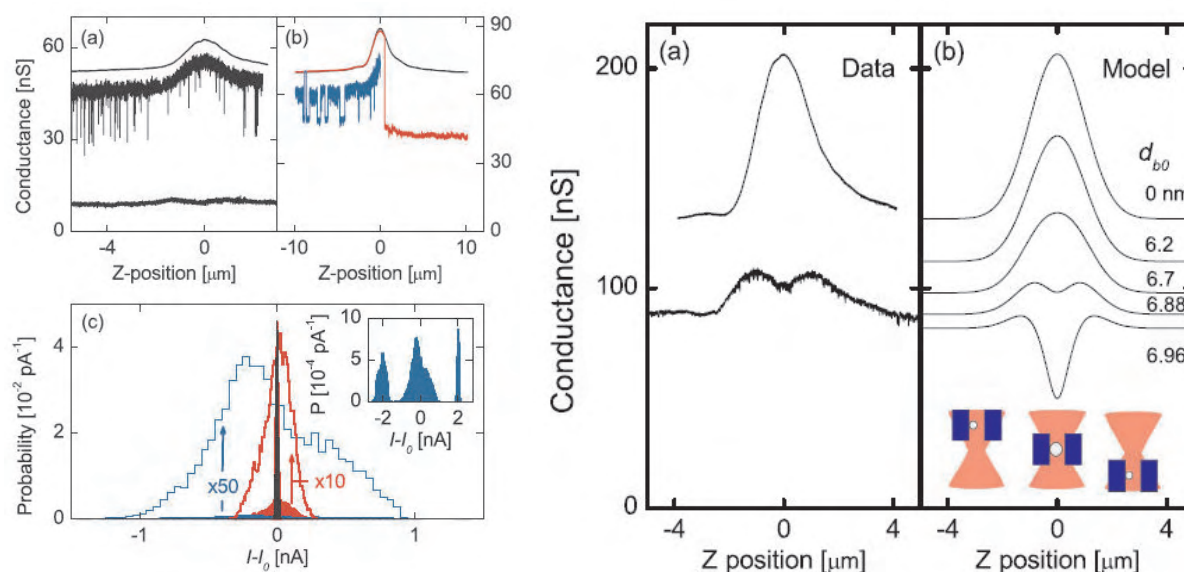
Figure 3.11: *Left*: Typical conductance curves of nanopores with five orders of magnitude different noise levels [2] (**a**)–(**c**). *Right*: (**a**) Conductance of a nanopore as a function of position of a laser focus with and without nanobubble. Please note the higher noise of the lower curve with nanobubble. (**b**) A simple model reproduces the measured data very well. We assume a circular bubble in a cylindrical channel and the expansion of the nanobubble follows the ideal gas law [2].

[1] R.M.M. Smeets et al.: Nano Lett. **6**, 89 (2006)
[2] R.M.M. Smeets et al.: Phys. Rev. Lett. **97**, 088 101 (2006)

3.11 Forces of Interaction Between Two Colloids in Media of Varying Ionic Strength

C. Gutsche, U.F. Keyser, F. Kremer

Optical Tweezers are employed to measure the forces of interaction within single pairs of colloids (Fig. 3.12) in media of monovalent and divalent ionic aqueous solutions of varying concentrations (Fig. 3.13). Artefacts are excluded in the measurements by
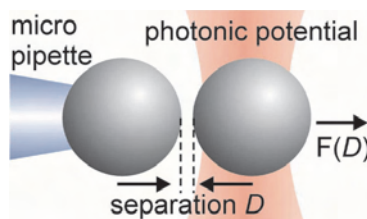
Figure 3.12: Scheme of the experimental set up: The force *F(D)* and separation between two identical, negatively charged colloids is measured using optical tweezers. One colloid is held with a micropipette (*blue*), the other in an optical trap created by a focused laser beam.
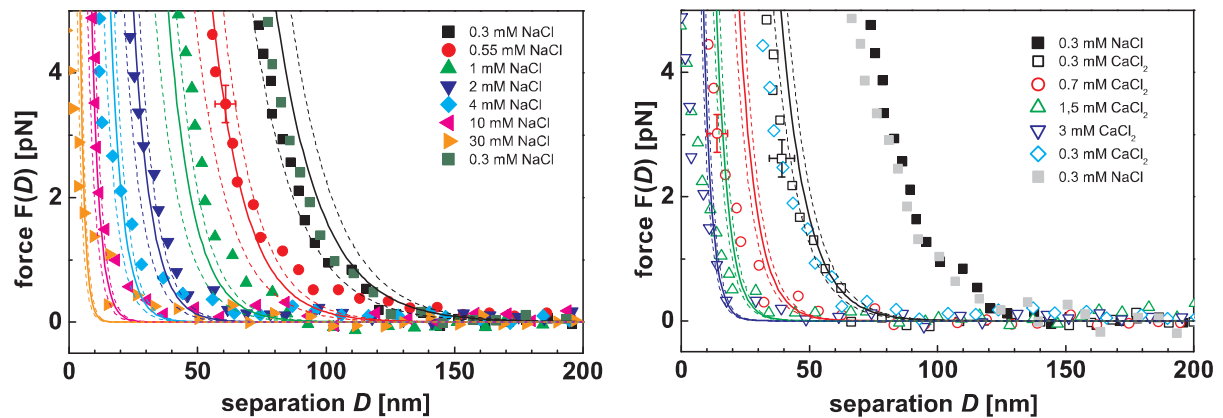
Figure 3.13: Force separation dependence for two isolated identical colloids in aqueous solution of monovalent (**a**) and divalent (**b**) ions of varying concentrations in sequence as indicated with global fit and its uncertainties.

cycling back to the initial salt conditions and find the same force–distance relation within experimental uncertainties. The data are well described for monovalent ions by a novel Poisson-Boltzmann approach based on the Derjaguin approximation and by the classical Derjaguin–Landau–Verwey–Overbeek (DLVO) theory. For the divalent ions significant deviations between theory and experiment are observed presumably caused by underestimating ion-ion correlations. Assuming for the Debye length the dependence as suggested by the DLVO theory, the charge per colloid is deduced, which is based on the full data set with different concentrations of the surrounding medium. From the measured force separation dependence an interaction length (at e.g. a force of 2 pN) is obtained, which enables one to analyse quantitatively the limits of the DLVO theory.

[1] B.V. Derjaguin, L. Landau: Acta Physicochim. URSS **14**, 633 (1941)
[2] E.J. Verwey, J.T.G. Overbeek: *Theory of the Stability of Lyophobic Colloids* (Elsevier, Amsterdam 1948)

3.12   Funding

Industrie- und Handelskammer Leipzig: Messplatz zur temperatur- und lösungsmitte-labhängigen Bestimmung der dielektrischen Funktion verschiedener Sensormaterialien
Prof. Dr. F. Kremer, Projektpartner: inotec FEG mbH Markkleeberg
AZ: 435011-6131 (2006)

DFG-Projekt "Confinement effects on the molecular dynamics of polymers with special architectures"
Prof. Dr. F. Kremer
KR 1138/17-1 (2006-2008)

DFG-Projekt "Physicochemical characterisation of ionic liquids-mediated peptide acylation reactions"
Prof. Dr. F. Kremer
KR 1138/18-1 (2006-2008)

DFG-Projekt "In-situ Untersuchung der Wechselwirkungskräfte an Polyelektrolyt-bürsten"
Prof. Dr. F. Kremer
KR 1138/20-1 (2006-2008)

3.13   Organizational Duties

F. Kremer
- Director of the Institute of Experimental Physics I
- Project Reviewer: Deutsche Forschungsgemeinschaft (DFG)
- Editor: J. Colloid Polymer Sci.
- Member of the Editorial Board: Macromol. Rapid Comm., Macromol. Chem. Phys., Polym. Adv. Technol.

3.14   External Cooperations

Academic

- Leipzig University
  K. Kroy

- Rostock University
  C. Schick

- Institute for Polymer Research, Dresden
  B. Voit, D. Appelhans, M. Stamm, P. Uhlmann

- Max Planck Institute of Microstructure Physics, Halle
  M. Alexe

- Martin Luther Universiy, Halle
  F. Bordusa, C. Wespe

- Max Planck Institute of Colloids and Interfaces, Golm
  M. Antonietti

- Experimental Soft Condensed Matter Group, Harvard University, USA
  C. Holze

- Universiy of Freiburg
  H. Finkelmann

- Technical University, Munich
  T. Scheibel, R. R. Netz

- Max Planck Institute for Metals Research, Stuttgart
  M. Rauscher

- University of Technology, Dresden
  A. Pich

- Lund University, Sweden
  P. Linse

Industry

- Novocontrol, Hundsangen, Germany

- Comtech GmbH, Munich, Germany

- Freudenberg Dichtungs- und Schwingungstechnik KG, Weinheim, Germany

- Kempchen Dichtungstechnik GmbH, Leuna, Germany

- inotec FEG mbH, Markkleeberg, Germany

3.15 Publications

Journals

C. Gutsche, M. Salomo, Y.W. Kim, R.R. Netz, F. Kremer: *The flow resistance of single DNA-grafted colloids as measured by Optical Tweezers*, Microfluid. Nanofluid. **2**, 381 (2006), doi:10.1007/s10404-006-0080-0

S. Höfl, F. Kremer, H.W. Spiess, M. Wilhelm, S. Kahle: *Effect of large amplitude oscillatory shear (LAOS) on the dielectric response of 1,4-cis-polyisoprene*, Polymer **47**, 7282 (2006)

C. Holtze, R. Sivaramakrishnan, M. Antonietti, J. Tsuwi, F. Kremer, K.D. Kremer: *The microwave absorption of emulsions containing aqueous micro- and nanodroplets: A means to optimize microwave heating*, J. Colloid Interface Sci. **302**, 651 (2006)

K. Kegler, M. Salomo, F. Kremer: *Forces of interaction between DNA-grafted colloids: An optical tweezers measuremen*, Phys. Rev. Lett. **98**, 41 801 2006

M. Salomo, C. Gutsche, K. Kegler, M. Struhalla, K. Kroy, J. Reinmuth, W. Skokow, C. Immisch and F. Kremer: *The binding of TmHU to single ds-DNA as observed by Optical Tweezers*, J. Mol. Biol. **359**, 769 (2006)

M. Salomo, K. Kegler, M. Struhalla, J. Reinmuth, W. Skokow, U. Hahn, F. Kremer: *The elastic properties of single double-stranded DNA chains of different lenght*, J. Colloid Polym. Sci. **284**, 1325 (2006)

A. Serghei, Y. Mikhailova, K.-J. Eichhorn, B. Voit, F. Kremer: *Discrepancies in the characterization of the glass transition in thin films of hyperbranched polyesters*, J. Polym. Sci. B Polym. Phys. **44**, 3006 (2006)

A. Serghei, M. Tress, F. Kremer: *Confinement effects on the relaxation time distribution of the dynamic glass transition in ultra-thin polymer films*, Macromolecules **39**, 9385 (2006)

A. Serghei, F. Kremer: *Broadband Dielectric Spectroscopy on ultra-thin organic layers having one free (upper) interface*, Rev. Sci. Instrum. **77**, 116 108 (2006)

A. Serghei, F. Kremer: *Unexpected preparative effects on the properties of thin polymer films*, Prog. Colloid Polym. Sci. **132**, 33 (2006)

U. Slotta, M. Tammer, F. Kremer, P. Kölsch, T. Scheibel: *Structural analysis of spider silk films*, Supramol. Chem. **18**, 59 (2006)

J. Tsuwi, L. Hartmann, F. Kremer, D. Pospiech, D. Jehnichen, L. Häußler: *Molecular dynamics in semifluorinated side-chain polyesters as studied by broadband dielectric spectroscopy*, Polymer **47**, 7189 (2006)

J. Tsuwi, D. Pospiech, D. Jehnichen, L. Häußler, F. Kremer: *Molecular dynamics in semifluorinated side-chain polysulfone as studied broadband dielectric spectroscopy*, J. Appl. Spectrosc. **47**, 7189 (2006)

Books

F. Kremer: *Broadband Dielectric Spectroscopy to study the molecular dynamics of polymers having different molecular architectures*, in *Physical properties of polymer handbook*, ed. by J. Mark (Springer, 2006)

A. Serghei, F. Kremer: *Molecular dynamics in thin polymer films*, in *Fractals, diffusion and relaxation in disordered complex systems*, Advances in Chemical Physics ACP, ed. by S.A. Rice, W.T. Coffey, Y.P. Kalmykov (Wiley, Weinheim 2006)

in press

D. Jehnichen, D. Pospiech, L. Häußler, P. Friedel, S.S. Funari, J. Tsuwi, F. Kremer: *Microphase separation in semifluorinated polyesters*, Z. Kristallogr. Suppl. (2006)

3.16 Graduations

Doctorate

- Dipl.-Phys. Anatoli Serghei
  Confinement-effects on the molecular dynamics in thin polymer films
  January 2006

- M.Sc. Julius Tsuwi Kazungu
  Dynamics in emulsions and fluorinated side-chain polymers studied by Broadband Dielectric Spectroscopy
  October 2006

- M.Sc. Michael Tammer
  Fourier-Transform-Infrarotspektroskopie an verstreckten Elastomernetzwerken
  December 2006

4

Physics of Interfaces

4.1   Introduction

In the year 2006, the "Physics of Interfaces" Department is happy to refer to some remarkable events reflecting recent success in teaching and research. Research on diffusion, particularly methodical enhancements of PFG NMR, interference microscopy and IR microscopy was in the center of the scientific activities. The investigations in the field of NMR diffusometry and NMR spectroscopy form an integral part of the activities of the Center of Magnetic Resonance (MRZ) of our university.

Of the 21 externally funded research projects that we succeeded to attain, we would like to particularly mention our activities in international research associations coordinated by us. These are: the International Research Training Group "Diffusion in Porous Media" in collaboration with the Dutch colleagues from the universities of Amsterdam, Delft, and Eindhoven, the International Research Group "Diffusion in Zeolites" jointly sponsored by EPSRC, CNRS and DPG and our work within the framework of the EU project (Network of Excellence) "In Situ Study and Development of Processes Involving Nanoporous Materials" (INSIDE PORES). An outstanding success was gained by Pavel Kortunov, who not only became the first graduate (PhD) of our international research training group, but received also the highest possible award of the German Zeolite Association, the George-Kokotailo-Prize.

After the accomplishment of the international conference "Diffusion Fundamentals I" in 2005, we especially focused in 2006 on the continuation of these activities and an ideal preparation of the second conference in this series in L'Aquila, Italy in August 2007 in cooperation with the University College London. The overwhelmingly positive response of the scientific community (250 participants) encouraged us to continue the publication of our online journal devoted to the publication of current scientific results as well as to the (poster and oral) presentations at regularly held conferences such as "Diffusion Fundamentals". The internationally exceptional position, that Leipzig has gained this way is in particular based on the high potential of the NMR-Diffusometry. After Petrik Galvosas returned to our group in 2005 as an assistant professor (junior professor) after several years abroad we are now especially happy to welcome Stefan Schlayer as a technical co-worker in our team. This way the premises are once again ensured that our technical base stands up to our high aims and to the expectations emerging from our international projects. The establishment of this assistant professorship is a significant milestone for the Department

which has not only to defend but even enhance its reputation as a leading center of NMR diffusometry.

A special highlight of the last year was the 8th conference "Magnetic Resonance in Porous Materials" in Bologna, Italy in September 2006. Since the conference's topic concerned the core of our activities it is not astonishing that with 11 participants our department provided the biggest group at this conference. However, with 4 talks and 10 posters we also decisively contributed to the scientific success of the event. Expression of the positive reception of our work of the more than 200 participants was the awarding of the Cesare-Borgia-Prize to our colleague Dr. Rustem Valliulin and the invitation to conduct the anniversary conference "Magnetic Resonance in Porous Materials X" 2010 in Leipzig.

The most prominent guest of our department in 2006 was Professor Dr. Dhananjai B. Shah from Cleveland State University, Ohio, USA. He came to us as a visiting "Mercator Professor" in summer 2005 for a stay of twelve months. Professor Shah's research is dedicated to the transport of different components in zeolites and zeolite membranes. Besides numerous publications we particularly appreciate the fact that our cooperation will be continued within the frame of our international research group "Diffusion in Zeolites", which in this way receives substantial reinforcement from overseas.

In conclusion, with pleasure we may mention that the two books *Diffusion Fundamentals* (J. Kärger, F. Grinberg, P. Heitjans, Leipziger Universitätsverlag 2005) and *Diffusion in Condensed Matter - Methods, Materials, Models* (P. Heitjans, J. Kärger, Springer-Verlag 2005) have been vividly asked for by the community so that work on a modified and enhanced edition for 2007 is in progress.

Jörg Kärger

4.2 Slow Cooperative Processes During Adsorption to Mesopores

S. Naumov, R. Valiullin, J. Kärger

Disordered materials are widely used in many processes of industrial and environmental importance. The equilibrium and dynamic processes that occur in the pore space of this material are strongly influenced by the confinement and the geometrical disorder of the porous matrix. In many porous materials, sorption hysteresis behavior is observed, i.e. adsorption and desorption isotherms do not coincide over a certain pressure interval. It is argued [1] that the hysteretic behavior is a consequence of the multiplicity of the metastable states, which are being passed by the system through different pathways during the adsorption and the desorption processes. While the adsorbate dynamics in the pressure range outside of the hysteresis loop is diffusive, inside of the hysteresis region late-stage dynamics is governed by a slow cooperative molecular rearrangement towards the global free-energy minimum. Though being predicted by computer simulations, this effect so far has not been addressed experimentally.

In the present work, the adsorbate transport properties in mesopores have been experimentally studied aiming at clarification of the internal dynamics leading to the

hysteresis phenomenon. The major idea behind was to combine microscopic and macroscopic experimental approaches in order to provide a self-consistent set of experimental data, which allows to separate different modes of molecular transport. In line with this idea, the pulsed field gradient NMR method, yielding information on the molecular microscopic diffusivities, and the transient uptake method, characterizing the overall adsorbate transport including single-molecular and cooperative modes, have been used [2]. In this way, the measured transient uptake functions in Vycor porous glass following a small stepwise change of the external gas pressure at different regions of the adsorption isotherm have been analyzed with help of the independently measured diffusivities using the pulsed field gradient NMR method. It is found that at low gas pressures, before the onset of the capillary condensation transition, the calculated uptake perfectly reproduces the measured one. This points out that in this region of the gas pressures the dynamics is exclusively diffusive. At the higher gas pressures, corresponding to the adsorption hysteresis region, the Fick's law approach predicts faster adsorption kinetics than experimentally observed, i.e. a slowing down of the uptake is unequivocally manifested.

Additionally, the experiments were performed by incomplete steps of adsorption followed by incomplete desorption and vice versa. At each point, the corresponding amounts adsorbed and the self-diffusion coefficients have been measured. In such a way, the so-called sorption and diffusivity scanning curves have been compiled (Fig. 4.1). The main result of this study is that, depending on the preparation history, within certain limits a state with almost any diffusivity can be prepared. We anticipate that this could be considered as an the manifestation of the multiplicity of metastable adsorbate distributions in mesoporous materials.
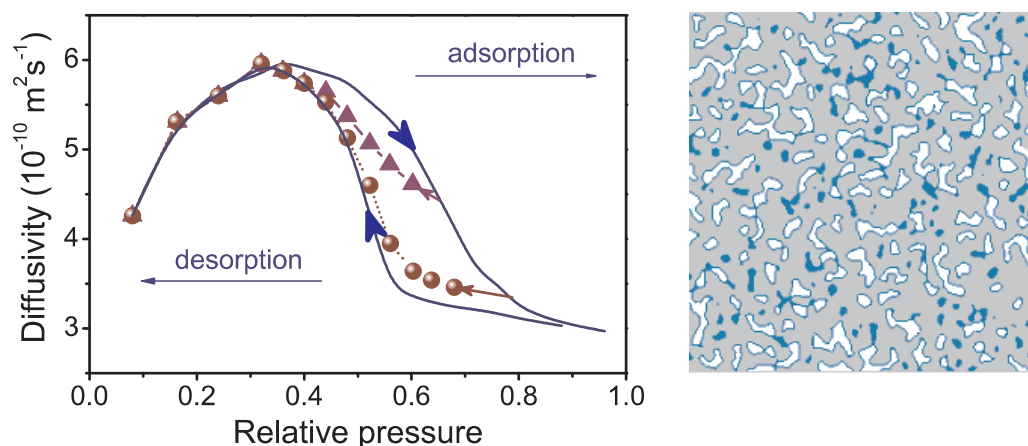
Figure 4.1: Self-diffusivity of cyclohexane in Vycor porous glass as a function of the external gas pressure. Different curves show different histories as a certain pressure had been attained. The right cartoon shows one of the possible distributions of the capillary-condensed phase (*blue*) along the porous matrix (*gray*).

The apparently slow adsorption kinetics in the hysteresis region obtained in our experiments is consistent with the picture given in the introduction refering to it as a consequence of the two-mode dynamics. At initial times, the created concentration gradients are eliminated via the adsorbate diffusion into the porous material and the system encounters a quasi-equilibrium metastable state, i.e. gets captured in one of the

local free-energy minima. Further uptake is controlled by the local density fluctuations and the density redistribution within the porous matrix. This process is essentially activated in nature because it requires crossing of free-energy barriers and resembles the main features of the random-field Ising model [3]. Thus, slow activated dynamics, prevailing at long times, explains the slowing down of the uptake in the region of capillary condensation. With the present studies, for the first time the dynamical features leading to adsorption hysteresis has been comprehensively investigated experimentally.

[1] H.J. Woo, P.A. Monson: Phys. Rev. E **67**, 041 207 (2003)
[2] R. Valiullin et al.: Nature **443**, 965 (2006)
[3] D.A. Huse: Phys. Rev. B **36**, 5383 (1987)

4.3 Transport Properties of Fluids in Nanopores at Sub- and Supercritical Conditions

M. Dvoyashkin, R. Valiullin, J. Kärger

Upon variation of the temperature in bulk liquids and in liquids completely saturating porous solids, the measured diffusivities often are reasonably well described by the Arrhenius model. This implies random molecular jumps with jump rates controlled by the activation energy of molecular propagation. When molecules, however, are confined to mesopores, the intermolecular and the molecule-pore wall interactions may vary in quantitatively different ways with changing temperature. Depending on the experimental conditions, this may lead to situations where the confined liquids may undergo phase transitions [1]. In the present contribution, dynamical properties of fluids in mesopores subjected to evaporation transition and transition to the supercritical state are explored using the pulsed field gradient NMR method.

In this route, molecular diffusion of n-pentane in Vycor porous glass within closed sample tubes has been studied [2]. It is found that the temperature dependence of the diffusivity dramatically depends on the state of the fluid surrounding the mesoporous monoliths. In an oversaturated sample, i.e. in a sample containing some amount of the liquid also outside of the porous material, the diffusivity in the mesopores followed the Arrhenius dependence. In samples with only the mesopores saturated by the liquid, i.e. without any excess fluid, with increasing temperature the diffusivity notably deviated from the Arrhenius dependence towards higher diffusivities. The analysis of the intensities of the respective NMR signals from the fluid within the porous material and in the surrounding phase has revealed that this anomaly is accompanied by the formation of a space free of liquid within the pore system. With the measured pore filling factors, the resulting overall diffusivity is estimated by a two-region approach with diffusion occurring in either the liquid phase or the free space within the pore volume.

A qualitatively new picture emerges if in the sample with the excess n-pentane the temperature interval is extended up to the n-pentane critical temperature T_c. Here, at a temperature $T \approx T_c - 30\,\mathrm{K}$, a sudden jump in the diffusivity of the intraporous fluid is observed (see Fig. 4.2). Remarkably, at temperatures up to T_c the diffusivity of the
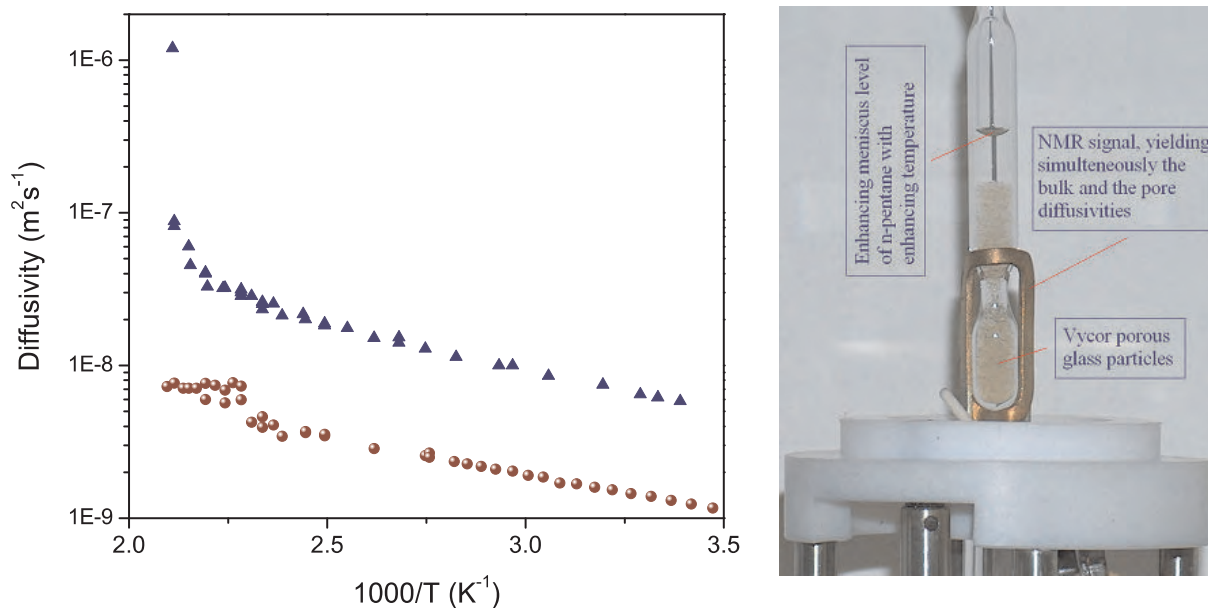
Figure 4.2: Arrhenius plot of the measured diffusivities of bulk n-pentane (*triangles*) and n-pentane in Vycor porous glass (*circles*) by PFG NMR. The *solid* and *dashed lines* show bulk and pore critical temperatures, respectively. The *right graph* shows the NMR glass tube with n-pentane and Vycor in the NMR probehead.

bulk surrounding phase does not exhibit any deviation from the normal (Arrhenius) behavior. These observations unequivocally point out that the critical state in pores is attained far below T_c in agreement with the literature. An important message of the present study is that NMR diffusometry provides an additional tool to study phase separation phenomena under confinement with novel information not accessible by other experimental techniques.

[1] L.D. Gelb et al.: Rep. Prog. Phys. 62, 1573 (1999)
[2] M. Dvoyashkin et al.: Phys. Rev. E., in press

4.4   Orientational Ordering of n-Alkane Molecules under Nanoscalic Confinement

A. Khokhlov, R. Valiullin, J. Kärger

Liquids under mesoscalic confinement exhibit different physical properties as compared to bulk state. This is brought about both by surface interactions and by effects of the confined space itself, leading to complex molecular organization. There is plenty of experimental evidence that n-alkane molecules tend to orient in the vicinity of surfaces, e.g. liquid-vapor interfaces [1] or under planar confinement [2]. In the present work [3], NMR spectroscopy has been exploited to study microscopic dynamics of n-alkane molecules introduced into silicon tubes of a few nanometers in diameter. It was found that the molecules possess incomplete sampling of all internuclear orientations due to a partial alignment of solute molecules leading to an observable residual dipolar
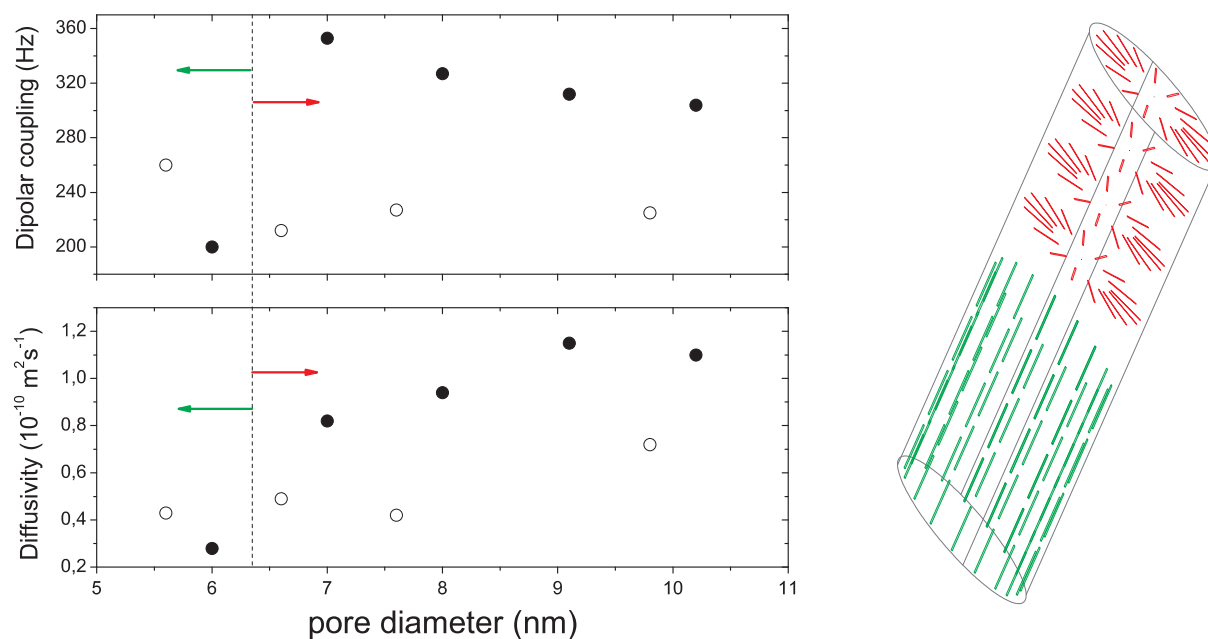
Figure 4.3: Residual dipolar coupling (*upper left graph*) and diffusivity (*lower left graph*) of eicosane ($C_{20}H_{42}$) as a function of the pore diameter d. The *filled* and *open symbols* refer to SiH_x- and SiO_2-terminated porous silicon, respectively. The *right graph* shows the two limiting molecular orientations, namely along the tube axis and perpendicular to the surface.

coupling D. The latter quantity has been measured experimentally as a function of the chain length, tube diameter and surface chemistry. These data have been complemented by the information on molecular diffusivities along the tubes.

In Fig. 4.3, typical dependencies of dipolar coupling on the pore size are shown. D increases with pore size decreasing from 10 nm to 7 nm, revealing stronger tendency to ordering. However, for PS with $d = 6$ nm a sudden decrease of D is observed. The latter is, presumably, a manifestation of a change of the orientation director. The simplest model explaining the experimental findings is that in the bigger pores the alkane molecules tend to orient along the pore axis, while in the smallest pores preferential alignment is parallel to the surface normal. The similar behavior has been found upon changing the molecular length revealing qualitative change in the behavior when the length is of the order of the pore radius. Measured self-diffusivities (Fig. 4.3) also support the picture emerging from the relaxation studies. Indeed, preferential stretching of the molecules along the pores should lead to a higher diffusivity as compared to the perpendicular orientation and this is exactly what we observe experimentally. In conclusion, n-alkane molecules are found to exhibit a rich variety of orientational ordering in silicon nanotubes depending on molecular length, pore size, and surface chemistry. NMR spectroscopy is shown to be a powerful tool which may provide important microscopic information on molecular behavior under nanoscopic confinement.

[1] B.M. Ocko et al.: Phys. Rev. E **55**, 3164 (1997)
[2] K. Nanjundiah, A. Dhinojwala: Phys. Rev. Lett. **95**, 154 301 (2005)
[3] R. Valiullin, A. Khokhlov: Phys. Rev. E **73**, 051 605 (2006)

4.5 Intracrystalline Self-Diffusion of Propane and Propylene in Metal Organic Framework Cu-BTC

M. Wehring, J. Gascon[*], F. Kapteijn[*], D. Dubbeldum[†], R.Q. Snurr[†], F. Stallmach

[*]Department for Catalysis Engineering, Delft University of Technology, The Netherlands
[†]Department of Chemical Engineering, Northwestern University, Evanston, USA

The metal-organic framework (MOF) compound copper(II) benzene-1,3,5-tricarboxylate, $(Cu_3(BTC)_2(H_2O)_3$: short Cu-BTC) is a nanoporous crystalline coordination polymer [1, 2]. The Cu-BTC structure forms a regular 3D pore system with interconnected 0.9 nm sized main pores and smaller side pores with 0.5 nm size. It has a specific pore volume of about $0.41\,cm^3g^{-1}$ and a high inner surface area. These properties are the reason for potential applications of CuBTC as microporous adsorbent in separation processes.

In this study we investigated the adsorption and self-diffusion of propane and propylene in Cu-BTC, which are both of interest for olefin separation using this material. Single-component adsorption isotherms were measured over a temperature range of 318 K to 383 K. They showed that propylene is stronger adsorbed in Cu-BTC than propane. The adsorption isotherms were analysed using a one-site Langmuir adsorption model, which yielded heats of adsorption of $31.3\,kJ\,mol^{-1}$ for propane and $42.9\,kJ\,mol^{-1}$ for propylene. The self-diffusion of propane and propylene adsorbed in Cu-BTC was measured using the proton (^{1}H) pulsed field gradient (PFG) NMR technique [3]. Due to the magnetic interactions with the electron spin of the copper ions of the Cu-BTC framework, the (^{1}H) nuclear magnetic relaxation times of the adsorbed molecules are rather short. For both types of molecules, the values are $5-10$ ms for the longitudinal (T_1) relaxation time and about 1.5 ms for the transverse (T_2) relaxation time at 298 K. These short values require that the PFG NMR studies are performed using the primary spin echo sequence with short diffusion times ($\Delta = 1.5$ ms) and short, but very high-intensity pulsed field gradients ($\delta = 400\,\mu s$, $g = 25\,Tm^{-1}$). The PFG NMR measurements were carried out in a temperature range of 298 K to 470 K.
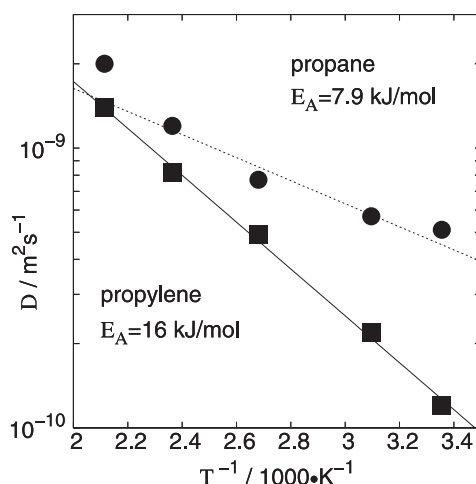
Figure 4.4: Intracrystalline self-diffusion coefficients of propane ($\bullet$) and propylene ($\blacksquare$) in metal organic framework Cu-BTC as obtained by ^{1}H PFG NMR studies.

The self-diffusion coefficients obtained are shown in an Arrhenius presentation (Fig. 4.4). The straight lines in the plot represent the temperature dependence and correspond to activation energies of the self-diffusion of $7.9\,\mathrm{kJmol^{-1}}$ for propane and $16\,\mathrm{kJmol^{-1}}$ for propylene. These values are significantly smaller than the corresponding heats of adsorption (see above), which indicates that the observed diffusion process is not influenced by intercrystalline diffusion of the C_3 hydrocarbons between neighbouring Cu-BTC crystals. Additionally, the experimentally determined self-diffusion coefficient of propane in CuBTC at $298\,\mathrm{K}$ ($5.1{\times}10^{-10}\,\mathrm{m^2s^{-1}}$) agrees well with results obtained by molecular simulations ($2.0{\times}10^{-10}\,\mathrm{m^2s^{-1}}$ to $5.1{\times}10^{-10}\,\mathrm{m^2s^{-1}}$ depending on the loading).

These results represent the first experimental data for intracrystalline diffusion of C_3 hydrocarbons in metal organic framework materials. They show that olefin separation with Cu-BTC may be based on differences in adsorption properties and may be facilitated by the reduced diffusivity of the olefin compared to the alkane.

[1] S.S.-Y. Chui et al.: Science **283**, 1148 (1999)
[2] A. Vishnyakov et al.: Nano Letters **3**, 713 (2003)
[3] F. Stallmach, P. Galvosas: In *Ann. Rep. NMR Spectrosc.*, Vol. 61 (Elsevier, London 2007) p 52

4.6   Surface Barriers on Nanoporous Particles: A New Method of Their Quantitation by PFG NMR

M. Krutyeva, S. Vasenkov, J. Kärger

The rate of molecular exchange between the intracrystalline space of nanoporous particles and their surroundings is among the limiting factors which determine the performance of zeolites and related nanoporous materials for their technological application in catalysis and adsorptive mass separation. This is in particular true since, during their industrial use, depositions of by-products on their outer surface or structural collapse close to their surfaces establish, or tend to enhance already existing, surface resistances. As a non-invasive technique and operating on the scale of micrometers which is particularly relevant for such systems, PFG (PGSE) NMR is ideally suited for quantitating such possible transport resistances on the particle surface.

A new method to determine the surface permeability of nanoporous particles was proposed [1]. It is based on a special analysis of the so-called NMR tracer desorption experiment, in which the normalized effective diffusivities of the molecules that after a given time have not yet left their particles are plotted as a function of their fraction related to the molecules initially in a particle, with the corresponding solutions of the diffusion equation via dynamical Monte Carlo simulations. These correlation curves are found to dramatically depend on the surface permeability. This is in particular true for the range where the transport resistances due to intraparticle ("intracrystalline") diffusion and surface barriers are comparable. It is this range where the conventional method of simply comparing the molecular mean exchange time with its estimate on the basis of the intracrystalline diffusivity [2] becomes questionable, as a consequence of the uncertainty in the primary quantities inherent to this method.
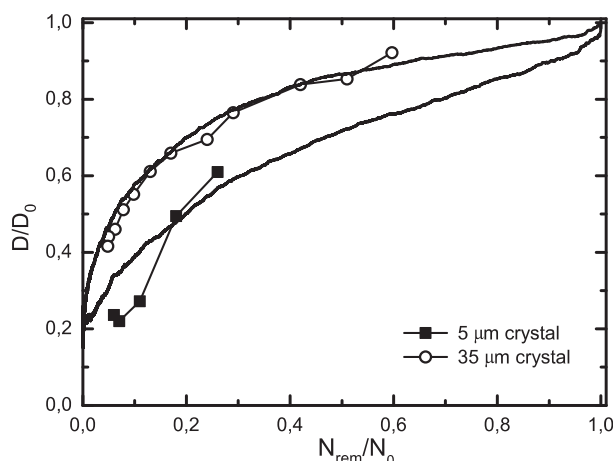
Figure 4.5: Correlation plot of restricted diffusion (D/D_0) and tracer desorption: experimental data obtained for methane in LTA zeolite crystals of different size (*symbols*) with the corresponding theoretical curves (*lines*) obtained by dynamic Monte Carlo simulations.

Figure 4.5 combines the two sets of experimental data, namely the relative numbers of molecules of methane still remaining in one and the same LTA zeolite crystal (abscissa) and effective diffusivities in relation to the corresponding values for diffusivities for unrestricted motion (ordinate). Direct comparison with the theoretical curves yields best agreement with the permeability values $\alpha = (0{,}8 \pm 0{,}5) \times 10^{-3}\,\mathrm{ms^{-1}}$ and $\alpha = (0{,}78 \pm 0{,}3) \times 10^{-3}\,\mathrm{ms^{-1}}$ for the zeolite crystals of 5 µm and 35 µm edge length, respectively. These values represent the first zeolite surface permeabilities ever obtained on the basis of direct experimental evidence.

In the temperature range from −20 °C to 100 °C the surface permeability of LTA zeolite crystallites for methane and ethane has been estimated [3]. It was observed that already without any further exposure, the surface of the crystallites studied reveals a finite transport resistance which is not negligibly small in comparison with that due to intracrystalline diffusion. The new method was found to be sensitive to different species of sorbate. The surface permeability increases from ethane to methane. Although the size of these molecules does not differ substantially, the surface permeabilities differ by one order of magnitude. With increasing temperature, the surface permeabilities were found to increase faster than the intracrystalline diffusivities, resulting in a decrease of the contribution of the surface resistance to the overall exchange rate. With the present study, a new tool for accessing surface permeabilities has been introduced. Even without any special treatment of the zeolite crystals, these permeabilities are found to be of notable influence on the overall transport. This work demonstrates that combined application of dynamic (lattice) MC simulations and PFG NMR measurements can lead to new insights into the details of translational dynamics of guest molecules on the external surface of microporous materials.

[1] M. Krutyeva et al.: J. Magn. Reson. **185**, 300 (2007)
[2] J. Kärger, D.M. Ruthven: *Diffusion in zeolites and other microporous solids* (Wiley, New York 1992)
[3] M. Krutyeva et al.: Micropor. Mesopor. Mat. (2007), in press

4.7 NMR Studies of Pore Formation and Water Diffusion in Self-Hardening Cut-Off Wall Materials

W. Schönfelder, J. Dietrich[*], A. Märten[*], K. Kopinga[†], F. Stallmach

[*]AZBUT Anneliese Baustoffe für Umwelt und Tiefbau GmbH, Ennigerloh
[†]Department of Applied Physics, Eindhoven University of Technology, The Netherlands

This project aims at the characterization of pore structure of hardening cut-off wall materials as well as the water self-diffusion of cured cut-off wall materials. It is performed within the International Research Training Group (IRTG) "Diffusion in Porous Materials".

Cut-off walls, which are vertical in-ground barriers of low hydraulic conductivity, are frequently used for the containment of polluted sites. It primarily consists of a watery suspension of a cement-based hydraulic binder and a cement-stable bentonite.

NMR relaxometry, cryoporometry and diffusometry indicate a direct relation between the solid content of the freshly mixed cut-off wall suspension, the pore size and the diffusive transport resistance of the cured cut-off wall material (Fig. 4.6). An increased content of solids in the cut-off wall suspension (I→III) leads to a decrease in relaxation times and diffusion coefficients, indicating a corresponding reduction of the pore sizes and an enhancement of the diffusion resistance. The self-diffusion coefficients of the pore water were found to be in the order of $D = 10^{-13}\,\mathrm{m^2s^{-1}}$.

They are about four orders of magnitude smaller than the self-diffusion coefficient of bulk liquid water, confirming an excellent diffusive resistance of the cut-off wall materials already on a microscopically small length scale. These NMR studies contribute to an improved characterization of self-hardening cut-off wall materials and may be used to optimize site-specific compositions.
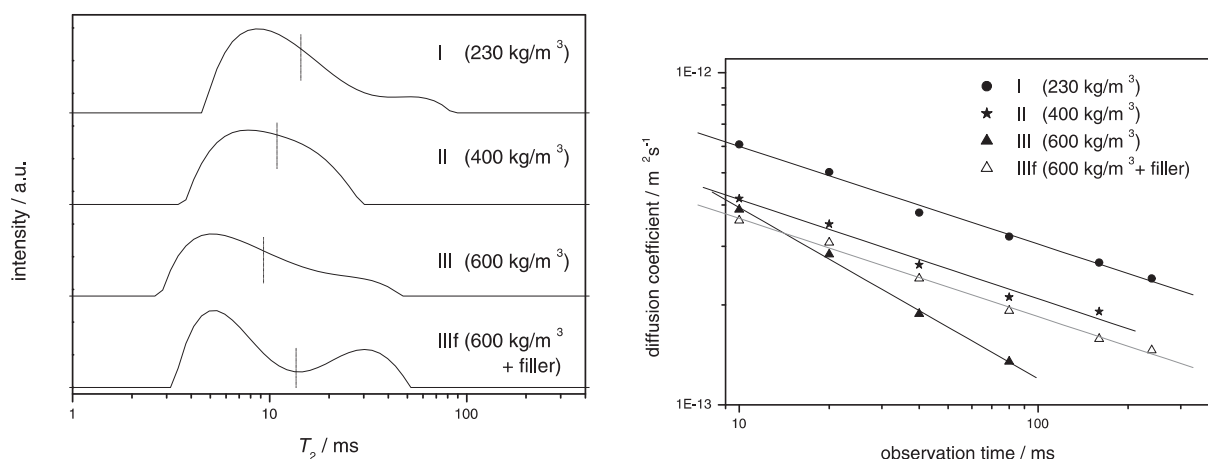
Figure 4.6: *Left*: distribution of transverse relaxation time T_2 of cured cut-off wall material of different solid content (*dotted lines* indicate mean T_2). *Right*: diffusion coefficient in dependency of the observation time observed for cured cut-off wall material with different content of solids (*I, II, III*) and additional filler material (*IIIf*).

4.8 Investigation of Uptake Processes in Silicalite-1 Fragments by Means of Interference Microscopy

D. Tzoulaki, W. Schmidt[*], J. Kärger

[*]MPI für Kohlenforschung, Mülheim a.d. Ruhr

MFI-type zeolites have excellent catalytic as well as separation properties allowing them to hold a prominent position in industry. In the literature, there can be found numerous articles about Silicalite-1 referring to its hourglass structure, which is indicative of regular intergrowth effects [1]. These zeolites have a three-dimensional pore system, consisting of straight and sinusoidal channels, of which only the sinusoidal primarily reach the external surface of an MFI crystals (Fig. 4.7b) [1].

For the first time only one segment of the crystal – and not the whole unity of MFI crystal – has been examined by means of interference microscopy. The segments [2] – obtained by disintegration of the intergrowths – do not have the shape expected according to literature (Fig. 4.7c,d), because of a preference to break in other positions,
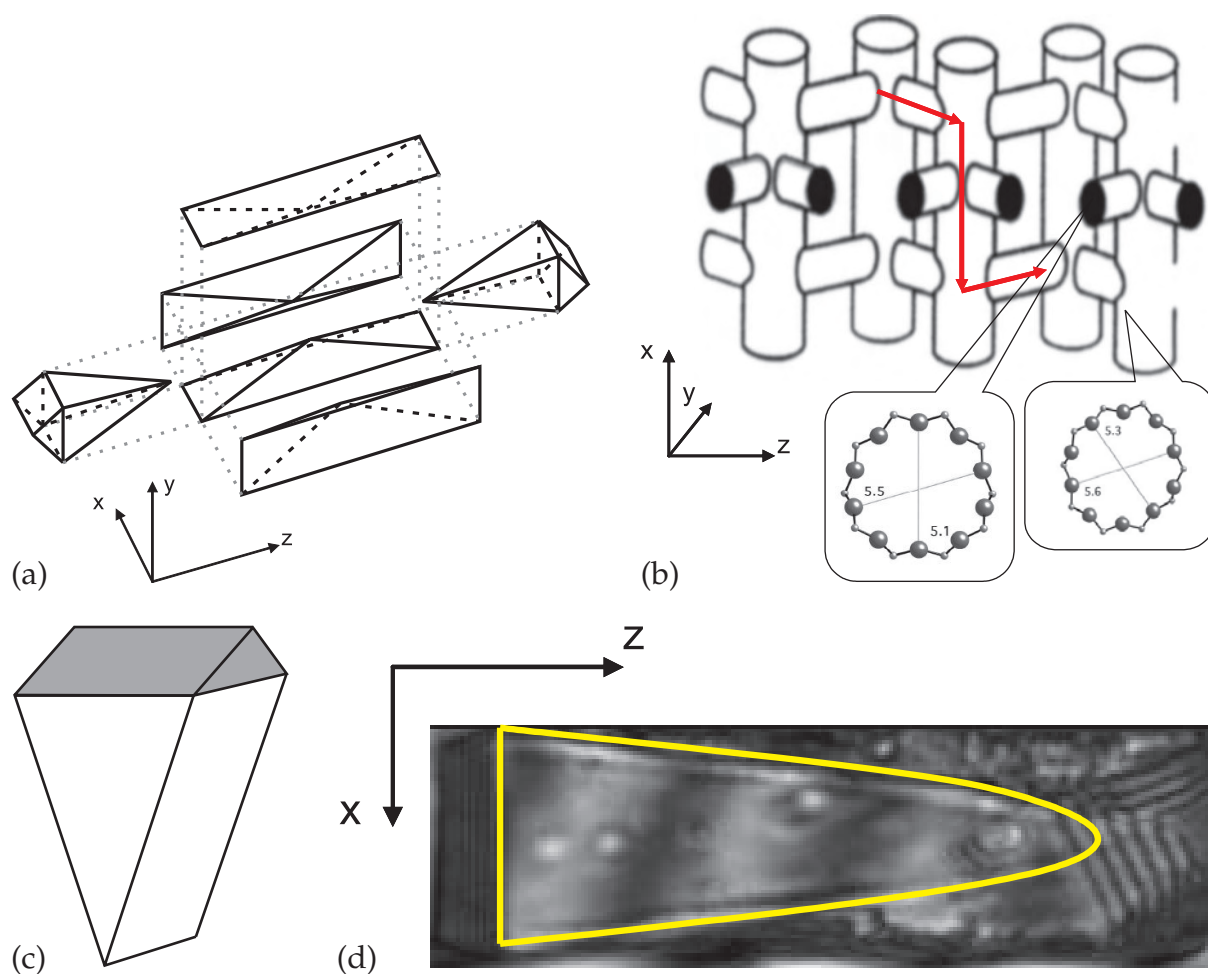
Figure 4.7: (a) Schematic representation of the internal structure of silicalite-1 crystals according to [1]. **(b)** 3D pore system of straight and sinusoidal channels. **(c)** Schematic representation of segments obtained after disintegration. **(d)** The segment under study.

where the crystal is not that tightly joined. Such kind of segments are investigated by our microscopic technique, which is based on the principle that the refractive index of a medium is a function of its composition, namely of the intracrystalline concentration of guest molecules [3]. As an output we obtain experimentally measured concentration profiles being of great importance because they reveal crucial information regarding the uptake processes, such as (i) the direction of internal transport, (ii) the presence of internal structural defects and (iii) surface/internal barriers. Four cycles of ad-/desorption of isobutane have been performed for a single fragment of silicalite-1 (Fig. 4.7d). For adsorption (desorption) measurements the pressure of isobutane in the surroundings of the zeolite was changed in a stepwise manner from 0 to 1 mbar and 1 to 2 mbar (2 to 1 and 1 to 0 mbar). By comparing uptake curves of adsorption for every cycle we observe that each time we perform a new cycle, the time needed for the molecules to fill the interior of the crystal rises whereas the equilibrium value of the amount adsorbed is practically not influenced (Fig. 4.8a). This phenomenon indicates that barriers near
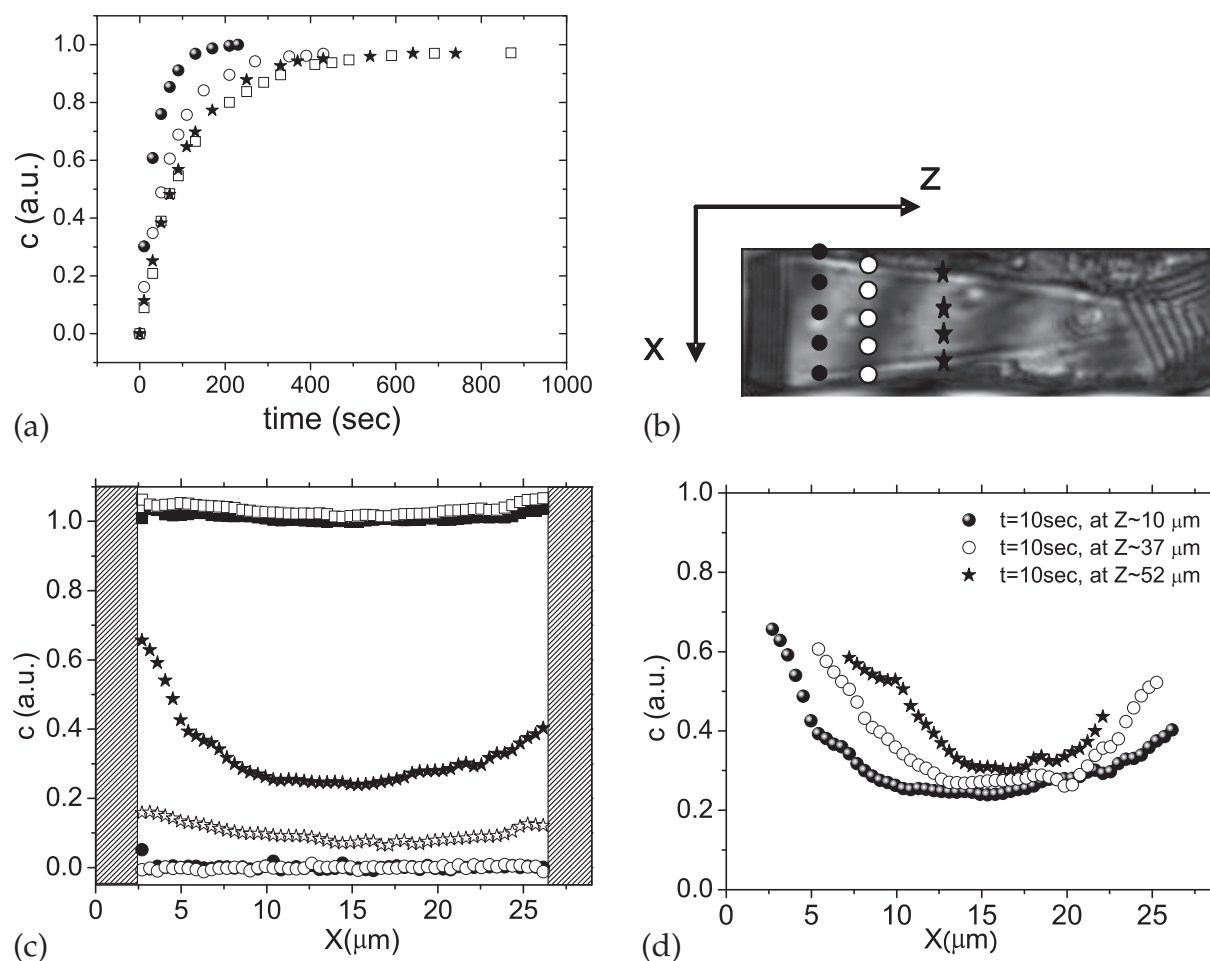
Figure 4.8: (a) Kinetics of adsorption $0-1$ mbar for (•) 1st, (∘) 2nd, (⋆) 3rd, and (□) 4th cycle. (b) Indication of the parts to which the profiles of (c) and (d) correspond to. (c) The evolution of one-dimensional intracrystalline profiles along *x*-axis during uptake of isobutan into the fragment for the first (*filled symbols*) and last cycle (*hollow symbols*). *Filled* and *hollow symbols* are in pairs: (•, ∘) at 0 sec, (⋆, ☆) at 10 sec and (■, □) at equilibrium. (d) The first one-dimensional intracrystalline profile along *x*-axis during uptake of isobutane into fragment at different parts.

the external surface of the crystal can be created as time goes by, and this assumption is verified by the intracrystalline concentration profiles (Fig. 4.8c). Although these profiles exhibit a pronounced curvature – due to the dominating diffusion resistance – for the first cycle, this curvature is no longer observed for the last cycle, where the profiles are almost flat. In addition to that, as we move closer to the right end of the segment, profiles show the expected behaviour, namely are more curved and show faster uptake (Fig. 4.8b, d).

[1] E.R. Geus et al.: Zeolites **14**, 82 (1994)
[2] U. Wilczok et al.: 18. Dt. Zeolith-Tagung (2006)
[3] O. Geier et al.: J. Phys. Chem. B **101**, 10 217 (2001)

4.9 Manipulating Molecular Uptake Rates of MFI Crystals by Surface Modification: An IR Microscopy Study

C. Chmelik, L. Heinke, A. Varma, U. Wilczok[*], W. Schmidt[*], D.B. Shah[†], J. Kärger

[*]MPI für Kohlenforschung, Mülheim a.d. Ruhr
[†]Dept. of Chem. & Biomed. Eng., Cleveland State University, Cleveland, USA

In many recent IR and interference microscopy investigations, presence of surface resistance was found in a variety of zeolites such as AFI, MFI and FER. Such surface barriers can have a substantial negative influence on the performance of zeolites in adsorption and catalysis. It is, therefore, important not only to learn more about the nature of these surface barriers, but also to find ways to increase/decrease surface barriers in a well defined way without affecting the intracrystalline diffusivity [1–3].

In the present study, the influence of a novel surface treatment of silicalite-1 with three different chlorosilanes $(CH_3)_3SiCl$, $(C_2H5)_3SiCl$ and $(C_3H_7)_3SiCl$ on the uptake rates of isobutane is investigated. The uptake curves of crystals from different samples are compared in Fig. 4.9. In contrast to the previous results, no effect on the uptake rate of the HF surface-etched zeolite crystals was observed. However, surface silanization significantly reduced the uptake rate. The extent of reduction was found to be proportional to the length of the alkyl group of the applied chlorosilane. This represents the main finding of this investigation, since it shows that surface silanization with chloroalkylsilanes represents a viable method for manipulating and controlling the surface resistance in a well-defined way.

[1] J. Kärger et al.: *Diffusion in Zeolites*, in *Handbook of Zeolite Science and Technology*, ed. by S.M. Auerbach et al. (Marcel-Dekker, New York 2003) p 341
[2] C. Weidenthaler et al.: *X-ray Photoelectron Spectroscopy on Surface Modified MFI Zeolites*, in *Proc. 18th German Zeolite Conf.* (Universität Hannover, Hannover 2006) p 191
[3] P. Kortunov et al.: Chem. Mater. **16**, 3552 (2004)
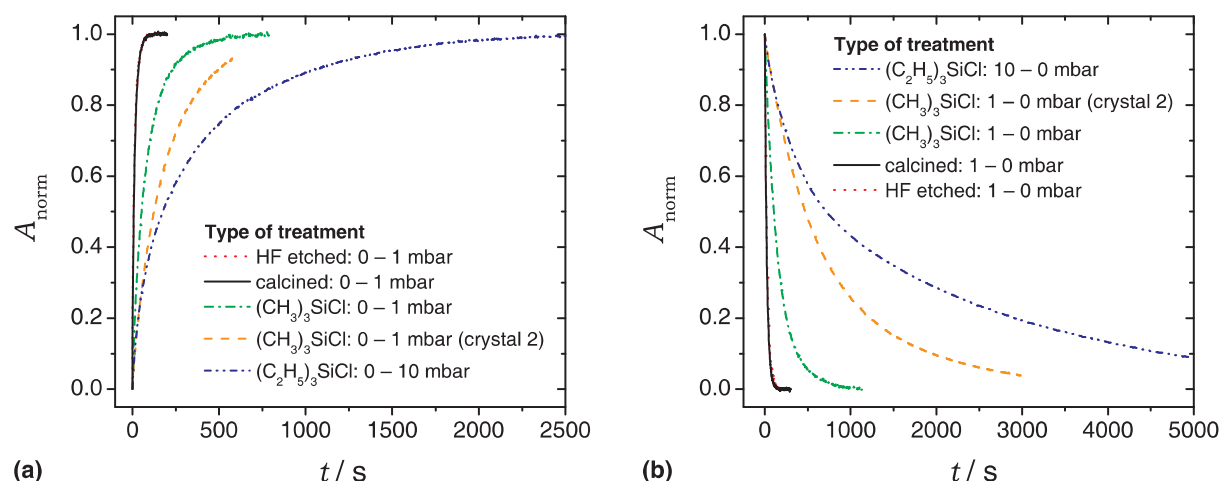
Figure 4.9: Adsorption (**a**) and desorption curves (**b**) of isobutane in different silicalite-1 samples. The HF treatment has no significant influence on the uptake rate, whereas the surface silanization leads to a progressively greater slowing down with increasing length of the alkyl group.

4.10   Assessing Guest Diffusion in Nanoporous Materials by Boltzmann's Integration Method

L. Heinke, P. Kortunov, J. Kärger

With the introduction of interference microscopy to diffusion studies in zeolites, for the first time the direct, space-resolved observation of transport diffusion in nanoporous materials has become possible. The method is based on recording transient concentration profiles during molecular uptake or release so that the local intracrystalline
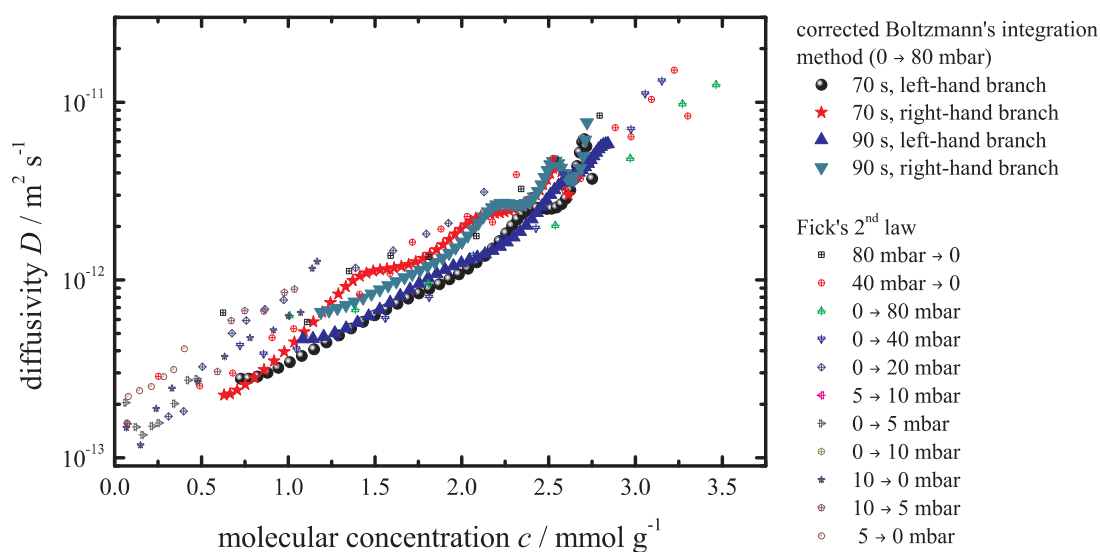
Figure 4.10: Methanol diffusivity in ferrierite calculated by Boltzmann's integration method for a pressure step of 0 to 80 mbar for $t = 70$ s and $t = 90$ s. The diffusivity calculated by Fick's 2nd law for several pressure steps is also pictured.

diffusivities directly result by a microscopic ("differential") application of Fick's 2nd law [1]. We show that under certain conditions the thus accessible wealth of information on the transport characteristics of nanoporous materials may be even surpassed by the application of an integration method which Ludwig Boltzmann invented more than a century ago and which thus encounters a large new field of application.

In many cases, however, the prerequisites for applying this method (one-dimensional mass transport without transport resistance at the surface) are not completely fulfilled. Therefore, the consequences of these deviations on the accuracy of the obtained results are discussed. It is found that the results of Boltzmann's integration method can be corrected by different considerations [2]. The discussion is focussed on the concentration profiles observed during the adsorption and desorption of methanol in ferrierite-type crystals as observable by interference microscopy (Fig. 4.10).

[1] J. Kärger et al.: Angew. Chem. Int. Ed. **45**, 7846 (2006)
[2] L. Heinke: Diff. Fundam. **4**, 9.1 (2006)

4.11   Internal Post-Curing of Hardening Cement Pastes of High-Performance Concretes Studied by NMR

K. Friedemann, F. Stallmach, J. Kärger

In the project "Water balance in high-performance concretes during internal post-curing (IPC) with innovative additives" (DFG: KA 953/22-1), NMR relaxometry and NMR diffusometry are used to investigate the availability of water added to cement pastes via appropriate additives. Within this project, we developed an NMR approach, which allows us to monitor how a water-containing polyelectrolyte gel releases its water into a hydrating white cement paste of moderately low initial w/c (water-to-cement-ratio) of 0.3 [1].
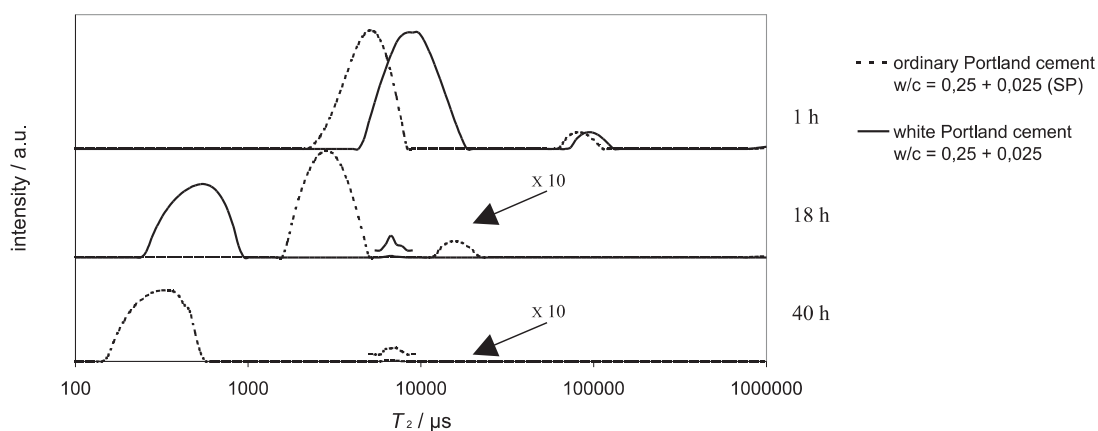
Figure 4.11: Distribution of the transverse relaxation times T_2 of physically-bound water in hydrating cements (*left peaks*) and gel-like water in the polyelectrolyte (*right peaks*) during the first 40 h of hydration.

These NMR-methods may also be applied to hydrating cement paste of even lower initial w/c-ratios and to practically relevant Portland cements with and without additional super-plasticizer (SP) [2]. As example, Fig. 4.11 shows the T_2 relaxation time distribution of a white Portland cement paste and an ordinary Portland cement paste with SP with an initial w/c-ratio of 0.25 and additional 25 g water-saturated polyelectrolyte gel per kilogram dry cement. The time dependence of the left peak shows the decreasing pore sizes due to cement hydration. The right peaks, which are characteristic for the water contained in the gel additive (T_2 = 100 ms), shift to shorter relaxation times and decrease in their intensity. It is observed that the consumption of the water from the additive occurs mainly during the accelerated period. In the sample containing super-plasticizer, the accelerated period and the consumption of the additional water from the gel is delayed due to the retarding influence of the SP (Fig.4.11).

[1] K. Friedemann et al.: Cem. Concr. Res. **36**, 817 (2006)
[2] K. Friedemann et al.: in: *Proc. Int. RILEM Conf. Volume Changes of Hardening Concrete* (PRO52), Denmark, August 2006, ed. by O.M. Jensen et al. (RILEM 2006) p 147

4.12   *In situ* ^{1}H and ^{13}C MAS NMR Kinetic Study of the Mechanism of Hydrogen Exchange for Propane on Zeolite HZSM-5

A.G. Stepanov[*], S.S. Arzumanov[*], H. Ernst, D. Freude

[*]Boreskov Institute of Catalysis, Novosibirsk, Russia

A simple reaction of hydrogen exchange between the Brönsted sites of zeolites and a small alkane molecule provides a pathway for claryfing the mechanism of alkane activation on solid acid catalysts. The existing data on the mechanism of the exchange for propane on acidic zeolites are contradictive [1–3]. Two mechanisms are mainly suggested. The first one implies intermediacy of propene in equlibrium with isopropyl cation to provide the exchange first into the methyl groups and then into methylene group by intramolecular hydrogen scrambling (consecutive scheme of the exchange) [1, 2]. The second mechanism suggests that both methyl and methylene groups are equally involved in the exchange via a direct proton/deuteron transfer between the catalyst acid sites and the alkane in a concerted step involving a pentacoordinated carbon atom (parallel scheme of the exchange) [3].

The kinetics of hydrogen (H/D) exchange between Brønsted acid sites of zeolite H-ZSM-5 and variously deuterated propane (propane-d_8, propane-1,1,1,3,3,3-d_6, propane-2,2-d_2) have been monitored *in situ* by ^{1}H MAS NMR spectroscopy within the temperature range of $503-556$ K. The contribution of intramolecular hydrogen transfer to the H/D exchange in the adsorbed propane was estimated by monitoring the kinetics of ^{13}C-label scrambling in propane-2–^{13}C *in situ* with ^{13}C MAS NMR at $543-573$ K. The rate constant (k_3) for intramolecular H/D exchange between the methyl and the methylene groups is $4-5$ times lower compared to the direct exchange of both the methyl (k_1) and the methylene (k_2) groups with Brønsted acid sites of the zeolite, the k_1
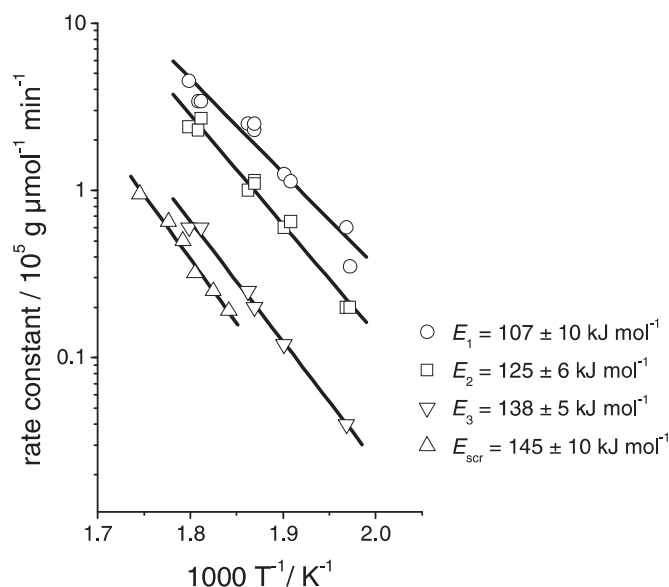
Figure 4.12: Arrhenius plot and activation energies for the H/D exchange reaction in deuterated propane on H-ZSM-5 and the ^{13}C-scrambling in propane-2-^{13}C on H-ZSM-5. k_1(○), k_2(□), k_3(∇), and k_{scr}(△).

being *ca.* 1.5 times higher than k_2 (Fig. 4.12). At lower temperature (473 K) the exchange is slower, and the expected difference between k_1 and k_2 is more essential, $k_1 \approx 3k_2$. This accounts for earlier observed regioselectivity of the exchange for propane on H-ZSM-5 at 473 K [1]. Faster direct exchange with the methyl groups compared to that with the methylene groups was attributed to a possible better spatial accessibility of the methyl groups for the exchange. Similar activation energies for H- and C-scramblings with two times more rapid rate of H-scrambling was rationalized by proceeding of these two processes through the intermediacy of isopropyl cation as in classical carbenium ion chemistry.

[1] J. Sommer et al.: J. Am. Soc. **117**, 1135 (1995)
[2] M. Haouas et al.: J. Am. Soc. **117**, 599 (2004)
[3] A.G. Stepanov: Catal. Lett. **54**, 1 (1998)

4.13   New Options for Measuring Molecular Diffusion in Zeolites by MAS PFG NMR

M. Fernandez, A. Pampel, J. Kärger, D. Freude

Combination of pulsed field gradient (PFG) NMR with magic-angle spinning (MAS) NMR is demonstrated to have remarkable advantages in comparison with conventional PFG NMR [1], if applied to diffusion measurements in beds of nanoporous particles, notably zeolites [2].

The contribution describes investigations that mainly profit from the elimination of the disturbing influence of the inhomogeneity of the sample susceptibility [3] playing a decisive role for PFG NMR diffusion measurements of molecules in beds of zeolites.
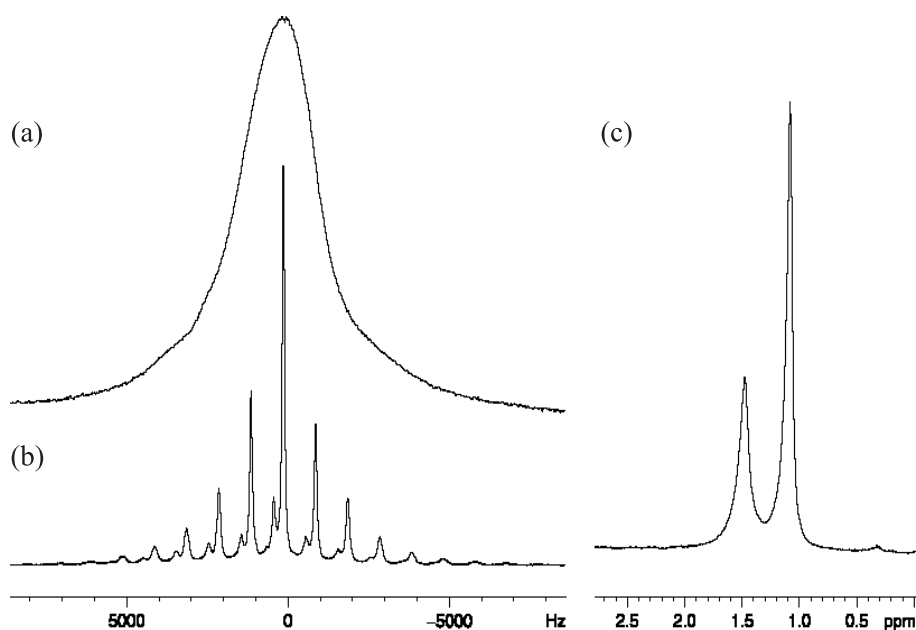
Figure 4.13: ^{1}H MAS NMR (observation frequency 749.98 MHz) spectra of *n*-butane adsorbed in silicalite-1 observed at room temperature. (**a**) Spectrum observed without sample spinning. **b**) Spectrum observed using MAS at 1 kHz rotation frequency. (**c**) Spectrum observed using MAS at 10 kHz rotation frequency.

In general, NMR spectra of polycrystalline materials are broadened by anisotropic interactions such as dipolar coupling, chemical shift anisotropy, quadrupolar coupling, and susceptibility effects. Depending on their strength and the achievable rotation frequency, MAS can reduce or even completely suppress these effects during the time course of an NMR experiment, see Fig. 4.13.

Using a 750 MHz spectrometer, at a rotation frequency of 10 kHz, the spectrum of *n*-butane is observed with a residual line width of 44 Hz and 73 Hz of the signals of the CH_3- and CH_2-groups, respectively. The performance of the PFG NMR diffusion experiment is straightforward under these conditions. The diffusion coefficient calculated from the decay of integrals of the signal of the CH_3 peak is 3.17×10^{-10} m^{2}s^{-1}.

MAS PFG NMR is able to provide spectral resolution that is suitable for the spectroscopic separation of signals from different components. Under these conditions diffusion experiments with binary mixtures absorbed in zeolites were carried out. Samples under study are mixtures of *n*-butane and isobutane absorbed in NaX and silicalite-1. The measurements show how it is possible to distinguish the diffusivities of both isomers. The diffusivities obtained for the binary mixture absorbed in NaX are 1.37×10^{-10} m^{2}s^{-1} and 1.12×10^{-10} m^{2}s^{-1} for *n*-butane and isobutane, respectively.

PFG NMR and MAS NMR have been combined to measure intracrystalline zeolitic diffusion. It has been demonstrated that in this way line broadening due to the susceptibility heterogeneities inevitable in such systems may be dramatically reduced. Thus, the bad resolution, one of the most decisive limitations of the application of PFG NMR to zeolitic host-guest systems, may be overcome. This opens broad application concerning intra-crystalline diffusion measurements for multicomponent mixtures in zeolitic host systems.

[1] A. Pampel et al.: Chem. Phys. Lett. **407**, 53 (2005)
[2] J. Kärger: in *Encyclopedia of Nuclear Magnetic Resonance*, Vol. 3, ed. by R.K. Harris et al. (Wiley, Chichester 1996) p 1656
[3] D. Michel et al.: J. Chem. Phys. **119**, 9242 (2003)

4.14 High Temperature ^{1}H MAS NMR Studies of the Proton Mobility in Zeolites

J. Kanellopoulos, H. Ernst, D. Freude

Bridging hydroxyl groups capable of donating protons to molecules in the cages of zeolites are Brønsted-acid sites in heterogeneous catalysis. ^{1}H NMR studies of the acid protons in dehydrated zeolites gave some insight into the proton mobility [1–3]. The proton mobility in hydrogen zeolites was observed from 160 K to 550 K by conventional heating of the bearing gas and to 790 K by means of the laser heating of dehydrated and fused samples. ^{1}H MAS NMR spectra of the bare Brønsted sites of zeolites were monitored in this temperature range. The full width at half maximum of the ^{1}H MAS NMR spectrum of the dehydrated unloaded samples narrows by a factor of 24 for zeolite H-ZSM-5 and a factor of 55 for zeolite 85 H-Y. For the latter, the activation energy of 78 kJmol^{-1} has been determined. Figure 4.14 shows the ^{1}H MAS NMR spectra of the dehydrated zeolite 85 H-Y with a rotation frequency of 1 kHz. There are two reasons for choosing such a low rotation frequency. First, the envelope of many sidebands gives a good picture of the static (without sample rotation) line width. Second, the condition $\omega_{rot}\tau_c \ll 1$ giving the line widths as a linear function of the correlation time is fulfilled at lower temperature for a lower rotation frequency. The narrowing onset takes place between 298 and 420 K, see Fig. 4.14. Independent of the line narrowing model it can be concluded that the correlation time τ_c which is given by the mean residence time τ of a proton at an oxygen atom is of the order of magnitude of the reciprocal low temperature line width ($\sim$ 100 μs) at the temperature of the narrowing onset.

Now the question arises whether the proton mobility is caused by jumps of hydrogen atoms over the oxygen framework of the zeolites or rather by a proton vehicle mecha-
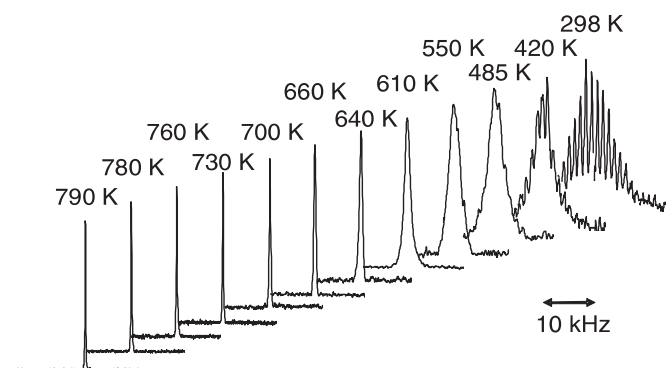
Figure 4.14: ^{1}H MAS NMR spectra of the dehydrated zeolite 85 H-Y for measuring temperatures from 298 K to 790 K. The rotation frequency is 1 kHz. No spinning sidebands can be observed at temperatures above 500 K, whereas at room temperature they are well-resolved.
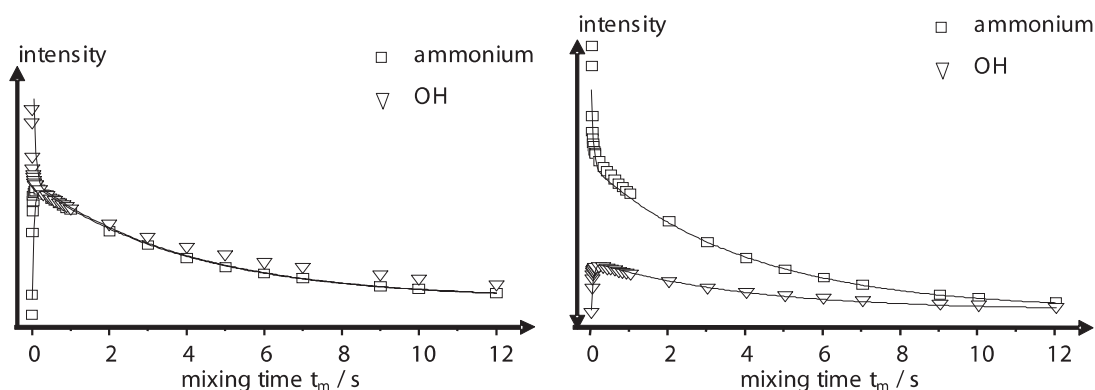
Figure 4.15: Amplitudes of the ^{1}H MAS NMR signal of ammonium ions and structural OH-groups as a function of the mixing time t_m. The zeolite H-Y was loaded with 1.5 ammonia molecules per supercage. For the *left panel*, the offset is shifted by the frequency difference between both signals from the left hand side of the left signal (ammonium ions). For the *right panel*, the offset is shifted by the same value to the right hand side from the right signal (bridging hydroxyl groups).

nism using residual water or ammonia molecules, which could not be removed from the zeolite by the activation procedure. Therefore, slightly reammoniated or rehydrated zeolites were investigated. One-dimensional exchange spectroscopy was performed by means of the NOESY pulse group, see Fig. 4.15.

In conclusion, zeolites H-Y and H-ZSM-5 were investigated by ^{1}H MAS NMR spectroscopy in the temperature range from 160 K to 790 K. We found that the hydrogen form of a zeolite, which contains almost residual ammonium ions, represents an ammonium conducting material for which the proton mobility is dominated by the high mobility of the ammonium ions in the zeolite. Thus, the proton vehicle mechanism by means of residual atoms in the zeolite seems to be responsible for the proton mobility at high temperatures.

[1] J. Kanellopoulos: PhD thesis, University of Leipzig 2006
[2] J. Kanellopoulos et al.: J. Catal. **237**, 416 (2006)
[3] D. Freude et al.: J. Catal. **49**, 123 (1977)

4.15   Progress of ^{17}O NMR for Zeolite Characterization

D. Schneider, D. Prochnow, H. Ernst, D. Freude

AlPO$_4$-14 and several zeolites of type A, X, Y, ZSM-5 isotopically enriched in ^{17}O were analysed by means of ^{17}O NMR in the field of 17.6 T using several solid-state NMR techniques for quadrupole nuclei. The influence of molecule adsorption is discussed including the question how the ^{17}O NMR shift reflects the basicity of the oxygen framework.

^{17}O MQ MAS (multi-quantum) experiments and ^{17}O DOR (double rotation) experiments were performed in the external magnetic field of 17.6 T (Bruker AVANCE 750 with wide-bore magnet) at 101.7 MHz. Probes constructed at the Institute of Chemical
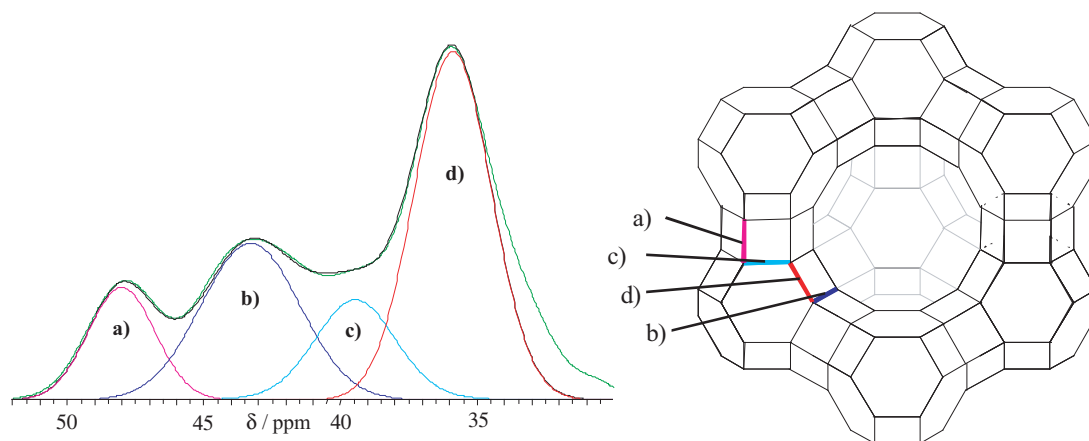
Figure 4.16: ^{17}O DOR NMR spectra of the dehydrated Na-LSX. The fit uses the fact that O_4-positions occur twice as much as the other crystallographic positions in the material.

Physics in Tallinn and Bruker MAS probes were used for the DOR (double rotation) and MQ (multi-quantum) MAS experiments, respectively. The repetition time was in the range from 200 ms to 1 s corresponding to the measured longitudinal relaxation times T_1, which vary from 100 ms to 500 ms for the various zeolite samples under study. The time step t_1 in the multiple-quantum dimension was increased in steps of the reciprocal spinning frequency, in order to avoid spinning sidebands. DOR experiments were performed typically in a synchronized manner [1] with an outer rotor speed of about 1.4 kHz and an inner rotor speed of $6.0-6.5$ kHz.

    Our studies confirm that the quadrupole coupling constant increases with increasing ionic character of the bonds T_α-O and O-T_β. Considering the values of C_{qcc} obtained from ^{17}O atoms in bridging positions in barium pyrophosphate (P-O-P) [2], in AlPO$_4$-
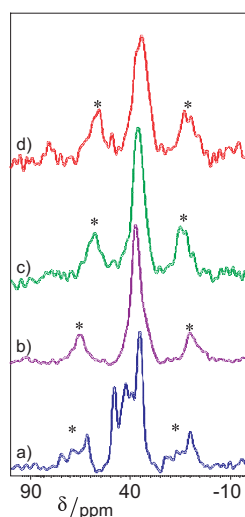
Figure 4.17: ^{17}O DOR NMR spectra of pure ^{17}O enriched Na-LSX (**a**), Na-LSX loaded with pyrrole (**b**), Na-LSX loaded with formic acid (**c**) and Na-LSX loaded with acetic acid (**d**). All samples were also immersed in octane to avoid hydration during the filling of the rotor. The spectra were measured in a magnetic field of $B_0 = 17.6$ T and at a spinning frequency of 1.2 to 1.4 kHz.

14 (Al-O-P) [2], in zeolites LSX [3] (Si-O-Al), see also Fig. 4.16, and in the layer silicate ilerit [2] (Si-O-Si) we obtain the relation

$$C_{\text{qcc}}(\text{P} - \text{O} - \text{P}) > C_{\text{qcc}}(\text{Al} - \text{O} - \text{P}) > C_{\text{qcc}}(\text{Si} - \text{O} - \text{Si}) > C_{\text{qcc}}(\text{Si} - \text{O} - \text{Al}) .$$

A similar connection can be found for the isotropic chemical shift of the ^{17}O NMR:

$$\delta_{\text{qcc}}(\text{P} - \text{O} - \text{P}) > \delta_{\text{qcc}}(\text{Al} - \text{O} - \text{P}) > \delta_{\text{qcc}}(\text{Si} - \text{O} - \text{Si}) > \delta_{\text{qcc}}(\text{Si} - \text{O} - \text{Al}) .$$

New experimental results claim that the ^{17}O-signals of the oxygen framework are shifted and also moved together due to adsorption of acid molecules, see Fig 4.17.

[1] A. Samoson, E. Lippmaa: J. Magn. Reson. **84**, 410 (1989)
[2] D. Prochnow: PhD thesis, Universität Leipzig, 2003
[3] D. Freude et al.: Solid. State. Nucl. Magn. Reson. **20**, 46 (2001)

4.16   Long-Time Scale Molecular Dynamics of Constrained Fluids Studied by NMR

F. Grinberg

Recent years have witnessed an expanding production of new materials with complex structures and tailored properties. A complex functionality of new materials is often achieved due to specific molecular ordering on the meso- and macroscopic length scales. Structure ordering is in turn accompanied by multiple molecular (individual or collective) dynamical processes tending to range over many time decades. The challenging problems of modern NMR methods are concerned with addressing hierarchic structures, multi-scale molecular dynamics and interfacial phenomena. This work demonstrates the experimental results of studying the effects produced by nano- to micrometer scale constraints on dynamical and structural properties of complex fluids using a combination of several NMR techniques: stimulated echo studies [1], temperature and frequency dependent measurements of the relaxation rates [2, 3] and diffusion studies with the help of Pulsed Field Gradient NMR [4].

All experimental data including transverse and longitudinal relaxation and diffusion demonstrate dramatic influence of cavity constraints on molecular collective and non-collective dynamical properties of confined liquids. This in particular refers to liquid crystals both above and below the bulk isotropization temperature. A strong pore size effect is reported for confined cyanobiphenyls (5CB).

For the interpretation, Monte Carlo computer simulations [2, 3] were carried out. A reduced dipolar correlation function, $G_0^{red}(t)$, was evaluated for a random walker diffusing in a closed spherical or cylindrical cavity with ordering and or adsorbing surface properties. Figure 4.18a shows typical results for a walker diffusing in a spherical cavity with ordered surface layer of thickness δr. The correlation function is characterized by fast and slowly decaying parts. Fast attenuation is due to dipolar correlation losses as the molecule diffuses from the ordered layer to the isotropic "bulk". The slowly decaying part is due to repeated returns of molecules to the ordered surface layer where the correlation to the initial orientation can partially be restored (the so-called process
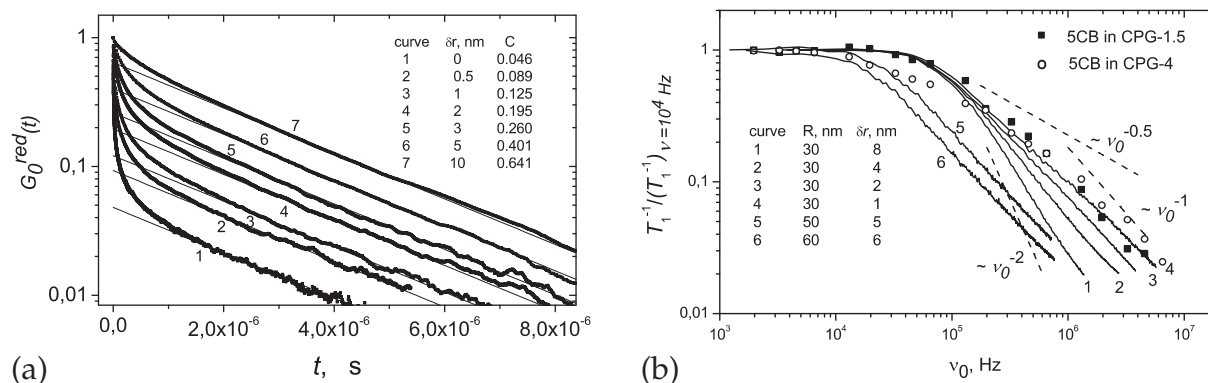
Figure 4.18: (**a**) Monte Carlo simulations of the reduced dipolar correlation function. The values of the thickness of the surface-ordered layer, δr, are indicated in the plot. The *solid lines* are fits of the function $C \times exp(-t/\tau_c)$ to the long tails of the simulated functions. (**b**) Normalised frequency dependencies of the spin-lattice relaxation rates, *curves* 1-6, evaluated from the simulated correlation functions. The curve parameter refers to different values of δr and R. The experimental data points refer to 5CB in CPG-1.5 and CPG-4 at 323 K.

of Reorientations Mediated by Translational Diffusion, see [2] and references therein). The correlation time of this process was examined as a function of δr, pore radius R and surface adsorbing strength. Simulated correlation functions were used for evaluating the frequency dependences of the spin-lattice relaxation rates, Fig. 4.18b, which were discussed in comparison to the experimental data.

[1] F. Grinberg et al.: In "NMR of Ordered Liquids", ed. by E.E. Burnell, C.A. de Lange (Kluver Academic, Dordrecht 2003)
[2] E. Anoardo et al.: Chem. Phys. **297**, 99 (2004)
[3] F. Grinberg: Magn. Reson. Imag. **25** (2007), in press
[4] J. Kärger: Diff. Fundam. **1**, 5.1 (2005)

4.17   NMR Velocimetry for Liquids under High Flow Rates

P. Galvosas, P.T. Callaghan[*]

[*]MacDiarmid Institute for Advanced Materials and Nanotechnology,
Victoria University of Wellington, New Zealand

NMR velocimetry has proven of considerable use as a tool for fluid mechanics investigations. Both the Lagrangian and Eulerian perspectives are available, using pure pulsed gradient spin echo encoding in the former case, and velocity imaging in the second. Ideally, velocity imaging allows one to determine the spatially dependent flow field $\vec{u}(\vec{r}, t)$ of the fluid under study which simplifies to $\vec{u}(\vec{r})$ in case of a stationary flow where the velocity is time independent. In practice, the resolution of velocity imaging may be limited, either by signal-to-noise or gradient strength availability in the case
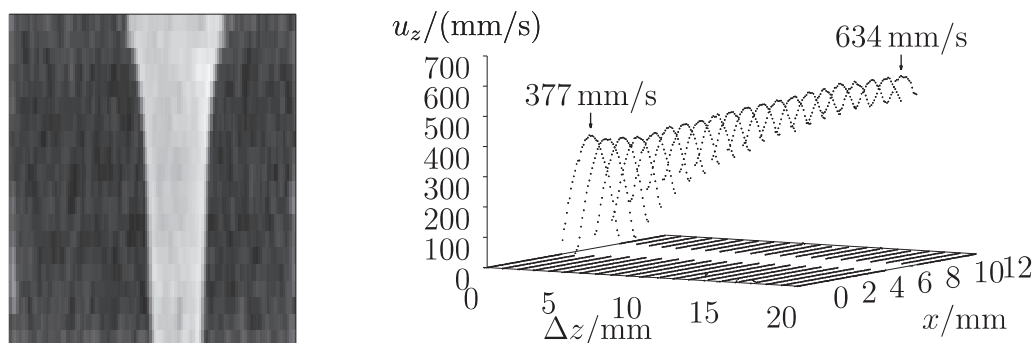
Figure 4.19: The NMR density image of a free liquid jet obtained from a slice in the centre of the jet with the nozzle at the upper border of the image (*left*) and its corresponding velocity field in dependency of x and the distance from the nozzle Δz (*right*).

of spatial coordinates, or by the finite time needed for position encoding in the case of temporal information. It is the latter limitation which is addressed in respect of NMR velocimetry in rapidly flowing liquids [1].

The goal of our investigation is to study a free liquid jet (see Fig. 4.19). The knowledge of its flow field and the changes to that flow introduced by added surfactants permits a study of a phenomenon known as the "Marangoni effect" [2]. The technique demonstrated here is aimed at a study of this effect via the changes of the properties of the liquid jet and, in particular, its dependency on the type of surfactant and its concentration.

We developed two approaches to imaging rapid flow. Both are based on a PGSE pulse sequence used to phase encode for the velocity. The first pulse sequence employs the RARE sequence in which a prior PGSE segment is used for the velocity encoding. This allows to measure two dimensional velocity profiles with velocities of up to 50 mm/s. A second pulse sequence was used, in fact able to acquire profiles across a free liquid jet. In Fig. 4.19 an example is given for a jet with a mean velocity of 192 mm/s and a peak velocity of 634 mm/s (see [1] for details). Both of the sequences proof to be useful for the investigation of flow fields in the corresponding ranges of velocity.

[1] P. Galvosas, P.T. Callaghan: J. Magn. Reson. **181**, 119 (2006), doi:10.1016/j.jmr.2006.03.020.
[2] C. Marangoni: Ann. Phys. Chem. **143**, 337 (1871)

4.18 Improvements in PFG NMR Probe Design

St. Schlayer, M. Gratz, F. Stallmach, P. Galvosas, J. Kärger

Pulsed field gradient (PFG) NMR diffusion studies in nanostructured materials are the key competence of our research group [1]. A continuous improvement and a high-quality maintenance of the necessary NMR spectrometer components are the basis for our successful involvements in many national and international research projects.

The generation of ultra-high intensity pulsed field gradients with the probes for the FEGRIS NMR spectrometers [2] requires to control the shape of short current pulses of

shielding coil

gradient coil
rf coil
sample

mechanical
coil support

current lead
dewar

gaskets

(a)   (b)   (c)
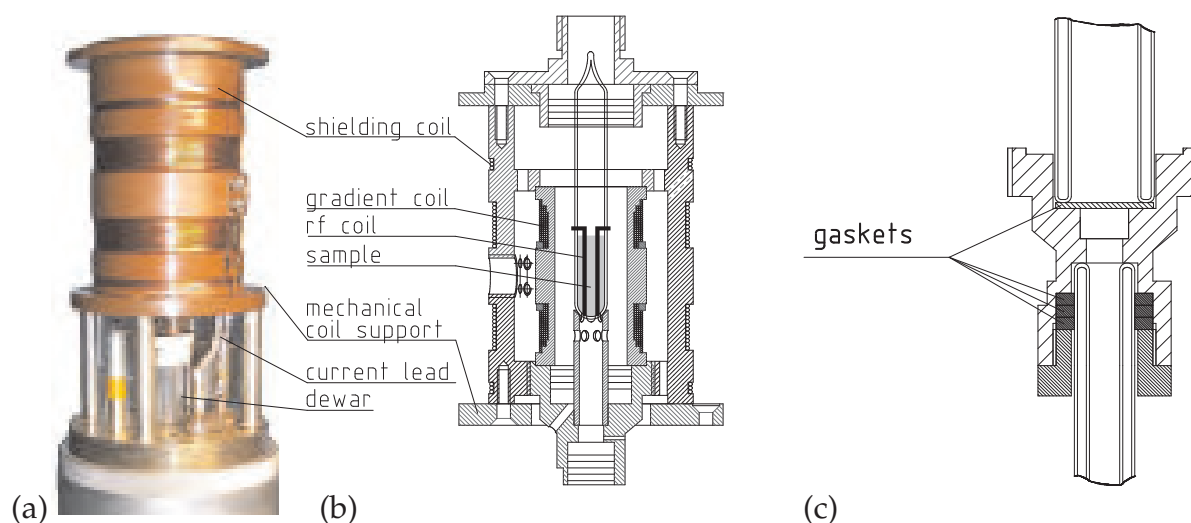
Figure 4.20: Top part of the PFG NMR probe for generation of ultra-high intensity pulsed field gradients [1, 2]. On the photograph (**a**), the shielding coil as well as the two solid copper leads to the gradient coil system are visible. The drawings represent the cross section through the gradient and shielding coils (**b**) and the new dewar sealing (**c**).

up to 100 A amplitude (Fig. 4.20). While flowing through the gradient coil, these current pulses generate high mechanical stress due to the Lorentz forces acting at the current leads and coil winding. This led to frequent malfunctions (break) of the originally used commercial feed-through capacitors for the current leads. They were replaced by solid (3 mm diameter) copper leads embedded in VESPEL insulators (see Fig. 4.20a). The necessary rf screen is achieved by 10 nF capacitors connected to the metal housing of the probe.

Additionally, a new sealing concept was developed, which improves the thermal insulation between the gradient coil and the NMR sample. This new seal consists of small teflon gaskets inserted between the glass dewar for controlling the NMR sample temperature and the mechanical rf and gradient coil supports (see Fig. 4.20c). It allows multiple use of the support materials and a much easier exchange of broken parts of the glass dewar. The PFG NMR probes may now be operated in a temperature range between 113 K and 523 K.

[1] F. Stallmach, P. Galvosas: In *Ann. Rep. NMR Spectrosc.*, Vol. 61 (Elsevier, London 2007) p 51
[2] P. Galvosas et al.: J. Magn. Reson. **151**, 260 (2001), doi:10.1006/jmre.2001.2381.

4.19   Funding

Combined NMR Studies of Diffusion and Reaction
Prof. Dr. D. Freude
im DFG-Projekt GRK 1056/1, International Research Training Group "Diffusion in Porous Materials"

Anwendungen der Doppelrotations- und Multiquanten-Messtechnik für Hochfeld-NMR-Untersuchungen an O-17-Kernen in porösen Festkörpern
Prof. Dr. D. Freude, Dr. H. Ernst
DFG-Projekt FR 902/16-2

Untersuchung der Protonen-Beweglichkeit in H-Zeolithen mit SFG NMR und MAS NMR im Temperaturbereich bis 800 K
Prof. Dr. D. Freude, Dr. H. Ernst
DFG-Projekt FR 902/12-2

Computersimulation und analytische Untersuchungen zum Einfluss der Kristallgrenze auf den Austausch von Gastmolekülen zwischen Zeolith-Nanokristallen und der Umgebung
Dr. S. Fritzsche, Prof. Dr. S. Vasenkov
DFG-Projekt FR 1486/2-1, SPP 1155 "Molekulare Modellierung und Simulation in der Verfahrenstechnik"

Reaktion und Diffusion in Single-File Netzwerken: Computersimulationen und statistisch-thermodynamische Untersuchungen
Prof. Dr. J. Kärger
DFG-Projekt KA 953/15-2

Studying Zeolitic Diffusion by Interference and IR Microscopy
Prof. Dr. J. Kärger
DFG-Projekt KA 953/18-2, International Research Group "Diffusion in Zeolites"

Bestimmung mikroskopischer Kenngrößen der Molekültranslation in Schüttungen nanoporöser Partikel mittels PFG NMR und Monte-Carlo-Simulation
Prof. Dr. J. Kärger
DFG-Projekt KA 953/19-1

Confinement Effects on Diffusion and Reaction in Zeolites, Studied by Dynamic MC Simulations, PFG NMR and Interference/IR Microscopy
Prof. Dr. J. Kärger
im DFG-Projekt GRK 1056/1, International Research Training Group "Diffusion in Porous Materials"

In situ study and development of processes involving nanoporous solids
Prof. Dr. J. Kärger
EU-Projekt NMP3-CT-2004-500895

Molecular diffusion in nanoporous materials
Prof. Dr. J. Kärger, Prof. Dr. H. Jobic
DFG-CNRS-Projekt KA 953/14-2

PFG NMR investigations on formulated catalysts; Bestimmung von Diffusionskoeffizienten an Katalysatoren
Prof. Dr. J. Kärger, Dr. F. Stallmach
BASF AG

Fourier-Transform-PFG-NMR mit starken Feldgradientenimpulsen zur selektiven Selbstdiffusionsmessung
Prof. Dr. J. Kärger, Dr. F. Stallmach
DFG-Projekt KA 953/16-1

Innovative Zugabestoffe für die Innere Nachbehandlung von Hochleistungsbeton unter Berücksichtigung der räumlichen und zeitlichen Wasserbilanz
Prof. Dr. J. Kärger, Dr. F. Stallmach
DFG-Projekt KA 953/22-1

Intelligent design of nanoporous sorbents
Prof. Dr. J. Kärger, Prof. Dr. S. Vasenkov
EU-Projekt CT-2004-005503

Fluid Transport in Porous Rocks and Sediments from Near-Surface Aquifers Studied by NMR and MRI
Dr. F. Stallmach
im DFG-Projekt GRK 1056/1, International Research Training Group "Diffusion in Porous Materials"

NMR and MRI studies of aquifer rocks; NMR- and MRI-Untersuchungen an Aquifergesteinen
Dr. F. Stallmach, Prof. Dr. J. Kärger
UFZ Halle/Leipzig GmbH

Messung intrakristalliner Diffusions-Reaktions-Profile in Zeolithen mittels IR-Imaging
Prof. Dr. J. Kärger
DFG-Projekt KA 953/21-1

Messung von Pasenübergangen in mesoskopisch beschränkten Systemen: kombinierter Einsatz von NMR und Molekulardynamik
Prof. Dr. J. Kärger, Dr. R. Valiullin
DFG-Projekt KA 953/20-1

Untersuchung der Diffusion in heterogenen Systemen mit PFG-MAS-NMR-Spektroskopie
Dr. A. Pampel, Prof. Dr. J. Kärger
DFG-Projekt PA 907/3-1

Mercator-Professur
Prof. Dr. D.B. Shah
Le 758/23-1

4.20 Organizational Duties

J. Kärger

- Ombudsman of Leipzig University
- Membership in the Programme Committee "Magnetic Resonance in Porous Media" (Bologna 2006), "Fundamentals of Adsorption" (Giardini Naxos, Sicily, Italy 2007), International Zeolite Conference (Peking 2007) and in the permanent DECHEMA committees Zeolites and Adsorption
- Membership in Editorial Boards: Micropor. Mesopor. Mat. (European Editor), Diff. Fundam. (Editor), Adsorption
- Referee: Phys. Rev., Phys. Rev. Lett., Europhys. Lett., J. Chem. Phys., J. Phys. Chem., Langmuir, Micropor. Mesopor. Mat., PCCP, J. Magn. Res.
- Project Reviewer: Deutsche Forschungsgemeinschaft, National Science Foundation (USA)

D. Freude

- Director of the Magnetic Resonance Centre (MRZ) of Leipzig University
- Membership in Editorial Boards: Solid State NMR; Diff. Fundam.
- Referee: Chem. Phys. Lett., J. Chem. Phys., J. Phys. Chem., J. Magn. Res., Solid State NMR

F. Grinberg

- Membership in "AMPERE Division of Spatially Resolved Magnetic Resonance" Polish German Radiospectroscopy Group (PGRG)
- Membership in Editorial Boards: Diff. Fundam. (Editor)

F. Stallmach

- Referee: Micropor. Mesopor. Mat., Angew. Chem., Membr. Sci., Am. Ceram. Soc.
- Project Reviewer: Deutsche Forschungsgemeinschaft

P. Galvosas

- Referee: Mag. Reson. Imag.
- Member of Faculty Board, Studienkommission and Prüfungskommission

R. Valiullin

- Membership in Scientific Advisory Committee "Bologna MRPM Conference (Ampere Event)"
- Referee: J. Phys. Chem. B, J. Membr. Sci., Micropor. Mesopor. Mat., Magn. Reson. Imag., Nature Photonics

4.21 External Cooperations

Academic

- Acad. Sci. Czech. Republ., Heyrovsky-Inst. Phys. Chem., Prague, Czech Republic
  Dr. Kocirik, Dr. Zikanova

- Delft University, Inst. Chem. Tech., The Netherlands
  Prof. Kapteijn

- Institut de Recherches sur la Catalyse, CNRS, Villeurbanne, France
  Dr. Jobic

- Institut Francais du Petrole, Malmaison, France
  Dr. Methivier

- Max Planck Institut für Kohlenforschung, Mülheim
  Dr. Schmidt, Prof. Schüth

- Max Planck Institut für Metallforschung, Stuttgart
  Dr. Majer

- Russian Acad. Sci., Boreskov Inst. Catalysis, Siberian Branch, Novosibirsk, Russia
  Dr. Stepanov

- TU München, Lehrstuhl Technische Chemie 2
  Prof. Lercher

- Università di Sassari, Dipartimento Chimica, Italy
  Prof. Demontis, Prof. Suffritti

- Universiät Eindhoven, Schuit Institute, The Netherlands
  Prof. van Santen

- Universität Erlangen Nürnberg, Dept. Chem. Engin.
  Prof. Emig, Prof. Schwieger

- Universität Hannover, Dept. Phys. Chem.
  Prof. Caro, Prof. Heitjans

- Universität Leipzig, Institut für Analytische Chemie
  Prof. Berger

- Universität Leipzig, Institut für Technische Chemie
  Prof. Einicke, Prof. Papp

- Universität Leipzig, Institut für Anorganische Chemie
  Prof. Krautscheid

- Universität Leipzig, Institut für Medizinische Physik und Biophysik
  Prof. Arnold, Prof. Gründer

- Universität Regensburg, Institut für Biophysik & Physikalische Biochemie
  Prof. Brunner

- Universität Stuttgart, Institut für Technische Chemie
  Prof. Hunger, Prof. Weitkamp

- University Athens, Dept Chem. Engn., Greece
  Prof. Theodorou

- University of Amterdam, The Netherlands
  Prof. Krishna

- University of Maine, Dept. Chem. Eng., Orono, USA
  Prof. Ruthven

- University College London, UK
  Prof. Brandani

- Westfälische Wilhelms-Universität Münster, Institut für Physikalische Chemie
  Dr. Schönhof

- Victoria University of Wellington, MacDiarmid Institute for Advanced Materials and
  Nanotechnology, New Zealand
  Prof. Callaghan

Industry

- Air Prod & Chem Inc., Allentown, USA
  Dr. Coe, Dr. Zielinski

- BASF, Ludwigshafen, Germany
  Dr. Müller, Dr. Nestle, Dr. Rittig

- Cepsa, Madrid, Spain
  Dr. Perez

- Grace, Worms, Germany
  Dr. McElhiney

- Resonance Instruments Ltd., Witney, UK
  J. McKendry

- SINTEF, Oslo, Norway
  Prof. Stöcker

- Tricat, Berlin, Germany
  Dr. Tufar, Dr. Lutz

4.22   Publications

Journals

P. Bräuer, A. Brzank, L.A. Clark, R.Q. Snurr, J. Kärger: *Guest-specific diffusion anisotropy in nanoporous materials: Molecular dynamics and dynamic Monte Carlo simulations*, Adsorption **12**, 417 (2006)

P. Bräuer, A. Brzank, J. Kärger: *Isotropic concentration profiles during diffusion-limited desorption from anisotropic media*, J. Colloid Interface Sci. **305**, 183 (2007)

P. Bräuer, A. Brzank, J. Kärger: *Two-component desorption from anisotropic pore networks*, J. Chem. Phys. **124**, 034 713 (2006)

A. Brzank, G.M. Schütz: *Amplification of molecular traffic control in catalytic grains with novel channel topology design*, J. Chem. Phys. **124**, 214 701 (2006)

J. Dietrich, W. Schönfelder, A. Märten, V. Klapperich, F. Stallmach: *Untersuchungen zum Schadstoffrückhaltevermögen von Einphasen-Dichtwandmassen*, Mitteilung des Instituts für Grundbau und Bodenmechanik Technische Universität Braunschweig **83**, 121 (2006)

K. Friedemann, F. Stallmach, J. Kärger: *NMR diffusion and relaxation studies during cement hydration - a non-destructive approach for clarification of the mechanism of internal post-curing of cementious materials*, Cem. Concr. Res. **36**, 817 (2006)

P. Galvosas, P.T. Callaghan: *Fast magnetic resonance imaging and velocimetry for liquids under high flow rates*, J. Magn. Reson. **181**, 119 (2006), doi:10.1016/j.jmr.2006.03.020

F. Grinberg: *Surface effects in liquid crystals constrained in nano-scaled pores investigated by Field-cycling NMR relaxometry and Monte Carlo simulations*, Magn. Reson. Imag. **25**, (2006), in press

F. Grinberg, G. Majer, S. Skripov: *Hydrogen diffusion in intermetallic Ta-V compounds*, J. Alloys Comp. **425**, 24 (2006)

J. Gulin-Gonzalez, A. Schüring, S. Fritzsche, J. Käger, S. Vasenkov: *The influence of the desorption barrier on the transport of molecules through the external surface of nanoporous crystals*, Chem. Phys. Lett. **430**, 60 (2006)

J. Jiao, J. Kanellopoulos, B. Behera, Y. Jiang, J. Huang, V.R.R. Marthala, S.S. Ray, W. Wang, M. Hunger: *Effects of Adsorbate Molecules on the Quadrupolar Interaction of Framework Aluminum Atoms in Dehydrated Zeolite H,Na-Y*, J. Phys. Chem. B **110**, 13 812 (2006)

H. Jobic, W. Schmidt, C.B. Krause, J. Kärger: *PFG NMR and QENS diffusion study of n-alkane homologues in MFI-type zeolites*, Micropor. Mesopor. Mater. **90**, 299 (2006)

J. Kanellopoulos, A. Unger, W. Schwieger, D. Freude: *Catalytic and multinuclear MAS NMR studies of a thermally treated zeolite ZSM-5*, J. Catal. **237**, 416 (2006)

J. Kärger, F. Grinberg: *A closer look at nanoporous materials*, Angew. Chem. Int. Ed. **45**, 3732 (2006)

J. Kärger, P. Kortunov, S. Vasenkov, L. Heinke, D.B. Shah, R.A. Rakoczy, Y. Traa, J. Weitkamp: *Unprecedented insight into diffusion by monitoring the concentration of guest molecules in nanoporous host materials*, Angew. Chem. Int. Ed. **45**, 7846 (2006)

J. Kärger, S. Vasenkov: *On the sticking probability of aromatic molecules on zeolites*, J. Phys. Chem. B **110**, 17 694 (2006)

P. Kortunov, L. Heinke, S. Vasenkov, C. Chmelik, D.B. Shah, J. Kärger, R.A. Rakoczy, Y. Traa, J. Weitkamp: *Internal concentration gradients of guest molecules in nanoporous host materials: Measurement and microscopic analysis*, J. Phys. Chem. B **110**, 23 821 (2006)

M.V. Luzgin, A.G. Stepanov, S.S. Arzumanov, V.A. Rogov, V.N. Parmon, W. Wang, M. Hunger, D. Freude: *Mechanism Studies of the Conversion of 13C-Labeled n-Butane on Zeolite H-ZSM-5 by Using 13C Magic Angle Spinning NMR Spectroscopy and GC-MS Analysis*, Chem. Eur. J. **12**, 457 (2006)

V. Meynen, P. Cool, E.F. Vansant, P. Kortunov, F. Grinberg, J. Kärger, M. Mertens, O.I. Lebedev, G. Van Tendelo: *Deposition of vanadium silicalite-1 nanoparticles on SBA-15 materials. Structural and transport characteristics of SBA-VS-15*, Micropor. Mesopor. Mat. **99**, 14 (2006)

A. Pampel, F. Engelke, P. Galvosas, C. Krause, F. Stallmach, D. Michel, J. Kärger: *Selective multi-component diffusion measurement in zeolites by pulsed field gradient NMR*, Micropor. Mesopor. Mat. **90**, 271 (2006)

D. Prochnow, A.-R. Grimmer, D. Freude: *Solid-state NMR studies of 17O-enriched pyrophosphates*, Solid. State. Nucl. Magn. Reson. **30**, 69 (2006)

F. Stallmach, S. Gröger, V. Künzel, J. Kärger, O.M. Yaghi, M. Hesse, U. Müller: *NMR studies on the diffusion of hydrocarbons on the metal-organic framework material MOF-5*, Angew. Chem. Int. Ed. **45**, 2123 (2006)

A.G. Stepanov, S.S. Arzumanov, H. Ernst, D. Freude: *1H MAS NMR monitoring of the 13C-labeled carbon scrambling for propane in zeolite H-ZSM-5*, Chem. Phys. Lett. **420**, 574 (2006)

R. Valiullin, M. Dvoyashkin, P. Kortunov, C. Krause, J. Kärger: *Diffusion of guest molecules in MCM-41 agglomerates*, J. Chem. Phys. **126**, 054705 (2007)

R. Valiullin, A. Khokhlov: *Orientational ordering of inear n-alkanes in silicon nanotubes*, Phys. Rev. E **73**, 051 605 (2006)

R. Valiullin, S. Naumov, P. Galvosas, J. Kärger, H.-J. Woo, F. Porcheron, P.A. Monson: *Exploration of molecular dynamics during transient sorption of fluids in mesoporous materials*, Nature **443**, 965 (2006)

Books

K. Friedemann, F. Stallmach, N. Nestle, J. Kärger: *Internal post-curing of hardening cement pastes of high-performance concretes studied by Low-field NMR relaxometry*, in *Proc. Int. RILEM Conf. Volume Changes of Hardening Concrete*, ed. by O.M. Jensen, P. Lura, K. Kovler (RILEM, 2006) p 147

K. Friedemann, F. Stallmach, N. Nestle, J. Ma, N.V. Tue, J. Kärger: *Hydratisierende Zemente mit innerer Nachbehandlung - Demonstration des Feuchteüberganges durch NMR Relaxations- und Diffusionsuntersuchungen*, in *Tagungsbericht 16. Int. Baustofftagung*, Band I, ed. by J. Stark (F.A. Finger-Institut für Baustoffkunde, Weimar 2006) p 367

Talks

T. Binder, F. Grinberg, J. Kärger: *Diffusion Fundamentals: Ein Buch über Leipzig, Einstein und die Physik*, Leipzig Book Fair, April 2006

J. Dietrich, W. Schönfelder: *Untersuchungen zum Schadstoffrückhaltevermögen von Einphasen-Dichtwandmassen*, Geotechn. Aspekte im Umweltschutz, Braunschweig, March 2006

M. Dvoyashkin, R. Valiullin, J. Kärger: *Temperature effects on phase equilibrium and diffusion in Vycor porous glass*, 4th Int. Research Training Group Workshop "Diffusion in Porous Materials", Leipzig, May 2006

M. Dvoyashkin, R. Valiullin, J. Kärger, W.-D. Einicke, R. Gläser: *Diffusion of supercritical fluids under confinements probed by PFG NMR method*, 5th Int. Research Training Group Workshop "Experimental and Theoretical Methods of Diffusion Studies in Nanostructured Materials", Frankfurt, October 2006

K. Friedemann: *Hydratisierende Zemente mit innerer Nachbehandlung - Demonstration des Feuchteüberganges durch NMR Relaxations- und Diffusionsuntersuchungen*, 16. Int. Baustofftagung, Weimar, September 2006

K. Friedemann: *Internal post-curing of hardening cement pastes of high-performance concretes studied by Low-field NMR relaxometry*, Int. RILEM Conf., Lyngby, Denmark, August 2006

P. Galvosas, Y. Qiao, M. Schönhoff, P.T. Callaghan: *On the Use of 2D Correlation and Exchange NMR Spectroscopy in Organic Porous Materials*, 8th Int. Conf. Magn. Res. Porous Media, Bologna, Italy, September 2006

F. Grinberg (invited): *What can NMR tell us about ordering, diffusion and re-orientational molecular dynamics in constrained fluids?*, IX. AMPERE NMR School, Poznan, Poland, June 2006

F. Grinberg *What Can NMR Tell Us About Ordering, Molecular Reorientations and Self-Diffusion of Fluids Constrained in Nano-Scaled Pores?*, 8th Int. Conf. Magn. Res. Porous Media, Bologna, Italy, September 2006

F. Grinberg (invited): *What Can NMR Tell Us about Structure and Molecular Dynamics of Fluids Constrained in Nano-Scaled Environments?*, Symp.: Horizons of NMR based research at the beginning of the 21st century, Ulm, October 2006

M. Krutyeva, J. Kärger, S. Vasenkov: *Influence of the surface of zeolite crystals on molecular transport: PFG NMR measurements and computer simulations*, 8th Int. Conf. Magn. Res. Porous Media, Bologna, Italy, September 2006

S. Naumov, R. Valiullin, P. Galvosas, J. Kärger, P.A. Monson (invited): *Diffusion hysteresis in mesoporous materials*, 3rd Int. Workshop on Dynamics in Confinement, Grenoble, France, March 2006

W. Schönfelder: *NMR- und SIP- Untersuchungen zur Charakterisierung von Aquifergesteinen*, 66. Jahrestagung Dt. Geophys. Ges., Bremen, March 2006

W. Schönfelder: *Studying diffusive water transport in bentonite cement mixtures of very low hydraulic conductivity* (Selected Poster Talk), 8th Int. Conf. Magn. Res. Porous Media, Bologna, Italy, September 2006

F. Stallmach: *NMR-Diffusometry von Gastmolekülen in nanoporösen Materialien*, Anorganisch-Analytisches Kolloquium, Ruhr-Universität Bochum, October 2006

F. Stallmach: *Probing pore structures and adsorbate-adsorbent interactions by NMR relaxometry and diffusometry*, Workshop des Graduiertenkollegs "Moderne Methoden der Magnetischen Resonanz", Universität Stuttgart, Blaubeuren, September 2006

F. Stallmach: *Probing pore structures and adsorbate-adsorbent interaction by NMR self-diffusion studies*, Annual Meeting French Zeolite Assoc. (GFZ Meeting), La Rochelle, March 2006

F. Stallmach: *Zerstörungsfreie Charakterisierung mineralischer Baustoffe mittels 1H-NMR des Porenwassers*, BASF Construction Chemicals GmbH, Trostberg, July 2006

R. Valiullin (invited): *New perspectives on anomalous dynamics during sorption hysteresis*, 373th Wilhelm und Else Heraeus Seminar "Anomalous Transport: Experimental Results and Theoretical Challenges", Bad Honnef, July 2006

R. Valiullin (invited): *Phase transitions and transport in nanoporous materials*, 4th Int. Research Training Group Workshop "Experimental and Theoretical Methods of Diffusion Studies", Leipzig, May 2006

R. Valiullin: *Dynamical aspects of the adsorption hysteresis phenomenon*, 8th Int. Conf. Magn. Res. Porous Media, Bologna, Italy, September 2006

R. Valiullin, S. Naumov, P. Galvosas, J. Kärger, H-J. Woo, F. Porcheron, P.A. Monson: *Experimental and theoretical studies of the relaxation processes associated with adsorption/desorption hysteresis in mesoporous materials*, 6th Int. Symp. Effects of Surface Heterogeneity in Adsorption and Catalysis on Solids, Zakopane, Poland, August 2006

Posters

M. Dvoyashkin, S. Naumov, R. Valiullin, J. Kärger: *Surface diffusion in nanoporous materials. Experimental study using pulsed field gradient NMR method*, 373th Wilhelm und Else Heraeus Seminar "Anomalous Transport: Experimental Results and Theoretical Challenges", Bad Honnef, July 2006

M. Dvoyashkin, R. Valiullin, J. Kärger, W.-D. Einicke, R. Gläser: *Transport properties of supercritical fluids in mesoporous materials probed by PFG NMR*, 8th Int. Conf. Magn. Res. Porous Media, Bologna, Italy, September 2006

K. Friedemann, W. Schönfelder, N. Nestle, F. Stallmach, J. Kärger: *Internal Post Curing of Hardening Cement Pastes of High Performance Concretes by a Water-containing Polyelectrolyte Gel*, 8th Int. Conf. Magn. Res. Porous Media, Bologna, Italy, September 2006

F. Grinberg: *Ultraslow Molecular Dynamics of Constrained Fluids Studied by NMR and MRI*, 5th Biotechnology Symp., Leipzig, May 2006

A. Khokhlov, R. Valiullin, J. Kärger: *Dynamics of linear n-alkanes in mesoporous silicon*, 1st Int. Workshop on IN-SItu Study and DEvelopment of Processes Involving PORous Solids, La Grande Motte, France, March 2006

A. Khokhlov, R. Valiullin, J. Kärger: *Freezing transition in linear mesopores of different shape*, 8th Int. Conf. Magn. Res. Porous Media, Bologna, Italy, September 2006

M. Krutyeva, J. Kärger, S. Vasenkov: *Exploring the influence of the surface of nanoporous materials on molecular transport: PFG NMR measurements and computer simulations*, IX AMPERE NMR School, Poznan, Poland, June 2006

S. Naumov, R. Valiullin, J. Kärger, P.A. Monson: *History-Dependent Adsorption and Diffusion in Nanoporous Materials*, 8th Int. Conf. Magn. Res. Porous Media, Bologna, Italy, September 2006

R. Valiullin, A. Khokhlov, J. Kärger: *Dynamics of linear n-alkanes in mesoporous silicon*, 8th Int. Conf. Magn. Res. Porous Media, Bologna, Italy, September 2006

4.23 Graduations

Doctorate

- Johanna Kanellopoulos
  NMR-Untersuchungen zur Protonenbeweglichkeit in dehydratisierten H-Zeolithen und zu verschiedenen Multiquanten-Verfahren für Quadrupolkerne mit dem Spin 5/2
  January 2006

- Andreas Brzank
  Molecular traffic control and two-species single-file diffusion
  October 2006

Diploma

- Lars Heinke
  Analytische Betrachtungen und IR-Experimente zum Sorptionsverhalten nanoporöser Materialien
  August 2006

- Markus Wehring
  Untersuchung der Mehrkomponentendiffusion in nanoporösen Materialien mittels PFG NMR
  July 2006

4.24 Guests

- D.B. Shah
  Cleveland State University, Ohio, USA
  until August 2006

- Alexander Stepanov
  Boreskov Institute of Catalysis, Novosibirsk, Russia
  January – April

4.25   Awards

- Dr. Rustem Valiullin
  Cesare-Borgia Prize
  at the 8th Conference on Magnetic Resonance in Porous Media

- Dr. Pavel Kortunov
  George-Kokotailo Prize
  from the German Zeolite Association

- Muslim Dvoyashkin
  2006 Participation Award
  at the 18th Meeting of Nobel Prize Winners in Chemistry

II

Institute for Experimental Physics II

5
Nuclear Solid State Physics

5.1 Introduction

Modern nuclear analysis methods, like the spatially resolved ion beam analysis as well as nuclear probes helps to solve current problems on special fields in material science and biomedical researches.

The working horse in the nuclear solid state physics division is the accelerator laboratory with the high energy ion nanoprobe LIPSION. The prevailing researches focus on quantitative trace element analysis in neuroscience, investigations of effects of single cell bombardment, elemental analysis of micro- and nanostructures and ion beam modification.

In addition, time differential perturbed angular correlation (TDPAC) is used to determine the nuclear quadrupole interaction in material of interest, e.g. TiO_2 bulk material and nanoparticles. These investigations are carried out with emphasis on biomedical and material science at the TDPAC-laboratory and at the isotope separator ISOLDE at CERN, Geneva.

Tilman Butz

5.2 The High-Energy Ion Nanoprobe LIPSION

T. Butz, D. Lehmann, A. Fiedler, M. Hohlweg, S. Jankuhn, C. Meinecke, F. Menzel, C. Nilsson, S. Petriconi, T. Reinert, M. Rothermel, D. Spemann, J. Vogt, S. Werner

The high-energy ion nanoprobe LIPSION at the University of Leipzig has been operational since October 1998. Its magnetic quadrupole lens system, arranged as a separated Russian quadruplet, has a symmetrical demagnification factor of about 130. The single-ended 3 MV SINGLETRON™ accelerator (High Voltage Engineering Europe B.V.) supplies H^+ and He^+ ion beams with a beam brightness of approximately $20\,A\,rad^{-2}m^{-2}eV^{-1}$. Due to this high brightness, the excellent optical properties of the focusing system of the nanoprobe and the suppression of mechanical vibrations by founding the bed-plates of accelerator and probe in greater depths separately from the surroundings, lateral resolutions below 100 nm for the low current mode (STIM) and 300 nm at a current of 50 pA (PIXE) were achieved routinely. The UHV experimental chamber is equipped with X-ray, and particle detectors to detect simultaneously the

characteristic X-rays (Particle Induced X-ray Emission, PIXE), as well as the backscattered ions (Rutherford Backscattering Spectrometry, RBS) and – in case of thin samples – the transmitted ions (Scanning Transmission Ion Microscopy, STIM, and Scanning Transmission Ion Micro-Tomography, STIM-T). A optical microscope allows sample positioning and inspection during measurement. The magnetic scanning system moves the focused beam across the sample within a scan field of adjustable extent. The data collection system MPSYS (MARC Melbourne) collects and stores the spectra of the several techniques at any beam position (Total Quantitative Analysis, TQA). In addition, optional windows can be set in the spectra for real-time elemental mapping. The pictures are viewed and printed as two-dimensional colour-coded intensity distributions.

The installation of an irradiation platform designed for single ion bombardment of living cells allows first patterned irradiations and hit verification tests.

Current work in nuclear nanoprobe performance is focused on:

1. Installation of the new target chamber with translation stages and goniometer inside the UHV-chamber.

2. Installation of the new irradiation platform for the single ion bombardment of living cells.

Accelerator Statistics 2006:

- operating hours: 2250 h
- maintenance and conditioning: 130 h

5.3 Proton Beam Writing

F. Menzel, D. Spemann, T. Reinert, J. Krüger*, M. Uhlmann*, J. Lenzner, T. Butz

*Wilhelm-Ostwald-Gymnasium, Leipzig

Within the continuous development of the technique of proton beam writing (PBW) at the LIPSION nanoprobe the minimal feature size of written structures was reduced to 130 nm with an aspect ratio of 75 (Fig. 5.1) [1]. For this purpose, 10 μm thick SU-8 was irradiated with 2.25 MeV protons under STIM conditions (~ 1 fA). First tests for the creation of buried structures in positive PMMA resist by one irradiation step utilizing the Bragg peak were successful. Furthermore, structures for applications in biomedical research were created, e.g. structures for the directed growing of neurons and Au contact structures on Si_3N_4 windows for so called intelligent Petri dishes by using resist templates [1]. In addition, the quality of Ni grids produced by electroplating could be clearly improved by using the easily removable negative resist ma-N 440 for the corresponding templates instead of the positive one PMMA (Fig. 5.2) [1, 2].

Microdimensional structures were created in Si [1], GaAs, and, for the first time, in InP by direct proton or helium ion irradiation and subsequent electrochemical etching of the semiconductor samples. The irradiation leads to a change in the electrical conductivity and therefore in an increased or reduced current during the etching step. This results in an amplified or an alleviated material removal in the irradiated region,
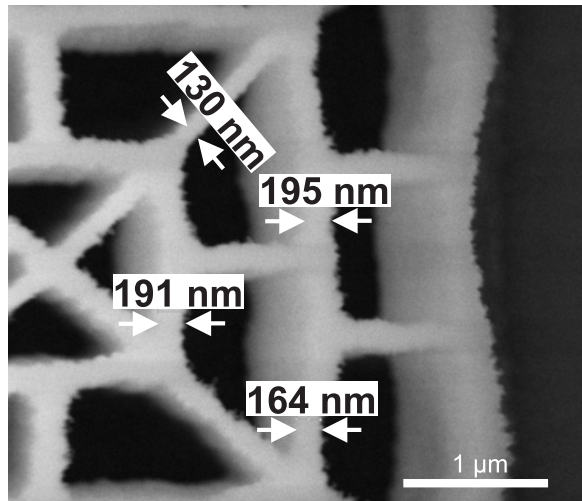
Figure 5.1: Structure written in $10\,\mu m$ thick SU-8 resist. The small walls with a thickness of down to 130 nm were produced with a low current beam of 2.25 MeV protons.
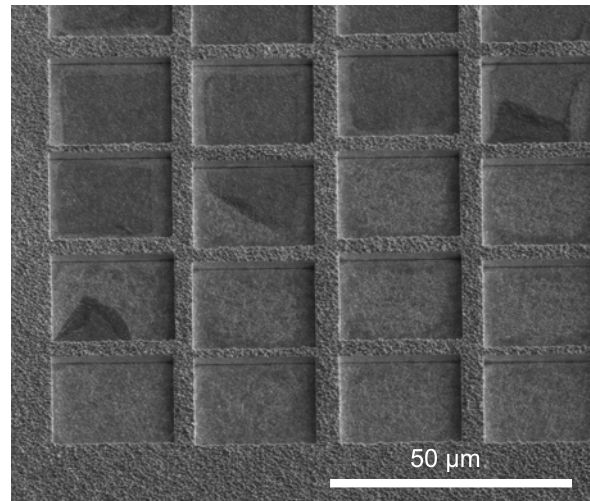
Figure 5.2: REM image of a Ni grid grown on a Si substrate by electroplating. The template for this structure, written in the negative resist ma-N 440, was removed after the plating step.
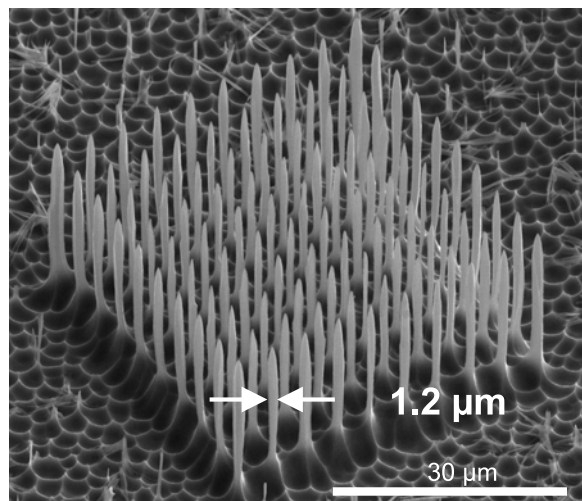
Figure 5.3: REM image of an array of Si pillars created by spot irradiation with 2.25 MeV protons with a dose of $12\,pC$/spot and subsequent electrochemical etching in an HF-solution. The pillar diameter depends on the dose applied and is $1.2\,\mu m$ in this case.
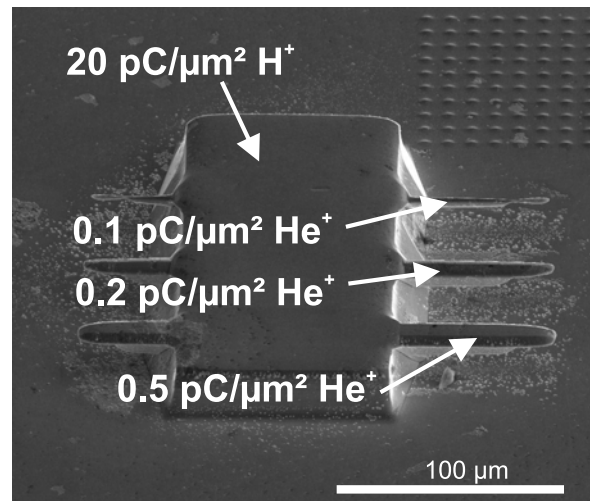
Figure 5.4: REM image of an GaAs structure consisting of a supporting block written with 2.25 MeV protons and 3 selfsupported plates written with 2.00 MeV helium ions after the electrochemical etching in a KOH-solution. Different irradiation doses (marked in the image) lead to different dimensions of these plates.

respectively. In this way, it was possible, e.g., to produce pillars with minimal diameters of $1.2\,\mu m$ (Fig. 5.3) and slanted pillars in Si as well as selfsupported plates in Si, GaAs (Fig. 5.4), and InP by underetching.

[1] F. Menzel et al.: *Proton beam writing of submicrometer structures at LIPSION.* Nucl. Instr. Meth. B, in print, doi:10.1016/j.nimb.2007.02.056

[2] F. Menzel et al.: Nucl. Instr. Meth. B **250**, 66 (2006)

5.4   The New Irradiation Platform at LIPSION

C. Nilsson, T. Reinert, S. Petriconi, T. Butz

The aim of the EU financed project CELLION is to gain information on the behaviour and reactions of living cells when exposed to single ion irradiation. To improve the experimental conditions at the LIPSION nanoprobe, a new experimental setup is being constructed. The new setup is composed of a new target chamber with a new translation stage and goniometer, along with a new irradiation platform for targeted single ion irradiation of living cells. Resent improvements and developments include programming of a user interface for the translation stage as well as construction of further needed parts, e.g. a replacement lid for the chamber for irradiation safety purposes and also preparations for the purchase of another microscope.

5.5   Ion Beam Analysis of Micro- and Nanostructures

C. Meinecke, J. Bauer[*], R. Kaden[†], J. Vogt, T. Butz

[*]Semiconductor Physics Division, Leipzig University
[†]Institute for Mineralogy, Crystallography and Material Research

In the framework of the research group "Architecture of nano- and microdimensional building blocks" (FOR 522) we investigated different micro- and nanostructures (wires).

The stoichiometry of cylindrite-microstructures was analysed to gain more information about the production of synthetic cylindrite. Different microstructures like thin plates [1] and cylinders with different cross-sections (round, squared) with a size of some µm revealed no significant differences in the stoichiometry within the error limits of the 3 cylindrite microstructures (see Tab. 5.1). Investigations on natural and synthetic cylindrite show that an increase of the (Fe+Pb)/(Sb+Sn) factor results in a decrease of the optical absorption edge [2]. However, the ratio (Fe+Pb)/(Sb+Sn) of these three microstructures when compared to the results of larger synthetic cylindrite samples (lateral size of some mm and thickness of more than 10 µm) [3], which were produced

Table 5.1: Stoichiometry of the cylindrite microstructures of different cross-section and bulk material.

	Fe	Sn	Pb	Sb	S	(Fe+Pb)/(Sn+Sb)
Cylindrite (round)	1.0	5.1	3.7	2.0	15.9	0.66
Cylindrite (squared)	1.0	5.0	3.7	2.0	16.0	0.67
Cylindrite (thin plate)	1.0	6.4	4.7	2.0	16.9	0.68
Cylindrite (bulk)	1.0	6.1	4.2	2.5	17.4	0.60

in the same way, exhibits a huge difference. For the cylindrite microstructures the (Fe+Pb)/(Sb+Sn) value is 0.66 to 0.68 (see Tab. 5.1). For the large cylindrite plates this value is less than 0.60 so that this factor seems to play a role in the structural formation of microstructures. The relationship between microstructure size, composition and band gap is currently under investigation.

Using these techniques we also investigated the stoichiometry of micro-dimensional, axial, hetero-structures consisting of gallium arsenide and aluminum arsenide in order to gain more information about the growing procedure. Therefore microwires produced by different growth procedures were investigated using μPIXE. We showed that the different metal-organic vapor phase epitaxy (MOVPE) growth procedures (abrupt and gradual GaAs to AlAs transition) do not lead to significant differences in the elemental distribution along the wire axis [4]. From the RBS- and PIXE-measurements of the GaAs/AlAs longitudinal hetero-structures we obtained the laterally resolved stoichiometry along the symmetry axis, which show that the designed elemental profile was not achieved, i.e. there were no microwires with a sharp GaAs–AlAs interface. We showed that there is an interdiffusion of the elemental components during the production process. The assumed oxidation of the AlAs could not be verified in this work due to the fixation of the microwires on conductive carbon.

[1] C. Meinecke et al.: Nucl. Instr. Meth. B (2007), in press, doi:10.1016/j.nimb.2007.02.040
[2] R. Kaden et al.: J. Mater. Chem. Phys., submitted
[3] F. Menzel et al.: Nucl. Instr. Meth. B **249**, 478 (2006)
[4] C. Meinecke et al.: Nucl. Instr. Meth. B (2007), in press, doi:10.1016/j.nimb.2007.02.039

5.6 Ion Beam Analysis of ZnO:(Mg, P, Al, Mn, Co, Cu and Nd) Thin Films Grown on c-Plane Sapphire

C. Meinecke, L. Hartmann[*], Q. Xu[*], J. Vogt, T. Butz

[*]Semiconductor Physics Division, Leipzig University

ZnO thin films, nominally undoped, alloyed with Mg, P, Al, Mn, Co, Cu and Nd grown epitaxially on c-plane sapphire by pulsed laser deposition (PLD) were investigated. In order to correlate the optical and electrical properties, e. g. the band gap energy and carrier concentration, as well as magnetotransport properties to the elemental composition, the films were analysed by Rutherford Backscattering Spectrometry (RBS) and Particle Induced X-ray Emission (PIXE) using He^+ and H^+ ion beams.

It was found that the element transfer from the PLD target to the film differs significantly for the individual doping and alloying elements, with concentration ratios between film and target ranging from less then 5 % for Al and Cu, over $10-20$ % for Nd and Mn, to $300-400$ % for Mg. In general, the films exhibited a metal to oxygen ratio of 1:1 (More details can be found in the reports of the Semiconductor Physics division).

5.7 Ion Beam Induced Ferromagnetism in Carbon Based Systems with Reduced Thermal Stress

M. Rothermel, J.L. Barzola-Quiquia[*], P. Esquinazi[*], T. Butz

[*]Division for Superconductivity and Magnetism, Leipzig University

To examine the effect of temperature on ion beam induced ferromagnetism in carbon based systems a new cooling device for the Leipzig ion-nanoprobe has been developed. Thus it was possible to irradiate highly oriented pyrolytic graphite (HOPG) with the 2.25 MeV proton-microbeam at room temperature (~ 300 K) and low temperature (~ 150 K). The samples were scrutinized concerning their magnetic properties using
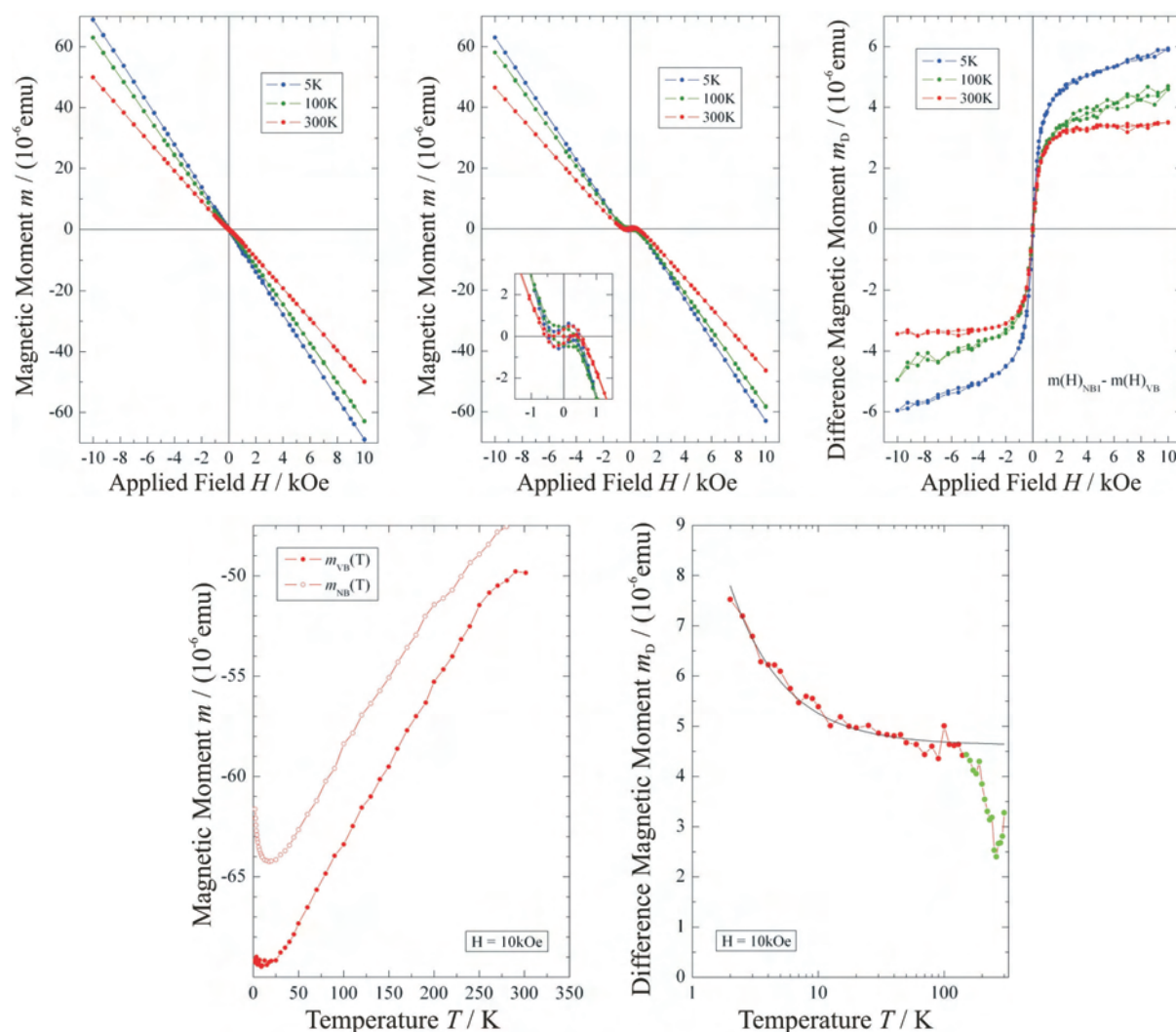
Figure 5.5: Ferromagnetic behavior of the cooled sample (hysteresis and temperature dependence). Initial diamagnetic signal of a HOPG sample (*top left*). Signal of the same sample after irradiation (*top middle*). Difference of the magnetic signal of the initial and irradiated sample (*top right*). Bottom: Absolute $m(T)$ measurements (*bottom left*). Difference of the initial and irradiated sample (*bottom right*), the *line* indicates the Curie-like paramagnetic part.

Table 5.2: Magnetic moments at saturation. The given change in susceptibility $\Delta\chi_m$ is the mass-susceptibility times sample mass.

	m_S (10^{-6} emu)			$\Delta\chi_m$ (10^{-10} emu/Oe)		
	at 5 K	100 K	300 K	at 5 K	100 K	300 K
room temperature	0.63	0.56	0.43	1.85	1.1	1.0
low temperature	4.55	3.34	3.26	1.4	1.2	0.2

a superconducting quantum interference device (SQUID). Taking the difference of the magnetic characterizations before and after each irradiation (see Fig. 5.5) the effect of the irradiation was obtained. The results show that cooling of the sample during irradiation leads to a saturation magnetization four times larger then for irradiation at room temperature (see Tab. 5.2). The paramagnetic moment, however, has been reduced.

By irradiating Kapton samples at beam currents of 840 pA and 15.7 nA large paramagnetic moments were induced. In the process of the second irradiation the material had locally transformed to a graphitic phase. Further investigations on thermally treated Kapton samples exhibited similar behavior. Because the concentration analysis by particle induced X-ray emission (PIXE) was performed simultaneously with the irradiation – with special regards on ferromagnetic impurities – we can conclude that we are dealing to be about with intrinsic properties of these materials.

5.8 Elemental Characterisation of Mn-, Mg- and Co-doped ZnO Nanostructures

C. Meinecke, A. Rahm*, J. Vogt, T. Butz

*Semiconductor Physics Division, Leipzig University

ZnO based nanostructures have attracted increasing interest in recent years due to their structural diversity. Furthermore, transition metal doping (e.g. by Co or Mn) of ZnO films has been shown to create a promising ferromagnetic material for spintronics.

We investigated the high-pressure pulsed laser deposition (PLD)growth of zinc oxide nanowires ($300 - 500$ nm in diameter) containing Co, Mg and Mn grown with NiO and Au catalysts.

Elemental analysis (PIXE, RBS) was carried out using a 2.25 MeV scanning proton beam with a spot size of approx. 500 nm. This high spatial resolution at beam currents of approx. 100 pA is necessary for the elemental analysis of single nanowires using RBS and PIXE.

Scanning electron microscopy, RBS and Particle induced X-ray emission measurements revealed differences between the compositions of nanowires compared to simultaneously grown films. For the Mg-doped ZnO, which was grown without a catalyst, we found a 3 times higher Mg content in the ZnO film compared to the nanowires. On the other hand, the analysis of the Mn-doped ZnO nanowires yielded the same Mn-concentration as the layer. The measurements of Mn-doped ZnO, which were grown using a NiO and gold catalyst, revealed that the ZnO-nanowire has a 3 times higher

Mn-content then the layer. The Co-doped ZnO-film possess a more then 2 times higher Co concentration then the ZnO-nanowire.

Finally, we can conclude that fabrication of doped ZnO-nanowires, using no catalyst, differs enormously from doped ZnO-films. Furthermore, the doping concentration of the ZnO-nanowires also depends on the doping material.

5.9 *In Situ* Quantitative Trace Element Analysis of Neuromelanin

N. Barapatre, T. Reinert, M. Morawski[*], T. Arendt[*], T. Butz

*Paul-Flechsig-Institut für Hirnforschung, Universität Leipzig

The role of neuromelanin has been long discussed in the still unresolved pathogenesis of the Parkinson's disease (PD), which affects $1-2\,\%$ of the general population over the age of 65 years. Neuromelanin's (NM) presence in the dopaminergic cells of the *substantia nigra* (SN), which degenerate selectively in the PD, its ability to chelate metal ions like iron, responsible for inducing oxidative stress and the reported alterations in iron level in SN of the Parkinsonian positive subjects led to the formulation of hypotheses that suggest the saturation of NM as cell apoptosis trigger [1, 2]. Nuclear microscopy (μPIXE) enables quantitative and simultaneous determination of various elements with sub-micron spatial resolution (see Fig. 5.6) and low detection limits ($\sim 50\,\mu\text{mol/l}$ for Fe).

A pilot study, however, indicated that the amount of iron bound to the NM is not significantly altered when a Parkinsonian case was compared with a control one. To
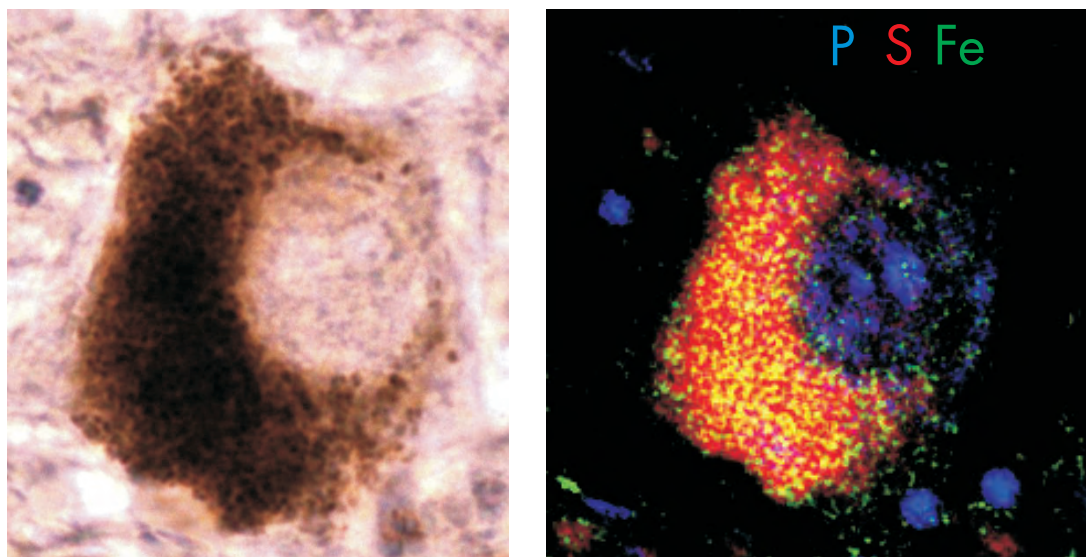
Figure 5.6: *Left*: Optical image of a cell containing neuromelanin from the brain tissue of a control subject. *Right*: Three element map of the same cell qualified and quantified using GeoPIXE. *Blue* represents the distribution of phosphorous and is seen mostly in the cell nucleus and cell membrane. *Red* represents the distribution of sulphur, the main constituent of the NM and *green colour* shows the distribution of Fe. *Yellow* is generated due to the overlap of *red* (S) and *green* (Fe). Fe can be seen mostly localised on NM.
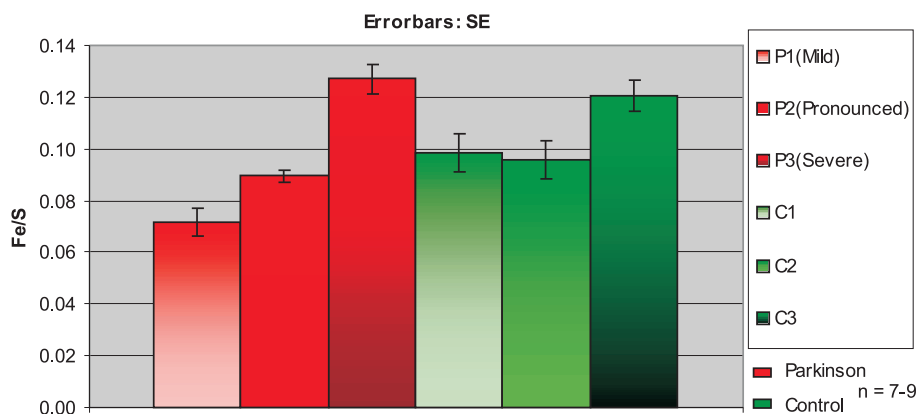
Figure 5.7: Fe content bound to NM normalised to sulfur. *Left three bars* represent three different idiopathic Parkinsonian cases with increasing severity of PD and the *right three* are control cases. No significant difference is noticed in the iron content.

make the findings of that study statistically relevant we analysed the NM from three different idiopathic Parkinsonian subjects and compared it with the NM from three normal subjects. Although one could see a significant increase in iron with the severity of PD, when compared to the control cases the difference was insignificant (Fig. 5.7). The result is striking, since well documented evidences are available that show increased Fe level in PD and subsequent oxidative stress.

Although the majority of studies have reported an overall increase in the iron levels in the SN of the Parkinsonian patients, none of them shows whether the increase is related to NM [3]. In this study NM was specifically analysed *in situ* and the trace element contents were determined. The findings of this study put a question mark on the present hypothesis of the increased iron level as a trigger of cell apoptosis.

[1] H. Federow et al.: Progr. Neurobiol. **75**, 109 (2005)
[2] L. Zecca et al.: J. Neural Transm. **109**, 663 (2002)
[3] M. Götz et al.: Ann. New York Acad. Sci. **1012**, 193 (2004)

5.10   Development of Specialized Petri Dishes for Radiobiological Experiments

M. Hohlweg, J. Krüger[*], M. Uhlmann[*], F. Menzel, T. Reinert, T. Butz

[*]Wilhelm-Ostwald-Gymnasium, Leipzig

In cell-biology more and more techniques are developed which use miniaturized structures for the analysis of cell-reaction on external stimuli. Our approach is to develop a microchip-like Petri dish using the micro-machining technique of proton beam writing (see Sect. 5.3). The structures could be used as a stencil for the implementation of electrical contacts and wiring or as mechanical barriers for compartimentalization on the Petri dish. The photoresists that we used were PMMA and SU-8, respectively.

Commercially available Petri dishes were equipped with a central hole to cover it with a 200 nm thin Si_3N_4 window that acts as irradiation entrance window. On these
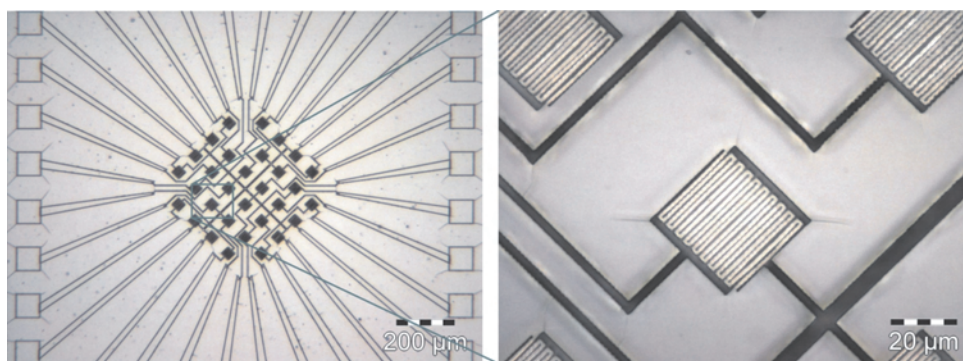
Figure 5.8: *Left*: Sensor field of 31 comb-like structures with their connections to outer contacts. *Right*: Magnified image of a sensor build up of two comb-like electrodes. *Light area* is the remaining PMMA-resist and *dark lines* are the developed regions, where the PMMA is taken off.

Si_3N_4 windows we created several micro-structures. One idea was to create electrodes in the form of interlocked fingers with minimum feature size below 500 nm. These electrodes could be used as sensitive impedance sensors for detecting changes in the cellular microenvironment. We are able to produce structures as small as 130 nm. However, first tests to create the electrodes surprisingly failed. The challenge was to write a large field (ca. 500 μm × 500 μm) of many small structures. This requires a very high writing precision of at least 0.05 %. The reason of the unsatisfactory precision was noise on the scanning signal. We have changed the electronics, successfully improving the signal-to-noise ratio. Figure 5.8 shows the structure written in PMMA and already developed. In order to process the electrodes and conducting paths the PMMA structure has to be sputtered with a thin gold layer followed by the removal of the residual PMMA.

Using SU-8, a negative resist, the written structures remain after development on the irradiation window. Thus, a compartimentalization of the Petri dish is achieved which separate sub-populations of cells. The communication between these sub-populations can only be mediated by medium-borne factors. Direct cell-cell communications are averted. The compartimentalization of Petri dishes on the irradiation window therefore enables us to study the cellular answer together with cell-cell communication after proton or helium irradiation.

5.11 Intracellular Iron: Quantitative Elemental Microscopy of Perineuronal Net-Ensheathed Neurons

A. Fiedler[*], M. Morawski[*], T. Reinert, G. Brückner[*], T. Arendt[*], T. Butz

[*]Paul-Flechsig-Institut für Hirnforschung, Universität Leipzig

A subpopulation of neurons with less vulnerability against neurodegenerative diseases possesses a specialised extracellular matrix in the form of a perineuronal net (PN). Due to its negatively charged chondroitin sulphate proteoglycans, the PN is able to bind large amounts of iron. Thus, the PNs possibly have a neuroprotective effect against
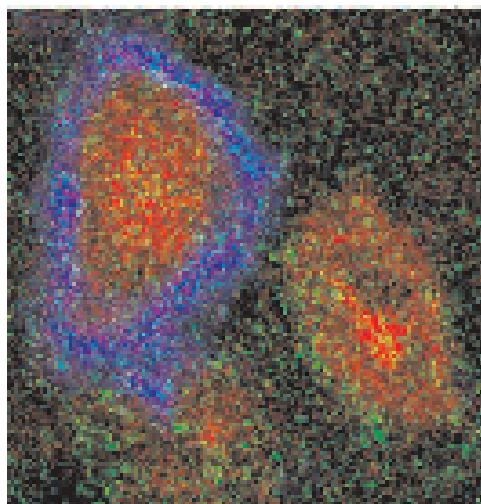
Figure 5.9: Nuclear microscopic elemental map (50×50 µm^2) of two neurons in the *subiculum*. The left neuron is enclosed with a perineuronal net (PN). PN are marked by nickel-enhanced staining (Ni: *blue*). The cytoplasm can be recognized by large phosphorus concentration (P: *red*). Iron is shown in green (Fe: *green*).
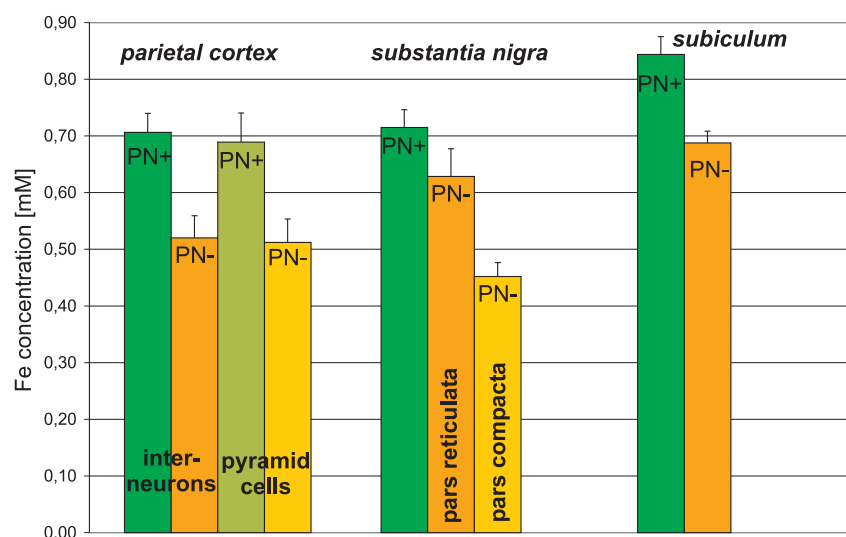
Figure 5.10: PN-positive neurons have a significantly (t-test < 0.02) increased intracellular concentration of iron than PN-negative neurons in several brain regions (*parietal cortex*, *substantia nigra*, *subiculum*). *Error bar*: standard error.

iron induced radical generation by reducing the local oxidative stress in the neuronal microenvironment. Within the Research Training Group INTERNEURO (GRK 1097) we have quantitatively analysed the elemental concentrations (especially iron) of perineuronal net-ensheathed neurons by using the nuclear microscopy technique PIXE (Particle Induced X-ray emission). We prepared brain sections (Wistar rat) of several brain areas (*substantia nigra*, *subiculum*, *parietal cortex*). The neurons with PNs were identified by immunohistochemical staining with lectin WFA intensified by DAB-nickel enabling the identification of the PNs for nuclear microscopy analysis (Fig. 5.9). The comparison of the intra-cellular iron concentration of neurons with and without a PN

in several rat brain regions showed that PN-ensheathed neurons had about 0.7 mM, whereby neurons without a PN had a significantly decreased iron concentration of approximately 0.55 mM (Fig. 5.10). The difference in intracellular iron concentrations could be an effect of the PNs. We hypothesise that there is an altered activity of iron specific proteins (transporters, reductases) in PN-associated neurons, which transform the iron into the less toxic Fe^{3+} state with subsequent storage inside the cell. This could probably delay functional changes as well as metabolic imbalances in the course of PD and AD.

5.12 TDPAC-Laboratory

T. Agne, S.K. Das, S.-B. Ryu, T. Butz

Nuclear probes were used to study the nuclear quadrupole interaction in macromolecules and various compounds which are of current use in material science. We used the highly sensitive spectroscopic method Time Differential Perturbed Angular Correlation (TDPAC). Here, a radioactive atom is placed at the site of interest and by correlating the emitted γ-quanta in space and on a nanosecond time scale local structural information is provided. Two modern 6-detector-TDPAC spectrometer are installed permanently at the Solid State Physics Lab of the ISOLDE on-line isotope separator at CERN. This outstation of the Leipzig TDPAC Laboratory is dedicated for TDPAC experiments with rather short-lived TDPAC isotopes, like ^{111m}Cd or ^{199m}Hg or ^{204m}Pb with half-lifes less than 70 minutes. Two further spectrometers are at Leipzig.

5.13 A New Isomeric TDPAC-Probe: ^{180m}Hf

S.K. Das, T. Agne, S.-B. Ryu, T. Butz

TDPAC usually employs unstable nuclei which decay to the neighboring daughter isotope via β^+/EC- or β^--decay.

Yet there are a few isotopes with longlived isomeric states like ^{111m}Cd, ^{199m}Hg and ^{204m}Pb. Here no nuclear transmutation occurs. We have shown for the first time that ^{180m}Hf with a first excited state halflife of 1.5 ns can be used successfully in $HfF_4 \cdot Hf \cdot 2H_2O$. This new isomeric probe can serve as Pu-analogue. The stretched cascade in ^{180m}Hf poses problems with conventional spectrometers but can be fully exploited with digital spectrometers.

5.14 ESRF: Development of a Spectrometer for SRPAC for ^{61}Ni Spectroscopy in Biomolecules

T. Agne, S.K. Das, T. Butz

Synchrotron-based Perturbed Angular Correlation (SRPAC) spectroscopy is a rapidly growing field because it complements nuclear forward scattering. Thus far, first experiments with ^{57}Fe and ^{61}Ni were successfully carried out at the European Synchrotron

Radiation Facility (ESRF) at Grenoble by various groups. For ^{61}Ni spectroscopy, efficient detectors for photon energies around 60 keV are required which yield ultrashort pulses. BaF_2 doped with Er in order to suppress the 600 ns fluorescence mounted on photomultipliers, are very promising. Since the prompt burst of scattered quanta is $3-4$ orders of magnitude larger than the delayed resonance fraction it remains to be seen whether the photomultipliers recover fast enough after the prompt burst. An alternativ are the new multi-pixel-photon counters.

5.15 Isolde: Development of a Fully-Digital, User-Friendly PAC-Spectrometer

T. Agne, S.K. Das, T. Butz

The new generation of PAC-spectrometers developed at Leipzig consists of fast digitizers with 1 GSample/s and massive data reduction on board using field programmable gated arrays (FPGA). A timing signal is generated, the pulse area is determined and selected, and the detector number is added as a tag to the data stream to the PC where the coincidences are detected and stored for real-time processing. The FPGA-programming is completed. The new spectrometer will use brand-new $LaBr_2$-(Ce)-scintillators which give excellent energy resolution and timing.

5.16 The Nuclear Quadrupole Interaction in Hf + 2.6 % Zr Alloys

S.K. Das, T. Butz

We used the ^{181}Hf(β^-)^{181}Ta nuclear probe to investigate the nuclear quadrupole interaction in $Hf_{1-x}Zr_x$ with $x = 0.026$ in the time range up to 120 ms, assuming Gaussian frequency distributions a fraction of about 70 % reveals NQI parameters close to pure Hf, i.e. there are 12 Hf nearest neighbours, and another fraction of 20 % which is attributed to 11 Hf and 1 Zr nearest neighbour. Surprisingly, this fraction exhibits a large deviation from axial symmetry which is not expected on the basis of the similarity of ionic radii of Zr and Hf.

5.17 Funding

ESRF: Aufbau eines SRPAC Spektrometers zur Untersuchung der Koordination und Dynamik von Nickel-Zentren in biologischen Systemen
Prof. T. Butz
BMBF, 05KS40LA/3

NANODERM – Quality of Skin as a barrier to ultra-fine particles
Prof. T. Butz
EU-Project, QLK4-CT-02678

Radioactive Metal Probes as Diagnostic Tools in Biomolecules
Prof. T. Butz
Deutsche Forschungsgemeinschaft, Tr327/8-1

ISOLDE: Aufbau eines volldigitalen, nutzerfreundlichen PAC-Spektrometers
Prof. T. Butz
BMBF, 05KK4OL1/4

5.18   Organizational Duties

T. Butz
- Member of the ISOLDE and Neutron Time of Flight Committee, CERN
- Vertrauensdozent der Studienstiftung des deutschen Volkes
- Sprecher der Ortsgruppe Leipzig des deutschen Hochschulverbandes
- Co-tutor for students of Tautenburg (astrophysics), LMU München (astrophysics), DESY/Zeuthen (particle physics)
- external Expert Scientific Committee on Consumer Products, DG Sanco, Brüssel
- Reviewer: DFG, Studienstiftung des deutschen Volkes, US Immigration Service, CNRS (France)
- Referee: J. of Physics C, Phys. Rev. B, Chem. Reviews, Phys. Rev. Lett., J. Biol. Inorg. Chem., Israeli Science Foundation, Alexander von Humboldt Foundation, Nucl. Instr. Meth. Phys. Res. B, Hyperfine Interact.

T. Reinert
- Referee: Nucl. Instr. Meth. Phys. Res. B

D. Spemann
- Referee: Nucl. Instr. Meth. Phys. Res. B

F. Menzel
- Referee: Nucl. Instr. Meth. Phys. Res. B

C. Meinecke
- Referee: Nucl. Instr. Meth. Phys. Res. B

C. Nilsson
- Referee: Nucl. Instr. Meth. Phys. Res. B

5.19 External Cooperations

Academic

- Centre d´Etudes Nucléaires de Bordeaux Gradignan (CENBG), Bordeaux, France
  Prof. Ph. Moretto

- European Organization for Nuclear Research (CERN), Genf, Switzerland
  ISOLDE Collaboration

- Commonwealth Scientific and Industrial Research Organisation (CSIRO), Exploration and Mining, Sydney, Australia
  Dr. C. Ryan

- European Molecular Biology Laboratory (EMBL), Outstation Hamburg
  Dr. W. Meyer-Klaucke, Dr. A. Vogel, O. Schilling

- Froschungsreaktor FRM II, Garching
  Prof. E. Wagner, Dr. U. Wagner

- FU Berlin
  Prof. U. Abram

- Gray Cancer Institute, London, UK
  Prof. B. Michael

- Gesellschaft für Schwerionenforschung (GSI), Darmstadt
  Dr. D. Dobrev, Dr. B. Fischer

- Hahn–Meitner Institut (HMI), Berlin
  Dr. D. Alber, Dr. H. Haas

- Institut für Interdisziplinäre Isotopenforschung (IIF), Leipzig
  K. Franke

- Institute of Physics, Kraków, Poland
  Dr. Z. Stachura

- Institute of Nuclear Technology, Sacavém, Portugal
  Dr. T. Pinheiro

- Leibnitz-Institut für Oberflächenmodifizierung (IOM), Leipzig
  Dr. K. Zimmer, Dr. J. Gerlach

- Royal Veterinary and Agricultural University (KVL), Copenhagen, Denmark
  Dr. L. Hemmingsen

- Martin-Luther-Universität Halle-Wittenberg
  Dr. J. Tanner

- Max Planck Institute for Demographic Research, Rostock
  A. Fabig

- Max-Planck-Institut für Mikrostrukturphysik, Halle/Saale
  Dr. J. Heitmann

- National University of Singapore
  Prof. F. Watt, Dr. T. Osipowicz

- Universität Leipzig, Paul-Flechsig-Institut
  Prof. T. Arendt, Dr. M. Morawski, Dr. G. Brückner

- The University of Melbourne, Australia
  Microanalytical Research Centre, Prof. D. Jamison

- TU Wien, Austria
  Prof. K. Schwarz, Prof. P. Blaha

- Universidade de Aveiro, Portugal
  Prof. V.S. Amaral

- Universität Hannover
  Arbeitskreis Prof. P. Behrens, Arbeitskreis Prof. C. Vogt

- Universität Leipzig
  Prof. R. Hoffmann

- Universität Zürich, Switzerland
  Prof. Vašak, Dr. P. Faller, Prof. R. Alberto

- Universitätskliniken Leipzig
  PD Dr. G. Hildebrandt

Industry

- Infineon Technologies Dresden GmbH & Co. OHG
  M. Jerenz

- Dechema
  Dr. E. Zschau, Self-employed expert in materials research

5.20 Publications

Journals

S.K. Das, F. Heinrich, T. Butz: *The nuclear quadrupole Interaction at inequivalent lattice sites in ammonium paramolybdate: a TDPAC study*, Chem. Phys. **327**, 291 (2006)

P. Esquinazi, D. Spemann, K. Schindler, R. Höhne, M. Ziese, A. Setzer, K.-H. Han, S. Petriconi, M. Diaconu, H. Schmidt, T. Butz, Y.H. Wu: *Proton irradiation effects and magnetic order in carbon structures*, Thin Solid Films **505**, 85 (2006)

M. Diaconu, H. Schmidt, H. Hochmuth, M. Lorenz, G. Benndorf, D. Spemann, A. Setzer, P. Esquinazi, A. Pöppl, H. von Wenckstern, K.-W. Nielsen, R. Gross, H. Schmid, W. Mader, G. Wagner, M. Grundmann: *Room-temperature ferromagnetic Mn-alloyed ZnO films obtained by pulsed laser deposition*, J. Magn. Magn. Mater. **307**, 212 (2006)

M. Diaconu, H. Schmidt, H. Hochmuth, M. Lorenz, H. von Wenckstern, G. Biehne, D. Spemann, M. Grundmann: *Deep defects generated in n-conducting ZnO:TM thin films*, Solid State Commun. **137**, 417 (2006)

K.-H. Han, P. Esquinazi, M. Diaconu, H. Schmidt, D. Spemann, T. Butz: *Aging and annealing effects on the magnetic ordering induced by proton irradiation in graphite*, J. Korean Phys. Soc. **48**, 1427 (2006)

L. Hartmann, Q. Xu, H. Schmidt, H. Hochmuth, M. Lorenz, C. Meinecke, M. Grundmann: *Spin polarization in $Zn_{0.95}Co_{0.05}O$:(Al, Cu) thin films*, J. Phys. D: Appl. Phys. **39**, 1 (2006)

A.D. Maynard, R.J. Aitken, T. Butz, V. Colvin, K. Donaldson, G. Oberdörster, M.A. Philbert, J. Ryan, A. Seaton, V. Stone, S.S. Tinkle, L. Tran, N.J. Walker, D.B. Warheit: *Safe handling of nanotechnology*, Nature **444**, 267 (2006)

C. Meinecke, M. Morawski, T. Reinert, T. Arendt, T. Butz: *Cellular distribution and localisation of iron in adult rat brain (substantia nigra)*, Nucl. Instr. Meth. B **249**, 688 (2006)

C. Meinecke, J. Vogt, R. Schmidt-Grund, T. Butz: *RBS studies on coated micro-dimensional glass fibers used as micro-resonators*, Nucl. Instr. Meth. B **249**, 387 (2006)

F. Menzel, R. Kaden, D. Spemann, K. Bente, T. Butz: *Ion beam analysis of synthetic cylindrite produced by CVT*, Nucl. Instr. Meth. B **249**, 478 (2006)

F. Menzel, D. Spemann, S. Petriconi, J. Lenzner, T. Butz: *Proton beam writing of microstructures at the ion nanoprobe LIPSION*, Nucl. Instr. Meth. B **250**, 66 (2006)

P. Reichart, D. Spemann, A. Hauptner, A. Bergmaier, V. Hable, R. Hertenberger, C. Greubel, A. Setzer, G. Dollinger, D.N. Jamieson, T. Butz, P. Esquinazi: *3D-Hydrogen analysis of ferromagnetic microstructures in proton irradiated graphite*, Nucl. Instr. Meth. B **249**, 286 (2006).

T. Reinert, D. Spemann, M. Morawski, T. Arendt: *Quantitative trace element analysis with sub-micron lateral resolution*, Nucl. Instr. Meth. B **249**, 734 (2006)

K. Schindler, D. Spemann, M. Ziese, P. Esquinazi, T. Butz: *Magnetism in Carbon: Writing Magnetic Structures with a Proton Micro-Beam on Graphite Surfaces*, Acta Phys. Pol. A **109**, 249 (2006)

H. Schmidt, M. Diaconu, H. Hochmuth, M. Lorenz, A. Setzer, P. Esquinazi, A. Pöppl, D. Spemann, K.-W. Nielsen, R. Gross, G. Wagner, M. Grundmann: *Weak ferromagnetism in textured $Zn_{1-x}(TM)_xO$ thin films*, Superlatt. Microstruct. **39**, 334 (2006)

R. Schmidt-Grund, A. Carstens, B. Rheinländer, D. Spemann, H. Hochmuth, G. Zimmermann, M. Lorenz, M. Grundmann, C.M. Herzinger, M. Schubert: *Refractive indices and band-gap properties of rocksalt $Mg_xZn_{1-x}O$ $(0.68 \leq x \leq 1)$*, J. Appl. Phys. **99**, 123 701 (2006)

S. Schorr, R. Höhne, D. Spemann, T. Doering, B.V. Korzun: *Magnetic properties investigations on Mn substituted ABX_2 chalcopyrite*, Phys. Stat. Sol A **203**, 2783 (2006)

S. Schorr, V. Riede, D. Spemann, T. Doering: *Electronic band gap of $Zn_{2x}(CuIn)_{1-x}X_2$ solid solution series (X=S,Se,Te)*, J. Alloy Compd. **414**, 26 (2006)

M. Schwertner, A. Sakellariou, T. Reinert, T. Butz: *Scanning transmission ion micro-tomography(STIM-T) of biological specimens*, Ultramicroscopy **106**, 574 (2006)

H.C. Semmelhack, R. Höhne, P. Esquinazi, G. Wagner, A. Rahm, K.H. Hallmeier, D. Spemann, K. Schindler: *Growth of highly oriented graphite films at room temperature by pulsed laser deposition using carbon–sulfur targets*, Carbon **44**, 3064 (2006)

D. Spemann, K. Schindler, P. Esquinazi, M. Diaconu, H. Schmidt, R. Höhne, A. Setzer, T. Butz: *Magnetic force microscopy studies on the magnetic ordering in organic materials induced by high energy proton irradiation*, Nucl. Instr. Meth. B **250**, 303 (2006)

Q. Xu, L. Hartmann, H. Schmidt, H. Hochmuth, M. Lorenz, R. Schmidt-Grund, D. Spemann, M. Grundmann: *Magnetoresistance effect in $Zn_{0.90}Co_{0.10}O$ films*, J. Appl. Phys. **99**, 013 904 (2006)

Q. Xu, L. Hartmann, H. Schmidt, H. Hochmuth, M. Lorenz, R. Schmidt-Grund, D. Spemann, A. Rahm, M. Grundmann: *Magnetoresistance in pulsed laser deposited 3d transition metal doped ZnO films*, Thin Solid Films **515**, 2549 (2006)

Q. Xu, L. Hartmann, H. Schmidt, H. Hochmuth, M. Lorenz, R. Schmidt-Grund, C. Sturm, D. Spemann, M. Grundmann: *Metal-insulator transition in Co-doped ZnO: Magneto-transport properties*, Phys. Rev. B. **73**, 205 342 (2006)

J. Zúñiga-Pérez, V. Muñoz-Sanjosé, M. Lorenz, G. Benndorf, S. Heitsch, D. Spemann, M. Grundmann: *Structural characterization of a-plane $Zn_{1-x}Cd_xO$ ($0 \leq x \leq 0.085$) thin films grown by metal-organic vapor phase epitaxy*, J. Appl. Phys. **99**, 023 514 (2006)

Books

T. Butz: *Fourier Transformation for Pedestrians* (Springer, Berlin 2006)

T. Butz et al.: *NFP - Scientific Activities*, in: *Report 2005 Institute für Physik*, ed. by M. Grundmann (Universität Leipzig, Leipzig 2006)

P. Esquinazi, R. Höhne, K.-H. Han, D. Spemann, A. Setzer, M. Diaconu, H. Schmidt, T. Butz: *Induced Magnetic Order by Ion Irradiation of Carbon Structures*, in *Carbon-Based Magnetism: an Overview of the Magnetism of Metal Free Carbon-Based Compounds and Materials*, ed. by T. Makarova, F. Palacio (Elsevier, Amsterdam 2006) p 437

Talks

T. Butz: *Can TiO$_2$ Nanoparticles Penetrate into vital Tissue of Skin?*, Int. Conf. Materials Chemistry, Mombai, 04. – 08. December 2006

T. Butz: *Das NANODERM-Projekt*, Bundesanstalt für Risikoforschung, Berlin, 28. March 2006

T. Butz: *Nukleare Sonden und Ionenstrahlen für die Zukunft*, Deutsche Tagung für Forschung mit Synchrotronstrahlung, Neutronen und Ionenstrahlen an Großgeräten 2006, Hamburg, 04. – 06. October 2006

T. Butz: *Studien zur Hautpenetration von Nanopartikeln: das NANODERM-Projekt*, IKW, Frankfurt/Main, 30. June 2006

T. Butz: *The LIPSION Facility*, NOTE Kick-off Meeting, Helsinki, 13. September 2006

M. Diaconu, H. Schmidt, H. Hochmuth, H. v. Wenckstern, D. Spemann, M. Lorenz, M. Grundmann, M. Fecioru-Morariu, K. Schmalbuch, G. Güntherodt: *ZnO films doped with rare earth metals*, Frühjahrstagung der DPG, Dresden, 27.–31. March 2006

L. Hartmann, Qingyu Xu, H. Schmidt, H. Hochmuth, M. Lorenz, R. Schmidt-Grund, D. Spemann, M. Grundmann: *Defect mediated ferromagnetism in* $Zn_{0.95}Co_{0.05}O:(Cu,Al)$ *thin films*, Frühjahrstagung der DPG, Dresden, 27.–31. March 2006

S. Heitsch, G. Zimmermann, H. Hochmuth, D. Spemann, G. Benndorf, H. Schmidt, M. Lorenz, M. Grundmann; *Photoluminescence properties on* $Mg_xZn_{1-x}O$ *thin films grown by pulsed laser deposition*, Frühjahrstagung der DPG, Dresden, 27.–31. March 2006

C. Meinecke, R. Kaden, K. Bente, J. Vogt, T. Butz: *Investigation of synthetic cylindrite microstructures*, 10th Int. Conf. Nuclear Microprobe Technology and Applications, Singapore, 09.–14. July 2006

C. Meinecke, R. Kaden, J. Vogt, K. Bente, T. Butz: *Ionenstrahlmikroskopische Untersuchungen an synthetischen Kylindrit-Mikrostrukturen*, Frühjahrstagung der DPG, Dresden, 27.–31. March 2006

C. Meinecke, J. Vogt, J. Bauer, V,. Gottschalch, T. Butz: *Stoichiometry investigations of interlayer of GaAs/AlAs nano-wires*, 10th Int. Conf. Nuclear Microprobe Technology and Applications, Singapore, 09.–14. July 2006

F. Menzel: *Protonenstrahlschreiben an der Hochenergie-Ionen-Nanosonde LIPSION – Erzeugung von Mikro- und Nanostrukturen mit hohem Aspektverhältnis in Photolacken und Halbleitern*, Seminarvortag am HMI, Berlin, 27. June 2006

F. Menzel, D. Spemann, S. Petriconi, J. Lenzner, T. Butz: *Proton beam writing of submicrometer structures at LIPSION*, 10th Int. Conf. Nuclear Microprobe Technology and Applications, Singapore, 09.–14. July 2006

T. Reinert: *The influence of high current densities in sub-micron nuclear microscopy on the quantitative elemental analysis of biological samples*, 10th Int. Conf. on Nuclear Microprobe Technology and Applications, Singapore, 09.–14. July 2006

H. Schmidt, M. Diaconu, H. Hochmuth, M. Lorenz, H. v. Wenckstern, G. Biehne, D. Spemann, M. Grundmann: *Deep defects generated in n-conducting ZnO:TM thin films*, Frühjahrstagung der DPG, Dresden, 27.–31. March 2006

Q. Xu, L. Hartmann, H. Schmidt, H. Hochmuth, M. Lorenz, R. Schmidt-Grund, D. Spemann, M. Grundmann: *Thickness dependent magnetoresistance of ZnCoO:Al thin films*, Frühjahrstagung der DPG, Dresden, 27.–31. March 2006

Posters

C. Bundesmann, R. Schmidt-Grund, D. Spemann, M. Lorenz, M. Grundmann, M. Schubert: *Phonon modes, dielectric contants, and exciton mass parameters in ternary $Mg_xZn_{1-x}O$*, MRS Spring Meeting, San Francisco, USA, 17.–21. April 2006

M. Diaconu, H. Schmidt, M. Fecioru-Morariu, G. Güntherodt, D. Spemann, H. Hochmuth, M. Lorenz, M. Grundmann: *Ferromagnetism in Zn(Mn,Sn)O and Zn(Mn,P)O films*, Frühjahrstagung der DPG, Dresden, 27.–31. March 2006

A. Rahm, E.M. Kaidashev, H. Schmidt, M. Diaconu, A. Pöppl, R. Böttcher, C. Meinecke, T. Butz, M. Lorenz, M. Grundmann: *Growth and characterization of Mn- and Co-doped ZnO nanowires*, Frühjahrstagung der DPG, Dresden, 27.–31. March 2006

T. Reinert, A. Fiedler, M. Morawski, T. Arendt: *High resolution quantitative element mapping of neuromelanin-containing neurons*, 10th Int. Conf. Nuclear Microprobe Technology and Applications, Singapore, 09.–14. July 2006

T. Reinert, C. Meinecke: *Charakterisierung von Mikrostrukturen mittels ortsaufgelöster RBS- und PIXE-Analyse*, Frühjahrstagung der DPG, Dresden, 27.–31. March 2006

5.21 Graduations

Diploma

- Stephan Werner
  Mikro-PIXE-Untersuchungen an mikrodimensionalen Strukturelementen mittels eines facettierten Röntgendetektors
  January 2006

- Silvio Petriconi
  On the proton beam writing and magnetic characterisation of microstructures in highly oriented pyrolytic graphite
  July 2006

- Martin Henze
  Search for novae in M31 on digitized Tautenburg Schmidt-plates
  November 2006

- Martin Rothermel
  Welche Rolle spielt die thermische Belastung bei ionenstrahlinduziertem Ferromagnetismus in kohlenstoffbasierten Systemen?
  December 2006

Master

- Seung-Beak Ryu
  The Nuclear Quadrupole Interactions at ^{44}Sc in the Anatase and Rutile Modifications of TiO_2 and Anatase Nanoparticles
  December 2006

5.22 Guests

- Dr. S.K. Das
  Babha Atomic Research Center, Kolkata, India
  March 2005 – June 2006

6

Semiconductor Physics

6.1   Introduction

In the following short articles we summarize our scientific activities of the year 2006. Our focus remained on the pulsed laser deposition (PLD) of ZnO thin films and nanostructures and their characterization. Based on our work on oxide dielectrics such as MgO, ZrO_2 or Al_2O_3 we achieved the fabrication of a planar all-oxide microcavity with quasi-bulk ZnO (60 nm) between two Bragg mirrors. The exciton-polariton formation with strong coupling was found at room temperature (Sect. 6.2). We will continue such investigations with the purpose to demonstrate Bose-Einstein condensation of massive (quasi-)particles at room temperature.

Unsurpassed control of surface and material quality in homoepitaxy of ZnO is demonstrated by us for PLD on ZnO (O-face) substrates (Sect. 6.3). Based on a thermal treatment of hydrothermal ZnO substrates yielding vicinal substrates, monolayer step surfaces prevail after 1 μm of PLD. Recently, even vicinal, epitaxial surfaces have been achieved (yet unpublished) and will build the basis to create close-to-ideal oxide heterostructures such as quantum wells, tunnel barriers, two-dimensional electron gases and the like.

Please go through our short articles and learn about our progress on epitaxy of ZnO-, III–V- and GaN-nanowires, lasing from ZnO microwires, ZnO Schottky diodes, semiconducting/ferroelectric $ZnO/BaTiO_3$ diodes, the theory and measurement of the dielectric function of ZnO and many more topics (you can look for even further information at http://www.uni-leipzig.de/~hlp).

We are grateful for the very positive evaluation of our DFG Research Unit 522, "Architecture of nano- and microdimensional building blocks", which will continue for another three years to 2009. Also the European Network of Excellence SANDiE, coordinated by us, received very good marks in a memorable review meeting in Madrid. These and other projects provide us with important means for our research activities and a lively cooperation with many colleagues, institutes and industrial companies. In particular the guests of our group contribute to intense scientific cooperation. Dr. Jesús Zúñiga Pérez will return in the coming years with a grant of the Alexander-von-Humboldt foundation.

Marius Grundmann

6.2 Exciton-Polariton Formation at Room Temperature in a Planar ZnO Resonator Structure

R. Schmidt-Grund, B. Rheinländer, C. Czekalla, G. Benndorf, H. Hochmuth, J. Lenzner, H. Schmidt, M. Lorenz, M. Grundmann

We report on strong coupling of exciton and photon modes in planar resonators consisting of a half-wavelength ZnO cavity, which acts as active medium [1]. The cavity is embedded between bottom and top Bragg reflectors consisting of quarter-wave stacks of the materials ZrO_2 and MgO (10.5 layer pairs) [2, 3] (Fig. 6.1). We have observed an energy splitting of the exciton-polariton branches of about 78 meV in maximum, which is as large as the best values reached for the technologically currently more advanced material systems CdZnTeSe and AlInGaN.

The resonator structure has been deposited on sapphire substrate using pulsed-laser deposition at approximately 700 °C in 20 Pa O_2 atmosphere. The exciton-polariton modes have been observed in both reflectivity and photoluminescence (PL) spectra for temperatures between 4 K and 306 K and at room temperature for various angles of incidence respective exit angles of the light. The PL was excited with a cw-HeCd laser operating at 325 nm. The excitation density at the resonator surface was 1 kW/cm^2 (spot diameter 4 µm). The reflectivity spectra of the Bragg reflectors used for the resonator have been obtained from layer-stack model analysis of ellipsometry data using materials dielectric functions determined previously from single films [3–5].

Within a resonator, coupling of electronic transitions with photonic modes is possible. The uncoupled modes can be excitonic, cavity, and Bragg band modes. For our
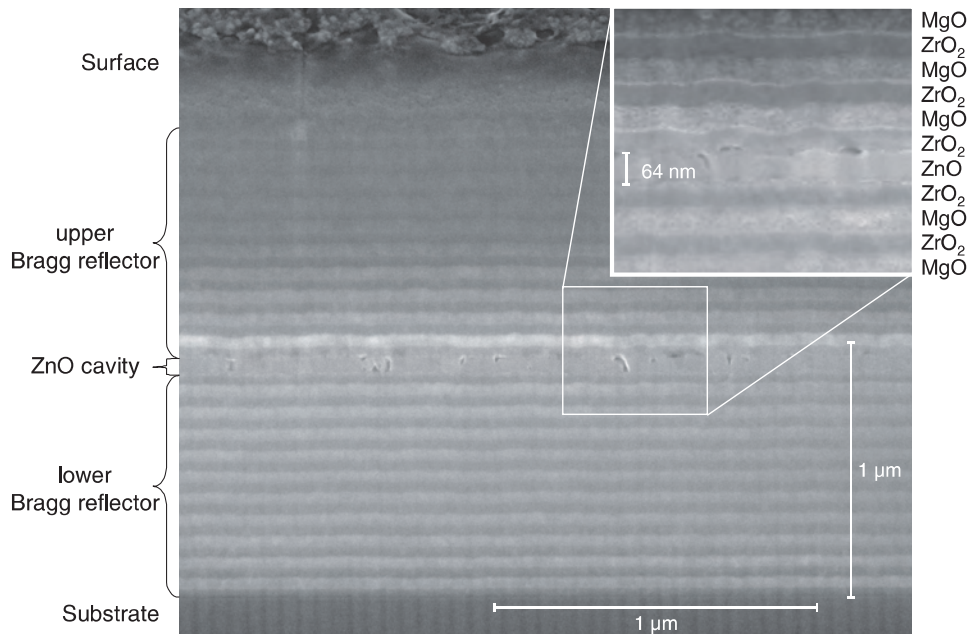
Figure 6.1: SEM image of a cross-section of our resonator structure. The cross-section was produced by writing a 12×2 µm sized hole in the resonator using a focused ion beam. The inset shows an enlarged region in the vicinity of the ZnO cavity. Note that the vertical scale is compressed due to the observation angle.
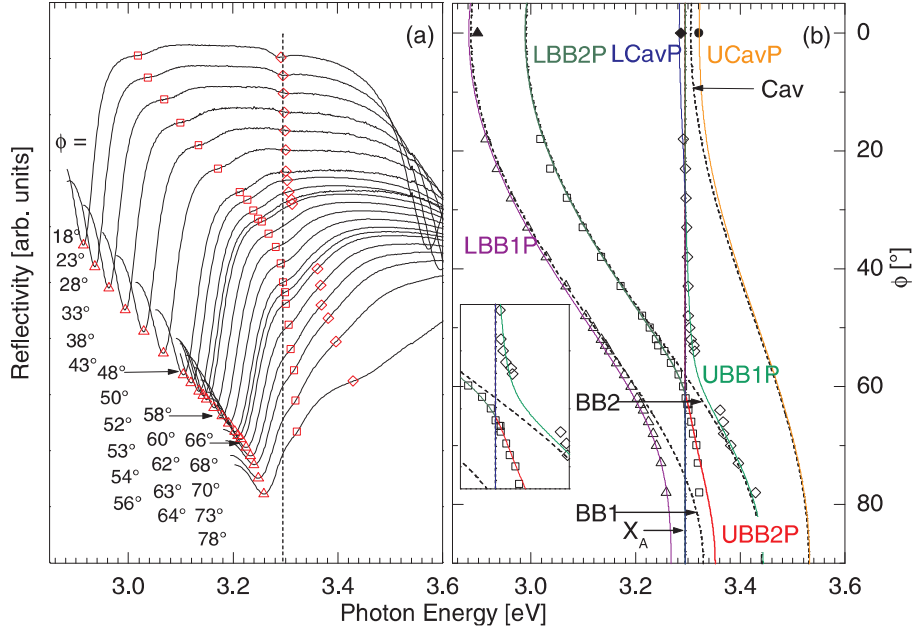
Figure 6.2: (a): Experimental reflectivity spectra of the resonator for various exit angles at 293 K. The experimentally determined mode positions are marked in *open symbols*. **(b)**: The calculated uncoupled modes are plotted as *dashed lines* along with the calculated exciton-polariton modes (*solid lines*) as a function of the angle.

resonator, the uncoupled modes are the discrete free exciton mode, the first order cavity mode (Cav), and two Bragg band-edge modes (BB1, BB2), with energies E_X, E_c, E_{B1}, and E_{B2}, respectively. The exciton can couple with all three photonic modes resulting in six exciton-polariton branches. The temperature as well as the angle dependency of the uncoupled modes has been calculated from the materials dielectric functions and the resonator geometry data.

The experimentally detected maxima and shoulders in the PL spectra respective minima and shoulders in the reflectivity spectra (Fig. 6.2) refer to cavity as well as Bragg band-edge exciton-polariton modes. In order to assign the experimentally observed modes to the six exciton-polariton branches mentioned above, we have calculated the exciton-polariton dispersions by taking into account the coupling of the free exciton mode with the cavity mode (LCavP and UCavP: lower and upper cavity polariton) and with the first and second Bragg band-edge mode (LBB1P/LBB2P and UBB1P/UBB2P: lower and upper Bragg band-edge 1/2 polariton). We have chosen a model based on a 6×6 Hamiltonian (after [6]):

$$\begin{pmatrix} E_X & 0 & 0 & \Delta_{1c} & \Delta_{1B2} & \Delta_{1B1} \\ 0 & E_X & 0 & \Delta_{2c} & \Delta_{2B2} & \Delta_{2B1} \\ 0 & 0 & E_X & \Delta_{3c} & \Delta_{3B2} & \Delta_{3B1} \\ \Delta_{1c} & \Delta_{2c} & \Delta_{3c} & E_c & 0 & 0 \\ \Delta_{1B2} & \Delta_{2B2} & \Delta_{3B2} & 0 & E_{B2} & 0 \\ \Delta_{1B1} & \Delta_{2B1} & \Delta_{3B1} & 0 & 0 & E_{B1} \end{pmatrix} . \tag{6.1}$$

Thereby the independent coupling of the exciton mode with each of the resonator modes is accounted and a consistent description of the mode dispersion is obtained for all three experimental setups. The mode coupling constants Δ_x can be calculated from

Table 6.1: Coupling constants for the exciton-polaritons and matrix elements of 6.1, which are consistent with the experimentally observed modes. All values are given in units of meV. The uncertainties amount to 10 %. The elements Δ_{ic} ($i = 1, 2, 3$) were found to be equal each and therefore abbreviated by Δ_{123c}.

	Δ_{123c}	Δ_{1B2}	Δ_{2B2}	Δ_{3B2}	Δ_{1B1}	Δ_{2B1}	Δ_{3B1}	Δ_c	Δ_{B2}	Δ_{B1}
PL(T)	11	22[a]	22[a]	0	0	55[a]	55[a]	19	31	78
PL(ϕ)	11[b]	22	22	0	0	55	55	19	31	78
R(ϕ)	11[b]	11	11	11	22	22	22	19	19	38

[a] Taken from the PL (ϕ) experiment.
[b] Taken from the PL (T) experiment.

the matrix elements Δ_{ix} by the relation $\Delta_x^2 = \sum_{i=1}^{3} \Delta_{ix}^2$, where x stands for c, $B1$, and $B2$ and $i = 1, 2, 3$ (Tab. 6.1). A maximum mode splitting of about 78 meV has been found. In contrast to previous findings [6] we have observed larger coupling strength between the exciton and the Bragg band-edge modes as between the exciton and the cavity modes. We explain this by a not ideal quality of our resonator, for which the energy barrier within the photonic band-gap is not that high and therefore energy transfer to the Bragg band-edge modes is possible.

[1] R. Schmidt-Grund et al.: Superlatt. Microstruct. (2007); R. Schmidt-Grund et al.: Phys. Rev. Lett. (submitted)
[2] M. Lorenz et al.: Ann. Phys. **13**, 59 (2004)
[3] R. Schmidt-Grund et al.: SPIE **6038**, 489 (2005)
[4] R. Schmidt et al.: Appl. Phys. Lett. **82**, 2260 (2003)
[5] R. Schmidt-Grund et al.: AIP Conf. Proc. **893**, 271 (2007)
[6] M. Richard et al.: Appl. Phys. Lett. **86**, 071 916 (2005).

6.3   Homoepitaxy of High-Quality ZnO PLD Thin Films

H. von Wenckstern, C. Hanisch, C. Czekalla, M. Brandt, G. Benndorf, G. Biehne, A. Rahm, H. Hochmuth, M. Lorenz, M. Grundmann

Homoepitaxial growth of ZnO remains up to today non-trivial. ZnO thin films deposited on as-received ZnO single crystalline substrates are usually textured and have rough surfaces caused by 3d growth. A low temperature buffer layer is needed to grow strain-free homoepitaxial thin films. This is due to damage of the substrate surface which is unintentionally introduced by the polishing by the vendors. The damaged layer extends 5 to 10 μm into the substrate. Thermal treatment at about 1000 °C in an oxygen ambient (850 mbar) recovers the polishing damage within two hours. The surface is vicinal after treatment, the miscut of about 0.06° causes terrace widths of about 200 nm (see Fig. 6.3a). After treatment the ZnO substrates are perfectly suited for homoepitaxy. We used pulsed-laser deposition for the growth of nominally undoped ZnO thin films with a thickness of about 1 μm as determined from the layer thickness oscillations in the 2θ–ω scan of the ZnO (0002) reflection. Additionally, we studied the initial growth process by depositing thin films with nominal thicknesses of 8 nm, 25 nm, 50 nm, and 80 nm by atomic force microscopy measurements depicted in Fig. 6.3 along
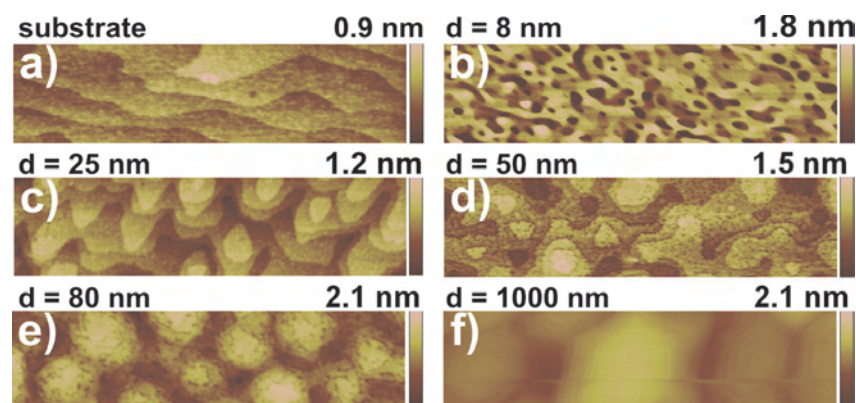
Figure 6.3: $2 \times 0.5\,\mu m^2$ AFM height scans of (**a**) an annealed ZnO substrate and homoepitaxial ZnO thin films (**b**)–(**f**) with a nominal thickness of d. *Labelled numbers* indicate height scale.

with the morphology of the treated substrate and that of a $1\,\mu m$ thick homoepitaxial ZnO thin film.

For a thickness of $8\,nm$ the epilayer still mimics the morphology of the substrate, however, the step lines begin to bend most probably caused by pinning by dislocations emerging from the substrate. For thicknesses of $25\,nm$ and above the pinned step lines cause the formation of closed loop spirals that coalesce to form hexagonally shaped islands with diameters up to $1\,\mu m$. Within such an island steps with height $c/2$ or c (depending on the growth conditions) are visible.

High resolution X-ray diffraction measurements revealed full width at half maximum (FWHM) of the 2θ–ω scan and the rocking curve of the ZnO (0002) reflection of $56''$ (which is, however, strongly influenced by the layer thickness oscillations and therefore only an upper limit) and $29''$, respectively. Comparing the FWHM of the rocking curve to that of heteroepitaxial ZnO PLD thin films ($370''$ for Al_2O_3/ZnO, $70''$ for $ScAlMgO_4/ZnO$) reveals the tremendous potential of homoepitaxial growth on optimally prepared ZnO substrates.

A low temperature ($2\,K$) photoluminescence (PL) measurement is depicted in Fig. 6.4 for a $1\,\mu m$ thick epilayer. The resolution of the detection equipment is $100\,\mu eV$. The recombination of free excitons is clearly visible. The participating holes stem either from the A (X_A) or the B valence band (X_B). At $3.42\,eV$ the excited state ($n = 2$) of the X_A is visible. The spectrum is dominated by the recombination of donor bound excitons (I6a/I6), the line I6 is ascribed to Al_X^0. Between the free exciton recombination and the I6a/I6 lines two additional transitions labelled I3a and I0 are visible, their origin is not clarified yet. A peak at lower energies labelled DBX is ascribed to recombination of excitons bound to structural defects. The inset of Fig. 6.4 depicts I6a/I6 with higher detail. At the high energy side their rotational states I6a*/I6* are visible emphasizing the high quality of the homoepitaxial thin film. The defect related green luminescence was not observed. PL area scans ($90\,\mu m \times 90\,\mu m$, 30×30 spectra, spatial resolution $3\,\mu m$, $10\,K$) revealed the extreme homogeneity of the best epilayer. The standard deviation of the spectrally integrated intensity is *only* $1\,\%$.

Thermal admittance spectroscopy was performed between $10\,K$ and $330\,K$. Three defect levels (T1, T2, T3) were found, the levels T2 and T3 superimpose such that a standard maximum evaluation with subsequent Arrhenius analysis was not possi-
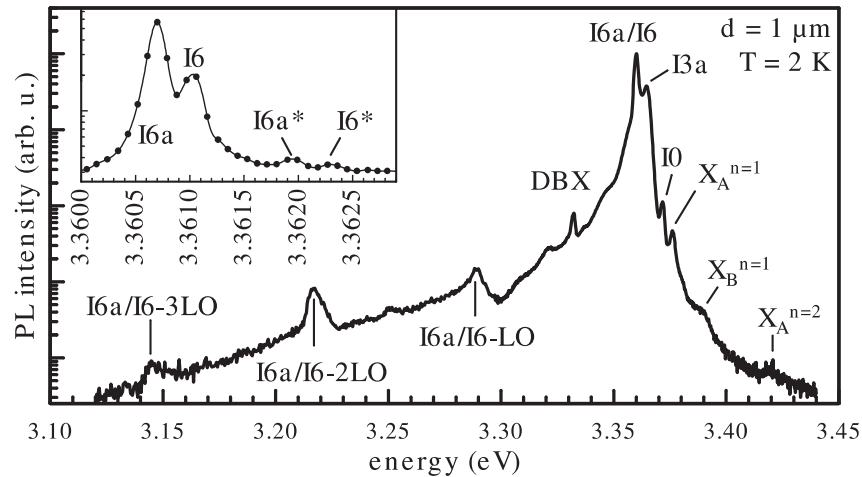
Figure 6.4: Low temperature PL spectrum of a homoepitaxial PLD thin film grown at $T_g \sim 650\,°C$. The inset shows the I6a/I6 transitions and the rotational states I6a*/I6* in higher resolution.

ble. However, their thermal activation energy was estimated to lie between 200 meV and 400 meV. The level T1 has a thermal activation energy of (56 ± 5) meV. Its density was estimated to be $3 \times 10^{13}\,cm^{-3}$, the net doping concentration of the sample is only $6 \times 10^{14}\,cm^{-3}$, a very good starting point for the realization of p-type ZnO.

In summary we have deposited high-quality homoepitaxial ZnO PLD thin films on vicinal ZnO substrates optimally prepared for epitaxy by heat treatment. The thin films show steps of $c/2$ or c, their structural properties are superior to heteroepitaxial thin films. The high quality of the homoepitaxial layers is also demonstrated by PL measurements showing excited states of donor bound and free excitons. Further the extreme homogeneity of the PL was revealed by area scans. The net doping concentration is only $6 \times 10^{14}\,cm^{-3}$, the concentration of Al is with $3 \times 10^{13}\,cm^{-3}$ orders of magnitude lower than in heteroepitaxial thin films.

6.4   A ZnO Microwire Laser

C. Czekalla, A. Rahm, T. Nobis, J. Lenzner, M. Grundmann

We report lasing phenomena in hexagonally shaped ZnO microwires grown by thermal evaporation of a pressed carbon/ZnO target (mass ratio 1:1). Structures with diameters in a range from a few hundred nanometers to several hundred micrometers can be achieved by this process [1]. The microwires show a high photoluminescence (PL) signal under low excitation conditions. They were isolated on a carbon gluepad, making PL emission from single structures observable by spatially resolved photoluminescence spectroscopy. The emitted light was detected perpendicular to the wire axis.

Figure 6.5a shows spectra measured under low (cw) and high (pulsed, 10 ns, 20 Hz) and high excitation conditions. The cw spectrum (grey curve) shows the emission peak of the free exciton at 3.28 eV and its first LO phonon replica at 3.20 eV. At higher excitation intensities (black curves) an additional peak arises on the lower energy side
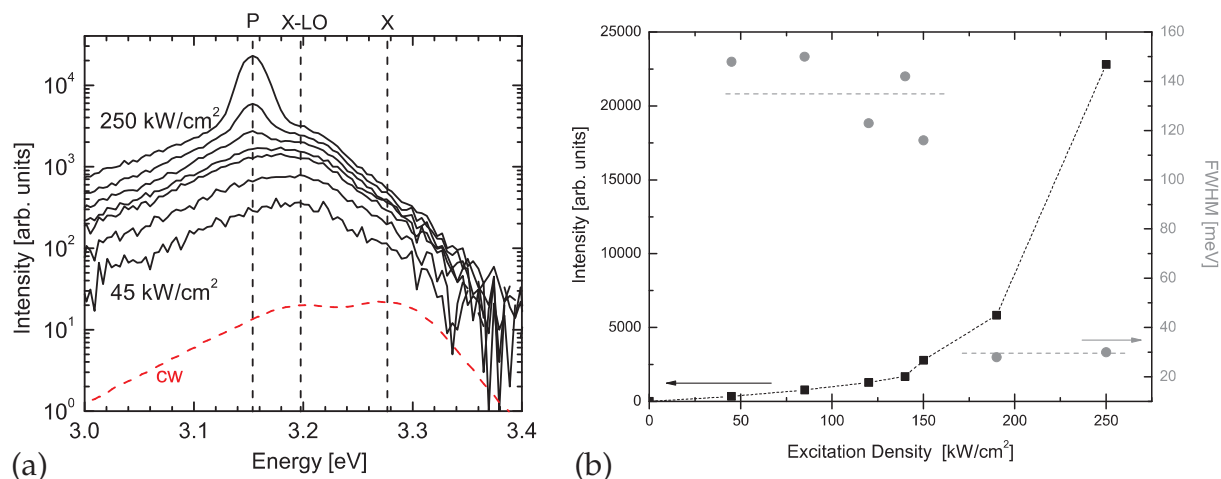
Figure 6.5: (**a**) PL specrta taken under low (*grey curve*) and high excitation conditions at room temperature. (**b**) Intensity of the peak at 3.15 eV and FWHM of the peak as a function of the excitation intensity. The lasing threshols is found to be 150 kW/cm^2.

of the free exciton peak at 3.15 eV. This is most probably related to exciton exciton collision processes and called P-band. The peak is growing superlinearly with the pump intensity as depicted in Fig. 6.5b. The FWHM is 88 meV for 85 kW/cm^2 and 29 meV for 250 kW/cm^2, indicating spectral narrowing and a phase transition to lasing at a threshold of 150 kW/cm^2.

This work was supported by the DFG within FOR522 and the EU within NANDOS.

[1] M. Lorenz et. al.: Ann. Phys. **13**, 39 (2004)

6.5 Ordered Growth of Tilted ZnO Nanowires: Morphological, Structural and Optical Characterization

J. Zúñiga-Pérez[*], A. Rahm, C. Czekalla, J. Lenzner, M. Lorenz, M. Grundmann

[*]present address: Centre de Recherche sur l'Hétéro-Epitaxie et ses Applications (CRHEA), Centre National de la Recherche Scientifique (CNRS), Valbonne, France

Semiconducting nanowires have shown up as excellent building blocks for nanodevices and nanosensors that make use of their doping possibilities and the ability to control their exact position. Currently, a huge effort is being devoted to studying ZnO nanostructures due to ZnO intrinsic properties, such as its high exciton binding energy or its piezoelectric character, as well as to the fact that ZnO presents the richest family of morphologies and branched structures [1]. The most common ZnO nanostructures consist on an array of ZnO nanowires growing perpendicularly to the substrate. However, new functionalities might require an ordered array of nanowires that, while maintaining a long range order, grow in directions other than the substrate normal.

With this aim we have grown tilted ZnO nanowires that are inclined at 30° with respect to the substrate normal, as can be seen in Fig. 6.6. The growth was carried out by
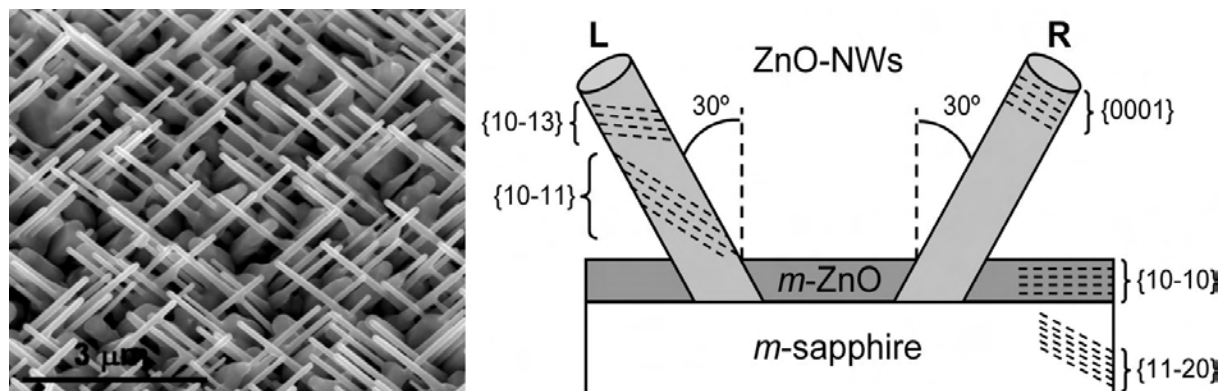
Figure 6.6: SEM image of ZnO nanowires grown on *m*-plane sapphire (*left*) and schematic representation of a typical sample (*right*).

high-pressure pulsed laser deposition (PLD) on *m*-plane sapphire without employing any catalyst species. The nanowires show well-defined epitaxial relationships with the *m*-plane sapphire substrate, the projection of the nanowires $\langle 0001 \rangle$ axis being parallel to the in-plane sapphire $[\bar{1}2\bar{1}0]$ direction [2]. High resolution X-ray diffraction indicates that all samples consist of two families of nanowires, tilted in opposite directions, and a nonpolar *m*-plane ZnO layer in between (see Fig. 6.6). Within the initial growth stages two sets of nanowires differing in diameter and length coexist, but only the narrowest and longest nanowires are found to keep on growing as deposition proceeds. A systematic study of the effects of growth conditions, including number of pulses, temperature, total pressure and oxygen partial pressure, has been carried out to determine those conditions under which a completely ordered array of tilted nanowires, with a minimum angular distribution, is obtained. Among the growth conditions, temperature and oxygen partial pressure are seen to mainly affect the nanowires axial and lateral growth rates, respectively, while the total chamber pressure allows monitoring of the evolution from thin film growth at low pressures, to a mixture of nanowires/nanobelt growth at high pressures. Finally, cathodoluminescence shows that low growth temperatures and high oxygen partial pressures improve the overall optical quality of the ZnO nanowires array.

[1] Z.L. Wang: Mater. Today **7**, 26 (2004)
[2] J. Zúñiga-Pérez et al.: Nanotechnology **18**, 195 303 (2007)

6.6 BaTiO₃-ZnO Heterojunctions Grown by Pulsed-Laser Deposition

M. Brandt, H. von Wenckstern, G. Biehne, H. Hochmuth, M. Lorenz, M. Grundmann V. Voora* M. Schubert*

*Department of Electrical Engineering, University of Nebraska-Licoln, Lincoln, USA

Both ZnO and BaTiO₃ (BTO) have received considerable interest by researchers in the past decades. While ZnO crystallizes in the wurzite structure, showing a spontaneous
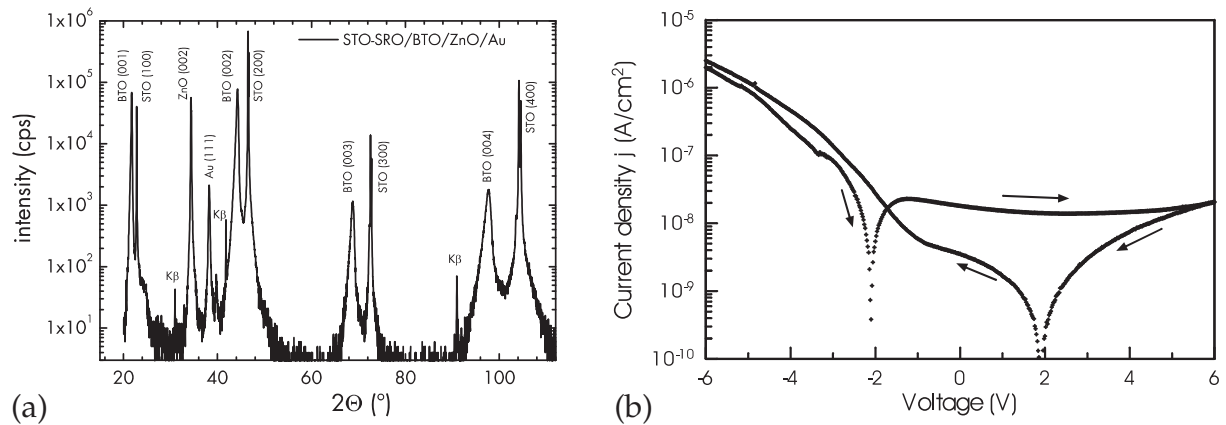
Figure 6.7: Results of XRD (**a**) and *I–V* (**b**) measurements, indicating the high crystalline quality and the low leakage currents of the junctions.

polarization, which is fixed parallel to the crystallographic c-axis, the spontaneous polarization in ferroelectric BTO can be controlled by an external electrical field. The formation of heterostructures of these materials results in a coupling of these polarizations enabling a variety of applications as polarization probes, optical switches, transparent non-volatile memory elements and transparent field effect transistors [1, 2].

Previously, BTO layers have been deposited by pulsed-laser deposition (PLD) on Si (100) and sapphire substrates, using a Pt back-contact in some cases [2]. Although these junctions did show the expected polarization coupling [3], significant drawbacks where observed. Polycrystallinity of the BTO layer resulted in high leakage currents through the junctions.

In order to overcome these problems, BTO thin films have been grown on lattice matched (100) $SrTiO_3$ substrates by PLD. To form ohmic back contacts, a conductive 70 nm thin $SrTiO_3$ layer has been deposited on the substrate prior to the deposition of the 800 nm thin BTO film. A 400 nm ZnO layer was grown ex situ, and ohmic Au contacts have been DC sputtered on the ZnO. XRD measurements have been performed on the heterostructures using a Philips X'Pert with Cu K_α radiation. A typical $2\Theta-\omega$ scan is depicted in Figure 6.7a showing (001) orientation of the BTO and (0001) orientation of the ZnO. Even the Au contact pads show a preferential (111) orientation. The junctions have been investigated by current-voltage (*I–V*) measurements. Figure 6.7b depicts an *I–V* curve showing both asymmetric current hysteresis and small leakage currents within the junctions, being three orders of magnitude smaller than in the previous structures [3].

[1] B.N. Mbenkum et al.: Appl. Phys. Lett. **86**, 091 904 (2005)
[2] J. Siddiqui et al.: Appl. Phys. Lett. **88**, 212 903 (2006)
[3] N. Ashkenov et al.: Thin Solid Films **486**, 153-157 (2005)

6.7   VLS-Growth of Binary and Ternary III–As Nanowires

J. Bauer[*], V. Gottschalch[*], G. Wagner[*], G. Benndorf

[*]Fakultät für Chemie und Mineralogie, AK Halbleiterchemie

The homoepitaxial vapor-liquid-solid (VLS) growth of GaAs and InAs nanowires was investigated using low-pressure metal-organic vapor phase epitaxy (MOVPE). To achieve an upright growth direction GaAs $(\bar{1}\bar{1}\bar{1})_{As}$ substrates were used. In the case of InAs nanowire growth the GaAs substrate was first covered by an upto 150 nm thick InAs island layer. For nanowire growth Au-based liquid alloy particles were used. They were formed due to alloying of a thin, evaporated gold film with the underlaying GaAs substrate or InAs island layer. Arsine was chosen as group-V source material and TMGa or TMIn as group-III precursor for GaAs or InAs, respectively. Typical SEM images are shown in Fig. 6.8 and Fig. 6.9. For GaAs nanowire growth three stages are found during the growth process. The starting point before TMGa is supplied is the liquid alloy droplet in a thermodynamic equilibrium composition state. At this time arsine is present in the gas-phase to stabilize the free GaAs substrate surface. With the supply of TMGa the droplet is driven to solve more gallium. Thus, the droplet volume increases, but the droplet wetting changes to a higher contact angle of the droplet on top of the already growing nanowire accompanied by a decrease in the contact area. The nanowire foot-section is formed (Fig. 6.8). The droplet composition reaches a quasi-stationary equilibrium state, where the same gallium amount that arrives the droplet also crystallizes to GaAs. So, the nanowire cross-section does not change and the column-like body-section grows until the TMGa is switches off. As a result, the excess gallium is crystallized from the droplet to form the neck-part of the GaAs nanowire. On top of the nanowires always the (Au,Ga,As) alloy particle is present. It has to be emphasized, that the arsenic in the gas-phase is necessary during the neck-formation. If arsine is switch off together with the TMGa, no neck is grown. The gallium depen-
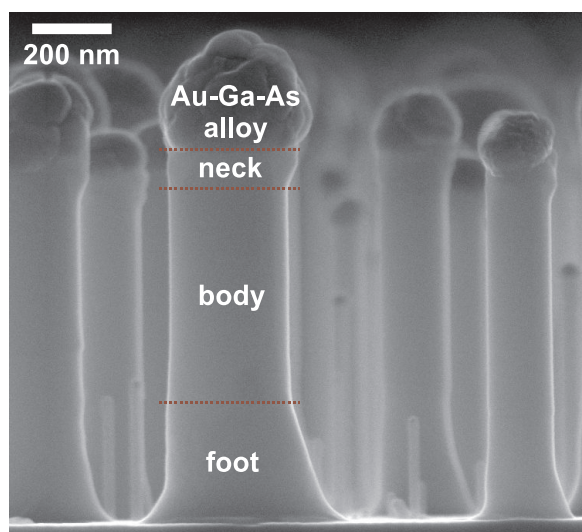
Figure 6.8: GaAs nanowires grown on GaAs $(\bar{1}\bar{1}\bar{1})_{As}$.
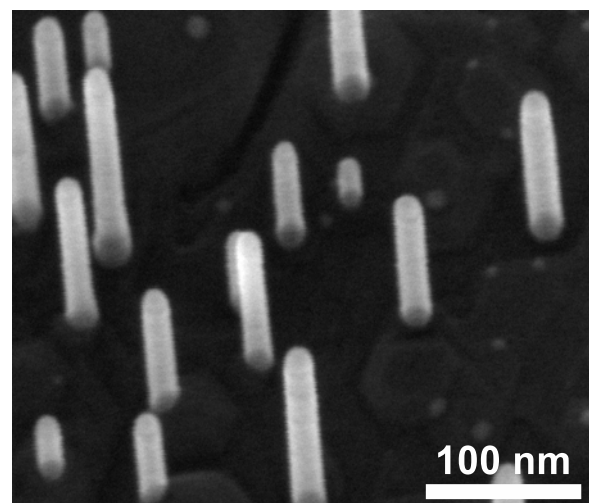
Figure 6.9: InAs nanowires grown on InAs/GaAs $(\bar{1}\bar{1}\bar{1})_{As}$.

dent wetting behavior can be applied to mark the nanowire with a bump by performing a TMGa break during nanowire growth. The GaAs nanowires have sphalerite structure. In $(\bar{1}\bar{1}\bar{1})_{As}$ growth direction twin sections are formed. The investigated InAs nanowires have wurtzite structure with almost twinned sphalerite lamella. However, they have a column-like structure with diameters less than 22 nm. Increasing the V/III ratio from 10 to 80, InAs layer growth was verified on the free GaAs substrate regions between the InAs islands. Furthermore, the InAs nanowires often exhibit a kind of foot-section. These appearances are still under investigation.

Beside the pure binary compounds we investigated the growth of (InGa)As sections embedded into GaAs nanowires. To create these hetero-structures TMIn was spontaneously supplied for a certain time with the partial pressure ratio TMGa/TMIn = 2. Using EDX mapping (Fig. 6.10) we verified the existance the (InGa)As-section in every nanowire. For a more quantitatively examination we made EDX linescans of single hetero-structure nanowires (Fig. 6.11). Obviously, the first hetero-junction is relatively abrupt not exceeding a few nm, while the second one shows a more diffusive slope over some 10 nm. We investigated the influence of important growth parameters on the composition of the (InGa)As-section. A very interesting result is, that with increasing growth time the In content increases. This fact indicates, that the In is first accumulated in the droplet and the incorporation may start later. In the temperature range of 450 to 490 °C the In content keeps constant. With increasing V/III ratio less In is incorporated into the (InGa)As segment. In contrast, the In fraction can be increased making a break
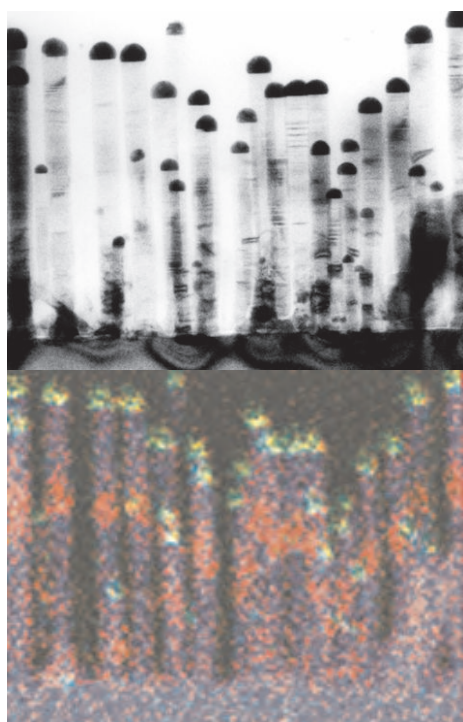
Figure 6.10: TEM bright-field (*top*) and EDX mapping (*bottom*) of GaAs/(InGa)As/GaAs double hetero-structure nanowires. The (InGa)As sections are marked *red*.
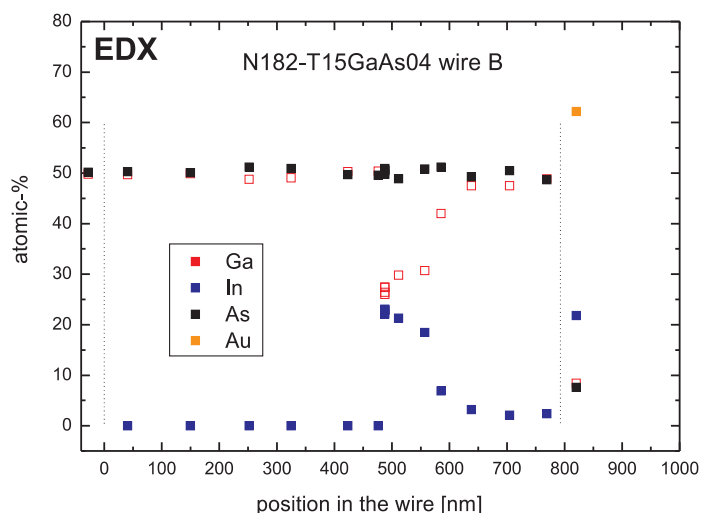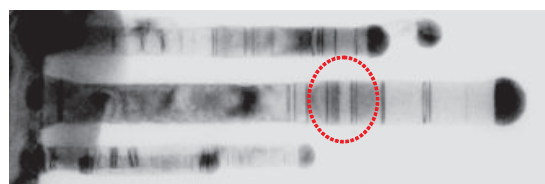
Figure 6.11: EDX line scan of a GaAs/(InGa)As/GaAs double hetero-structure nanowire.

before and after the (InGa)As growth. First RT photoluminescence investigations show a broad emission band in the IR region (1 eV).

[1] J. Bauer et al.: J. Cryst. Growth **298**, 625 (2007)

6.8　Temperature-Dependence of the Refractive Index and the Optical Transitions at the Fundamental Band-Gap of ZnO

R. Schmidt-Grund, N. Ashkenov[*], M. Schubert[†], W. Czakai[‡], D. Faltermeier[§], G. Benndorf, H. Hochmuth, M. Lorenz, M. Grundmann

[*]present adress: OPTEG GmbH, Leipzig
[†]Department of Electrical Engineering, University of Nebraska-Lincoln, Lincoln, USA
[‡]present adress: X-FAB Semiconductor Foundries AG, Erfurt
[§]1. Physikalisches Institut, Universität Stuttgart

We report on the temperature dependence of the dielectric function (DF) of ZnO determined using spectroscopic ellipsometry at temperatures between 5 K and 829 K and on energies and broadening parameters of the fundamental Γ-point band-to-band transitions and their respective excitonic properties as well as the below-band-gap refractive index, obtained from an (0001)-oriented ZnO thin film sample (thickness: 800 nm), which has been grown using pulsed laser deposition (PLD) on sapphire substrate [1].

　　Using spectroscopic ellipsometry with subsequent layer model analysis of the measured spectra, the DF for the polarization perpendicular to the wurtzite c-axis have been determined (Fig. 6.12). The analysis of the DF spectra using line shape model functions including contributions due to the fundamental band-to-band transitions ($\epsilon^{3DM_0;A;B;C}$) and their free discrete ($\epsilon^{dex;A;B;C}$) as well as continuum ($\epsilon^{exc;A;B;C}$) excitonic polarizabilities yields transition energies, exciton properties, and the below-band-gap refractive
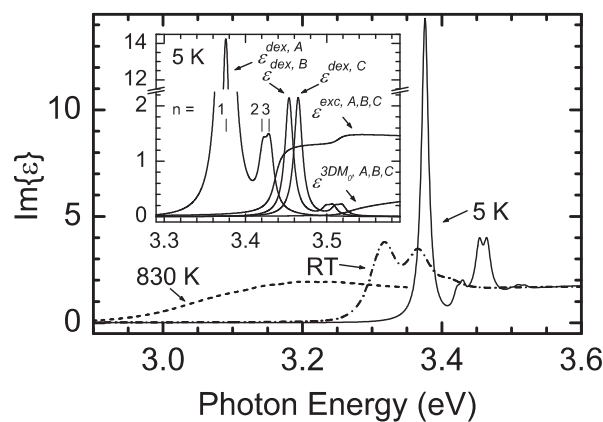
Figure 6.12: ZnO dielectric function for polarization perpendicular to the c-axis for selected temperatures. In the *inset*, the individual contributions to the DF are shown for $T = 5$ K.
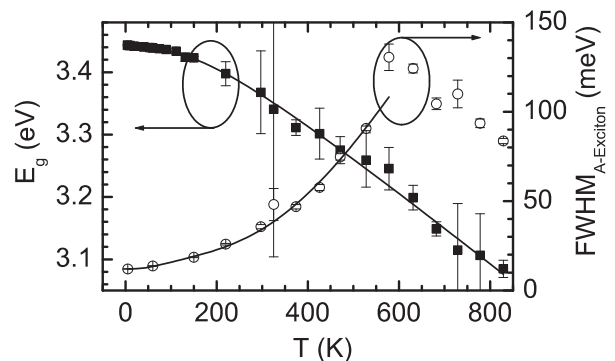
Figure 6.13: Temperature dependence of E_g (*filled symbols*) and the *FWHM* of the *A*-exciton (*open symbols*). The lines represent two-oscillator model calculations (6.2) (see Tab. 6.2).

Table 6.2: Two-Oscillator model parameters (6.2). Note that $W_2 = 1 - W_1$.

	$E_g(0\,\text{K})/FWHM(0\,\text{K})$ (eV)	α (10^{-4} eV/K)	θ_1 (K)	θ_2 (K)	W_1
$E_g(T)$	3.4427 ± 0.0006	5.9 ± 0.6	127 ± 15	616 ± 30	0.3 ± 0.2
$FWHM_{A-\text{exciton}}(T)$	$(12.1 \pm 0.2) \times 10^{-4}$	5.5 ± 0.8	110 ± 25	uncertain	uncertain

index as function of temperature [2]. A, B, and C denote the fundamental band-to-band transitions from the three topmost valence bands to the lowest conduction band E^A, E^B, and E^C, respectively. The low temperature ellipsometry data are supplemented by photoluminescence data taken in the temperature range $4-200$ K.

From the transition energies A, B, and C the spin orbit coupling (Δ_{so}) and crystal-field splitting (Δ_{cf}) parameters have been found using the quasi-cubic model approach [3], which allows for separation of the fundamental band-to-band transition energy E_g. A strong temperature-dependence of Δ_{cf} was found. We explain this behaviour as caused by internal strain within the thin film due to different thermal expansion coefficients between the film and the substrate. The strong redshift of E_g with increasing temperature can be well explained by electron-phonon interactions, which causes also the strong increase of the homogeneous broadening ($FWHM$) of the exciton transition. The two-oscillator model [4]:

$$X(T) = X(0\,\text{K}) \mp \alpha \sum_{i=1}^{2} \frac{W_i \theta_i}{\exp(\theta_i/T) - 1} \,, \tag{6.2}$$

where X stands for E_g and $FWHM$, θ_i denotes the phonon temperatures, W_i their relative weights, and α the high temperature slope, accounts for acoustic and optic phonon branches and was used for interpretation of the observed temperature dependence of E_g and the $FWHM$ of the A-exciton ($FWHM_{A-\text{exciton}}$), which can be seen in Fig. 6.13. In Tab. 6.2, the two-oscillator model parameters are given. The model parameters for E_g and $FWHM_{A-\text{exciton}}$ match well with each other. As can be seen in Fig. 6.13, $FWHM_{A-\text{exciton}}(T)$ can be well described by electron-phonon interactions up to temperatures of about 550 K.

The ZnO below-band-gap refractive index n for the polarization perpendicular to the c-axis was found, within the error bars, to depend linearly on the temperature. The temperature dependence dn/dT further depends almost linearly on the photon energy E:

$$dn/dT = (dn/dT)_0 + (dn/dT)_1 \times E \,, \tag{6.3}$$

with $(dn/dT)_0 = 4.1 \times 10^{-5}\,\text{K}^{-1}$ and $(dn/dT)_1 = 2.3 \times 10^{-5}\,(\text{eV K})^{-1}$. Note, these values are valid for the thin film and depend on the internal strain because of the strain induced shift of the band-to-band transition energies. The influence of the strain on dn/dT can be estimated to be less than $1 \times 10^{-5}\,\text{K}^{-1}$.

[1] R. Schmidt-Grund et al.: AIP Conf. Proc. **893**, 271 (2007)
[2] R. Schmidt et al.: Appl. Phys. Lett. **82**, 2260 (2003)
[3] J.J. Hopfield: J. Phys. Chem. Solids **15**, 97 (1960)
[4] R. Pässler: J. Appl. Phys. **89**, 6235 (2001)

6.9   The Influence of the Orientation and Thickness of ZnO-Layers on the Dielectric Function

C. Sturm, R. Schmidt-Grund, T. Chavdarov, B. Rheinländer, H. Hochmuth, J. Zúñiga-Pérez*, M. Lorenz, M. Grundmann

*present address: Centre de Recherche sur l'Hétéro-Epitaxie et ses Applications (CRHEA),
Centre National de la Recherche Scientifique (CNRS), Valbonne, France

ZnO is a direct band gap semiconductor with a wurtzite crystal structure. Due to its optical properties, such as the band-gap energy of $E = 3.4\,\mathrm{eV}$, it is an interesting material for optoelectronic devices. Due to the wurtzite structure of ZnO the dielectric function (DF) is a tensor with the two independent components $\varepsilon_\perp$ and $\varepsilon_\parallel$. The DF of ZnO single bulk crystals is well known, however, the influence of the film orientation and thickness on the DF is mostly unknown. We use generalized Ellipsometry to study a-plane and m-plane ZnO films with layer thicknesses of 30 nm to 610 nm in the spectral range $0.05 - 0.15\,\mathrm{eV}$ and $(0.75 - 4.5)\,\mathrm{eV}$.

The a-plane and m-plane ZnO films were deposited on r-plane and m-plane sapphire, respectively, by Pulsed Laser Deposition (PLD). The DF was obtained using a line shape analysis which contain a model dielectric function (MDF) approach. At the infrared spectral range the MDF consists of contributions of the lattice vibrations and free charge carriers. In the band-gap energy range an approach suggested by Adachi [2] was used.

In comparison with the DF of an a-plane single bulk crystal and c-plane films, which agree very well with each other, the exciton peaks of the a-plane and m-plane films are shifted to higher energies and are broader (Fig. 6.14a). The DF of a-plane films with different film thicknesses were compared to each other and agree very well for film thicknesses $d \geq 200\,\mathrm{nm}$. However we found for film thicknesses $d \leq 75\,\mathrm{nm}$ a shift of the exciton peak energy and an increased broadening compared to the thickest one. Infrared spectroscopic ellipsometry shows a high free charge carrier concentration of the ZnO layer at the ZnO-sapphire interface for the a-plane and m-plane ZnO samples. However, the concentration is too small to explain the shift only with help of Burstein-Moss effect
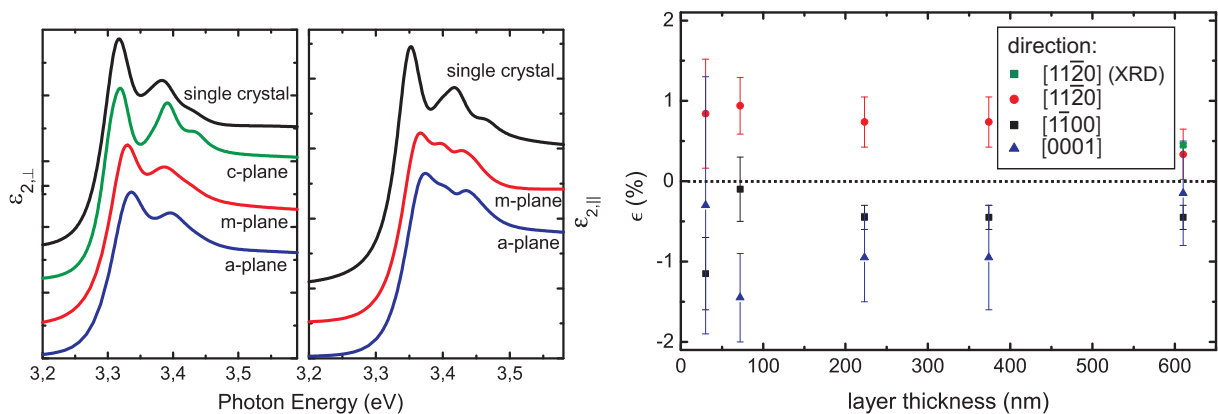
Figure 6.14: (a) Imaginary part of the DF for different orientations of the ZnO layer. Due to the low sensivity $\varepsilon_{2,\parallel}$ is not shown for c-ZnO . (b) Calculated strain for the a-plane ZnO layers.

and band-gap renormalization. X-ray diffraction measurements yield a larger value of the [11$\bar{2}$0]-lattice constant of the a-plane films compared to the single bulk crystal one. Since surface over layer effects and thickness non-uniformity can be excluded as responsible for the shift we evoke strain effects. To estimate the strain of the layers we use $\mathbf{k} \cdot \mathbf{p}$ theory [1]. The results are shown in Fig. 6.14b. We obtained a tensile strain in [11$\bar{2}$0]-direction which is in good agreement to the result of the XRD measurements $\varepsilon_{[11\bar{2}0]} = (0.45 \pm 0.02)\,\%$ of the thickest a-plane layer. We can conclude that the strain effects are sufficiently to explain the observed shifts.

[1] M. Suzuki et al.: J. Appl. Phys. **80**, 6868 (1996)
[2] S. Adachi: *Properties of group-IV, III–V and II–VI Semiconductors* (Wiley, Chichester 2005)

6.10   Electronic and Optical Properties of Group-II Oxides

D. Fritsch, H. Schmidt, M. Grundmann

The Empirical Pseudopotential Method (EPM) has been used to investigate the electronic and optical properties of the semiconducting group-II compounds wurtzite ZnO and rocksalt MgO. Thereby, the adjustable parameters of the ionic model potential have been fitted to experimentally well-known low-temperature transition energies through a simplex-like fitting procedure [1]. The calculations account for relativistic effects in form of the spin–orbit interaction as well as for the nonlocality of the pseudopotential through additionally applied nonlocal correction terms. Special emphasis has been laid on the transferability of the model potential parameters between different crystal structures. The electronic properties, such as band energies and derived Luttinger and Luttinger-like parameters for the rocksalt MgO and wurtzite ZnO are in favourable agreement with other experimental and theoretical findings. The whole data set regarding the electronic and optical properties of MgO and ZnO can be found in [2].

The eigenfunctions of the pseudo-wave-equation have been used to calculate the polarization-dependent transition matrix elements. A subsequent Brillouin zone integration by means of the Linear Tetrahedron Method (LTM) [3] yielded the imaginary part of the dielectric function for wurtzite ZnO. Thereby, the irreducible part of the Brillouin zone has been transferred to surface integrals in subprisms which can be evaluated numerically a lot easier. A grid of 135 $\mathbf{k}$ points defines the vertices of those subprims. For illustration, a division of the irreducible part of the Brillouin zone in only eight subprims is schematically shown in Fig. 6.15a.

The contributions to the dielectric function from the eight subprisms together with the whole dielectric function of wurtzite ZnO are shown in Fig. 6.15b. Based on the subprism data, the contributions to the dielectric function are attributed to special regions (subprisms) of the Brillouin zone. It has been shown that contributions to the low-energy part of the dielectric function solely originate from the subprism which contains the Γ-point.

In summary, $\mathbf{k}$-points at high-symmetry lines and within the Brillouin zone have been identified whose band-band-transitions contribute mainly to the dielectric function. The localisation of the $\mathbf{k}$ values within the Brillouin zone and the identification
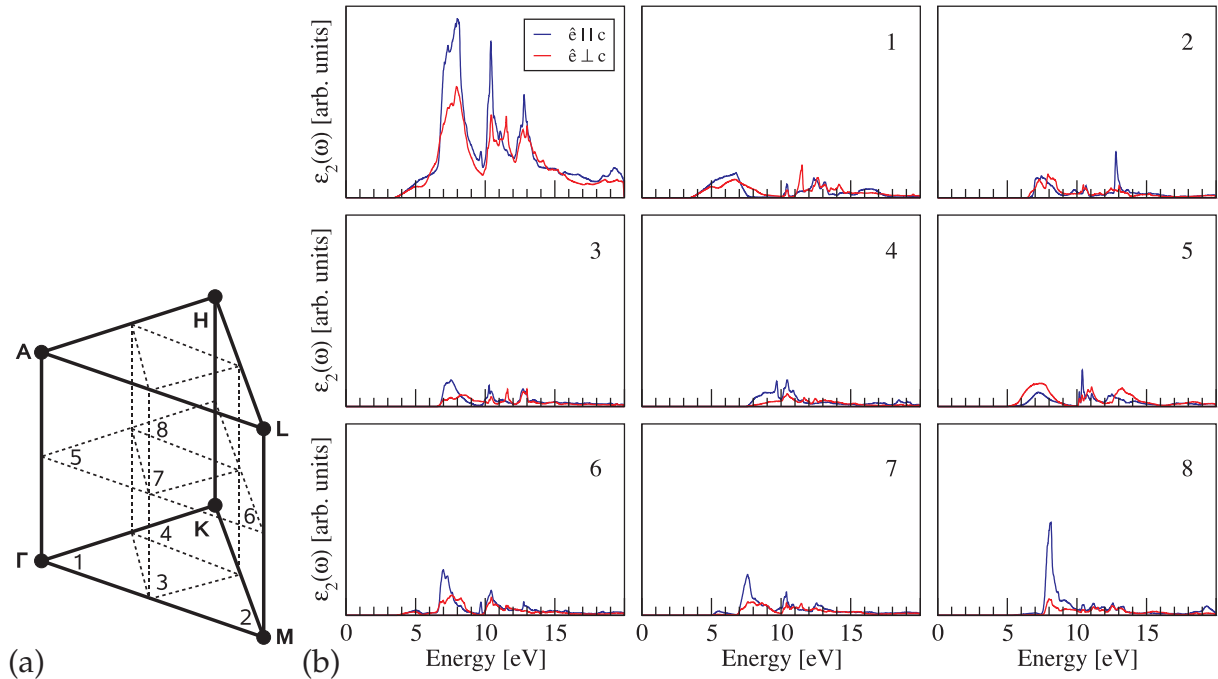
Figure 6.15: (**a**) Subdivision of the irreducible part of the hexagonal Brillouin zone into eight subprisms. (**b**) Polarisation dependent imaginary part of the dielectric function of wurtzite ZnO. Shown are the contributions from the subprisms 1 to 8 and its sum (upper left). For $\hat{e}\|c$ and $\hat{e}\perp c$ the component of electric field of the electromagnetic wave with energy from 0 eV to 20 eV lies parallel and perpendicular to the c-axis of ZnO, respectively.

of band-band-transitions allow for an assignment of band-band-transitions in the electronic band structure to critical points in the dielectric function. This identification of band-band-transitions which contribute to critical points in the dielectric function is only possible by band structure calculations. Therefore, the presented dielectric function is an important step towards the detailed understanding of the optical properties of wurtzite ZnO.

This work was financially supported by the Network of Excellence SANDiE (NMP4-CT-2004-500101).

[1] M. Goano et al.: J. Appl. Phys. **88**, 6467 (2000)
[2] D. Fritsch: PhD thesis, submitted December 2006
[3] G. Lehmann, M. Taut: Phys. Stat. Sol. B **54**, 469 (1972)

6.11   Electronic Properties of Group-III Nitrides

D. Fritsch, H. Schmidt, M. Grundmann

The electronic and optical properties of the group-III nitride compound semiconductors AlN, GaN, and InN have been calculated by means of the Empirical Pseudopotential Method (EPM). Thereby, the model potential parameters of the ionic model potential used [1] have been adjusted to experimentally well-known low-temperature transition energies with special emphasis laid on the transferability between the different crystal
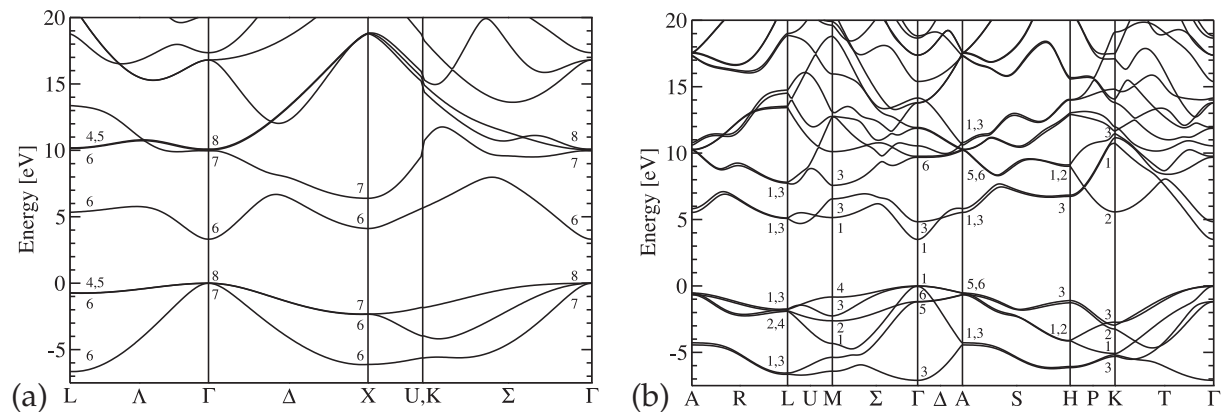
Figure 6.16: Calculated band structure of (**a**) zinc-blende GaN and of (**b**) wurtzite GaN along high symmetry lines in the Brillouin zone.

structures. Additionally, relativistic correction terms and nonlocal model potentials have been taken into account to allow for the accurate description of the spin–orbit interaction and the nonlocality of the pseudopotential. The various parameters have been obtained through a simplex-like fitting procedure [2]. As an example the electronic band structures of zinc-blende and wurtzite GaN are shown in Fig. 6.16a and 6.16b. The electronic properties such as band energies are in favourable agreement with other theoretical and experimental findings.

The accurate description of the valence and conduction band energies allows for the determination of the Luttinger and Luttinger-like parameters of the zinc-blende and wurtzite type crystals and their related effective masses. It has been shown that the calculated material parameters are again in favourable agreement with other published results. The full set of transition energies at critical points in the zinc-blende and wurtzite Brillouin zone, the material parameters such as Luttinger and Luttinger-like parameters and related effective masses and polarization-dependent transition matrix elements can be found in [3].

This work was financially supported by the Network of Excellence SANDiE (NMP4-CT-2004-500101).

[1] N.W. Ashcroft: Phys. Lett. **23**, 48 (1966)
[2] M. Goano et al.: J. Appl. Phys. **88**, 6467 (2000)
[3] D. Fritsch: PhD thesis, submitted December 2006.

6.12 Development of High-Speed ZnO Schottky Diodes

H. von Wenckstern, G. Biehne, M. Grundmann

High-speed ZnO Schottky diodes have been fabricated on insulating sapphire substrates. Normally Schottky diodes are processed in a so-called front-to-front contact configuration as depicted in Fig. 6.17. In such a configuration a circular Schottky contact is surrounded by an ohmic annulus. The separation between the Schottky and the ohmic contact is usually several hundreds of microns. This is the region determining the series
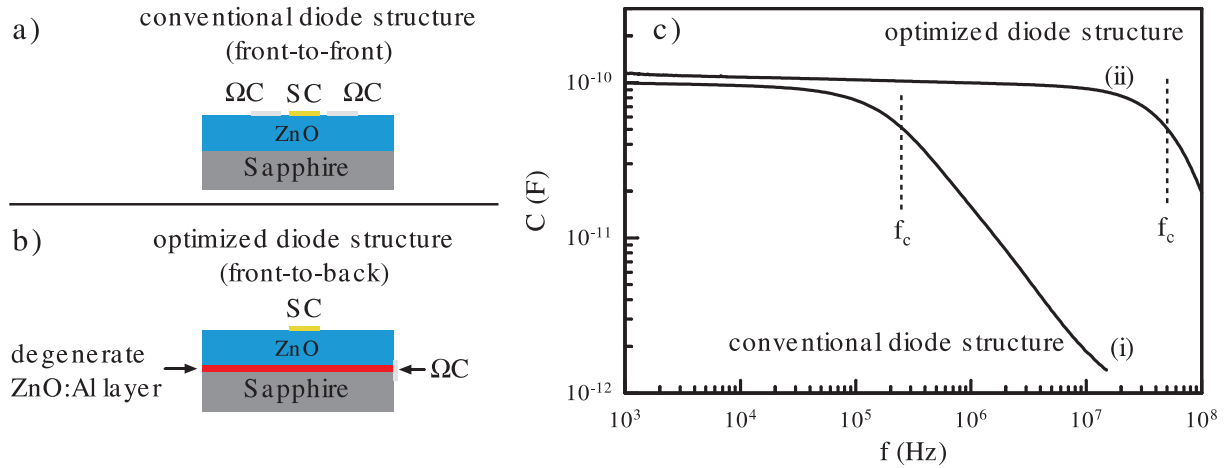
Figure 6.17: Schottky diode contact schemes (**a**,**b**) and frequency dispersion of the diode capacitance (**c**). *SC* denotes the Pd Schottky contacts and *ΩC* the ohmic contacts.

resistance of the diode structure. We developed an alternative way enabling a tremendous reduction of the diodes series resistance. For that a degenerately doped ZnO:Al layer of about $50-100\,\mathrm{nm}$ thickness is grown first. On top of that the about $1\,\mu\mathrm{m}$ thick ZnO main layer is grown. The degenerate ZnO:Al layer serves as ohmic back contact and the region determining the series resistance of such a front-to-back contact configuration extends only from the end of depletion region towards the ZnO:Al. This distance is smaller than the sample thickness ($< 1\,\mu\mathrm{m}$). The series resistance of a conventional front-to-front ZnO Schottky diode is in the $\mathrm{k}\Omega$ range, whereas the series resistance of our novel diode structures ranges between 20 and about $200\,\Omega$ [1]. Figure 6.17 demonstrates the advantage of the novel diode layout, for which the maximal frequency of operation f_c (the 3db cut-off frequency) is $3\times10^7\,\mathrm{Hz}$ and thus more than a factor of hundred higher than for the conventional front-to-front contact configuration.

[1] H. von Wenckstern et al.: Appl. Phys. Lett. **88**, 092 102 (2006)

6.13 Exact Solution for the Capacitance of a Current-Free Schottky Diode

M. Schmidt, R. Pickenhain, M. Grundmann

Up to now there are only approximate solutions for the capacitance C of a Schottky diode existing. In this work we developed general expressions for the capacitance of homogeniously doped space charge regions (SCR) at semiconductor interfaces, which have been applied to Schottky diodes.

Usually a completely depleted SCR of width w without mobile charge carriers is assumed. The potential distribution $\Phi(x)$ is calculated from Poisson's equation and the capacitance can be obtained. In this work free carriers in the SCR are treated only under the assumption of a non-degenerate semiconductor. The capacitance of a Schottky diode can be calculated analytically without solving Poisson's equation explicitly [1].
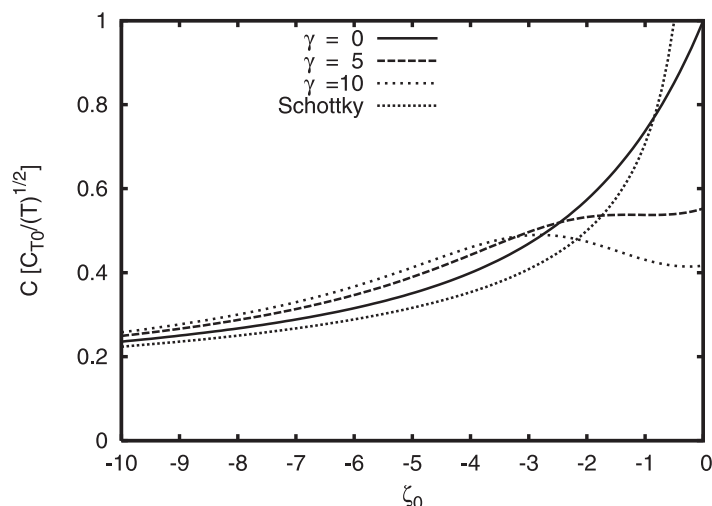
Figure 6.18: Capacitance of a Schottky diode in classical theory and exact solution ($\zeta_0 = e\Phi/k_\text{B}T$).

For a reverse biased diode our solution coincides with the capacitance obtained from classical Schottky theory. While in the classical theory the capacitance diverges in the flatband case, the exact solution takes a finite value (Fig. 6.18). As shown in [2] the temperature dependence of the concentration of free charge carriers can be obtained from capacitance–voltage measurements at different temperatures, an approach directly arising from our new theory.

[1] M. Schmidt et al.: Sol. State. Electron. (2007), in press
[2] M. Schmidt: Diplomarbeit, Universität Leipzig 2006

6.14 Electrical Properties of ZnO Thin Films Grown under Different Oxygen Partial Pressures

H. von Wenckstern, M. Brandt, H. Hochmuth, M. Lorenz, M. Grundmann

Four nominally undoped ZnO thin films were grown heteroepitaxially on a-plane sapphire substrates by pulsed-laser deposition. The growth temperature was 750 °C and the oxygen partial pressure (p_{O_2}) was set between 10^{-2} and 1 mbar. After growth electrical contacts were realized by sputtering Au contacts at the corners of the samples. The current-voltage characteristics of these contacts exhibit linear behavior; the contacts are well suited for Hall measurements using the van der Pauw method. Such measurements were carried out between about 20 K and about 325 K for all of the four samples. The temperature dependence of the free carrier concentration n_H and the Hall mobility μ_H are depicted in Fig. 6.19. Samples grown at $p_{O_2} \leq 3 \times 10^{-2}$ mbar turn insulating due to carrier freeze-out for $T < 80$ K. The two samples grown at the larger p_{O_2} show an unexpected behavior for $T < 80$ K: n_H shows a minimum, increases again and remains than constant for the lowest temperatures; μ_H becomes independent off T. Such behavior can be understood considering two parallel conduction paths. One, determining the electrical properties (n_2, μ_2) at low temperatures, is a thin degenerate layer being most
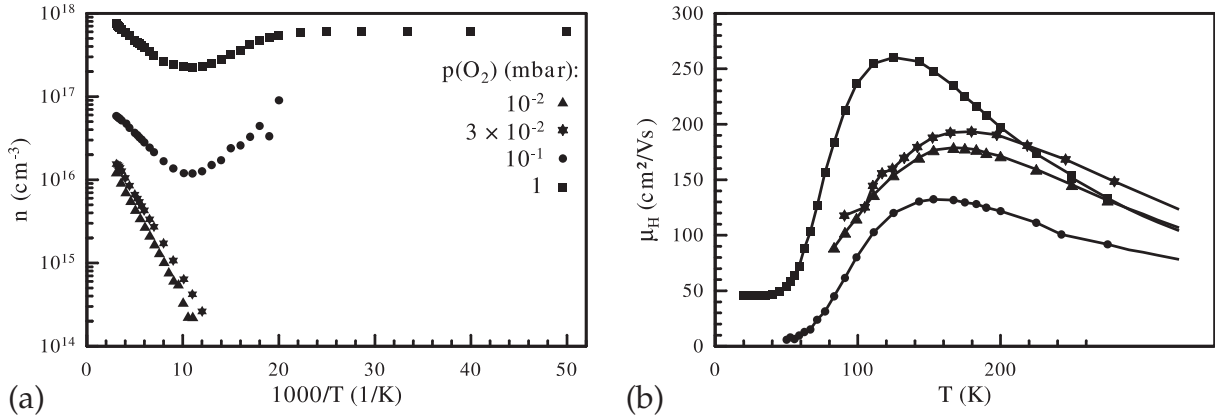
Figure 6.19: Free electron concentration (**a**) and Hall mobility (**b**) of ZnO thin films grown using different oxygen partial pressures as indicated in (**a**).

probably localized at the sapphire/ZnO interface, the other is the comparatively thick (about 1 μm) ZnO main layer (n_1, μ_1). Since the electrical properties of the degenerate layer are independent of T the parallel conduction paths can be easily separated as

$$n_1 = \frac{(\mu_H n_H - \mu_2 n_2)^2}{\mu_H^2 n_H - \mu_2^2 n_2} \tag{6.4}$$

$$\mu_1 = \frac{\mu_H^2 n_H - \mu_2^2 n_2}{\mu_H n_H - \mu_2^2 n_2} . \tag{6.5}$$

The values of n_2 and μ_2 are obtained from the low temperature data as indicated at the axis of Fig. 6.20. The electrical properties of the ZnO main layer are than obtained using (6.4) and (6.5). The corrected free carrier concentration and Hall mobility of the sample grown at the highest p_{O_2} are depicted exemplarily in Fig. 6.20 (the same procedure was applied to the sample grown at 0.1 mbar, for the other two samples such
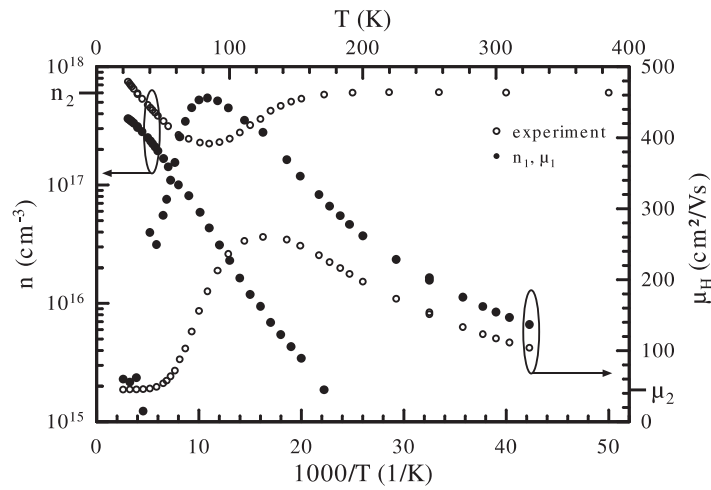
Figure 6.20: Measured Hall data (n_H, μ_H) of PLD thin film grown at oxygen partial pressure of 1 mbar and calculated Hall data (n_1, μ_1) of the main layer using the carrier concentration and mobility (n_2, μ_2) of the degenerate layer read off the graphs.

Table 6.3: Parameters of dominant donors of ZnO thin films grown at different $p(O_2)$.

p_{O_2} (mbar)	N_{d1} (10^{16} cm^{-3})	E_{d1} (meV)	N_{d2} (10^{16} cm^{-3})	E_{d2} (meV)	N_a (10^{15} cm^{-3})
10^{-2}	2	96	0.6	47	3
3×10^{-2}	1	110	0.5	51	3
10^{-1}	4	64	5	29	20
1	60	31	3	16	40

a procedure was not necessary). The Hall mobility of the ZnO main layers was fitted using Matthiessen's rule considering the following scattering mechanisms: ionized impurity, acoustic deformation potential, piezoelectric potential, polar-optical, and grain boundary scattering. From that, the density of compensating acceptors, the grain size, and the average barrier height between adjacent grains was obtained. The free carrier concentration was fitted using a two donor charge balance equation considering compensation. Here, the density and the thermal activation energy of the most shallow donor levels are deduced. The parameters obtained from the fitting procedure are listed in Tab. 6.3. The thermal activation energy of the free electron concentration decreases with increasing p_{O_2} as already obvious from Fig. 6.19. The samples grown at the lowest p_{O_2} have two dominant shallow donors with thermal activation energies of about 55 meV and about 100 meV, respectively. The more shallow defect might be an effective mass type defect, the deeper has a thermal activation energy being similar to that of E1. Its concentration decreases by increasing p_{O_2} and it is not a dominant donor for samples grown with $p_{O_2} \geq 0.1$ mbar. This suggests that this 100 meV donor is connected to the oxygen sublattice. The effective mass type donor is besides a shallow donor with thermal activation energy of about 29 meV also present in the sample grown at 0.1 mbar. The chemical origin of this 30 meV donor is so far unknown, however, it is the only dominant donor in the sample grown at the highest p_{O_2} of 1 mbar.

6.15 Investigation of Electron States in ZnO Using Thermal Admittance Spectroscopy

H. von Wenckstern, G. Biehne, M. Grundmann

Shallow and dominant donors in *n*-type semiconductors are usually investigated with Hall effect measurements yielding their thermal activation energy and their concentration. Deep defects (which means here, that the density of such a deep defect is about an order of magnitude lower than the density of the defect determining the position of the Fermi level) in semiconductors are characterized by deep level transient spectroscopy yielding their thermal activation energy, their density and the capture cross-section of the defect. Admittance spectroscopy provides a link between the two methods. The frequency dispersion of the capacitance and the conductance G of a diode is measured. Due to the temperature dependence of the emission rate e_n of a defect ($e_n \sim \sigma T^2 \exp(-E_t/kT)$, σ is the cross-section and E_t the thermal activation energy of the defect) the freeze-out temperature of a defect level depends on the measuring frequency (a defect responses only if the emission rate is smaller than the frequency of the alternating test voltage, the
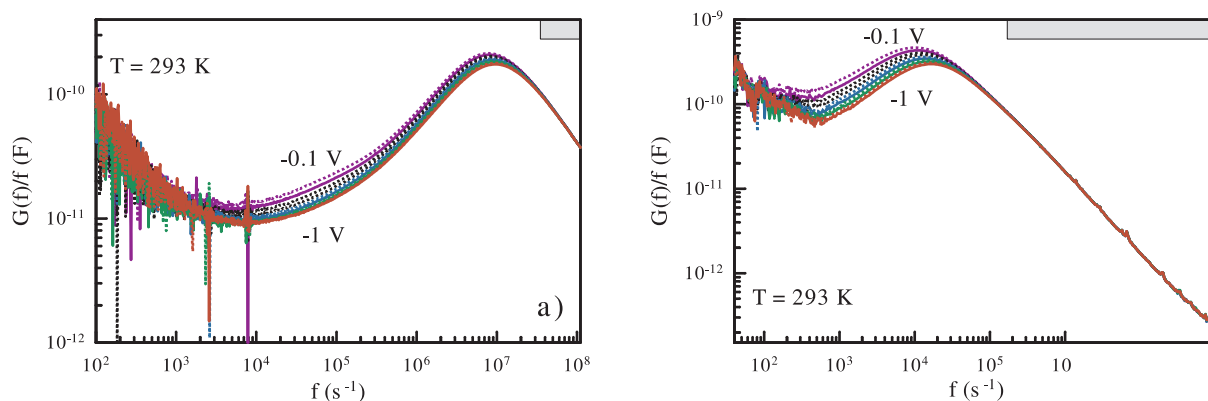
Figure 6.21: $G(f)/f$ plot of (**a**) ZnO PLD thin film and (**b**) ZnO single crystal for different biases measured at room temperature. The *grey boxes* indicate the frequency range for which the series resistance of the samples does not allow measurements of the samples capacitance (see text).

freeze-out temperature is here the temperature for which a defects does not respond anymore to the ac test voltage of frequency f). Therefore, the thermal activation energy of a defect can be obtained from thermal admittance spectroscopy (TAS). This was done for ZnO Schottky diodes in the temperature range from 20 K to 330 K applying test frequencies between 100 Hz and 1 MHz. Here, we compare TAS on ZnO single crystals (SC) grown by the hydrothermal method and a ZnO thin film grown by pulsed-laser deposition (PLD) on sapphire substrates. The Schottky barriers are realized in both cases by thermal evaporation of Pd after chemical cleaning of the surface. The diodes are
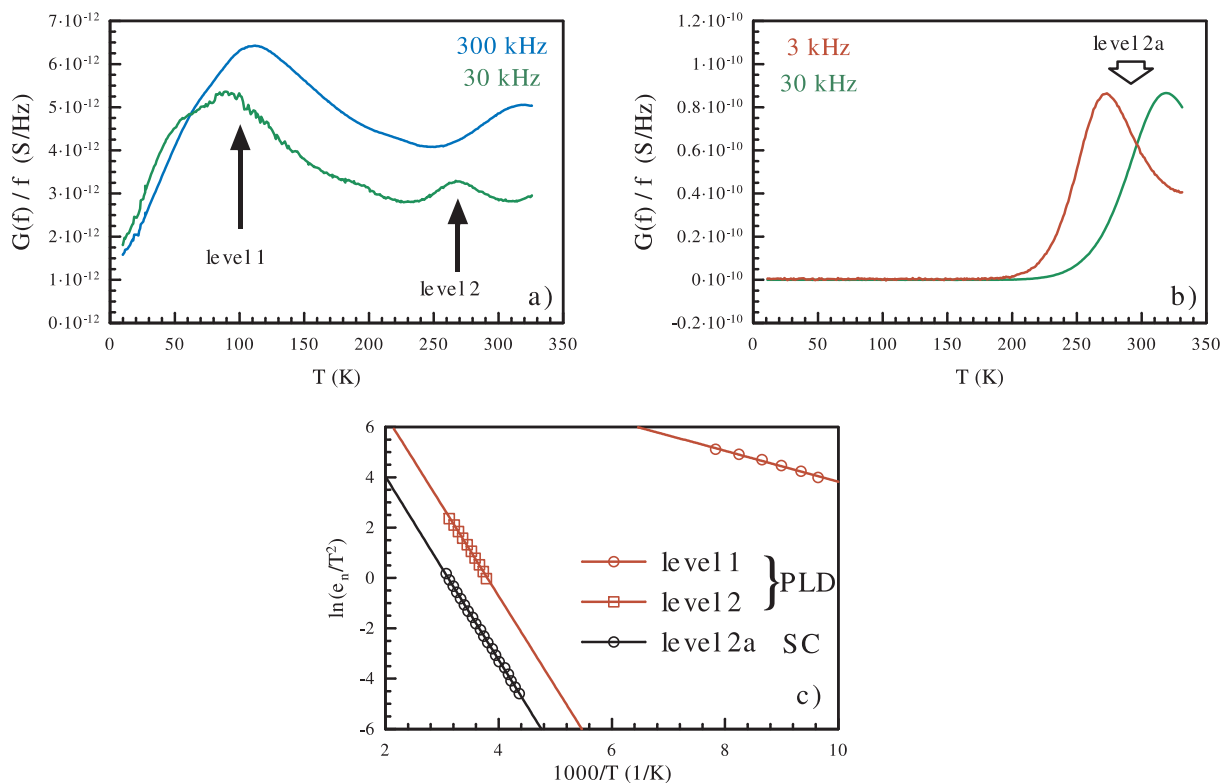
Figure 6.22: Thermal admittance spectroscopy for (**a**) PLD thin film and (**b**) ZnO single crystal for selected frequencies. The Arrhenius plots are shown for each level in (**c**).

processed in the front-to-back contact configuration. For that, a special growth scheme was applied for the PLD thin film [1]. Figure 6.21 depicts $G(f)/f$ measurements at room temperature (RT) for the PLD thin film and the ZnO single crystal in dependence on the reverse bias. It can be clearly seen, that for the PLD thin film a defect freezes out at RT for $f \sim 10\,$MHz (maximum in the $G(f)/f$ representation). For the hydrothermally grown single crystal the freeze-out of a defect is seen for $f \sim 20\,$kHz. For both kinds of samples the $G(f)/f$-plots become independent on the applied reverse bias for frequencies (indicated by the grey boxes of Fig. 6.21) for which the series resistance of the diode acts as low pass not allowing reliable measurements of the diode capacitance.

Figure 6.22 shows the TAS measurements (different frequencies were applied to the PLD and the single crystal sample due to the their different series resistance) and the Arrhenius analysis of levels 1, 2, and 2a from which the thermal activation energies were determined to be 53 meV, 310 meV, and 314 meV, respectively. The levels 2 and 2a have a very similar E_t, however, their cross-section must be different as already evident from Fig. 6.21 and as reflected in the vertical shift seen in Fig. 6.22c. At low measuring temperatures a superposition of two shallow levels is found for the PLD thin film sample, however, only one of these two levels could be evaluated (level 1).

In conclusion a ZnO PLD thin film and a ZnO single crystal were investigated by TAS. The dominant defect in the PLD sample has $E_t \sim 53\,$meV. Both samples contain a defect with $E_t \sim 310\,$meV, however, the cross-sections of these defects are dissimilar implying that they have different microscopic origins.

[1] H. von Wenckstern et al.: Appl. Phys. Lett. **88**, 092 102 (2006)

6.16 Meyer-Neldel Rule Behavior of Deep Electron Traps in ZnO

H. Schmidt, M. Wiebe[*], B. Dittes[*], M. Grundmann

[*]Wilhelm-Ostwald-Gymnasium, Leipzig

70 years ago Meyer and Neldel investigated the temperature dependence of the specific conductivity in ZnO and other oxidic compounds and found that the conductivity depends exponentially on temperature [1]. We investigated the Meyer-Neldel (MN) rule behavior of deep electron defects in ZnO using a correct analysis of DLTS data where the capture cross section σ_i, $[\sigma_i]$ = cm^2, is assumed to be temperature dependent [2]. The DLTS spectrum of a Co-doped ZnO film [3] with the apparent capture cross section being 2 orders of magnitude smaller than in most of the probed deep electron traps is shown for three differen trate windows in the inset of Fig. 6.23. DLTS peaks occur where the emission rate of the traps

$$e_i(T) = 1/\tau = N_B v_{th} \sigma_i \exp\left(-E_a/k_B T\right) = e_0 T^2 \exp\left(-E_a/k_B T\right) \tag{6.6}$$

lies within the period width [4], i.e. the response peak shifts to lower temperatures with increasing period width. Assuming thermal emission processes, the standard Arrhenius
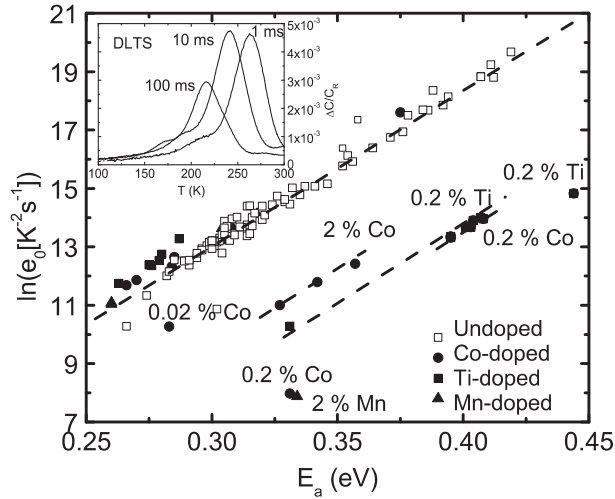
Figure 6.23: The MN plot of $\ln(e_0)$ vs E_a was generated using standard DLTS analysis for electron traps in 3d transition metal doped ZnO and nominally undoped ZnO. The $(E_a, \ln(e_0))$-coordinates of the Co-doped ZnO film from the *inset* are (0.395 eV, 13.34). *Inset:* DLTS spectrum measured at several rate windows ($T_w = 1, 10, 100$ ms) on a ZnO film doped with 0.2 at. % Co.

evaluation yields the thermal activation energies E_a and capture cross sections σ_i. In the standard DLTS analysis e_0 is defined by

$$e_0 = N_B v_{th} \sigma_i / T^2 = 4\pi \left(\frac{m^\star k^2}{h^3} \right) \sqrt{6\pi} \sigma_i \, , \tag{6.7}$$

where σ_i is assumed to be temperature independent, i.e. possible detrapping entropy changes are neglected. However, we find a linear relationship between $\ln(e_0)$ and E_a (Fig. 6.23). The slope of the MNR line in Fig. 6.23 is $(k_B T_{iso})^{-1}$ with $T_{iso} = 226$ K. The single capture cross section of deep electron traps in ZnO lying on the MN line has been determined by including entropy changes in a detailed balance analysis and amounts to $\sigma_i = 5.7 \times 10^{-23}$ cm^2. Finally, we would like to state that the MN behaviour can only be explored by investigating thermally activated processes with well-known temperature dependent prefactors in a large set of samples.

[1] W. Meyer, H. Neldel: Z. Tech. Phys. (Leipzig) **12**, 588 (1937)
[2] J.A.M. AbuShama et al.: Appl. Phys. Lett. **87**, 123 502 (2006)
[3] M. Diaconu et al.: Sol. Stat. Comm. **137**, 417 (2006)
[4] D.V. Lang: J. Appl. Phys. **45**, 3023 (1974)

6.17 Strong Electron Confinement in Mg$_x$Zn$_{1-x}$O/ZnO Quantum Wells Grown by Pulsed Laser Deposition

S. Heitsch, A. Müller, G. Zimmermann, H. Hochmuth, G. Benndorf, M. Lorenz, M. Grundmann

ZnO possesses a large exciton binding energy of 60 meV, which opens the possibility to observe and use excitonic effects at room temperature. The increase of the exciton
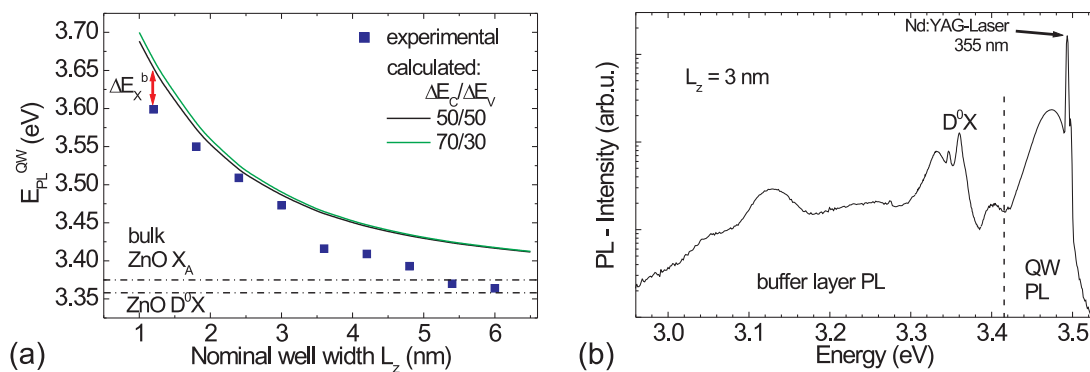
Figure 6.24: (**a**) Comparison of the QW PL energies measured at 2 K (*squares*) with the corresponding calculated PL energies (*solid lines*). The *dash-dotted lines* mark the energy positions of the free exciton (X_A) and of the donor bound exciton (D^0X) PL from bulk ZnO. (**b**) PL spectrum of a resonantly excited $Mg_{0.15}Zn_{0.85}O/ZnO$ QW with $L_z = 3$ nm at 2 K.

binding energy and oscillator strength in $Mg_xZn_{1-x}O/ZnO$ quantum wells (QWs) makes ZnO a promising candidate for the realization of room-temperature polariton lasers [1].

We have grown $Mg_xZn_{1-x}O/ZnO$ QWs ($x = 0.14 - 0.15$) with nominal well widths 1.2 nm $\leq L_z \leq 6$ nm by PLD [2] and investigated their photoluminescence (PL) properties. In Fig. 6.24a the QW PL emission energies are compared with calculated transition energies. The calculations were done with the model of a QW with finite barriers. The used parameters are $m_e = 0.24\,m_0$, $m_h = 0.59\,m_0$, and the band-gap difference was determined to be $\Delta E_{cv} = 475$ meV from spectroscopic ellipsometry. The energy only weakly depends on the band-offset ratio $\Delta E_c/\Delta E_v$. In the QW structures with $L_z > 3$ nm, the QW luminescence lies below the calculated transition energies because of the occurrence of the quantum-confined Stark-effect (QCSE) [3]. In the thin QWs the quantum confinement effects dominate over the QCSE, and in the $Mg_{0.14}Zn_{0.86}O/ZnO$ QW with $L_z = 1.2$ nm we achieved a high-energy shift of the QW emission of 222 meV with respect to the free exciton emission in bulk ZnO. This is the strongest possible confinement achievable for $Mg_{0.14}Zn_{0.86}O/ZnO$ QWs. The expected increase of the exciton binding energy ΔE_X^b in narrow QWs reveals itself as the difference between calculated and measured PL energy. Having in mind that the QW widths are nominal values, the exciton binding energy increases by about 53 to 65 meV for $L_z = 1.2$ nm, depending on the value taken for $\Delta E_c/\Delta E_v$.

The $Mg_{0.15}Zn_{0.85}O/ZnO$ QW with $L_z = 3$ nm was excited resonantly at $\lambda_{exc} = 355$ nm, so that no excitation of the $Mg_{0.15}Zn_{0.85}O$ barrier layers took place. We found (Fig. 6.24b) that the integrated QW PL is as intense as the PL from the 100 nm thick ZnO buffer layer. This means that the quantum yield from the QW is approximately thirty times larger than that of the ZnO buffer layer, which is a proof of the good optical quality of our QWs.

[1] M. Zamfirescu et al: Phys. Rev. B **65,** 161 205(R) (2002),
     doi:10.1103/PhysRevB.65.161205
[2] S. Heitsch et al: *Interface and Luminescence Properties of Pulsed Laser Deposited Mg_xZn_{1-x}O/ZnO Quantum Wells with Strong Confinement*, in *Zinc Oxide and Related Materials*, ed. by J. Christen et al., Mater. Res. Soc. Symp. Proc. **957** (MRS, Warrendale 2007)
[3] C. Morhain et al: Phys. Rev. B **72**, 241 305(R) (2005), doi:10.1103/PhysRevB.72.241305

6.18 FTIR Photocurrent Spectroscopy of Deep Levels in ZnO Thin Films

H. Frenzel, H. von Wenckstern, A. Weber, H. Schmidt, G. Biehne, H. Hochmuth, M. Lorenz, M. Grundmann

Epitaxial ZnO(0001) thin films have been grown by pulsed laser deposition (PLD) on a-Al_2O_3 and investigated by deep level transient spectroscopy (DLTS) and by Fourier transform infrared photocurrent (FTIR-PC) spectroscopy in the mid-infrared wavelength range. With DLTS, only rechargeable defects with a sufficiently large electron capture cross-section are observable. FTIR-PC probes optical transitions of deep levels either into a band or into shallow states below the band edge. However, FTIR-PC is not capable to distinguish between minority and majority traps.

Figure 6.25 depicts an investigation of the annealing behavior of nominally undoped ZnO thin films. The FTIR-PC and DLTS spectra show a defect distribution, which is typical for ZnO. The commonly observed defects E1 at ~ 110 meV, L2 at ~ 250 meV, and E3 at ~ 320 meV have been detected by both methods at similar optical ionization energies and thermal activation energies. However, there are more details visible in FTIR-PC. A2 at ~ 160 meV is most probably a hole trap, because it is not visible in DLTS spectra, where only majority transients are observable in n-type ZnO. In ZnO doped with cobalt, there is a superposition of this defect with the electron trap L1 at ~ 170 meV (not shown here). In DLTS spectra, E3 is often very broad. After oxygen annealing, a shoulder is visible at the high-temperature side of this peak. Thus, it is a double peak, labeled E3/E3′, with E3′ at ~ 370 meV. E3′ is also visible in FTIR-PC at this energy and can be related to the oxygen sublattice. The dominance of E1 in the oxygen-treated sample implies a connection to oxygen, too [1]. For L2, an extended defect structure is more probable than a single point defect. This would explain the broad width of this peak in the spectra and the fact that it has mostly been detected in polycrystalline ZnO.

Further annealing experiments (not shown here) reveal that the concentration of E3 is highest for the vacuum annealed sample, which supports our conclusion [2] that E3 is the second ionization of the zinc interstitial.
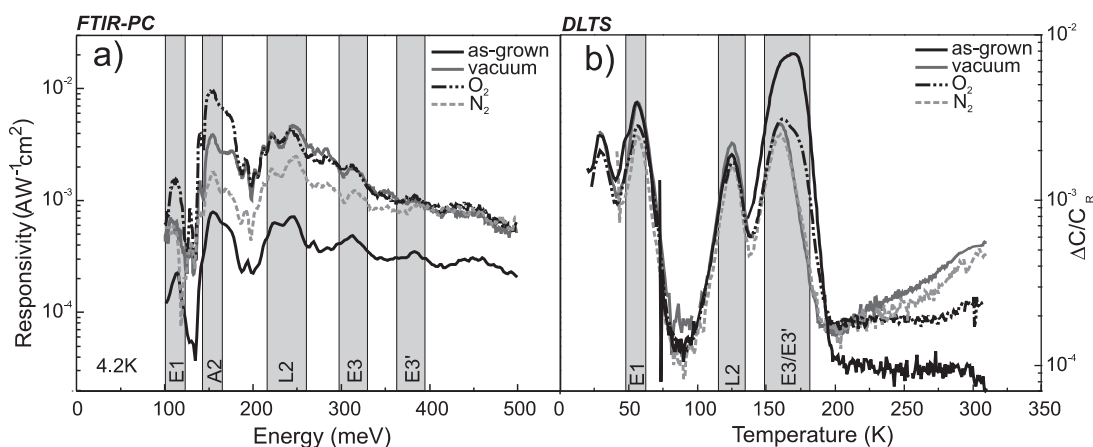
Figure 6.25: FTIR-PC (**a**) and DLTS (**b**) spectra of differently annealed nominally undoped ZnO thin films. The *grey boxes* show defect levels detected by FTIR-PC and DLTS, respectively.

In ZnO doped with the transition metal manganese (Mn), FTIR-PC is able to probe the Mn^{2+}-related hole trap at ~ 450 meV and two additional hole traps at ~ 380 meV and ~ 270 meV. Such hole traps have also been observed in nitrogen-implanted p-type ZnO at ~ 150 meV (A2) and ~ 280 meV (A3) [3].

[1] H. Frenzel et al.: Proc. 28th ICPS, Vienna, Austria, July 24–28, 2006
[2] G. Brauer et al.: Phys. Rev. B **74**, 045 208 (2006)
[3] H. von Wenckstern et al.: Appl. Phys. Lett. **89**, 092 122 (2006)

6.19   ZnO Films Doped with $3d$ or $4f$ Magnetic Ions

M. Ungureanu, H. Schmidt, M. Fecioru-Morariu[*], G. Güntherodt[*], H. Hochmuth, M. Lorenz, M. Grundmann

[*]II. Physikalisches Institut, RWTH Aachen

ZnO-based diluted magnetic semiconductors, formed by substituting a fraction of Zn-cations with magnetic ions, were analyzed for future applications in spintronics [1]. We investigated ZnO films doped with Mn or with Gd. In ZnO:Mn films P or Al was added, while in ZnO:Gd films Al was added to vary the electrical properties. Films were grown by pulsed laser deposition (PLD) on a-Al_2O_3 substrates in O_2 pressures between 2×10^{-5} and 0.3 mbar. No secondary phases were found in X-ray diffraction (XRD). XRD also indicated large internal stress, shifting the ZnO peaks, for films containing 1 % Gd.

ZnO:Mn films grown at O_2 pressures above 0.1 mbar were insulating and films grown below 0.1 mbar were n-conducting. By adding 0.2 % Al to ZnO:Mn, n-conducting films were obtained for growth below 0.01 mbar O_2. The ZnO:(Mn,P) films grown below 10^{-3} mbar O_2 pressure were n-conducting. The ZnO:Gd films grown below 0.2 mbar O_2 were n-conducting. All investigated ZnO:(Gd,Al) films were n-conducting.

Magnetic properties were investigated in a SQUID magnetometer. For the investigated films, superparamagnetic and spin-glass behavior can be excluded from the shape of the temperature dependent magnetization curves, measured between 5 K and 350 K at 250 Oe as field cooled (FC) and zero field cooled (ZFC), since no peak was detected on the ZFC curve. The presence of magnetic hysteresis was checked at 5 K and at 300 K.

Ferromagnetism above 300 K was observed in insulating ZnO:Mn films with around 5 % Mn, with a maximum average magnetic moment of 0.06 μ_B/Mn ion at 5 K. Al addition to ZnO:Mn films induces a decrease of ferromagnetism. By adding 0.1 % P to the ZnO:5 % Mn films, the magnetic moment was increased up to 0.2 μ_B/Mn ion at 5 K, ferromagnetism still being present above 300 K (Fig. 6.26) [2]. The presence of P could provide holes to mediate exchange in ZnO:Mn [3]. For ZnO:1 % Gd films, ferromagnetism was observed below 150 K. By adding 0.2 % Al to ZnO:1 % Gd films, ferromagnetism above 300 K was obtained (Fig. 6.26), with maximum magnetic moment of 0.3 μ_B/Gd ion at 5 K, indicating that exchange in ZnO:Gd films may be electron-mediated.
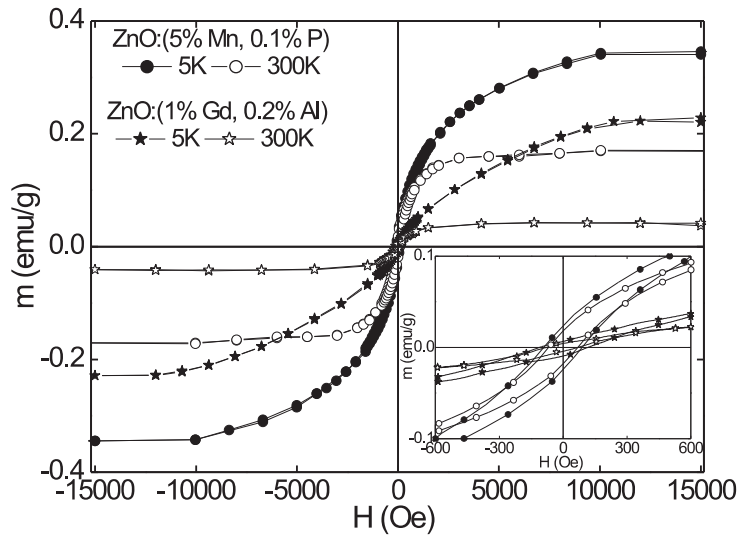
Figure 6.26: Magnetic hysteresis loops for Zn(Mn,P)O and Zn(Gd,Al)O films. Substrate contributions were subtracted.

[1] G.A. Prinz: Science **282**, 1660 (1998)
[2] M. Diaconu et al.: Phys. Lett. A **351**, 323 (2006)
[3] T.Dietl et al.: Science **287**, 1019 (2000)

6.20   Magnetoresistance and Anomalous Hall Effect in Magnetic ZnO Films

Q. Xu, L. Hartmann, H. Schmidt, H. Hochmuth, M. Lorenz, D. Spemann, M. Grundmann

The magnetotransport properties of Mn-doped ZnO and Co-doped ZnO films prepared by pulsed laser deposition (PLD) on a-plane sapphire substrates were studied in dependence on magnetic field strength ($0-6$ T) and temperature ($5-290$ K) [1]. The free electron concentration in the films was controlled by the PLD growth conditions (substrate temperature, oxygen partial pressure) and by the film thickness. A critical electron concentration has been observed in Co-doped ZnO related to the metal insulator transition but not in Mn-doped ZnO. An inverse relationship between the positive magnetoresistance (MR) and electron concentration at 5 K has been observed for both Co-doped ZnO films and Mn-doped ZnO films (Fig. 6.27). Clear anomalous Hall effect (AHE) was observed in Co-doped ZnO, but no AHE was observed in Mn-doped ZnO, indicating the possible ferromagnetism in n-type conducting Co-doped ZnO but not in n-type conducting Mn-doped ZnO. The saturated anomalous Hall resistivity has a dependence of $n^{-1.4}$ on electron concentration and $\rho^{1.4}$ on resistivity (Fig. 6.28), indicating that both skew scattering and side-jump mechanisms may contribute.

[1] Q. Xu et al.: J. Appl. Phys. **101**, 063 918 (2007)
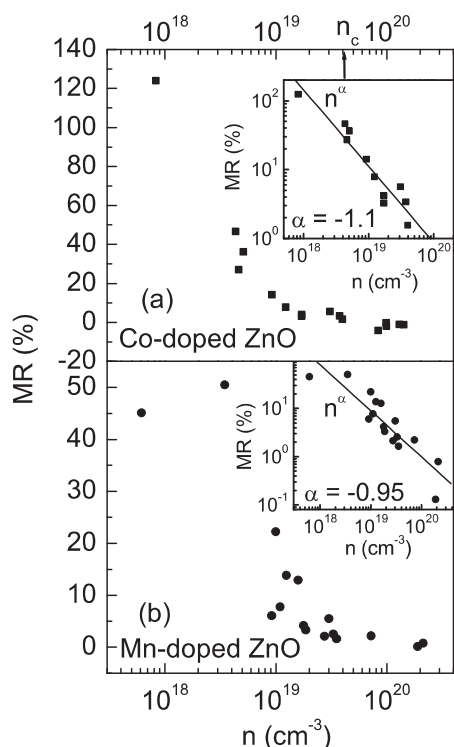
Figure 6.27: The positive MR value in dependence on the free electron concentration n at 5 K for (**a**) Co-doped ZnO and (**b**) Mn-doped ZnO. The insets show the inverse relationship between MR and n.
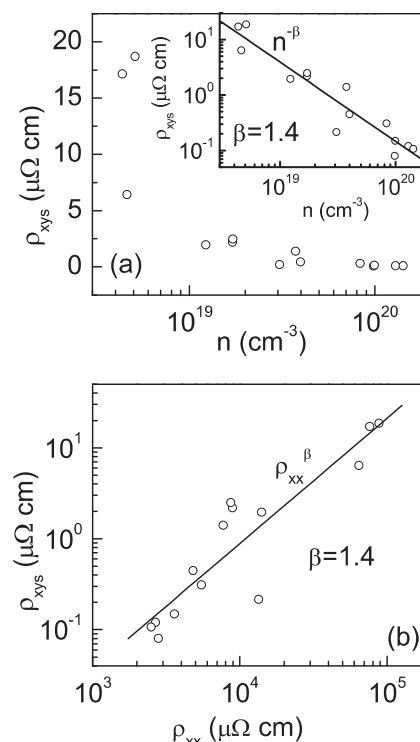
Figure 6.28: (**a**) The saturated anomalous Hall resistivity in dependence on the free electron concentration at 5 K for Co-doped ZnO. (**b**) The saturated anomalous Hall resistivity in dependence on resistivity at 5 K for Co-doped ZnO.

6.21 BP and $B_xGa_{1-x-y}In_yP$ Layer Structures Grown by MOVPE

V. Gottschalch[*], H. Paetzelt[*], K. Schollbach[*], J. Bauer[*], G. Leibiger[†], G. Wagner[*], G. Benndorf, D. Hirsch[‡]

[*]Fakultät für Chemie und Mineralogie, AK Halbleiterchemie
[†]Freiberger Compound Materials GmbH
[‡]Leibniz-Institut für Oberflächenmodifizierung Leipzig

BP, ternary $B_xGa_{1-x}P$ and related quaternary alloys like $B_xGa_{1-x-y}In_yP$ are novel indirect transition type materials for light emitters or detectors in the visible spectral range but systematic investigations are rare or missing completely. Intermediate layers of cubic BP are a possible substrate material due to its low thermal expansion and lattice mismatch compared to GaN ($\Delta a/a(\text{BP/GaN}) = -0.6\%$) and ZnO ($\Delta a/a(\text{BP/ZnO}) = 0.7\%$).

We have studied the metal-organic vapor-phase epitaxial growth of BP, $B_xGa_{1-x}P$ and $B_xGa_{1-x-y}In_yP$ thin films on GaP, GaAs and Si substrates of different orientation using the standard precursors Triethylboron, Trimethylgallium, Trimethylindium and Phosphine. The growth of the heterostructures has been performed by low-pressure MOVPE ($p_{tot} = 50$ mbar) in a commercial reactor (AIX 200, AIXTRON Corp.). The
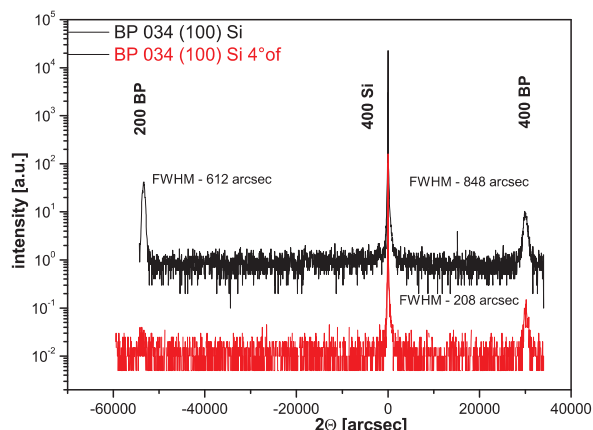
Figure 6.29: Symmetrical 400 DCXRD pattern of (100) Si/BP epitaxial layer grown at 1030 °C.
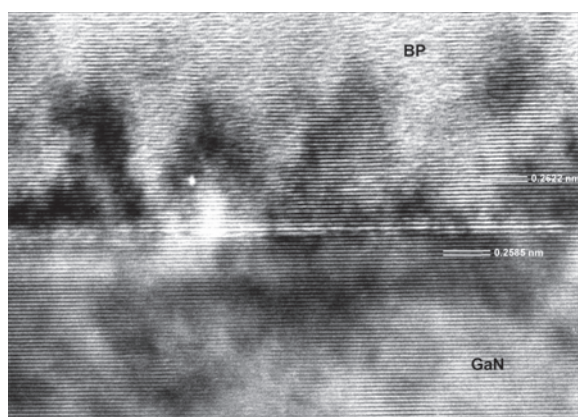
Figure 6.30: HRTEM image of lattice fringes from BP grown on (0001)GaN. The distance between the lattice fringes in GaN is $c_0/2 =$ 0.258 5 nm. If GaN is used as standard we obtain a $d_{(111)}$(BP) = 0.262 nm.

growth temperature was changed from 550 to 1000 °C and the total gas flow was 7000 sccm during each run. The growth rate ranged from 0.2 to 1 µm/h, The properties of the deposited thin film were determined using double-crystal X-ray diffraction, spectroscopic ellipsometry, chemical-etching techniques, transmission electron microscopy, photoluminescence, Raman scattering, and Secondary Ion Mass Spectroscopy.
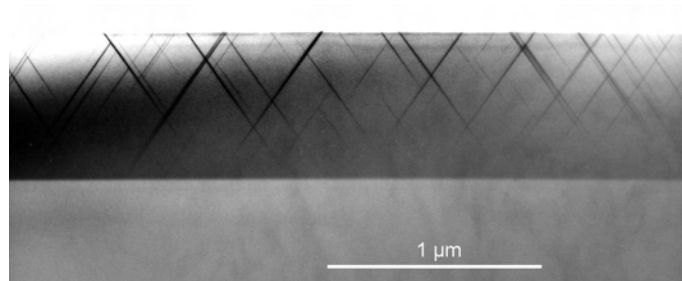
Figure 6.31: TEM bright-field image of a BGaInP layer (tickness 690 nm). The dark contrasts result from stacking faults exclusively, B = [1$\bar{1}$0]. Viewing along [110] no stacking faults are visible.

Figure 6.32: DCXRD-spectra of $B_x Ga_{1-x-y} In_y P$/GaP-layers with different Boron concentration: *a*) 3 %, *b*) 3.5 %, *c*) 5.4 %, *d*) 6.1 %, (FWHM< 30 arcsec).

Figure 6.33: Cross section TEM image of the GaP/$B_{0.03}Ga_{0.67}In_{0.3}P$ superlattice.

Figure 6.34: SIMS investigations of $B_{0.02}Ga_{0.98}P$ (3.2 nm) / $Ga_{0.79}In_{0.21}P$ (5.7 nm) / GaP (32 nm) superlattice.

BP single crystalline layers have been successfully grown on different substrates or layers (GaAs, GaAs, Si, GaN) and were continuous and free of cracks (Fig. 6.29). In the temperature range of 750 to 1000 °C smooth surfaces and interfaces have been observed (Fig. 6.30). TEM investigation shows that the BP layer involved {111} twins. In the temperature range of $650-800$ °C mirror-like surfaces for the $B_xGa_{1-x}P$ and $B_xGa_{1-x-y}In_yP$/GaP layer structures have been observed. The mole fraction of Boron in the epitaxial alloy-layers was varied from $x = 0$ to 0.05. In particular, the measurements of (BGa)P/GaP superlattices have shown excellent interface characteristics.

Lattice matched material ($B_xGa_{1-x-y}In_yP$/GaP) was grown at $T_{growth} = 580$ °C. We have demonstrated that $B_xGa_{1-x-y}In_yP$-bulk-like layers (lattice matched to GaP) with high structural quality can be successfully grown using MOVPE (Figs. 6.31 and 6.32). A possible influence of the Indium on the Boron incorporation has not been detected.

In addition, we have grown highly compressively strained $B_xGa_{1-x-y}In_yP$/GaP-(Fig. 6.33) and $B_xGa_{1-x}P$/$Ga_xIn_{1-x}P$/GaP-superlattices (Fig. 6.34) on (001) GaP substrates. SIMS and X-ray investigations of these structures are compared with vapor pressure data.

6.22 States of III–V and II–VI Compounds in VLS Growth

H. Paetzelt[*], J. Bauer[*], A. Vogel[*], V. Gottschalch[*], W. Schmitz[*], G. Zimmermann

[*]Fakultät für Chemie und Mineralogie, AK Halbleiterchemie

The vapour-liquid-solid (VLS) growth method is well-established in fabrication of freestanding III–V- and II–VI-nanowires using metal-organic vapour-phase epitaxy. Some aspects of VLS growth are not yet well understood. The crystalline structure as well as the chemical composition of the so called catalyst may have great influence on the structure of the grown one-dimensional nanostructures.

On this account we deposited thin gold films varying from 6 to 26 nm in thickness on GaAs ($\bar{1}\bar{1}\bar{1}$) and c-plane sapphire. Those films were analyzed using a texture goniometer, atomic force microscopy, conventional and temperature-sensitive X-ray diffraction offering the opportunity to capture in-situ scans up to 900 °C. We discuss the interactions observed between substrate, gold and precursor material.

Au films on Al_2O_3

A 25 nm thick gold film was deposited on c-plane Al_2O_3 and heated. While heating at different temperatures X-ray diffraction measurements were obtained. As shown in Fig. 6.35 even at 850 °C the Au 111 peak is still visible thus the gold is not yet molten. However an alignment of the gold particles resulting in a more intense diffraction peak is observed. Figure 6.36 shows AFM images of gold clusters possibly formed by diffusion during the heating-process. The formation of gold clusters also explains the more intense diffraction peaks at higher temperatures.

Au - TEGa interaction (GaN nanowire growth)

Using c-plane Al_2O_3 as a substrate a 6 nm thick gold film was deposited and heated under N_2-atmosphere up to 600 °C. Figure 6.37 shows the X-ray measurements after cooling down. The 600 °C heating-process leads to a more intense an narrow diffraction
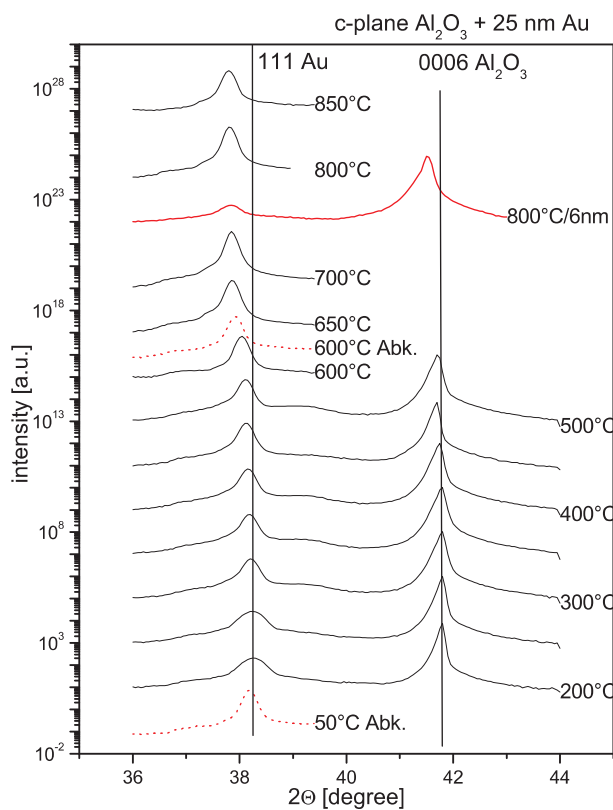
Figure 6.35: X-ray measurements of c-plane Al_2O_3 with 25 nm Au at different temperatures.
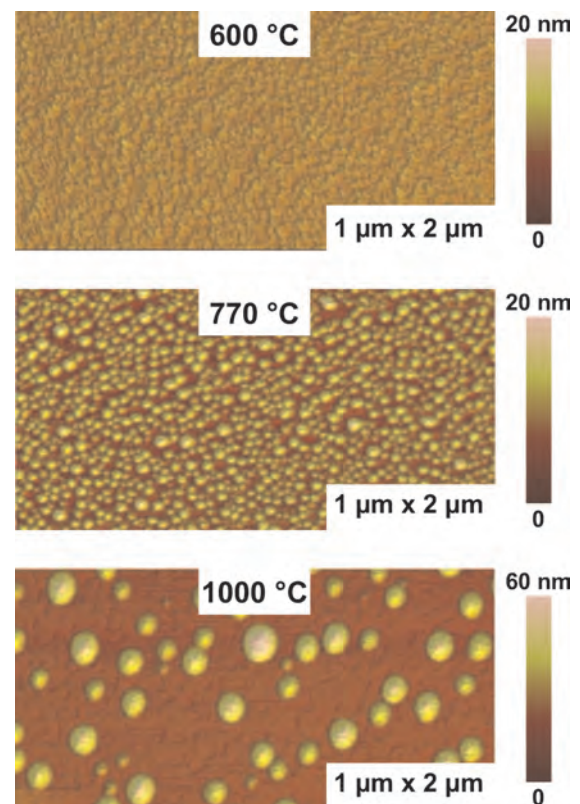
Figure 6.36: AFM images of Au layers heated to 600, 770 and 1000 °C respectively (measurement after cooling down).
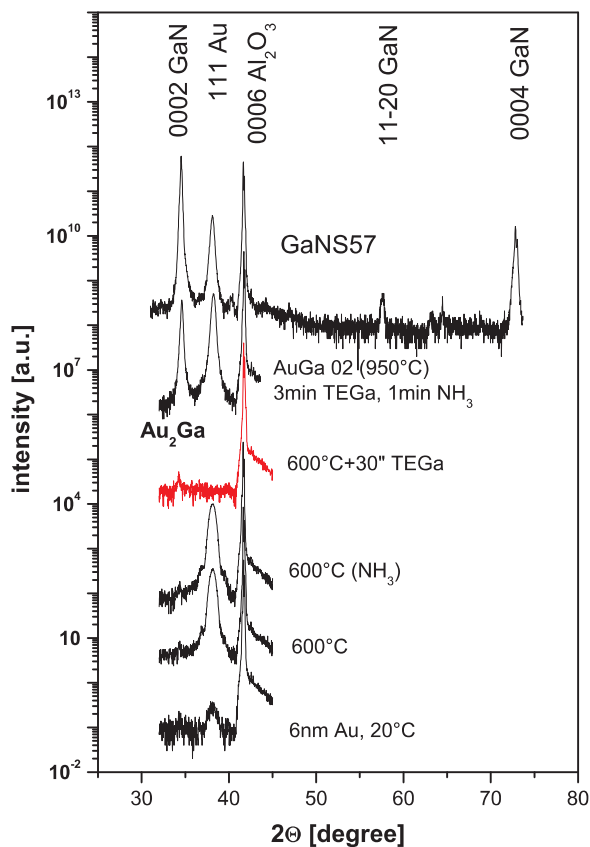
Figure 6.37: X-ray diffraction pattern obtained on 6 nm Au/(0001) Al$_2$O$_3$ specimen at different treatments.
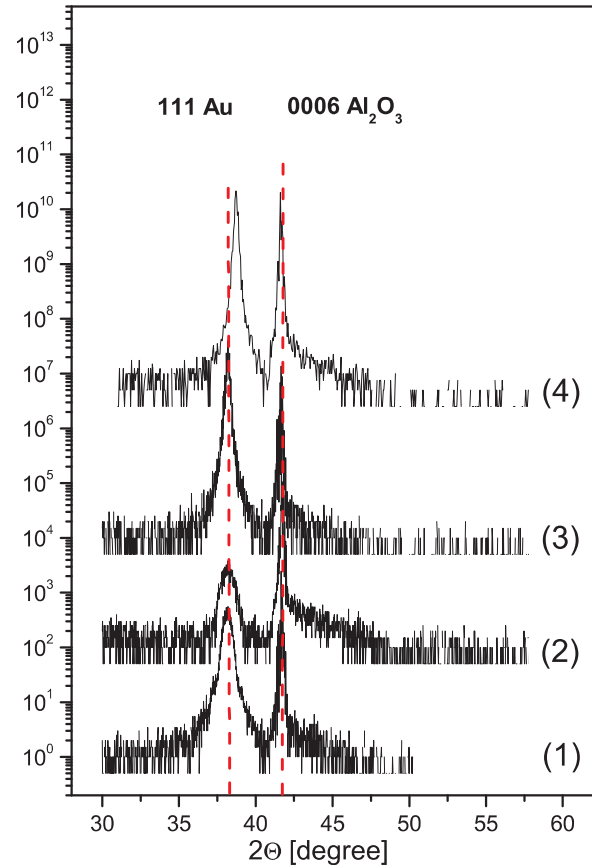
Figure 6.38: XRD spectra of gold on c-Al$_2$O$_3$. A 14 nm Au layer (*1*), Laser-ordered Au droplets (*2*), Au layer after 10 min DEZn treatment at 960 °C (*3*) and Au layer after 60 min DEZn treatment at 700 °C (*4*). The Au 111 peak of (*4*) is shifted 0.52° this correlates an Zn–Au alloy with 26 at. % Zn.

peak. Supplying 30 seconds of TEGa the gold peak vanished which indicats a reaction between Ga and Au. This polycrystalline alloy generats only a weak diffraction peak.

More evidence for the existence of such an alloy is presented while adding NH$_3$ after the TEGa treatment resulting in the growth of GaN nanowires using the Ga supplied by the Ga–Au-alloy. Diffraction patterns obtained after the nanowire growth at 950 °C showed straight GaN and Au peaks indicating that pure gold crystallized on top of the wires.

Au - DEZn interaction (ZnO nanowire growth)

14 nm thick gold films as well as Laser-ordered gold droplets were deposited on c-plane Al$_2$O$_3$ showing more or less intense diffraction peaks (Fig. 6.38). The layer was treated with DEZn at 960 °C for 10 min showing no Zn-Au-alloy as a result of the high Zn-pressure at this temperature. But supplying DEZn at 700 °C for a total amount of

60 min, the diffraction peak shifted towards larger angles correlating to a Zn–Au alloy with 26 at. % Zn.

Au-GaAs and Au-TMGa Interaction (GaAs nanowire growth)

A 26 nm layer was deposited on GaAs($\bar{1}\bar{1}\bar{1}$) showing no azimuthally distorted correlations (Fig. 6.39). Heating the film up to a temperature of 480 °C showed an incorporation of Ga into the Gold film resulting in a shift of the obtained diffraction peak (Fig. 6.40). Furthermore an alloy was formed producing additional peaks. Since diffraction peaks are still visible no complete melting takes place leaving solid state diffusion as one possible mechanism for Ga incorporation. These X-ray patterns are showing the interaction between Au and GaAs while annealing under AsH_3/H_2-atmosphere. forming an Au–Ga alloy and resulting in VLS growth of GaAs nanowires (Fig. 6.41). This alloy can also be observed when examining the gold droplets on top of already grown wires.
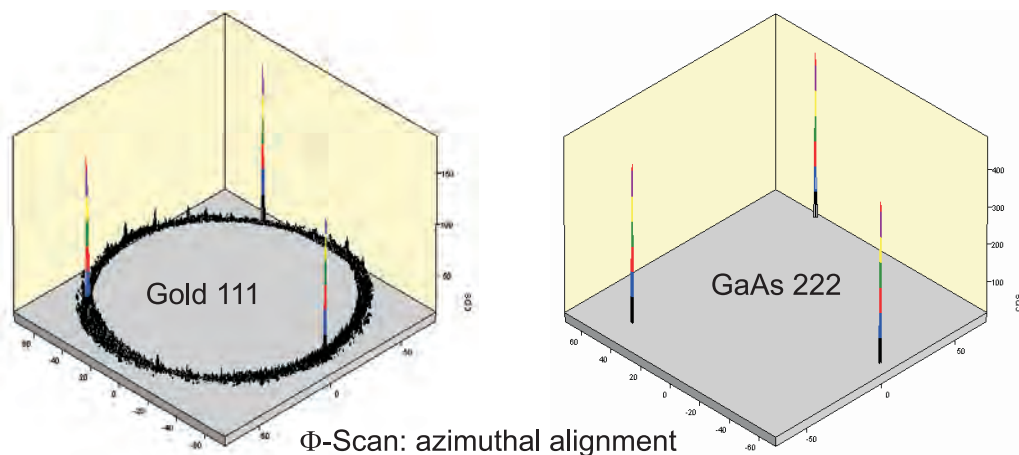
Figure 6.39: XRD-investigation: $(111)_{Au} \parallel (\bar{1}11)_{GaAs}$.
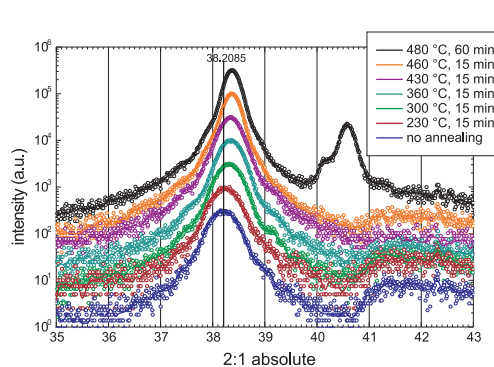
Figure 6.40: XRD-investigation: Au/GaAs($\bar{1}\bar{1}\bar{1}$)$_{As}$ annealed in N_2-atmosphere.
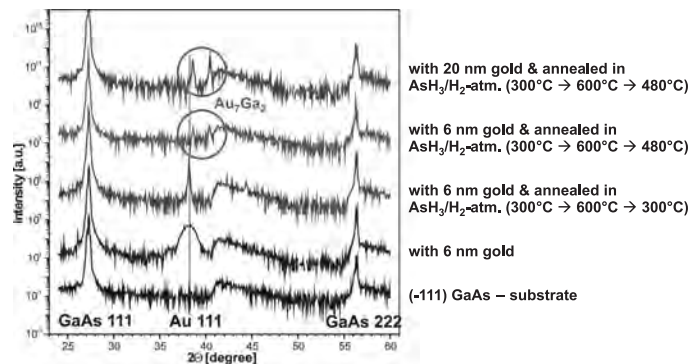
Figure 6.41: XRD-investigation: Au/GaAs($\bar{1}\bar{1}\bar{1}$)$_{As}$ annealed in N_2-atmosphere.

6.23 (InGa)As/GaAs ($\lambda \sim 1.2\,\mu$m) Horizontal Cavity Surface-Emitting Laser (HCSEL)

V. Gottschalch[*], J. Kováč jr.[†], J. Kováč[†], H. Herrnberger[‡], T. Gühne[*], R. Schmidt-Grund, B. Rheinländer, J. Zajadacz[‡], J. Dienelt[‡], A. Schindler[‡]

[*]Fakultät für Chemie und Mineralogie, AK Halbleiterchemie
[†]Slovak University of Technology & International Laser Center, Bratislava, Slovakia
[‡]Leibniz-Institut für Oberflächenmodifizierung e.V

Surface emitting lasers (SEL) are of great interest for their various potential applications, e.g., monolithic two dimensional arrays for optical processing and interconnect. We present the properties of the integrating stripe laser structure including the horizontal laser cavity with an etched front facet and dielectric Bragg mirror at the rear facet.

We have grown laser structures with $Ga_{1-x}In_xAs$ double quantum wells [1]. Laser structures were fabricated as oxide stripe lasers with stripe widths of $(8-35)\,\mu$m and cavity lengths between 400 and 800 μm. The active region consists of a double quantum well (DQW) of 8 nm $In_{0.37}Ga_{0.63}As$ embedded in 180 nm GaAs barrier. This active region structure is sandwiched between two doped $Al_{0.35}Ga_{0.65}As$-cladding layers. For broad area lasers we found laser activity in an emission range from 1130 to 1190 nm with a threshold current density between 0.25 and 0.35 kA cm^{-2} ($X_{In} \sim 32-37\,\%$, $T_0 \sim 103$ K, $\eta_{\text{diff}}^{\text{max}} \sim 48\,\%$) (Fig. 6.42).

HCSEL structure with a cleaved facet and an ion beam etched outcoupler facet, coated with PECVD SiO_x/Si bragg mirror, was fabricated [2]. The HCSEL incorporates the oxide stripe resonator part and deflector part coupled through the air slit terminated by 45° etched facet that produce total internal reflection perpendicular to the laser cavity (Fig. 6.43). Electron beam lithography and chemically assisted ion beam etching (Cl_2/Ar^+) was used to form vertical air slit and 45° deflector micro mirror. The front laser mirror facet was fabricated using chemically assisted ion beam etching while the cleaved rear facets were coated with SiO_x/Si Bragg mirrors. Finally, HCSELs were fabricated as oxide stripe lasers with different stripe widths of $6-35\,\mu$m. The edge
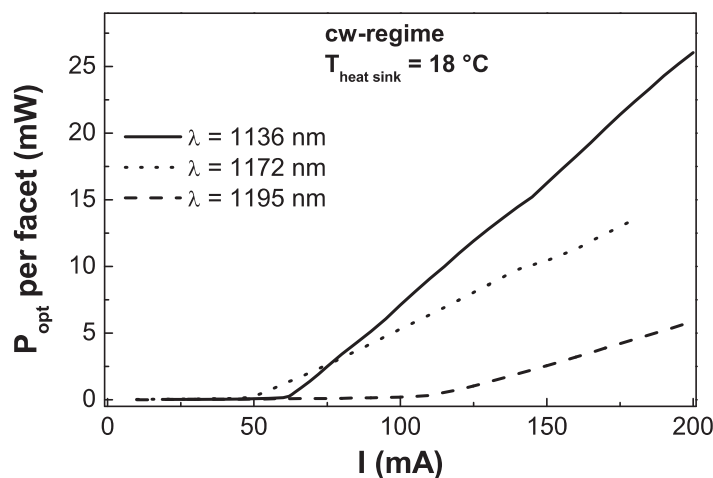
Figure 6.42: Optical output power versus injection current in CW-operation of laser structures.
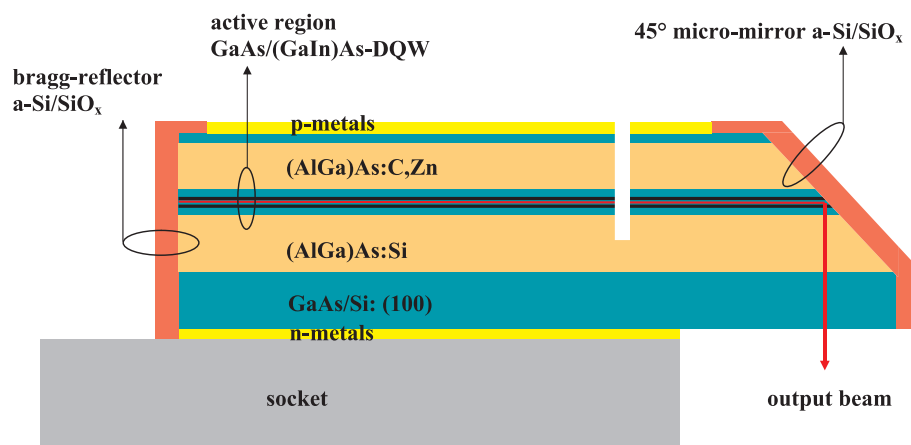
Figure 6.43: Schematic structure of fabricated (InGa)As/GaAs rear surface-emitting laser with vertical (cleaved face) and 45° micro-mirrors.
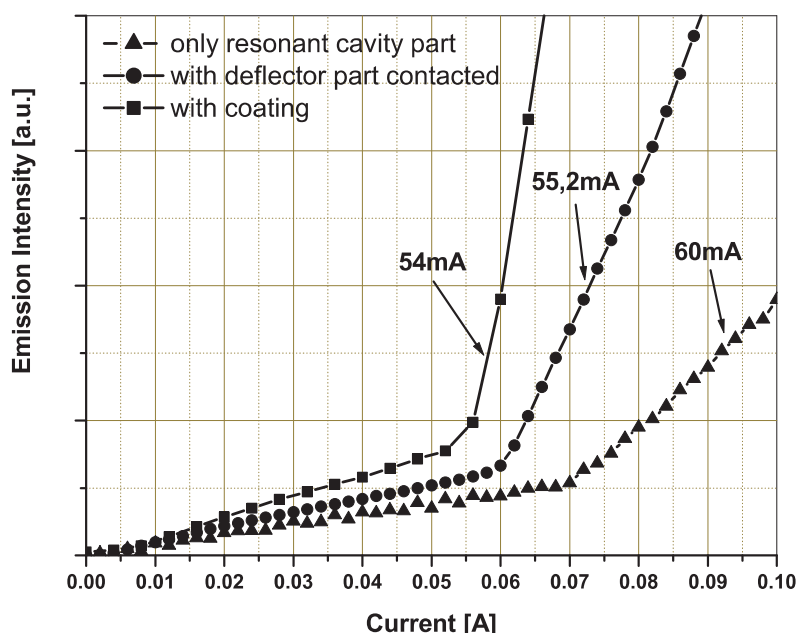
Figure 6.44: The light power vs. input current measured at the rear-surface facet from the same laser diode: With ion beam etched air slit and 45° facet (▲); with cleaved facet and ion beam etched 45° facet (with bridge of the LS) (●); with cleaved facet, ion beam etched 45° facet and bragg reflectors (■).

emitting laser cavity with lengths of $200-600\,\mu m$ is coupled to fixed $150\,\mu m$ tilted cavity laser part. The emission spectra and optical power were measured in the impulse operation for the different injection currents in both parts of the laser structure [3]. The L–I characteristics of the devices were measured in the impulse operation using Ge or InGaAs photodetector (Fig. 6.44). The presented devices are characterized by improved slope efficiency documented in L–I characteristics and the stable single-longitudinal mode operation at 1165.22 nm with narrow line width of 0.1 nm. The etched air slit in the laser cavity and a dielectric Bragg mirrors at the rear facet improved the filtering and reflection of the propagated light.

[1] V. Gottschalch et al.: J. Cryst. Growth **272**, 642 (2004)
[2] T. Gühne et al.: Laser Phys. **16**, 441 (2006)
[3] J. Ková č et al.: Laser Phys. Lett. **4**, 200 (2007)

6.24 MOVPE-Growth of GaN-Nanowires on Various III–V-Substrates

V. Gottschalch[*], J. Bauer[*], H. Paetzelt[*], M. Shirnow[*], G. Wagner[*], G. Benndorf, J. Lenzner

[*]Fakultät für Chemie und Mineralogie, AK Halbleiterchemie

GaN nanoscale structures (nanowires) have great potential for realizing new optoelectronic devices. We compare the anisotropic growth of freestanding GaN wires on various substrates and templates using the precursor combinations 1.1-dimethylhydrazine (DMHy)/Trimethylgallium (TMG), and the VLS-growth using NH_3/Triethylgallium (TEG).

GaN-Growth using DMHy/TMGa

The combination DMHy/TMGa was used to grow GaN at low substrate temperatures ($T_{growth} < 800\,°C$) in order to limit the nitridation damage of the substrate materials, and to study the formation of wurtzite or the cubic GaN structure. Structural and growth characteristics of the initial layer and the nanowires were investigated using transmission and scanning electron microscopy, X-ray diffraction, atomic force microscopy and cathodoluminescence techniques. We have investigated the GaN growth on GaAs $(111)_{As}$-, $(111)_{Ga}$- and (100)-substrates, on (111), $(\bar{1}11)$, (100), (110) GaAs/BP- and GaP/BP-structures. It is possible to use cubic BP as substrate material due to its low thermal expansion and lattice mismatch compared to GaN.

By variation of the growth temperature in the range from $550\,°C$ to $750\,°C$ and the partial pressure a small range of "catalyst-free" formation was found, where cubic GaN wires ($T_{growth} = 550-650\,°C$, V/III $\sim$ 27) can grow directly on GaAs-substrates (Fig. 6.45). Between the substrate and the wires a closed intermediate GaN layer exists (thickness $30-50nm$). Cross-section TEM investigations revealed the transition from the wurtzite structure to the cubic GaN in growth direction. GaN wires deposited on an intermediate BP layer (Fig. 6.46) above $750\,°C$ show the wurtzite type structure. The GaAs/BP- and GaP/BP-structures are favoured for growth of hexagonal GaN nanowires at higher-temperature ($T_{growth} \sim 800\,°C$). The hexagonal GaN has the following epitaxial relationship: $(0001)_{GaN} \parallel (111)_{BP}$, $\langle 11\bar{2}0\rangle_{GaN} \parallel \langle 110\rangle_{BP}$.

GaN-Growth using NH_3/TEGa

We grew GaN wires on (0001) and $(10\bar{1}2)$ Al_2O_3 surfaces using the precursors TEGa and NH_3 and N_2 as the carrier gas in a temperature range from 900 to $1000\,°C$. TEGa and NH_3 were separately introduced into the horizontal cold wall reactor in order to prevent prereactions. We used Ni and Au as initiators for vapour-liquid-solid (VLS)
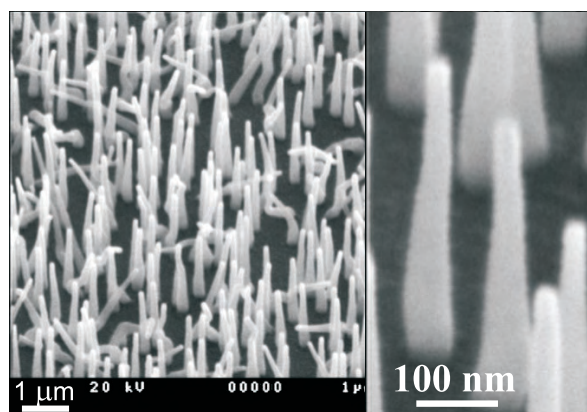
Figure 6.45: SEM images of cubic GaN wires on ($\bar{1}11$) GaAs substrate (T_{growth} = 600 ℃, V/III ∼ 27).
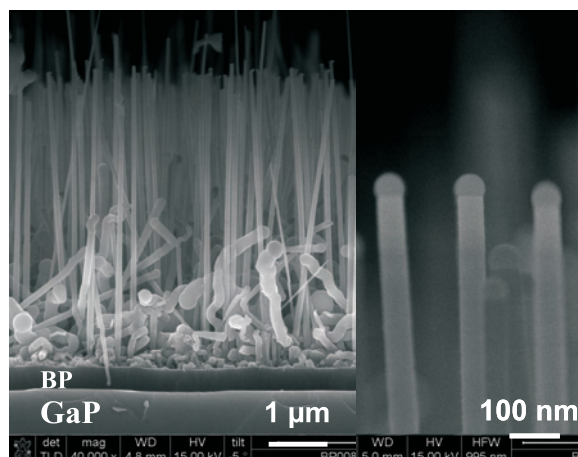
Figure 6.46: SEM images of hexagonal GaN wires grown at 780 ℃ on ($\bar{1}11$) GaP/BP-template.
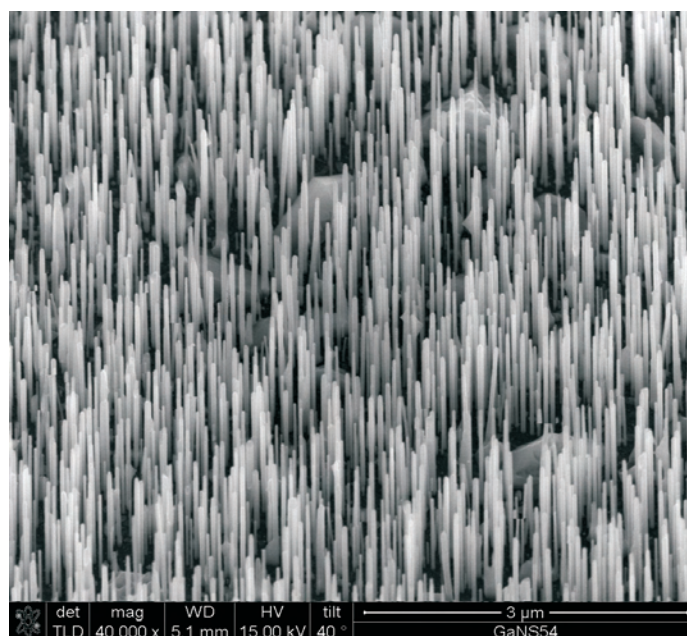
Figure 6.47: SEM images of GaN wires grown on c-plane Al_2O_3 substrates, the thickness of Au-layer as initiator for VLS-growth was 5 nm.

wire growth. We observed hexagonal GaN wires with Au-droplet (prefered growth in ⟨0001⟩) and grains grown in the temperature range 700−1000 ℃. We obtained wires with high aspect ratios (possible length up to 20 µm, see Fig. 6.47).

Additionally, we have studied GaN-wires-growth using Ga-sublimation in a sandwich technique (Ga/NH_3). Cathodoluminescence spectra at 300 K of GaN wires grown on (0001) Al_2O_3-substrates at 650 ℃ using DMHy/TMGa consist of one broad emission feature between 2.0 and 3.3 eV. The bands result from defects and/or carbon incorporation. By using the precursor combination Ga or TEGa/NH_3 and growth temperatures between 800 and 1000 ℃ band-edge luminescence dominates at structures with low defect densities, otherwise a strong yellow band appears at twinned regions.

6.25 Funding

Nanophotonic and nanoelectronic Devices fom Oxide Semiconductors (NANDOS)
Prof. Dr. M. Grundmann
EU STReP Contract No. 016424

BMBF-Nachwuchsgruppe "Nano-Spinelektronik"
Dr. H. Schmidt
BMBF FKZ 03N8708

Deutsch-Chinesische Kooperation zur Entwicklung von transparenten und halbleiten-den GMR und TMR Prototyp-Bauelementen
Dr. H. Schmidt
BMBF CH05/010

Ferromagnetism in transition metal doped ZnO
Dr. H. Schmidt
DFG Schm 1663/1-1

6.26 Organizational Duties

M. Grundmann
- Vertrauensdozent der Studienstiftung des deutschen Volkes
- Direktor des Institut für Experimentelle Physik II
- Coordinator of the European Network of Excellence on 'Self-Assembled semiconductor Nanostructures for new Devices in photonics and Electronics' (SANDiE, www.sandie.org)
- Sprecher der DFG Forschergruppe 'Architektur von nano- und mikrodimensionalen Strukturelementen' (FOR 522, http://www.uni-leipzig.de/~for522)
- Sprecher der Fächerübergreifenden Arbeitsgemeinschaft Halbleiterforschung Leipzig (FAHL, http://www.uni-leipzig.de/~fahl)
- Mitglied des Beirat Ionenstrahlzentrum, FZR, Rossendorf
- Berufungskommission: Nachfolge Michel, Vorsitzender; Nachfolge Lösche, Vorsitzender
- Project Reviewer: Deutsche Forschungsgemeinschaft (DFG), Alexander-von-Humboldt Stiftung (AvH), Schweizerischer Nationalfonds zur Förderung der wissenschaftlichen Forschung (FNSNF), Fonds zur Förderung der Wissenschaften (FWF)
- Referee: Appl. Phys. Lett., Electr. Lett., J. Appl. Phys., Nature, Physica E, Phys. Rev. B., Phys. Rev. Lett., Phys. Stat. Sol., Science

M. Lorenz
- Project Reviewer: United States - Israel Binational Science Foundation (BSF)
- Referee: Appl. Phys. Lett., IEEE Transact. Appl. Supercond., J. Am. Chem. Soc., J. Phys. D Appl. Phys., Thin Solid Films, J. Cryst. Growth, Mater. Lett., Appl. Surf. Sci., Appl. Phys. A, J. Phys. Chem., Mat. Sci. Eng. B, Semicond. Sci. Technol.

H. Schmidt
- Referee: Phys. E, Appl. Phys. Lett., Phys. Stat. Sol. A, J. Appl. Phys., Opt. Mat., J. Phys. Cond. Matter
- Reviewer: European Young Investigators Awards 2006 (EURYI)

6.27 External Cooperations

Academic

- Leibniz-Institut für Oberflächenmodifizierung e.V., Leipzig
  Prof. Dr. B. Rauschenbach, Dr. E. Schubert

- Universität Leipzig, Fakultät für Biowissenschaften, Pharmazie und Psychologie
  Prof. Dr. A. Beck-Sickinger

- Universität Leipzig, Fakultät für Chemie und Mineralogie
  Dr. V. Gottschalch, Prof. Dr. H. Krautscheid, Prof. Dr. K. Bente

- Universität Halle-Wittenberg
  Prof. Dr. I. Mertig, Prof. Dr. W. Widdra

- Max-Planck-Institut für Mikrostrukturphysik, Halle/Saale
  Prof. Dr. U. Gösele, Dr. O. Breitenstein, Dr. A. Ernst, Dr. P. Werner, Dr. D. Hesse

- Forschungszentrum Dresden-Rossendorf
  Prof. Dr. M. Helm

- Technische Universität Berlin
  Prof. Dr. D. Bimberg, Dr. A. Hoffmann

- Universidade de Aveiro, Portugal
  Prof. Dr. N. Sobolev

- Kinki University, Dept. of Electronics Systems and Information Engeneering, Japan
  Dr. M. Kusunoki

- Paul Scherer Institut, Villingen
  Prof. Dr. H. Sigg

- Université Paris-Sud, France
  Prof. Dr. F. Julien

- Chinese Academy of Sciences, Institute of Physics, Beijing, P.R. China
  Prof. Dr. Yusheng He

- Universität Gießen
  Prof. Dr. B. Meyer, Dr. D. Hofmann, Prof. Dr. J. Janek

- Universität Magdeburg
  Prof. Dr. A. Krost, Dr. A. Dadgar, Prof. Dr. J. Christen

- Universität Bonn
  Prof. Dr. W. Mader

- Universität Hannover
  Prof. Dr. M. Binnewies

- Göteborg University, Sweden
  Prof. Dr. M. Willander

- NCSR "Demokritos", Institute of Materials Science, Greece
  Prof. Dr. A. Travlos

- Univerité Joseph Fourier, Grenoble, France
  Prof. Dr. D. Le Si Dang

- University of Pretoria, South Africa
  Prof. F.D. Auret

- University of Canterbury, Christchurch, New Zealand
  Prof. S. Durbin

Industry

- Solarion GmbH, Leipzig
  Dr. Alexander Braun

- El-Mul Technologies, Yavne, Israel
  Dr. Armin Schön

- PhysTech GmbH, Moosburg
  Dr. L. Cohausz

- OSRAM Opto-Semiconductors GmbH, Regensburg
  Dr. V. Härle

- Freiberger Compound Materials GmbH, Freiberg
  Dr. G. Leibiger

6.28 Publications

Journals

G. Brauer, W. Anwand, W. Skorupa, J. Kuriplach, O. Melikhova, J. Cizek, I. Prochazka, C. Moisson, H. von Wenckstern, H. Schmidt, M. Lorenz, M. Grundmann: *Defects in virgin and N^+-implanted ZnO single crystals studied by positron annihilation, Hall effect, and deep-level transient spectroscopy*, Phys. Rev. B **74**, 045 208 (2006), doi:10.1103/PhysRevB.74.045208

G. Brauer, W. Anwand, W. Skorupa, H. Schmidt, M. Diaconu, M. Lorenz, M. Grundmann: *Structure and ferromagnetism of Mn^+ ion-implanted ZnO thin films on sapphire*, Superlatt. Microstr. **39**, 41 (2006), doi:10.1016/j.spmi.2005.08.030

C. Bundesmann, A. Rahm, M. Lorenz, M. Grundmann, M. Schubert: *Infrared optical properties of $Mg_x Zn_{1-x}O$ thin films ($0 \leq x \leq 1$): Long-wavelength optical phonons and dielectric constants*, J. Appl. Phys. **99**, 113 504 (2006), doi:10.1063/1.2200447

M. Diaconu, H. Schmidt, M. Fecioru-Morariu, G. Guentherodt, H. Hochmuth, M. Lorenz, M. Grundmann: *Ferromagnetic behavior in Zn(Mn,P)O thin films*, Phys. Lett. A **351**, 323 (2006), doi:10.1016/j.physleta.2005.10.097

M. Diaconu, H. Schmidt, H. Hochmuth, M. Lorenz, G. Benndorf, D. Spemann, A. Setzer, P. Esquinazi, A. Pöppl, H. von Wenckstern, K.-W. Nielsen, R. Gross, H. Schmid, W. Mader, G. Wagner, M. Grundmann: *Room-temperature ferromagnetic Mn-alloyed ZnO films obtained by pulsed laser deposition*, J. Magn. Magn. Mat. **307**, 212 (2006), doi:10.1016/j.jmmm.2006.04.004

M. Diaconu, H. Schmidt, H. Hochmuth, M. Lorenz, H. von Wenckstern, G. Biehne, D. Spemann, M. Grundmann: *Deep defects generated in n-conducting ZnO:TM thin films*, Sol. Stat. Comm. **137**, 417 (2006), doi:10.1016/j.ssc.2005.12.028

D. Fritsch, H. Schmidt, M. Grundmann: *Pseudopotential band structures of rocksalt MgO, ZnO, and Mg$_{1-x}$Zn$_x$O*, Appl. Phys. Lett. **88**, 134 104 (2006), doi:10.1063/1.2188382

K. Goede, M. Grundmann, K. Holland-Nell, A. Beck-Sickinger: *Cluster properties of peptides on (100) semiconductor surfaces*, Langmuir **22**, 8104 (2006), doi:10.1021/la0605236

M. Gonschorek, H. Schmidt, J. Bauer, G. Benndorf, G. Wagner, G.E. Cirlin, M. Grundmann: *Thermally assisted tunneling processes in InGaAs/GaAs quantum dot structures*, Phys. Rev. B **74**, 115 312 (2006), doi:10.1103/PhysRevB.74.115312

T. Gühne, V. Gottschalch, G. Leibiger, H. Herrnberger, J. Kováč, J. Kováč jr., R. Schmidt-Grund, B. Rheinländer, D. Pudiš: *Properties of (InGa)As/GaAs QW (∼ 1.2 μm) Facet-Coated Edge Emitting Diode Laser*, Laser Phys. **16**, 441 (2006)

L. Hartmann, Q. Xu, H. Schmidt, H. Hochmuth, M. Lorenz, C. Sturm, C. Meinecke, M. Grundmann: *Spin polarization in Zn$_{0.95}$Co$_{0.05}$O:(Al,Cu) thin films*, J. Phys. D Appl. Phys. **39**, 4920 (2006), doi:10.1088/0022-3727/39/23/003

S. Heitsch, G. Zimmermann, A. Rahm, C. Bundesmann, G. Wagner, H. Hochmuth, M. Lorenz, H. Schmidt, M. Schubert, M. Grundmann: *Structural and optical properties of ZnO thin films grown on silicon by pulsed laser deposition*, Thin Solid Films **496**, 234 (2006), doi:10.1016/j.tsf.2005.08.305

S. Jaensch, H. Schmidt, M. Grundmann: *Quantitative scanning capacitance microscopy*, Physica B **376**–**377**, 913 (2006), doi:10.1016/j.physb.2005.12.227

C. Klingshirn, M. Grundmann, A. Hoffmann, B. Meyer, A. Waag: *Zinkoxid - Ein alter, neuer Halbleiter*, Phys. J. **5**(1), 33 (2006)

M. Lorenz, R. Johne, H.P.D. Schenk, S.I. Borenstain, A. Schön, C. Bekeny, T. Voss, J. Gutowski, T. Nobis, H. Hochmuth, J. Lenzner, M. Grundmann: *Fast, high-efficiency, and homogeneous room-temperature cathodoluminescence of ZnO scintillator thin films on sapphire*, Appl. Phys. Lett. **89**, 243 510 (2006), doi:10.1063/1.2405392

C. Meinecke, J. Vogt, R. Schmidt-Grund, T. Butz: *RBS studies on coated micro-dimensional glass fibers used as micro-resonators*, Nucl. Instr. Meth. B **249**, 387 (2006), doi:10.1016/j.nimb.2006.04.035

T. Nobis, A. Rahm, M. Lorenz, M. Grundmann: *Numerical Modelling of Zinc Oxide Nanocavities to Determine Their Birefringence*, Proc. SPIE **6122**, 61 220V (2006), doi:10.1117/12.660550

L. Peternai, J. Kováč, J. Jakabovic, V. Gottschalch, B. Rheinländer: *Investigation of GaN$_x$P$_{1-x}$/GaP LED structures optical properties*, J. Electron. Mater. **35**, 654 (2006)

V.M. Polyakov, F. Schwierz, D. Fritsch, H. Schmidt: *Monte Carlo study of steady-state and transient transport in wurtzite InN*, Phys. Stat. Sol. C **3**, 598 (2006), doi:10.1002/pssc.200564146

A. Rahm, E.M. Kaidashev, H. Schmidt, M. Diaconu, A. Pöppl, R. Böttcher, C. Meinecke, T. Butz, M. Lorenz, M. Grundmann: *Growth and characterization of Mn- and Co-doped ZnO nanowires*, Microchim. Acta **156**, 21 (2007), doi:10.1007/s00604-006-0602-1

H. Schmidt, M. Diaconu, H. Hochmuth, M. Lorenz, A. Setzer, P. Esquinazi, A. Pöppl, D. Spemann, K.W. Nielsen, R. Gross, G. Wagner, M. Grundmann: *Weak ferromagnetism in textured $Zn_{1-x}TM_xO$ thin films*, Superlatt. Microstr. **39**, 334 (2006), doi:10.1016/j.spmi.2005.08.059

R. Schmidt-Grund, A. Carstens, B. Rheinländer, D. Spemann, H. Hochmut, G. Zimmermann, M. Lorenz, M. Grundmann, C.M. Herzinger, M. Schubert: *Refractive indices and band-gap properties of rocksalt $Mg_xZn_{1-x}O$ ($0.68 \leq x \leq 1$)*, J. Appl. Phys. **99**, 123 701 (2006), doi:10.1063/1.2205350

R. Schmidt-Grund, T. Gühne, H. Hochmuth, B. Rheinländer, A. Rahm, V. Gottschalch, J. Lenzner, M. Grundmann: *Cylindrical resonators with coaxial Bragg reflectors*, Proc. SPIE **6038**, 489 (2006), doi:10.1117/12.638585

E. Schubert, J. Fahlteich, B. Rauschenbach, M. Schubert, M. Lorenz, M. Grundmann, G. Wagner: *Recrystallization behavior in chiral sculptured thin films from silicon*, J. Appl. Phys. **100**, 016 107 (2006), doi:10.1063/1.2207728

H. von Wenckstern, G. Biehne, R. Abdel Rahman, H. Hochmuth, M. Lorenz, M. Grundmann: *Mean barrier height of Pd Schottky contacts on ZnO thin films*, Appl. Phys. Lett. **88**, 092 102 (2006), doi:10.1063/1.2180445

H. von Wenckstern, R. Pickenhain, H. Schmidt, M. Brandt, G. Biehne, M. Lorenz, M. Grundmann: *Deep acceptors states in ZnO single crystals*, Appl. Phys. Lett. **89**, 092 122 (2006), doi:10.1063/1.2335798

Q. Xu, L. Hartmann, H. Schmidt, H. Hochmuth, M. Lorenz, R. Schmidt-Grund, D. Spemann, A. Rahm, M. Grundmann: *Magnetoresistance in pulsed laser deposited 3d transition metal doped ZnO films*, Thin Solid Films **515**, 2549 (2006), doi:10.1016/j.tsf.2006.04.024

Q. Xu, L. Hartmann, H. Schmidt, H. Hochmuth, M. Lorenz, R. Schmidt-Grund, D. Spemann, M. Grundmann: *Magnetoresistance effects in $Zn_{0.90}Co_{0.10}O$ films*, J. Appl. Phys. **100**, 013 904 (2006), doi:10.1063/1.2208691

Q. Xu, L. Hartmann, H. Schmidt, H. Hochmuth, M. Lorenz, R. Schmidt-Grund, C. Sturm, D. Spemann, M. Grundmann: *Metal-insulator transition in Co-doped ZnO: Magneto-transport properties* Phys. Rev. B **73**, 205 342 (2006), doi:10.1103/PhysRevB.73.205342

J. Zúñiga-Pérez, V. Munoz-Sanjose, M. Lorenz, G. Benndorf, S. Heitsch, D. Spemann, M. Grundmann: *Structural characterization of a-plane $Zn_{1-x}Cd_xO$ ($0 \leq x \leq 0.085$) thin films grown by metal-organic vapor phase epitaxy*, J. Appl. Phys. **99**, 023 514 (2006), doi:10.1063/1.2163014

Books

C. Bundesmann, M. Lorenz, M. Grundmann, M. Schubert: *Phonon modes, dielectric constants, and exciton mass parameters in ternary $Mg_xZn_{1-x}O$*, in: *Current and Future Trends of Functional Oxide Films*, ed. by D. Kumar, V. Craciun, M. Alexe, K.K. Singh, Mat. Res. Soc. Symp. Proc. **928E** (MRS, Warrendale 2006)

M. Grundmann: *The Physics of Semiconductors, An Introduction including Devices and Nanophysics* (Springer, Heidelberg 2006)

M. Grundmann (Ed.): *The Physics Institutes of Universität Leipzig, Report 2005* (Universität Leipzig, Leipzig 2006)

M. Grundmann, A. Rahm, T. Nobis, H. von Wenckstern, M. Lorenz, C. Czekalla, J. Lenzner: *Growth and Characterization of Optical and Electrical Properties of ZnO Nano- and Microwires*, in *Zinc Oxide and Related Materials*, ed. by J. Christen et al., Mater. Res. Soc. Symp. Proc. **957** (MRS, Warrendale 2007)

S. Heitsch, G. Zimmermann, A. Müller, J. Lenzner, H. Hochmuth, G. Benndorf, M. Lorenz, M. Grundmann: *Interface and Luminescence Properties of Pulsed Laser Deposited MgZnO/ZnO Quantum Wells with Strong Confinement*, in *Zinc Oxide and Related Materials*, ed. by J. Christen et al., Mater. Res. Soc. Symp. Proc. **957** (MRS, Warrendale 2007)

H. von Wenckstern, M. Brandt, J. Lenzner, G. Zimmermann, H. Hochmuth, M. Lorenz, M. Grundmann: *Temperature dependent Hall measurements on PLD thin films*, in *Zinc Oxide and Related Materials*, ed. by J. Christen et al., Mater. Res. Soc. Symp. Proc. **957** (MRS, Warrendale 2007)

in press

C. Czekalla, J. Lenzner, A. Rahm, T. Nobis, M. Grundmann: *A Zinc Oxide Microwire Laser*, Superlatt. Microstruct.

R. Schmidt-Grund, B. Rheinländer, C. Czekalla, G. Benndorf, H. Hochmut, A. Rahm, M. Lorenz, M. Grundmann: *ZnO based planar and micro-pillar resonators*, Superlatt. Microstruct.

H. von Wenckstern, M. Grundmann: *Electrical properties of ZnO bulk and thin films*, Adv. Mater.

Talks

J. Bauer, V. Gottschalch, H. Paetzelt, G. Wagner, G. Benndorf: *MOVPE-growth, real-structure and physical properties of vertical-aligned GaAs-Nanowires*, 13th Int. Conf. Metal Organic Vapor Phase Epitaxy, Miyazaki, Japan, 22.–25. May 2006

G. Brauer, W. Anwand, W. Skorupa, J. Kuriplach, O. Melikhova, J. Cizek, I. Prochazka, H. von Wenckstern, M. Brandt, M. Lorenz, M. Grundmann: *Defects in N$^+$ ion-implanted ZnO single crystals studied by positron annihilation and Hall effect*, 19th Int. Conf. Application of Accelerators in Research and Industry (CAARI2006), Fort Worth/Texas, USA, 20.–25. August 2006

G. Brauer, W. Anwand, W. Skorupa, J. Kuriplach, O. Melikhova, J. Cizek, I. Prochazka, H. von Wenckstern, M. Brandt, M. Lorenz, M. Grundmann: *Defects in N^+ ion-implanted ZnO single crystals studied by positron annihilation and Hall effect*, 14th Int. Conf. Positron Annihilation (ICPA-14), Hamilton/Ontario, Canada, 23.–28. July 2006

C. Bundesmann, R. Schmidt-Grund, D. Spemann, M. Lorenz, M. Grundmann, M. Schubert: *Phonon modes, dielectric contants, and exciton mass parameters in ternary $Mg_xZn_{1-x}O$*, MRS Spring Meeting, San Francisco, USA, 17.–21. April 2006

C. Bundesmann, R. Schmidt-Grund, D. Spemann, M. Lorenz, M. Grundmann, M. Schubert: *Infrared optical studies of ternary $Mg_xZn_{1-x}O$: Phonons, dielectric constants, and effective mass parameters*, 4th Workshop Ellipsometry, Berlin, 20.–22. February 2006

H. Frenzel, A. Weber, H. von Wenckstern, G. Biehne, H. Hochmuth, M. Lorenz and M. Grundmann: *Mid-infrared photocurrent spectroscopy of thin ZnO films*, DPG spring meeting Dresden, 28. March 2006

L. Hartmann, Q. Xu, H. Schmidt, H. Hochmuth, M. Lorenz, R. Schmidt-Grund, D. Spemann, M. Grundmann: *Defect mediated ferromagnetism in $Zn_{0.95}Co_{0.05}O$:(Cu,Al) thin films*, German Physical Society Spring Meeting, Dresden, 27.–31. March 2006

S. Heitsch, G. Zimmermann, C. Schulz, J. Lenzner, H. Hochmuth, D. Spemann, G. Benndorf, H. Schmidt, T. Nobis, M. Lorenz, M. Grundmann: *Photoluminescence properties of $Mg_xZn_{1-x}O$ thin films grown by pulsed laser deposition*, German Physical Society Spring Meeting, Dresden, 27.–31. March 2006

H. Schmidt: *NanoFutur: Verbesserung der industriellen Kooperationsmöglichkeiten*, nanoDE 2006, 3. BMBF-Nanotechnologietage, Berlin, 06./07. November 2006

H. Schmidt: *ZnO als Basismaterial für Spintronik-Bauelemente*, FWIN und FWIM Seminar Series, Forschungszentrum Dresden-Rossendorf, Institut für Ionenstrahlphysik und Materialforschung, 20. November 2006

H. Schmidt, S. Jaensch, C. Henkel, M. Brandt, M. Grundmann: *2D-Dotierprofile von Halbleitern auf der Nanometerskala*, Physikalisches Kolloquium der TU Bergakademie Freiberg, 24. Mai 2006

H. Schmidt, M. Ungureanu, Q. Xu, L. Hartmann, H. Hochmuth, M. Lorenz, M. Grundmann: *ZnO as a basis material for spintronic devices*, NSF-MRSEC Seminar Series, University of Nebraska, Lincoln, USA, 22. September 2006

R. Schmidt-Grund, T. Gühne, H. Hochmuth, B. Rheinländer, A. Rahm, V. Gottschalch, J. Lenzner, M. Grundmann: *ZnO micro-pillar resonators with coaxial Bragg-Reflectors*, 6th Int. Conf. Physics of Light-Matter Coupling in Nanostructures (PLMCN6), Magdeburg, 25.–29. September 2006

R. Schmidt-Grund, B. Rheinländer, C. Czekalla, T. Gühne, G. Benndorf, H. Hochmut, A. Rahm, V. Gottschalch, R. Heimbuch, J. Lenzner, M. Grundmann: *Towards cylindrical ZnO resonators with coaxial Bragg-Reflectors*, FAHL Academia, Int. Workshop Self-assembly of Complex Nanostructures, Leipzig, 25./26. September 2006

M. Schubert, C. Bundesmann, N. Ashkenov, H. v. Wenckstern, H. Schmidt, M. Lorenz, T. Nobis, H. Hochmuth, M. Diaconu, D. Fritsch, A. Rahm, R. Schmidt-Grund, M. Grundmann: *ZnO-based thin films and nanostructures: Phonons, plasmons, band gap energies, magnetism and electric polarization exchange: A Leipzig review* [Invited talk], SPIE Photonics West, San Jose, USA, 21. – 26. January 2006

C. Sturm, R. Schmidt-Grund, R. Kaden, B. Rheinländer, K. Bente, M. Grundmann: *Ellipsometry and Microreflection on Cylindrite*, German Physical Society Spring Meeting, Dresden, 27. – 31. March 2006

H. von Wenckstern, J. Sann, M. Brandt, G. Benndorf, S. Heitsch, A. Krtschil, M. Lorenz, M. Grundmann, A. Krost, B.K. Meyer: *Optical and electrical properties of phosphorous doped ZnO thin films*, German Physical Society Spring Meeting, Dresden, 27. – 31. March 2006

H. von Wenckstern, H. Schmidt, R. Pickenhain, G. Biehne, M. Brandt, G. Brauer, M. Lorenz, M. Grundmann: *Electrical characterization of deep acceptor states in N implanted ZnO single crystals*, German Physical Society Spring Meeting, Dresden, 27. – 31. March 2006

H. von Wenckstern, H. Schmidt, R. Pickenhain, G. Biehne, M. Brandt, M. Lorenz, G. Brauer, A. Dadgar, A. Krost, M. Grundmann: *Electrical Characterization of Deep Acceptor States in ZnO*, 2006 MRS Fall Meeting, Boston, USA, 27. November – 01. December 2006

H. von Wenckstern, H. Schmidt, R. Pickenhain, G. Biehne, M. Brandt, M. Lorenz, M. Grundmann, G. Brauer: *Deep Acceptor States in ZnO Single Crystals*, E-MRS 2006, Nice, France, 29. May – 02. June 2006

Q. Xu, L. Hartmann, H. Schmidt, H. Hochmuth, M. Lorenz, R. Schmidt-Grund, D. Spemann, M. Grundmann: *Thickness dependent magnetoresistance of ZnCoO:Al thin films*, German Physical Society Spring Meeting, Dresden, 27. – 31. March 2006

Posters

G. Brauer, W. Anwand, W. Skorupa, J. Kuriplach, O. Melikhova, J. Cizek, I. Prochazka, C. Moisson, H. von Wenckstern, H. Schmidt, M. Lorenz, M. Grundmann: *Comparative characterization of differently grown ZnO single crystals by positron annihilation and Hall effect*, E-MRS 2006, Nice, France, 29. May – 02. June 2006

G. Brauer, W. Anwand, W. Skorupa, J. Kuriplach, O. Melikhova, J. Cizek, I. Prochazka, H. von Wenckstern, M. Brandt, M. Lorenz, M. Grundmann: *Defects in N$^+$ ion-implanted ZnO single crystals studied by positron annihilation and Hall effect*, 4th Int. Wokshop on ZnO and Related Materials, Giessen, 03. – 06. October 2006

H. Frenzel, H. von Wenckstern, A. Weber, G. Biehne, H. Hochmuth, M. Lorenz, M. Grundmann: *Measurement of deep intrinsic defects in thin ZnO films via mid-infrared photocurrent spectroscopy*, 28th Int. Conf. Physics of Semiconductors, Vienna, Austria, 24. – 28. July 2006

D. Fritsch, H. Schmidt, M. Grundmann: *Pseudopotential investigations of electronic and optical properties of wurtzite ZnO and GaN*, German Physical Society Spring Meeting, Dresden, 27. – 31. March 2006

D. Fritsch, H. Schmidt, M. Grundmann: *Calculated optical properties of wurtzite GaN and ZnO*, 28th Int. Conf. Physics of Semiconductors, Vienna, Austria, 24. – 28. July 2006

D. Fritsch, H. Schmidt, M. Grundmann: *Pseudopotential investigation of the electronic and optical properties of wurtzite ZnO*, 4th Int. Workshop ZnO and Related Materials, Giessen, 03. – 06. October 2006

V. Gottschalch, J. Bauer, H. Paetzelt, M. Shirnow, G. Wagner, J. Lenzner: *MOVPE-growth of GaN-nanowires on various III-V-substrates*, FAHL Academia, Int. Workshop Self-assembly of Complex Nanostructures, Leipzig, 25./26. September 2006

V. Gottschalch, H. Herrnberger, T. Gühne, J. Kováč jr., G. Leibiger, J. Kováč, R. Schmidt-Grund, J. Zajadacz, J. Dienelt, A. Schindler: *(InGa)As Oberflächenemitter mit horizontaler Kavität (HCSEL)*, German Physical Society Spring Meeting, Dresden, 27. – 31. March 2006

S. Heitsch, G. Zimmermann, J. Lenzner, H. Hochmuth, G. Benndorf, M. Lorenz, M. Grundmann: *Photoluminescence of $Mg_xZn_{1-x}O$/ZnO Quantum Wells Grown by Pulsed Laser Deposition*, FAHL Academia, Int. Workshop Self-assembly of Complex Nanostructures, Leipzig, 25./26. September 2006

S. Heitsch, G. Zimmermann, J. Lenzner, H. Hochmuth, G. Benndorf, M. Lorenz, M. Grundmann: *Photoluminescence of $Mg_xZn_{1-x}O$/ZnO Quantum Wells Grown by Pulsed Laser Deposition*, 28th Int. Conf. Physics of Semiconductors, Vienna, Austria, 24. – 28. July 2006

J. Kováč, J. Kováč jr., D. Pudiš, A. Šatka, F. Uherek, V. Gottschalch, B. Rheinländer, H. Herrnberger, J. Zajadacz, K. Zimmer, A. Schindler: *Properties of InGaAs/GaAs QW Coupled Edge and Surface Emitting Tilted Cavity Lasers*, 15th Int. Laser Physics Workshop, Lausanne, Switzerland, 24. – 28. July 2006

M. Lorenz, H. Hochmuth, H. von Wenckstern, M. Brandt, H. Schmidt, R. Johne, R. Schmidt-Grund, G. Benndorf, J. Lenzner, M. Schubert, M. Grundmann: *Advances in high-quality ZnO thin films and heterostructures grown by Pulsed Laser Deposition*, 4th Int. Workshop ZnO and Related Materials, Giessen, 03. – 06. October 2006

R. Schmidt-Grund, N. Ashkenov, M. Schubert, W. Czakai, D. Faltermeier, G. Benndorf, H. Hochmuth, M. Lorenz, J. Bläsig, M. Grundmann: *Temperature-dependent band-gap and excitonic properties of ZnO*, 4th Int. Workshop ZnO and Related Materials, Giessen, 03. – 06. October 2006

R. Schmidt-Grund, N. Ashkenov, M. Schubert, W. Czakai, D. Faltermeier, G. Benndorf, H. Hochmuth, M. Lorenz, J. Bläsig, M. Grundmann: *Temperature-dependent band-gap and excitonic properties of ZnO* 28th Int. Conf. Physics of Semiconductors, Vienna, Austria, 24. – 28. July 2006

R. Schmidt-Grund, N. Ashkenov, M. Schubert, W. Czakai, D. Faltermeier, G. Benndorf, H. Hochmuth, M. Lorenz, J. Bläsig, M. Grundmann: *Temperature-dependent band-gap and excitonic properties of ZnO*, 4th Workshop Ellipsometry, Berlin, 20. – 22. February 2006

R. Schmidt-Grund, T. Gühne, H. Hochmuth, B. Rheinländer, A. Rahm, V. Gottschalch, J. Lenzner, M. Grundmann: *Cylindric resonators with coaxial Bragg-Reflectors*, FAHL Academia, Int. Workshop Self-assembly of Complex Nanostructures, Leipzig, 25./26. September 2006

R. Schmidt-Grund, T. Gühne, H. Hochmuth, B. Rheinländer, A. Rahm, V. Gottschalch, J. Lenzner, M. Grundmann: *Cylindric resonators with coaxial Bragg-Reflectors*, 28th Int. Conf. Physics of Semiconductors, Vienna, Austria, 24. – 28. July 2006

R. Schmidt-Grund, T. Gühne, H. Hochmuth, B. Rheinländer, A. Rahm, V. Gottschalch, J. Lenzner, M. Grundmann: *Cylindric Resonators With Coaxial Bragg-Reflectors*, German Physical Society Spring Meeting, Dresden, 27. – 31. March 2006

M. Shirnow, V. Gottschalch, G. Wagner, J. Bauer, H. Paetzelt, J. Lenzner: *MOVPE-Wachstum von GaN Nadeln*, German Physical Society Spring Meeting, Dresden, 27. – 31. March 2006

C. Sturm, T. Chavdarov, R. Schmidt-Grund, B. Rheinländer, H. Hochmuth, M. Lorenz, M. Grundmann: *Anisotropy of the band-gap of ZnO thin films*, 4th Int. Workshop ZnO and Related Materials, Giessen, 03. – 06. October 2006

C. Sturm, R. Schmidt-Grund, R. Kaden, B. Rheinländer, K. Bente, H. von Wenckstern, M. Grundmann: *Optical Properties of Cylindrite*, FAHL Academia, Int. Workshop Self-assembly of Complex Nanostructures, Leipzig, 25./26. September 2006

C. Sturm, R. Schmidt-Grund, R. Kaden, B. Rheinländer, K. Bente, H. von Wenckstern, M. Grundmann: *Optical Properties of Cylindrite*, 28th Int. Conf. Physics of Semiconductors, Vienna, Austria, 24. – 28. July 2006

C. Sturm, R. Schmidt-Grund, R. Kaden, B. Rheinländer, K. Bente, M. Grundmann: *Generalized Ellipsometry on Cylindrite*, 4th Workshop Ellipsometry, Berlin, 20. – 22. February 2006

H. von Wenckstern, M. Brandt, H. Schmidt, H. Hochmuth, M. Lorenz, M. Grundmann: *Comprehensive study of donors states in ZnO thin films*, 4th Int. Wokshop on ZnO and Related Materials, Giessen, 03. – 06. October 2006

H. von Wenckstern, M. Brandt, H. Schmidt, G. Zimmermann, R. Johne, J. Lenzner, H. Hochmuth, M. Lorenz, M. Grundmann: *Integral electrical and micro-electrical investigations of ZnO thin films*, German Physical Society Spring Meeting, Dresden, 27. – 31. March 2006

H. von Wenckstern, J. Sann, M. Brandt, A. Krtschil, M. Lorenz, M. Grundmann, B.K. Meyer, A. Krost: *Optical and electrical properties of phosphorous-doped ZnO thin films*, E-MRS 2006, Nice, France, 29. May – 02. June 2006

Q. Xu, L. Hartmann, H. Schmidt, H. Hochmuth, M. Lorenz, R. Schmidt-Grund, C. Sturm, D. Spemann, M. Grundmann: *The magnetotransport properties of Co-doped ZnO films*, 28th Int. Conf. Physics of Semiconductors, Vienna, Austria, 24. – 28. July 2006

6.29   Graduations

Doctorate

- Thomas Nobis
  Beobachtung und Modellierung des optischen Flüstergalerie-Effekts in hexagonalen Zinkoxid-Nanoresonatoren
  September, 2006

Diploma

- Matthias Brandt
  Elektrische Eigenschaften von Zinkoxid bei erhöhten Temperaturen
  Mai 2006

- Christian Czekalla
  Hochanregungsspektroskopie an Zinkoxid-Strukturen
  September 2006

- Heiko Frenzel
  Fourier-Transform-Infrarot-Photostrom-Spektroskopie an ZnO-Schottkydioden
  September 2006

- Lars Hartmann
  Transportuntersuchungen an ZnO Dünnfilmen im elektrischen und magnetischen Feld
  August 2006

- Robert Johne
  Kathodolumineszenz-Untersuchung von Zinkoxid Dünnfilmen für Szintillator-Anwendungen – Experiment und Modellierung
  Januar 2006

- Hendrik Paetzelt
  Herstellung und Charakterisierung von $A^{III}B^{V}$ Nano- und Mikrorollen
  Januar 2006

- Mario Saenger
  Dielectric Function, Phonon, and Polaron modes in Electrochemically colored Tungsten Oxide Thin Films
  Oktober 2006

- Chris Sturm
  Verallgemeinerte Ellipsometrie an a-plane und m-plane orientierten ZnO-Schichten
  Dezember 2006

Master

- Ra'ed Abdel Rahman
  Schottky Contacts on n-type ZnO Thin Films
  Mai 2006

6.30   Guests

- Amélia Ankiewicz
  Universidade de Aveiro, Portugal
  05. – 29. July 2006

- Dr. Evgeny M. Kaydashev
  Rostov-on-Don State University, Russia
  29. July – 29. October 2006

- Yu-Zi Liu, M.Sc.
  Institute of Physics, Chinese Academy of Science, Beijing, PR China
  01. April – 31. July 2006

7

Solid State Optics and Acoustics

7.1 Development of a Miniaturized Advanced Diagnostic Technology Demonstrator 'DIAMOND' - Technology Study Phase 2

W. Grill, R. Wannemacher

A miniaturized universal scanning microscope ('space microscope') is being developed for potential operation on board of the International Space Station ISS, which allows diagnostics of samples by means of optical scanning microscopy, partly combined with spectral resolution, as well as by means of acoustic microscopy with vector contrast. Foreseen microscopic techniques are confocal optical microscopy in reflection, scanning microscopy in transmission, as well as spectrally resolved fluorescence and Raman microscopy. Acoustic microscopy permits spatially resolved determination of micromechanical sample properties.

7.2 Ultrasound Diagnostics of Directional Solidification

W. Grill, E. Twerdowski, M. von Buttlar, R. Wannemacher

An ultrasonic measuring device based on guided waves has been developed in order to determine the growth rate of alloys, in particular of opaque metallic alloys. Experimental tests show that a high resolution is achievable in the determination of the position of the solid-liquid interface, down to 0.01 mm. The ultrasonic technique is therefore an appropriate tool for the measurement of the solidification velocity for stable as well as unstable solidification processes. The aim consists in the investigation of the impact of process parameters on the resulting material properties. Controlled non-stationary growth presently appears to become a main research object for the next future, in particular in the context of industrial applications. The measurement of the solidification velocity by ultrasound is a diagnostic tool for directional solidification experiments. It was developed in the framework of the Technological Research Programme of the European Space Organization. An ultrasound pulse launched from the cold end of the

sample and being reflected from the phase boundary of solidification allows to determine the position of the solid-liquid interface. Given the speed of sound in the sample the position of the phase boundary can be determined as a function of time and, hence, the solidification velocity via precise measurement of the propagation time by means of an autocorrelation technique.

7.3 Development and Verification of the Applicability of Ultrasonic Methods

W. Grill, Z. Kojro

Possible applications associated with the company Schott GLAS of the ultrasound techniques developed and published by our group are investigated. Techniques, sensors, and measurement devices are being developed. The work is conducted in cooperation with Schott GLAS. New techniques were developed and tested.

7.4 Multi-Contrast Imaging of Soft Matter Samples by Combinatory Scanning Confocal Laser and Acoustic Vector Contrast Microscopy

A.E. Kamanyi, R. Wannemacher, W. Grill

A number of combinations of different microscopes have been used and are still used by scientists, in an attempt to realize a more productive and cost effective characterization of samples. We present another such combination. We constructed and tested a combinatory confocal laser scanning microscope (CLSM) and phase-sensitive scanning acoustic microscope (PSAM) resulting in good quality multi-contrast images (electromagnetic and mechanical contrast). The microscopes are both confocal in nature, but the similarities end there. The CLSM is a more established and widely used form of optical microscopy. It is very valuable for obtaining high-resolution images and 3D reconstructions. The fluorescence detection mode of the CLSM makes it an instrument of choice in the biological and medical sciences. It can be particularly useful in viewing only selected components of an object, by selective staining with fluorescent dyes or fluorescent markers. However, the CLSM is limited to non-opaque samples. This limitation is complemented in this combination by the PSAM acoustic waves' ability to penetrate the sample and image what lies beneath. Acoustic microscopy uses high frequency acoustic waves instead of optical waves for qualitative (imaging) and quantitative characterization of materials. The image contrast also differs in that the acoustic microscope is sensitive to changes in acoustic impedance (density $\times$ velocity) while the laser scanning microscope like all other light microscopes is sensitive to changes in refractive index, n. This leads to different characteristics for the contrast in the two techniques.
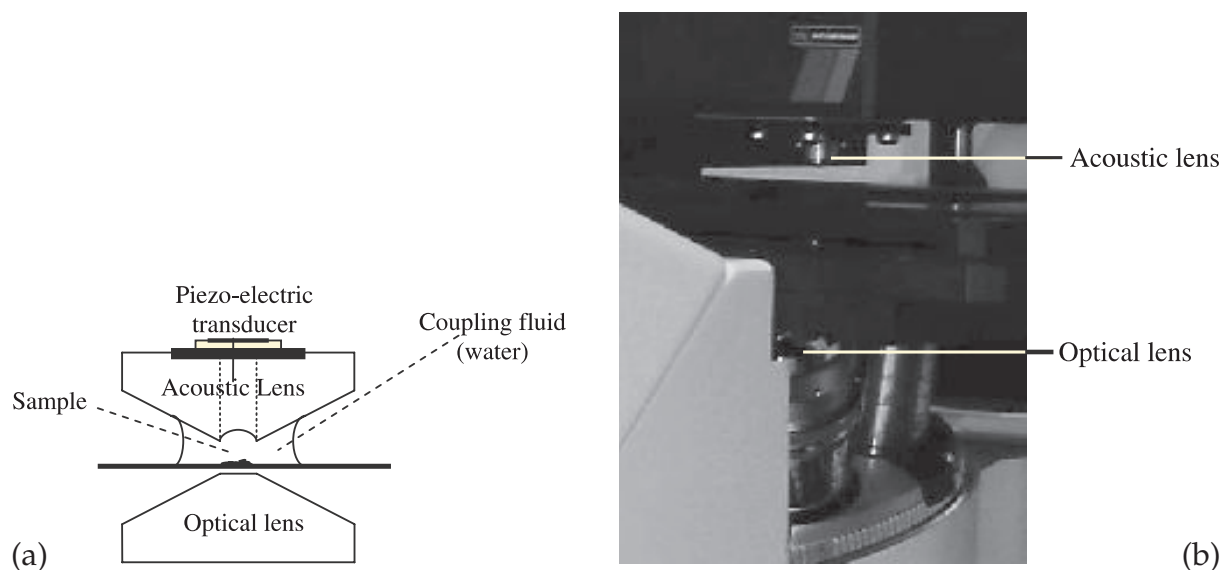
Figure 7.1: (**a**) Lens set-up of combined PSAM-CLSM. (**b**) Digital camera image of lens arrangement.
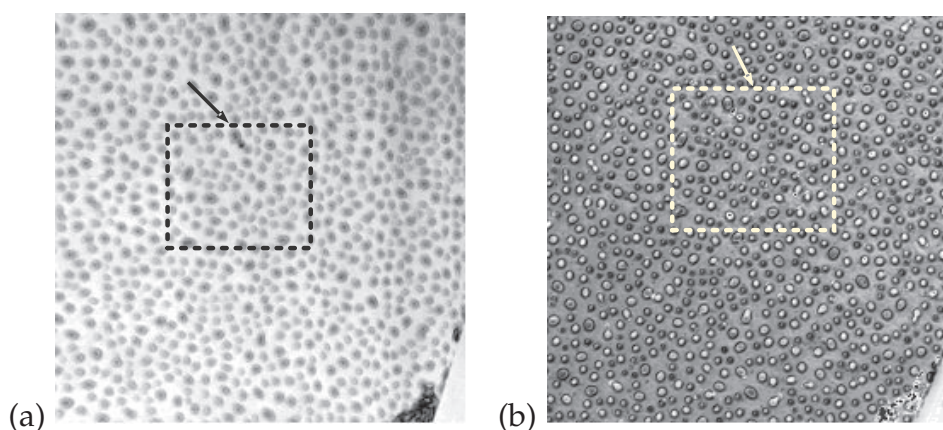
Figure 7.2: Images taken by combined PSAM and CLSM of sample 1. (**a**) PSAM image, (**b**) CLSM image (PSAM Image size: 150×160 µm; CLSM Image: 150×150 µm).

The experimental set-up is based on a modified commercial confocal Laser scanning microscope (Zeiss LSM510) and is shown in Fig. 7.1 [1]. Figures 7.2 and 7.3 display results for a PS/PMMA blend spin-coated on a glass substrate. A significant difference in contrast is observed in the acoustic and optical images, respectively, while the basic structures are the same. From the acoustic image, the darker areas (some have black spots in them) are assigned to polystyrene since it has lower acoustic impedance, $Z \sim 2.5$ MRayls, while the brighter areas, which seem interconnected in the background, are PMMA with higher acoustic impedance, $Z \sim 3.2$ MRayls. The contrast in the optical images is different, and almost reverse in gray scale. This is attributed to the refractive indices of PS and PMMA, which are known to be $n_{PS} \sim 1.60$, $n_{PMMA} \sim 1.49$ at $\lambda = 543$ nm (measurement wavelength for the CLSM image). Substantially more information is obtainable from the PSAM images. The morphology can be studied and corresponding 3D images can be created. The average film thickness and height profile can also be obtained from the PSAM phase image. Volume imaging is also possible
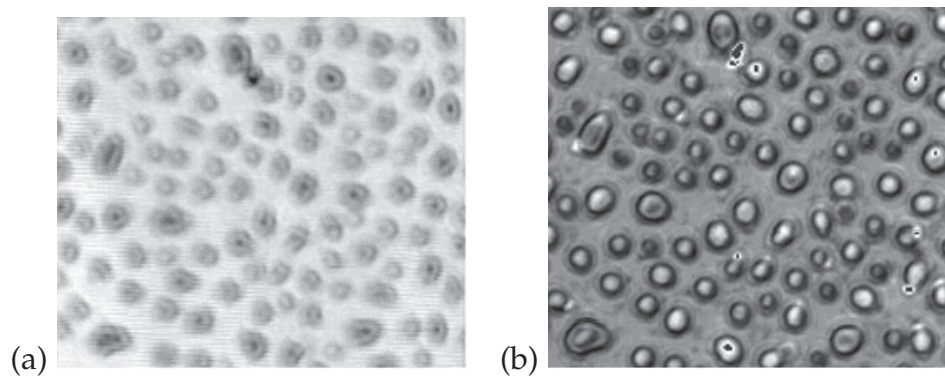
Figure 7.3: Zoomed-in images of areas marked in Fig. 7.2. (**a**) Acoustic image, (**b**) optical image.

Figure 7.4: Pseudo-3D images of fibroblast with height profile from PSAM phase image. (**a**) PSAM amplitude (brightness contrast), (**b**) CLSM Fluorescence (brightness), (**c**) CLSM reflection (brightness).

with the PSAM. The micro-elastic properties of the blend can be investigated by taking y–z images and calculating the surface wave velocities from the $V(z)$ curves. The CLSM can be used to image surface and bulk structures in the blends as well as to study the surface morphology.

As another example fibroblasts were studied using the combinatory PSAM/CLSM technique. Fibroblasts are cells that make up the structural fibers and ground substance for connective tissues. They are characterized by an abundant and branched cytoplasm surrounding an elliptical, speckled nucleus. The cells imaged here were stained for f-actin with phalloidin in order to observe fluorescence. Fig. 7.4 displays the unique 3D multi-contrast images obtainable from this combinatory microscope.

[1] A.E. Kamanyi et al.: Proc. SPIE **6177**, 617 712 (2006)

7.5 Modeling of Local Piezoelectric Coupling and Acoustic Wave Propagation in Piezoelectric Materials

M. Pluta, A. Habib, E. Twerdowski, M. von Buttlar, M. Schmachtl, R. Wannemacher, W. Grill

Anisotropic propagation of sound waves in crystals is associated with a number of remarkable phenomena. One of them is the appearance of caustics, that is directions in which the energy flow becomes very large, in fact infinite in the limit of geometric acoustics. Even cubic crystals can exhibit caustics in the propagation of sound. The study of this so-called phonon focusing phenomenon in crystals has attracted great attention in the last few decades. Piezoelectric materials are of special interest due to their industrial applications. In describing the elastic behavior of the piezoelectric

(a)   (b)   (c)
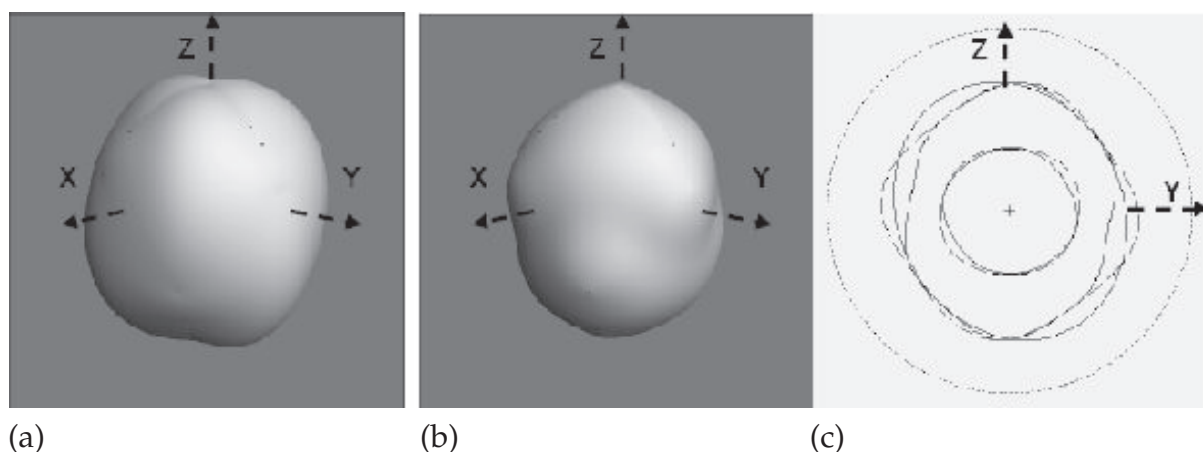
Figure 7.5: Lithium niobate slowness surfaces with piezoelectric stiffening included. ST mode (**a**), FT mode (**b**). Dots are visible on both sheets at conic points. (**c**) Shows the y–z cross-section of slowness surfaces calculated without (*dashed lines*) and with (*solid line*) piezoelectric stiffening for all modes. The inner sheets correspond to the longitudinal mode, and the outer ones to the two transversal modes. The *dotted circle* at $s = 0.4\,\text{s/km}$ defines the scale of the images. (Values along the oval line in (**c**) are not affected by the piezoelectric stiffening, so both lines coincide).

crystals, the standard procedure is to include both, the strain-induced stress and the electric-field-induced stress in Newton's equation of motion for continuous media. The crystal then appears elastically stiffened, and the phase velocity and polarization of the wave are altered compared to the case without the piezoelectric effect. The effect of piezoelectric stiffening must be taken into account in interpreting ultrasonic data, phonon focusing patterns, ballistic heat transport, and other transport phenomena. Due to piezoelectric stiffening caustics may vanish, appear, or be shifted substantially. Piezoelectricity also reduces the acoustic symmetry. This happens, because piezoelectricity, even in the electrostatic approximation, increases the degree of the equation of the slowness surface from 6 to 8. Using the material constants reported in the literature slowness surfaces for $LiNbO_3$ have been calculated with and without the piezoelectric effect. The transversal slowness sheets with the piezoelectric stiffening included are presented in Fig. 7.5. Points of the conical degeneracy are noticeable as spots on the surface. Piezoelectric stiffening generally increases phase velocities, which is equivalent to contraction of the slowness surface (compare Fig. 7.5c). Group velocity surfaces corresponding to the slowness sheets shown in Fig. 7.5 are displayed in Fig. 7.6.

Phonon focusing. Where the curvature of the slowness surface is small, the rays are strongly bunched together in direction, and consequently the energy flux in their direction is large, and vice versa. A measure of phonon focusing is related to the mapping of directions from slowness to the group velocity space. Calculated results of phonon focusing are shown in Fig. 7.7.

Arrival time. For a point source at a crystal surface, the group velocity determines not only the direction, but also the timing of acoustic energy arrival at the opposite surface. Results of calculations of wave arrival times, based on that, are presented in Fig. 7.8. Brightness presented in the phonon images is proportional to the Maris phonon enhancement factor.

(a)   (b)   (c)
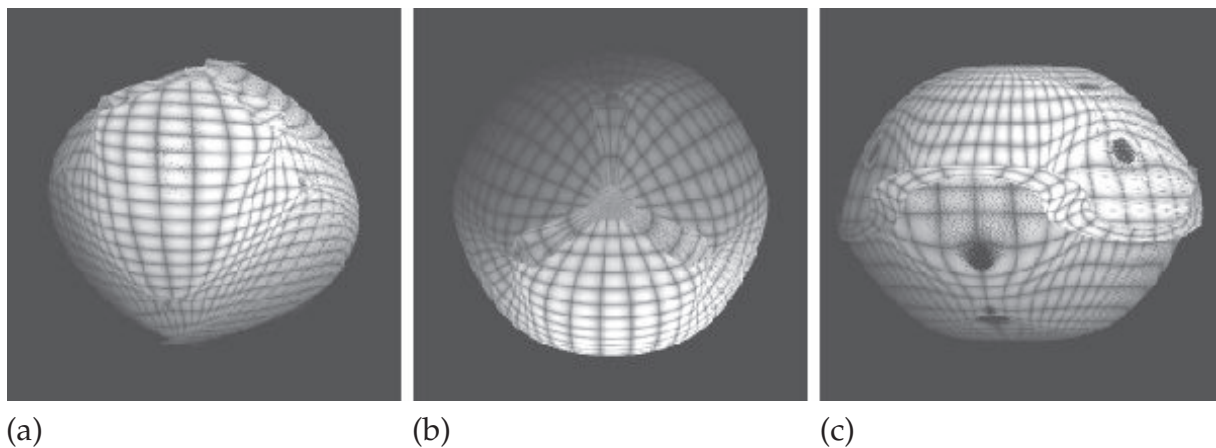
Figure 7.6: Lithium niobate wave surfaces created by the end points of group velocity vectors. ST mode (**a**) and (**b**), FT mode (**c**). Perspective in (**a**) and (**c**) is similar to that in Fig. 7.5, while (**b**) is the top view along the z axis of the wave surface for the ST mode. *Dark lines* demonstrate mapping from equidistant directions in spherical coordinates to the ray vectors. The mapping reveals folds of the wave surface – three arms visible at the top for the ST mode (**a**, **b**) and a curved belt in the equator area (**c**). *Dark areas* in (**c**) correspond to directions, into which very few ray vectors are pointing.

(a) (b) (c)
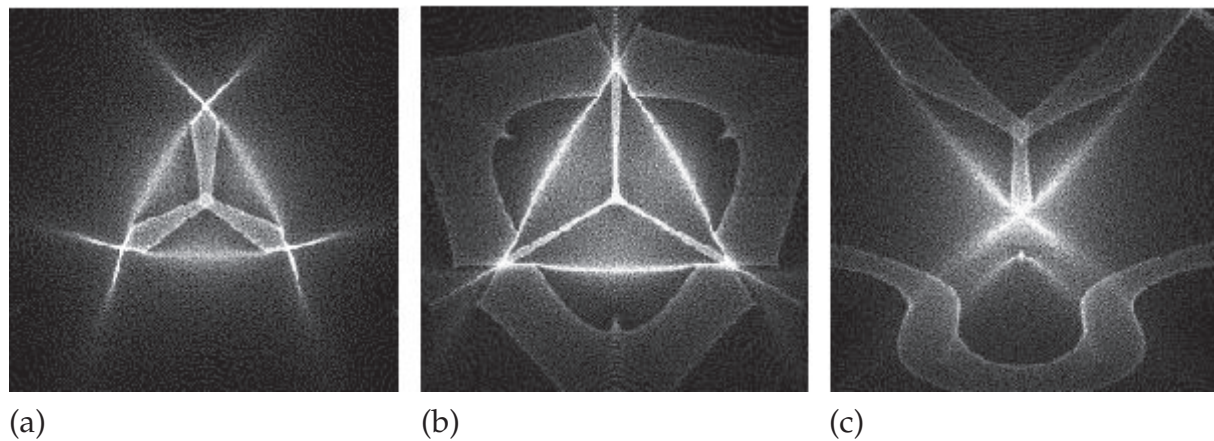
Figure 7.7: Calculated phonon focusing patterns of lithium niobate. ST and FT modes, viewed along the z axis with (**a**) and without (**b**) piezoelectric stiffening. Piezoelectric stiffened ST and FT modes, viewed along the direction $\theta = 37°$, $\phi = 180°$ (**c**).

(a) (b) (c)
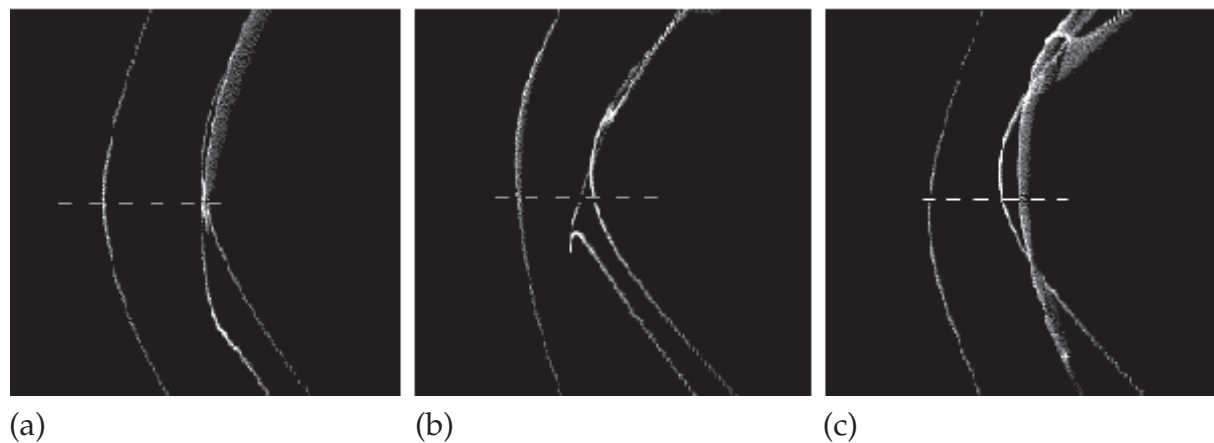
Figure 7.8: Calculated phonon arrival times for a 5 mm thick lithium niobate crystal, for longitudinal and both transverse modes. Vertical coordinates are in the range -4.25 mm to $+4.25$ mm along the 0–y direction for a z-cut plate (**a**), 0–z direction for a y-cut crystal with (**b**) and without (**c**) piezo-stiffening. The horizontal coordinate is the arrival time in the range $0 - 2.84$ µs.

A 3D set (x, y, t) of complex number data were experimentally acquired in single 2D scans employing Coulomb excitation and quadrature detection. Selected 2D cross-sections of such a 3D data set are shown in Fig. 7.9. The time scales as well the vertical scales in Figs. 7.8 and 7.9 are the same, and the results may be compared. Comparison shows similar relative delays between the individual modes. That confirms that the values of the material constants of the model are close to the real ones. A predominant planar wave component propagating perpendicular to the crystal surface is visible.

Knowing the slowness surface and making assumptions on the source directionality diffraction may be included in the calculations by the angular spectrum technique. Field distributions in Fig. 7.10 show features that may be identified as wave front folds in Fig. 7.6b and as lines of phonon focusing in Fig. 7.7b. The difference may be explained as the effect of diffractive broadening of those features at limited frequency. Angular spectrum + 2D FFT modeling may be applied to the determination of the material constants.

(a)　　　　　　　　　(b)　　　　　　　　　(c)
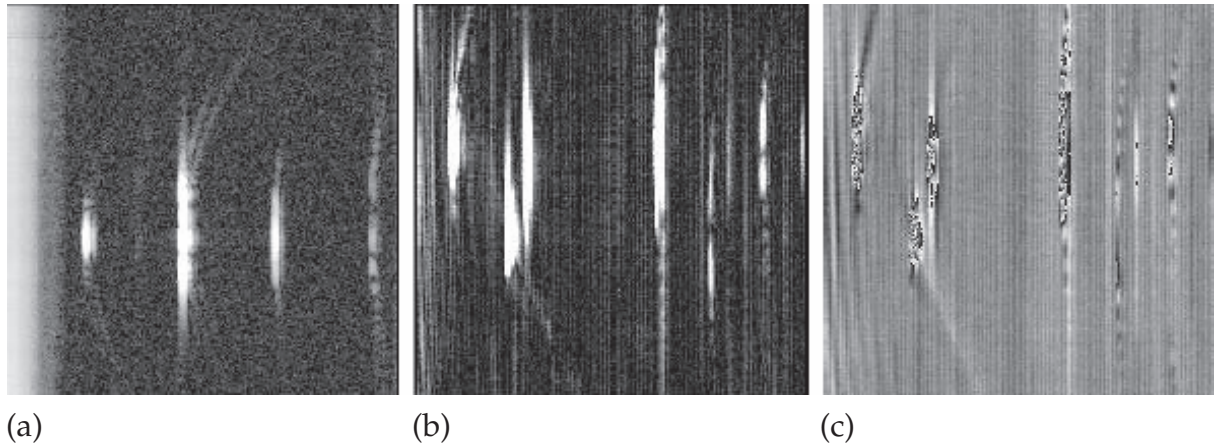
Figure 7.9: Measured arrivals of the wave fronts for a 5 mm thick lithium niobate crystal. Vertical: Spatial coordinates in the range −4.25 mm to 4.25 mm. Horizontal coordinate: Time span of 2.84 μs with an initial delay of 0.43 μs in (**b**, **c**) relative to the excitation burst to avoid the cross-talk. Logarithm of the signal amplitude scanned along the 0–*y* direction for a *z*-cut plate (**a**). Amplitude (**b**) and real part (**c**) scanned along 0–*z* direction for a *y*-cut crystal. Beside of the first arrivals of the basic modes seen at the *left side* of each picture, multiple reflections are visible on the *right*.

(a)　　　　　　　　　(b)　　　　　　　　　(c)
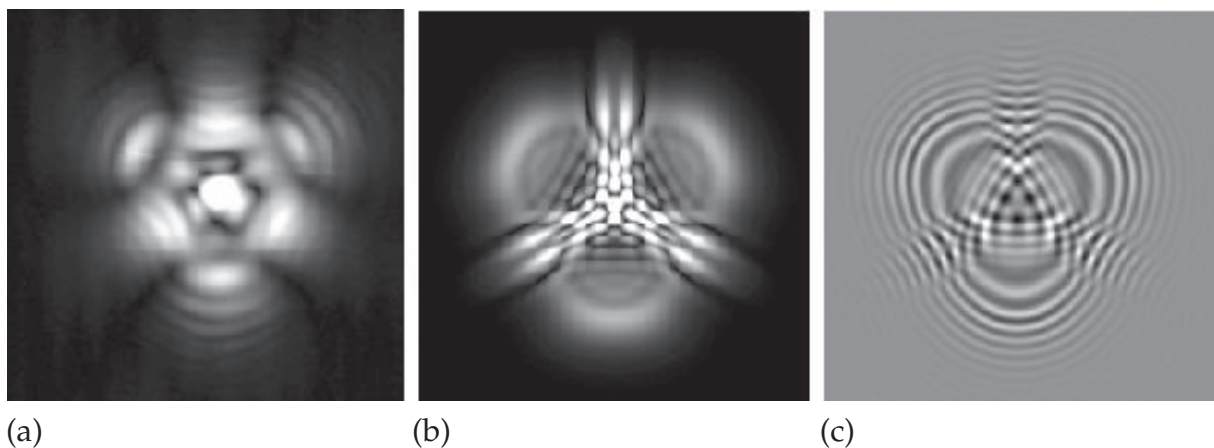
Figure 7.10: Lithium niobate wave surfaces created by the end points of group velocity vectors. ST mode (**a**) and (**b**), FT mode (**c**). Perspective in (**a**) and (**c**) is similar to that in Fig. 7.5, while (**b**) is the top view along the *z* axis of the wave surface for the ST mode. *Dark lines* demonstrate mapping from equidistant directions in spherical coordinates to the ray vectors. The mapping reveals folds of the wave surface – three arms visible at the *top* for the ST mode (**a**, **b**) and a curved belt in the equator area (**c**). *Dark areas* in (**c**) correspond to directions, into which very few ray vectors are pointing.

7.6 Apodized Non-Confocal Acoustic Transmission Microscopy

E. Twerdowski, W. Grill

Two non-confocally adjusted spherical transducers are employed to implement an acoustic microscope operating in transmission with an approximately line-shaped point

spread function (PSF). Such a PSF is of advantage in acoustic transmission line tomography and spatially resolved velocity measurements in solids. The foci of the transducers are viewed as diffraction-limited point transducers and appropriate time-selective signal acquisition is designed to restrict the ultrasound wave paths to the line connecting them. It is found that for typical commercially available transducers the largest contribution to the detected signal is not due to the direct ultrasound wave but due to the edge waves emanating from the rim of the focusing transducer. This poses constraints on achieving a line-shaped PSF in defocused acoustic transmission microscopy. It is shown that, due to the strong contribution from edge waves, it is impossible to achieve a line-shaped PSF in the case of application of a long exciting toneburst. The influence of the exciting pulse length, as well as the position of the time gate on the obtainable PSF is investigated.

The ability to measure local elastic properties of materials is one of the most attractive applications of acoustic microscopy. One of the possibilities to accomplish this is the utilization of the "through-transmission substitution technique" [1]: the sample is prepared in the form of a parallel-sided slab of known thickness and is interposed between a coaxially aligned sender-receiver transducer pair. Changes in signal amplitude and arrival time produced by insertion of the sample within the water path are used to derive the transmission loss and propagation velocity in the sample. Planar transducers are successfully used for measurement of attenuation and phase velocity in samples made of homogeneous materials, since the lateral resolution is irrelevant.In materials that manifest spatial variation of the mechanical properties, such as functionally graded materials (FGM), the lateral resolution of the sender-receiver pair is of interest. In order to perform such spatially resolved measurements of the mechanical properties, focusing instead of planar transducers were successfully employed [2, 3]. Planar and point-focusing transducers are widely used in acoustic microscopy and their characterization has been the subject of study for many researchers. Both the theory as well as experiments give support to modelling the pressure field radiated from the transducers as a combination of two wave types: the direct wave (sometimes called geometrical wave) that emanates from the transducer surface orthogonally to it, and the edge wave, generated by the discontinuities of the transducer and propagating in all directions.

Such models have been developed for both planar as well as for focusing transducers [4–6]. If not treated properly, the phenomenon of edge wave generation can lead to errors in NDE applications. This has lead to the extensive studies devoted to characterization of the properties of the pressure fields radiated by transducers. In the case of application of planar transducers in NDE these studies resulted among others (a) in correction methods that take the phenomenon of edge wave generation into account, and (b) in manufacturing transducers that produce either the direct wave or edge wave only. The application of focusing transducers to spatially resolved velocity measurements in FGM materials is also affected by the edge wave generation phenomenon, which therefore has to be treated properly. In order to achieve high lateral resolution, the two ultrasonic lenses are focused on the opposite surfaces of a planeparallel sample that is scanned relative to the lenses (Fig. 7.11). The foci of the lenses can in this case be treated as diffraction-limited point transducers. Application of fast switching and gating allows suppressing signals resulting from scattering or reflections from internal discontinuities in the sample, which restricts the signal path essentially to the path-

Figure 7.11: Schematic of the spatially resolved velocity measurement setup.

way with the shortest time of flight between the foci. This is equivalent to obtaining a lineshaped point spread function (PSF). After determination of the time of flight of the ultrasound between the foci, one is able to derive the speed of sound in the plane-parallel sample. Unfortunately, edge waves do not follow the geometrical path of the direct wave. As has been shown before for the case of a single transducer operating in reflection and positively defocused from a liquid-solid boundary, the edge wave contributions are even larger than those of the direct wave. This has been found in the present work to be the case also in measurements using defocused transmission microscopy. It has been found that edge waves influence strongly the obtainable PSF. The goal of this paper was to optimize the obtainable PSF by varying the following parameters of the defocused microscopy setup: (a) length of the exciting burst, (b) position and width of the time window (gate) applied to the transmitted signal, and (c) directly suppressing the edge waves by ultrasound-opaque masks in front of the lenses (apodization).

A straight piece of carbon fibre with a diameter of 3 µm served as an object in the experiments determining the line spread function of defocused transmission microscopy setup. The diameter of the fibre was chosen smaller than the wavelength of the ultrasound in water at the frequency used (about 18 µm) in order to resolve possible fine structures in the obtained images. As was expected, such a thin fibre produced very small signal variations during the scan. This led to relatively noisy images which are therefore not shown here. Nevertheless, those experiments served as a proof of validity for measurements employing a thicker wire. It was found out that the finest structure of interest observed in the experiments was larger than 100 µm, thus an application of a wire of 50 µm thickness does not influence the results. Indeed, experiments with a piece of copper wire of diameter 50 µm gave qualitatively the same results as those with the fibre. These results are shown in Figs. 7.12 and 7.13. The former figure presents an amplitude waveform acquired at the centre of the scanning region. The amplitude peaks labelled by letters "a" to "f" denote the position of the time gate that was applied in the postprocessing stage to the acquired data in order to generate the corresponding C-scan images represented in 7.13.
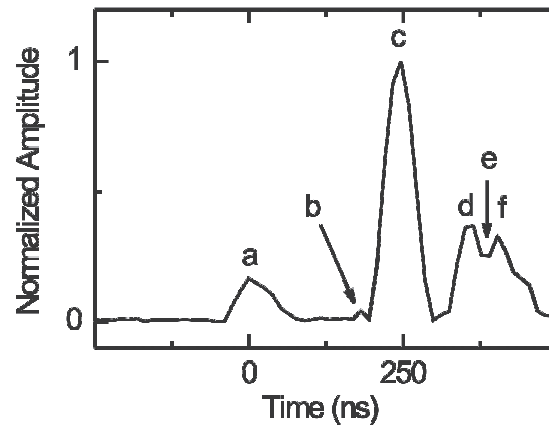
Figure 7.12: Amplitude waveform acquired on the axis of symmetry halfway between the transducers in the experiment with the short burst excitation. Excitation burst length 24 ns. Defocus F_1F_2 5 mm (see Fig. 7.11).
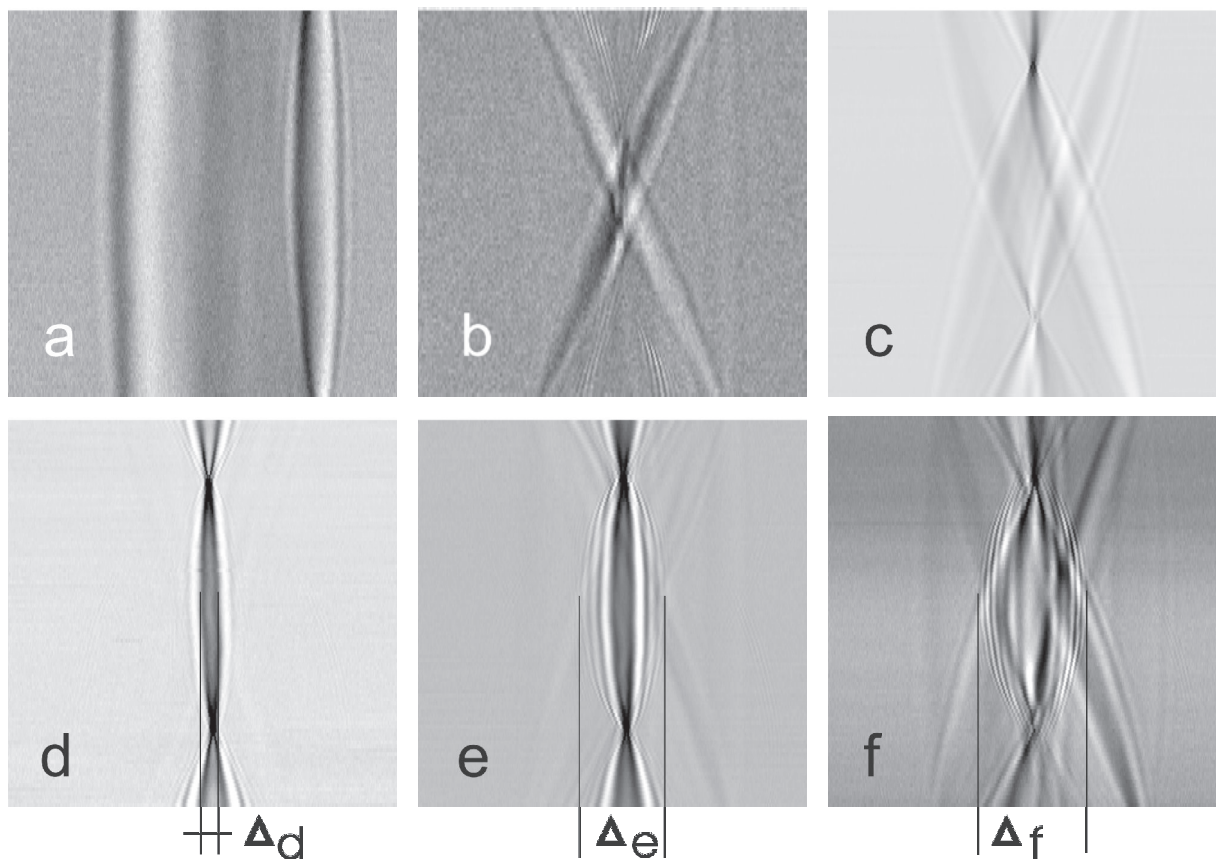
Figure 7.13: Images, corresponding to conventional C-scan output, obtained by application of a time gate of 12 ns width to the acquired 3D data set at positions labelled as **a**, **b**, **c**, **d**, **e**, and **f** in Fig. 7.12. Horizontal and vertical image ranges are 4 mm and 8 mm, respectively.

[1] B. Zeqiri: J. Acoust. Soc. Am. **99**, 996 (1996)
[2] J. Ndop et al.: Ultrasonics **36**, 461 (1998)
[3] J. Ndop et al.: Mater. Sci. Forum **308**, 873 (1999)
[4] J. Zhang et al.: J. Appl. Phys. **86**, 2825 (1999)

[5] H. Djelouah et al.: Ultrasonics **29**, 188 (1990)
[6] D. Cathignol et al.: Acta Acust. **83**, 410 (1997)

7.7 Imaging of Directly Bonded Semiconductor Wafers: Application of Apodized Non-Confocal Acoustic Transmission Microscopy

E. Twerdowski, R. Wannemacher, N. Razek, A. Schindler, W. Grill

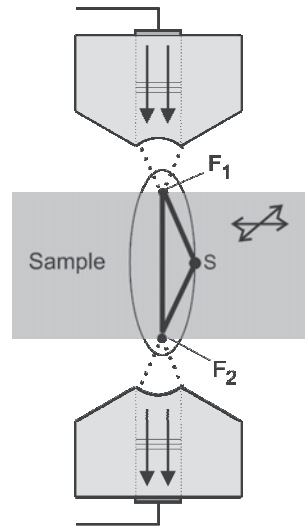Application of a line-shaped point spread function (PSF) to imaging of void defects in directly bonded wafers is investigated. Two non-confocally adjusted spherical transducers are employed to implement an acoustic microscope operating in transmission with a time dependent point spread function, whose shape is optimized by both temporal apodization of the received signal and spatial apodization of the transducer aperture. Strong imaging artifacts resulting from the generation and detection of edge waves are eliminated in this way. It is shown by several examples that only a broadband system can be utilized in order to obtain a line-shaped PSF suitable for imaging.

Direct semiconductor wafer bonding has increasingly become a technology of choice for materials integration in microelectronics, optoelectronics, and microelectromechanical systems (MEMS), being widely used for joining semiconductor wafers without employing any intermediate layers. It makes use of the phenomenon that mirror-polished, flat and clean surfaces, when brought into contact at room temperature, are locally attracted to each other due to both van-der-Waals forces, and the formation of hydrogen bonds between the OH-terminated surfaces and adsorbed water molecules. Subsequent thermal annealing allows for elimination of water molecules, oxygen, and hydrogen atoms, resulting in covalent bonding across the interface. An
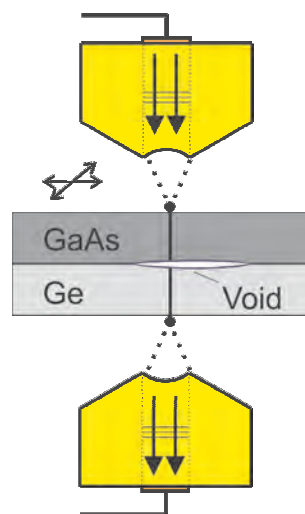
Figure 7.14: Application of non-confocal transmission microscopy to disbond defect imaging in directly bonded wafers.

introduction to the direct wafer bonding technique can be found in [1]. One problem frequently associated with wafer bonding is the formation of interface bubbles, sometimes referred to as voids, induced by imperfections in the topography of the surfaces, prebonding surface contamination, gas bubbles, and dust particles. To give an example, a particle with a diameter of only $0.5\,\mu m$ trapped between two silicon wafers with a thickness of $525\,\mu m$ each will yield an unbonded area of approximately $5\,mm$ radius. It is therefore essential to monitor the homogeneity of the bonded interface. Ultrasound is very sensitive to variations of the elastic properties of materials and is particularly receptive to locating gaps (delaminations and voids) in the sample. This sensitivity manifests itself in a drastic drop of the transmitted signal amplitude, allowing for straightforward detection of the defect. The most typical defect in bonded wafers is a completely disbonded area between them, known as a dis-
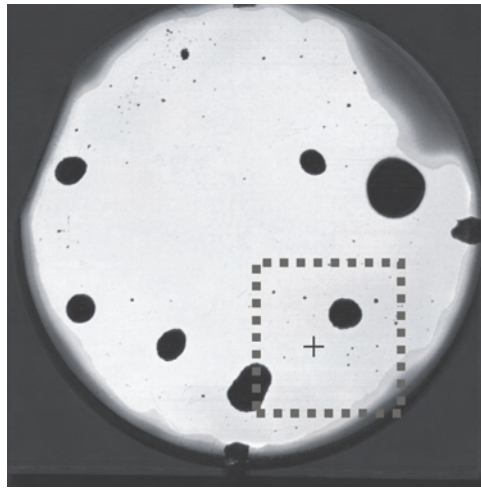
Figure 7.15: Overview image of GaAs–Ge bonded wafer scanned in transmission. The figure was obtained in the experiment with short toneburst excitation (24 ns) by application of a time gate of 12 ns duration at position "4" to the acquired signal (see Fig. 7.16). Horizontal and vertical image ranges are $52 \times 52\,mm^2$.
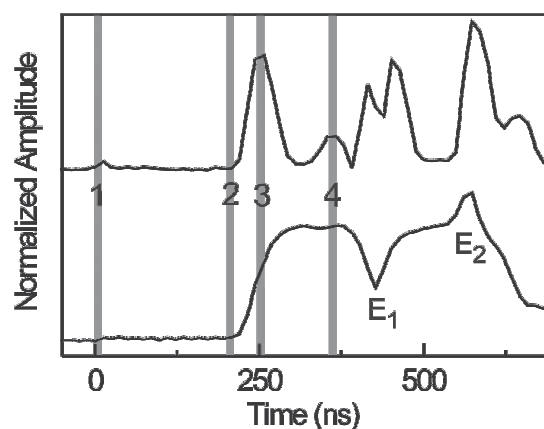
Figure 7.16: Waveforms acquired at a defect-free location of the bonded wafer (location marked by *cross* in Fig. 7.15). *Upper* and *lower* graphs correspond to application of short (24 ns) and long (1020 ns) tonebursts for excitation, respectively.

```
0 0 0 0 0 0 0 0 0 0 0 0 0 0 0 0 0
0 0 0 0 0 0 0 0 0 0 0 0 0 0 0 0 0
0 0 0 0 0 0 0 0 0 0 0 0 0 0 0 0 0
0 0 0 0 0 0 1 1 1 1 1 0 0 0 0 0 0
0 0 0 0 1 1 1 1 1 1 1 1 1 0 0 0 0
0 0 0 0 1 1 1 1 1 1 1 1 1 0 0 0 0
0 0 0 1 1 1 1 0 0 0 1 1 1 1 0 0 0
0 0 0 1 1 1 0 0 0 0 0 1 1 1 0 0 0
0 0 0 1 1 1 0 0 0 0 0 1 1 1 0 0 0
0 0 0 1 1 1 0 0 0 0 0 1 1 1 0 0 0
0 0 0 1 1 1 1 0 0 0 1 1 1 1 0 0 0
0 0 0 0 1 1 1 1 1 1 1 1 1 0 0 0 0
0 0 0 0 1 1 1 1 1 1 1 1 1 0 0 0 0
0 0 0 0 0 0 1 1 1 1 1 0 0 0 0 0 0
0 0 0 0 0 0 0 0 0 0 0 0 0 0 0 0 0
0 0 0 0 0 0 0 0 0 0 0 0 0 0 0 0 0
0 0 0 0 0 0 0 0 0 0 0 0 0 0 0 0 0
```
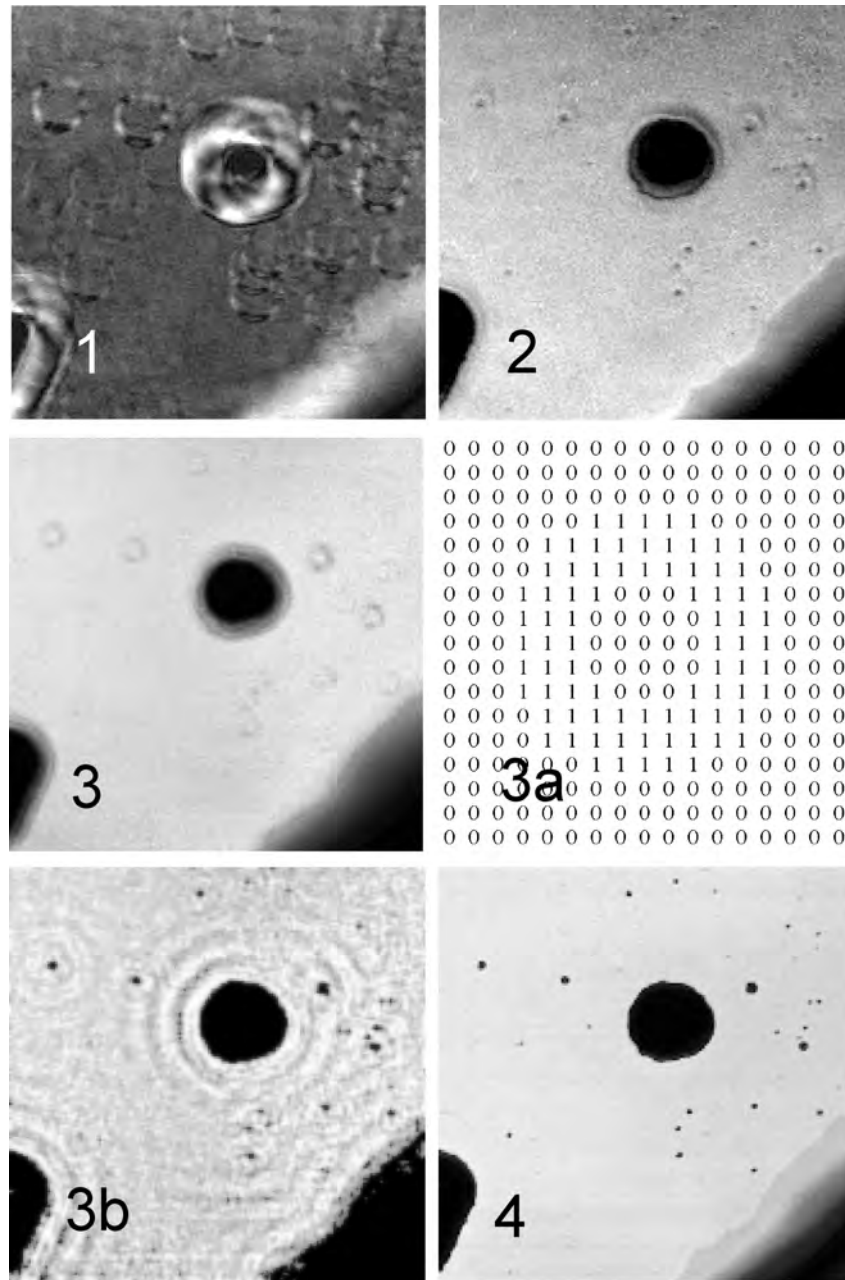
Figure 7.17: Images of the bonded wafer obtained with short (24 ns) toneburst excitation through time gating of the experimental data. The imaged region corresponds to the area marked with *dashed lines* in Fig. 7.15, and the numbers in the images correspond to time positions labeled by 1–4 in Fig. 7.16. Strong dependence of resolution upon position of the time gate is observed. Best resolution is achieved by imaging with the "direct" wave (image *4*). Image *3a* illustrates the deconvolution kernel applied to the image *3*; image *3b* presents the result of the deconvolution. Horizontal and vertical image ranges are 17×17 mm^2.

bond. Its detection is successfully performed by conventional imaging systems utilizing C-mode scanning acoustic microscopes (SAM) operating in reflection. In this paper a non-confocally adjusted phase sensitive acoustic microscope (PSAM) operating in transmission is employed for imaging. Under certain conditions to be specified below, this mode of operation results in a line-shaped point spread function (PSF)
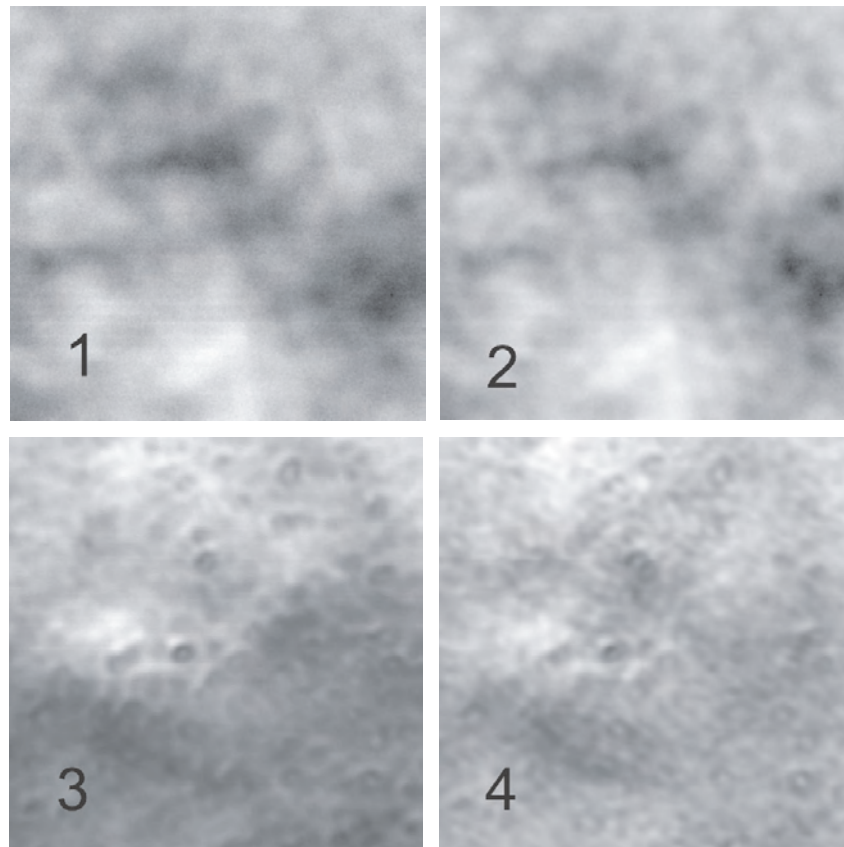
Figure 7.18: Images of a 1.5×1.5 mm^2 region of the bonded wafer obtained with long (1020 ns) toneburst excitation through time gating of the experimental data. The numbers correspond to time gate positions labeled in Fig. 7.16. No bond defects can be resolved independent of the time gate position.

of the system that can be advantageous in material characterization applications. It is worth mentioning that bonded interface may also exhibit so-called "weak" bonds. These are areas that can be treated as an interface state intermediate to fully bonded and completely disbonded states. In the case of a weak bond, normal components of stress and displacement are preserved across the boundary. Compressional waves are therefore not perceptive to this type of interfacial defect, which makes it very difficult to detect it using only compressional ultrasound waves. Investigations concerning the NDT of adhesive joints have shown that such areas are more susceptive to transversal as compared to longitudinal waves. Another method for characterization of the bonding quality is based on the anharmonicity caused by weak bonds and was developed especially for semiconductor wafers. In that approach, measuring of the anharmonic content of the transmitted high-power ultrasonic wave serves as a source for the analysis of the bonding quality. In the present work, we are dealing only with disbondtype defects demonstrating the application of a lineshaped PSF to imaging.

Non-confocal transmission microscopy has been applied to non-destructive characterization of GaAs and Ge bonded wafers (Fig. 7.14). The sending and receiving ultrasonic lenses are focused on opposing surfaces of the bonded wafers or even into the coupling medium outside of the wafers. The foci of the lenses are viewed
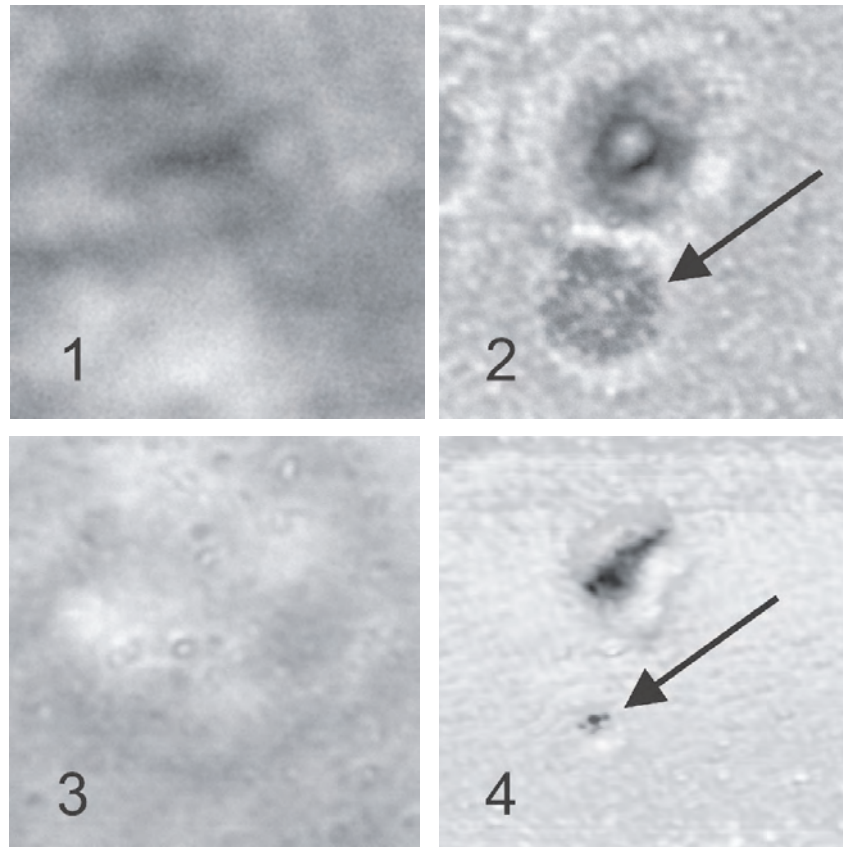
Figure 7.19: The same region of the bonded wafer as that in Fig. 7.18 imaged with short tonebursts (24 ns). Images are obtained through time gating of the experimental data. The numbers correspond to time gate positions labeled in Fig. 7.16. Short toneburst allows for discrimination among all the wave types and utilization of each of them for imaging: "straight edge-to-edge" (image *1*), "diagonal edge-to-edge" (image *2*), "edge-to-focus" (image *3*), and "direct" wave (image *4*). Imaging with "direct" wave results in best resolution, while imaging with the strongest wave contribution ("edge-to-focus" wave, image *3*) obscures the defects completely.

as diffraction-limited point transducers and appropriate time gating of the acquired signal is designed to restrict the ultrasound wave paths to the line connecting the focus points, which is equivalent to obtaining a lineshaped PSF of the system. Such a shape of the PSF is of advantage in those tomography applications, where, on one hand, one has to determine the time-of-flight and/or attenuation integrated along the ultrasound propagation path, and, on the other hand, high lateral resolution along the axis of the sending-receiving transducer pair is of interest. This requires the lateral resolution of the setup to be uncoupled from the location on the axis of the transducers. An application of this technique in spatially resolved non-destructive measurement of mechanical properties in functionally graded materials has been reported in [2]. Conventionally, a line-shaped PSF can be achieved by a confocal configuration of weakly focusing transducers operating in transmission. Such a configuration was utilized, e.g., in [3], in NDT of adhesive joints in fused silica. Confocal configuration, however, exhibits a pronounced trade-off between the achievable lateral resolution and the depth of focus. The idea behind nonconfocal transmission microscopy is to relax this tradeoff by means

of creating a quasi line-shaped PSF by application of time selective signal recording. The task of this paper is twofold. On one hand, it illustrates the successful construction of a line-shaped PSF by non-confocal transmission microscopy and its application to imaging of the delamination defects within GaAs-Ge fusion bonded wafers. On the other hand, it demonstrates examples of the imaging artifacts arising from generation and detection of edge waves that manifest themselves in an apparent loss of resolution in the scanned images.

[1] Q.Y. Tong, U. Gösele: *Semiconductor Wafer Bonding: Science and Technology* (Wiley, New York 1998)
[2] J. Ndop et al.: Ultrasonics **36**, 461 (1998)
[3] M. Rothenfusser et al.: Ultrasonics **38**, 322 (2000)

7.8 Funding

7.9   Organizational Duties

Wolfgang Grill

- Adjunct Professor and Member of the Graduate School, The University of Georgia, Athens, GA, USA
- Project Reviewer: Deutsche Forschungsgemeinschaft, Alexander von Humboldt Foundation

7.10   External Cooperations

Academic

- University of the Witwatersrand, Johannesburg, South Africa
  Prof. Dr. A. Every

- Wroclaw Institute of Technology, Wroclaw, Poland
  Dr. M. Pluta

- University of Arizona, Tucson, Arizona, USA
  Prof. Dr. T. Kundu

- University of Central Florida, Orlando, Forida, USA
  Prof. Dr. W. Luo, Dr. W. Ngwa

- Johann Wolfgang Goethe-Universität Frankfurt
  Prof. Dr. J. Bereiter-Hahn

- Universität Dortmund
  Prof. Dr. U. Woggon

International Organizations

- European Space Organization ESA/ESTEC

Industry

- Schott GLAS Mainz
- Kayser-Threde GmbH

7.11   Publications

Journals

E. Twerdowski, M. von Buttlar, N. Razek, R. Wannemacher, W. Grill: *Combined surface-focused acoustic microscopy in transmission and scanning ultrasonic holography*, Ultrasonics **44**, e1301 (2006)

E. Twerdowski, W. Grill: *Temporal and spatial apodization in defocused acoustic transmission microscopy*, Ultrasonics **44**, 25 (2006)

E. Twerdowski, M. von Buttlar, W. Grill: *Scanning acoustic defocused transmission microscopy with vector contrast combined with holography for weak bond imaging*, Proc. SPIE **6177**, 617 718 (2006)

M. von Buttlar, E. Twerdowski, M. Schmachtl, S. Knauth, W. Grill: *Ultrasonic monitoring for directional solidification experiments onboard of the International Space Station*, Proc. SPIE **6177**, 617 702 (2006)

E. Twerdowski, R. Wannemacher, W. Grill: *Application of spatially and temporally apodized non-confocal acoustic transmission microscopy to imaging of directly bonded wafers*, Ultrasonics **44**, 54 (2006)

A. Habib, E. Twerdowski, M. von Buttlar, M. Pluta, M. Schmachtl, R. Wannemacher, W. Grill: *Transmission acoustic holography of piezoelectric materials by Coulomb excitation*, Proc. SPIE **6177**, 61 771A (2006)

A. Kamanyi, W. Ngwa, T. Betz, R. Wannemacher, W. Grill: *Combined phase-sensitive acoustic and confocal laser scanning microscopy*, Ultrasonics **44**, e1295 (2006)

A. Kamanyi, R. Wannemacher, W. Grill: *Combinatory scanning confocal laser and acoustic vector contrast microscopy: multi-contrast imaging of soft matter samples*, Proc. SPIE **6177**, 617 712 (2006)

E.T. Ahmed Mohamed, S. Schubert, T. Gilberger, A. Kamanyi, R. Wannemacher, W. Grill: *Characterization of malaria infected red blood cells by scanning confocal laser and acoustic vector contrast microscopy*, Proc. SPIE **6177**, 617 716 (2006)

Books

M. Pluta, A. Habib, E. Twerdowski, M. von Buttlar, M. Schmachtl, R. Wannemacher, W. Grill: *Wave propagation modeling for piezoelectric materials with Coulomb excitation*, in *Proc. 9th Western Pacific Acoustics Conf.* (2006)

M. von Buttlar, E. Twerdowski, A. Habib, M. Pluta, R. Wannemacher, W. Grill: *Bulk wave excitation and acoustic holography in piezoelectric wafers by scanning contact electrodes*, in: *Proc. IX. Int. Conf. for Young Researchers: Wave Electronics and Its Applications in the Information and Telecommunication Systems*, St. Petersburg, Russia (2006)

8

Superconductivity and Magnetism

8.1 Introduction

The research of the Division of Superconductivity and Magnetism is concerned with the study of magnetic ordering and superconductivity in a range of materials. The present focus is on ferromagnetic ordering in carbon-based materials, superconductivity in MgB_2 and magnetotransport properties of ferromagnetic oxide heterostructures. With the installation of a dual beam microscopic a facility for the preparation of nanostructures has become available and the fabrication of ferromagnetic and superconducting heterostructures on the nano- and micrometer scale has begun.

Pablo Esquinazi

8.2 Bistable Resistance State Induced by Joule Self-Heating in Manganites

Y.F. Chen, M. Ziese, P. Esquinazi

The magnetotransport properties of $La_{0.7}Sr_{0.3}MnO_3$, $La_{0.8}Ca_{0.2}MnO_3$, $La_{0.7}Ca_{0.3}MnO_3$ and Fe_3O_4 films were investigated in the nonlinear regime of strong Joule self-heating. In this regime in case of the manganite films the resistance–current characteristics exhibit two sharp transitions between bistable resistance values, see Fig. 8.1. The critical currents corresponding to the transitions depend on base temperature, magnetic field, current sweep rate, film resistance, and thermal coupling to the surroundings. This phenomenon opens up the possibility for the development of a magnetoresistance sensor based on Joule self-heating tuned colossal magnetoresistance. Indeed, in $La_{0.8}Ca_{0.2}MnO_3$ and $La_{0.7}Ca_{0.3}MnO_3$ films the colossal magnetoresistance can be strongly enhanced by using the interplay between negative magnetoresistance and Joule heating.
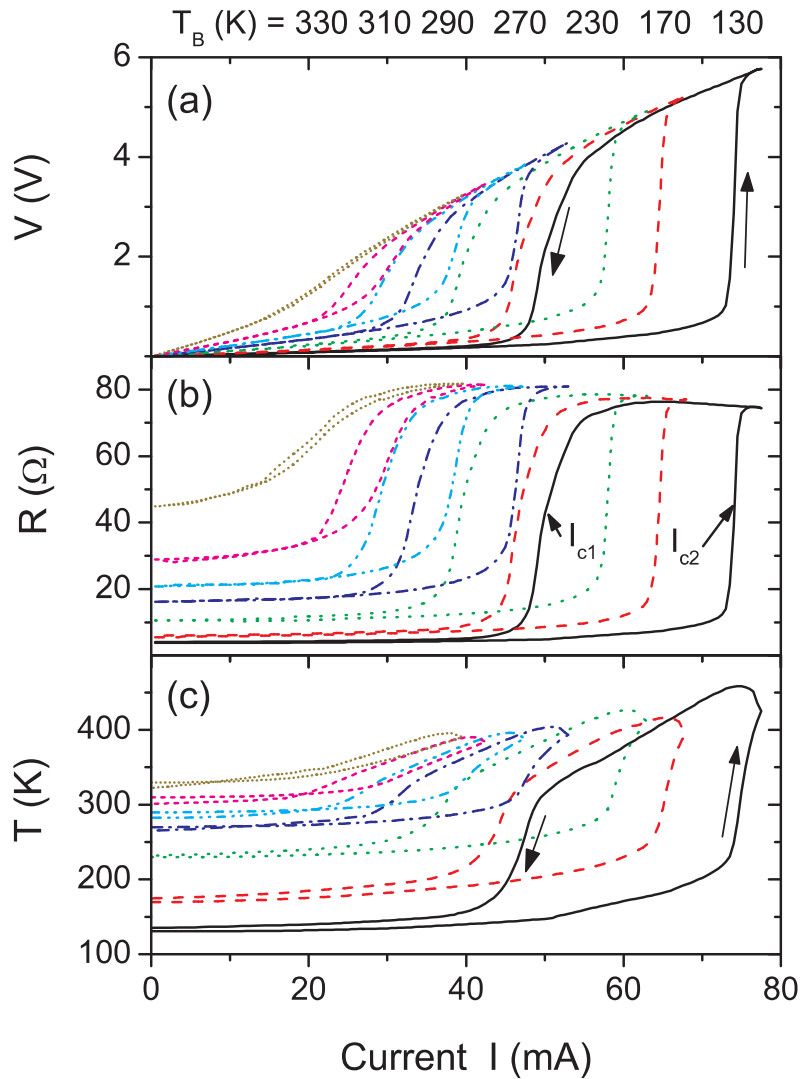
Figure 8.1: (**a**) Voltage–current, (**b**) resistance–current, and (**c**) temperature–current curves measured on a $La_{0.7}Sr_{0.3}MnO_3$ film in zero magnetic field for various base temperatures T_B as indicated in the figure.

8.3 Magnetoresistance Switch Effect in a Multiferroic $Fe_3O_4/BaTiO_3$ Bilayer

M. Ziese, A. Bollero[*], I. Panagiotopoulos[†], N. Moutis[‡]

[*]SPINTEC, CEA/CNRS, Grenoble, France
[†]Department of Materials Science and Engineering, University of Ioannina, Greece
[‡]Institute of Materials Science, NCSR "Demokritos", Athens, Greece

Multiferroic bilayers composed of a magnetite Fe_3O_4 and a $BaTiO_3$ layer show nonlinear current–voltage characteristics in current perpendicular to plane configuration. The magnetoresistance of the bilayers is strongly bias dependent and can be switched from negative at low bias to positive at large bias. These effects do not arise from charge-carrier modulation in the magnetite layer by an electric field effect. Therefore both the

nonlinear transport characteristics and the switchable magnetoresistance are attributed to interfacial transport phenomena.

8.4 Carrier-Induced Ferromagnetism in n-Type ZnMnAlO and ZnCoAlO Thin Films at Room Temperature

X.H. Xu[*], H.J. Blythe[*], M. Ziese, A.J. Behan[*], J.R. Neal[*], A. Mokhtari[*], R.M. Ibrahim[*], A.M. Fox[*], G.A. Gehring[*],

[*]Department of Physics and Astronomy, University of Sheffield, UK

The realization of semiconductors that are ferromagnetic above room temperature will potentially lead to a new generation of spintronic devices with revolutionary electrical and optical properties. Transition temperatures in doped ZnO are high but, particularly for Mn doping, the reported moments have been small. By careful control of both oxygen deficiency and aluminium doping is was shown that the ferromagnetic moments measured at room temperature in n-type ZnMnO and ZnCoO are close to the ideal values of 5 μ_B and 3 μ_B, respectively. Furthermore a clear correlation between the magnetization per transition metal ion and the ratio of the number of carriers to the number of transition metal donors was established as is expected for carrier-induced ferromagnetism for both the Mn and Co doped films. The dependence of the magnetization on carrier density is similar to that predicted for the transition temperature for a dilute magnetic semiconductor in which the exchange between the transition metal ions is through the free carriers. A positive magnetoresistance was observed in the films, but no anomalous Hall effect or anisotropic magnetoresistance.

8.5 Electrostatic Force Microscopy on Oriented Graphite Surfaces: Coexistence of Insulating and Conducting Behaviour

Y. Lu[*], M. Muñoz[*], C.S. Steplecaru[*], C. Hao[*], M. Bai[*], N. Garcia[*], K. Schindler, P. Esquinazi

[*]CSIC, Madrid, Spain

Measurements of the electric potential fluctuations on the surface of highly oriented pyrolytic graphite were performed using electrostatic force and atomic force microscopy. Micrometric domain-like potential distributions were observed even when the sample was grounded. Such potential distributions are unexpected given the good metallic conductivity of graphite because the surface should be an equipotential. The results indicate the coexistence of regions with "metallic-like" and "insulating-like" behaviour showing large potential fluctuations of the order of 0.25 V, see Fig. 8.2. In lower qual-
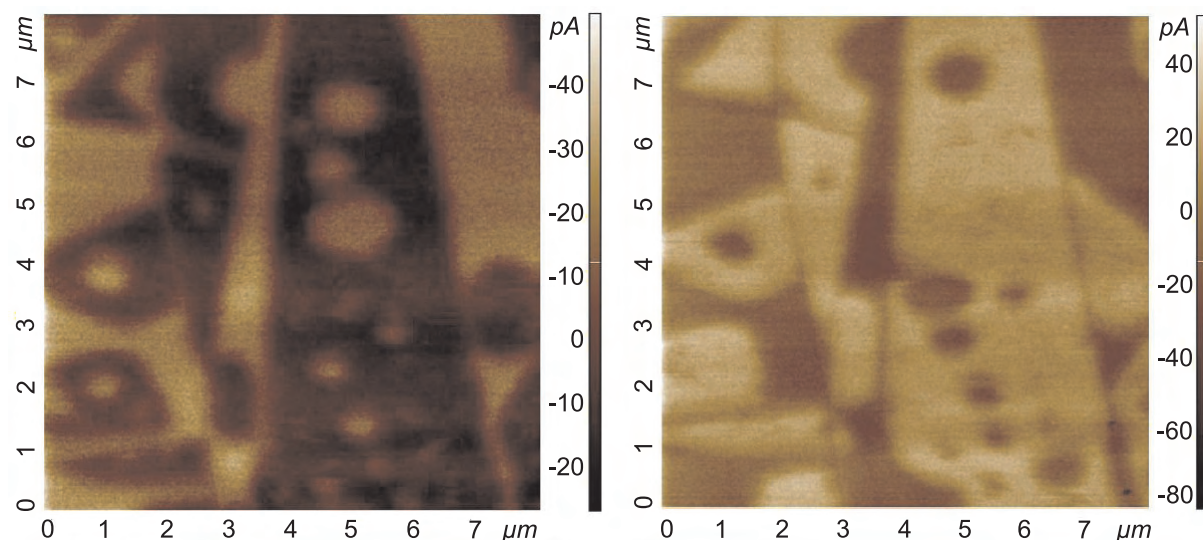
Figure 8.2: EFM images obtained for different polarities of the tip voltage. *Left*: 3 V, *right*: −3 V.

ity graphite, this effect is not observed. Experiments were performed in Ar and air atmospheres.

8.6   Growth of Highly Oriented Graphite Films from Carbon–Sulfur Targets Using PLD at Room Temperature

H.C. Semmelhack, R. Höhne, P. Esquinazi, G. Wagner[*], A. Rahm[†], K.H. Hallmeier[‡], D. Spemann[§], K. Schindler

[*]Institut für Mineralogie, Kristallographie und Materialwissenschaft
[†]Abteilung Halbleiterphysik
[‡]Wilhelm-Ostwald-Institut für Physikalische und Theoretische Chemie
[§]Abteilung Nukleare Festkörperphysik

Carbon–sulfur films were grown by pulsed laser deposition at room temperature using different graphite–sulfur mixtures as targets. The structure of the films was characterized by X-ray diffraction and transmission electron microscopy. The composition and the chemical bonds were analyzed by Rutherford-backscattering spectroscopy, X-ray photoelectron spectroscopy and energy dispersive X-ray analysis. The films were composed of amorphous carbon with sp^2-, sp^3- and S−C−C−S bonds and textured graphite on the top of the film. The thin graphite layer on top of the carbon-sulfur films is highly oriented, comparable to highly oriented pyrolytic graphite, and free of sulfur in the graphite lattice, see Fig. 8.3. The lateral size of the oriented graphite grains in the films was up to 8 μm.
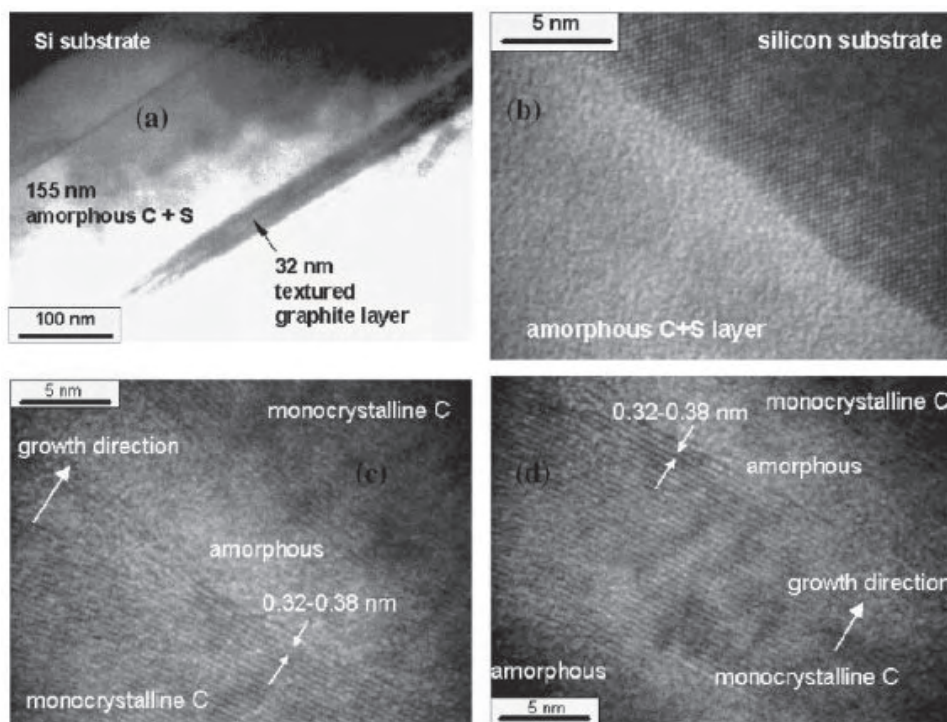
Figure 8.3: Cross-section (110) of a film made from a 50 wt. % C–50 wt. % S target. (**a**) TEM bright-field image of a film package consisting of an amorphous carbon and sulfur and a textured graphite layer grown on a Si (001) substrate, HRTEM images (**b**) of the interfacial region between the (001)-oriented Si substrate and the amorphous carbon–sulfur layer, (**c**) and (**d**) of the textured graphite layer which is interrupted by amorphous regions.

8.7   Funding

8.8 Organizational Duties

P. Esquinazi

- Project Reviewer: Deutsche Forschungsgemeinschaft (DFG), National Science Foundation (USA), German-Israeli Foundation
- Referee: Phys. Rev. Lett, Phys. Rev. B., Physica C, Phys. Lett. A, Phys. Stat. Sol., J. Low Temp. Phys., Carbon, J. Chem. Phys., Eur. J. Phys. B, J. Magn. Magn. Mater.

M. Ziese

- Project Reviewer: U.S.-Israel Binational Science Foundation, European Science Foundation
- Referee: Phys. Rev. Lett., Phys. Rev. B., J. Phys.: Condens. Matter, J. Phys. D: Appl. Phys., Phys. Stat. Sol., J. Magn. Magn. Mater., Eur. J. Phys. B, Thin Solid Films

8.9 External Cooperations

Academic

- State University of Campinas, Campinas, Brazil
  Prof. Dr. Yakov Kopelevich

- Umea University, Sweden
  Dr. Tatiana Makarova

- Universidad Autónoma de Madrid, Spain
  Prof. Dr. Miguel Angel Ramos, Prof. Dr. Sebastian Vieira

- Institute for Metal Physics of National Academy of Sciences of Ukraine, Kiev, Ukraine
  Prof. Dr. V.M. Pan

- Max-Planck-Institut für Metallforschung, Stuttgart
  Dr. E.H. Brandt

- University of Ioannina, Greece, Ioannina, Greece
  Prof. I. Panagiotopoulos,

- Institute for Materials Science, National Center of Scientific Research "Demokritos", Athens, Greece
  Dr. Nikos Moutis

- Trinity College Dublin, Ireland
  Prof. J.M.D. Coey

- IFW Dresden
  Dr. Kathrin Dörr

- University of Sheffield, UK
  Prof. G. Gehring

- University of the Negev, Beer Sheva, Israel
  Dr. Evgeny Rozenberg

- Institut für Oberflächenmodifizierung, Leipzig
  Dr. Klaus Zimmer

8.10 Publications

Journals

Y.F. Chen, M. Ziese, P. Esquinazi: *Bistable resistance state induced by Joule self-heating in manganites: a general phenomenon*, Appl. Phys. Lett. **88**, 222 513 (2006), doi:10.1063/1.2209204

Y.F. Chen, M. Ziese, P. Esquinazi: *Joule heating enhanced colossal magnetoresistance in $La_{0.8}Ca_{0.2}MnO_3$ films*, Appl. Phys. Lett. **89**, 082 501 (2006), doi:10.1063/1.2337280

P. Esquinazi, D. Spemann, K. Schindler, R. Höhne, M. Ziese, A. Setzer, K.-H. Han, S. Petriconi, M. Diaconu, H. Schmidt, T. Butz, Y.H. Wu: *Proton irradiation effects and magnetic order in carbon structures*, Thin Solid Films **505**, 85 (2006), doi:10.1016/j.tsf.2005.10.056

H. Kempa, P. Esquinazi, Y. Kopelevich: *Integer quantum Hall effect in graphite*, Solid State Commun. **138**, 118 (2006), doi:10.1016/j.ssc.2006.02.020

Y. Lu, M. Muñoz, C.S. Steplecaru, C. Hao, M. Bai, N. Garcia, K. Schindler, P. Esquinazi: *Electrostatic Force Microscopy on Oriented Graphite Surfaces: Coexistence of Insulating and Conducting Behaviors*, Phys. Rev. Lett. **97**, 076 805 (2006), doi:10.1103/PhysRevLett.97.076805

J.R. Neal, A.J. Behan, R.M. Ibrahim, H.J. Blythe, M. Ziese, A.M. Fox, G.A. Gehring: *Room-Temperature Magneto-Optics of Ferromagnetic Transition-Metal-Doped ZnO Thin Films*, Phys. Rev. Lett. **96**, 197 208 (2006), doi:10.1103/PhysRevLett.96.197208

J.G. Ossandón, J.L. Giordano, P. Esquinazi, H. Kempa, U. Schaufuß, S. Sergeenkov: *Nonlinear response of ac conductivity in narrow YBCO film strips at the superconducting transition*, J. Phys. Conf. Ser. **43**, 655 (2006), doi:10.1088/1742-6596/43/1/160

I. Panagiotopoulos, N. Moutis, M. Ziese, A. Bollero: *Magnetoconductunce and hysteresis in milled $La_{0.77}Sr_{0.33}MnO_3$ powder compacts*, J. Magn. Magn. Mater. **299**, 94 (2006), doi:10.1016/j.jmmm.2005.03.088

V. Pantin, J. Avila, M.A. Valbuena, P. Esquinazi, M.E. Dávila, M.C. Asensio: *Electronic properties of high oriented pyrolitic graphite: Recent discoveries*, J. Phys. Chem. Solids **67**, 546 (2006), doi:10.1016/j.jpcs.2005.10.169

D.S. Rana, M. Ziese, S.K. Malik: *Direct Correlation between 1/f-magneto-noise and magnetoresistance in $La_{0.7}Sr_{0.3}MnO_3$ and $(La_{0.5}Pr_{0.2})Ba_{0.3}MnO_3$ manganites*, Phys. Rev. B. **74**, 094 406 (2006), doi:10.1103/PhysRevB.74.094406

K. Schindler, D. Spemann, M. Ziese, P. Esquinazi, T. Butz: *Magnetism in Carbon: Writing Magnetic Structures with a Proton Micro-Beam on Graphite Surfaces*, Acta Phys. Pol. A **109**, 249 (2006)

H. Schmidt, M. Diaconu, H. Hochmuth, M. Lorenz, A. Setzer, P. Esquinazi, A. Pöppl, D. Spemann, K.-W. Nielsen, R. Gross, G. Wagner, M. Grundmann: *Weak ferromagnetism in textured $Zn_{1-x}(TM)_xO$ thin films*, Superlatt. Microstruct. **39**, 334 (2006), doi:10.1016/j.spmi.2005.08.059

S. Schorr, R. Höhne, D. Spemann, Th. Döring, B.V. Korzun: *Magnetic properties investigations of Mn substituted ABX$_2$ chalcopyrites*, Phys. Stat. Sol. A **203**, 2783 (2006), doi:10.1002/pssa.200669515

H.C. Semmelhack, R. Höhne, P. Esquinazi, G. Wagner, A. Rahm, K.H. Hallmeier, D. Spemann, K. Schindler: *Growth of highly oriented graphite films at room temperature by pulsed laser deposition using carbon-sulfur targets*, Carbon **44**, 3064 (2006), doi:10.1016/j.carbon.2006.05.004

D. Spemann, K. Schindler, P. Esquinazi, M. Diaconu, H. Schmidt, R. Höhne, A. Setzer, T. Butz: *Magnetic force microscopy studies on the magnetic ordering in organic materials induced by high-energy proton irradiation*, Nucl. Instr. Meth. B **250**, 303 (2006), doi:10.1016/j.nimb.2006.04.128

X.H. Xu, H.J. Blythe, M. Ziese, A. Behan, J.R. Neal, A. Mokhtari, M.R. Ibrahim, A.M. Fox, G.A. Gehring: *Carrier-induced ferromagnetism in n-type ZnMnAlO and ZnCoAlO thin films at room temperature*, New J. Phys. **8**, 135 (2006), doi:10.1088/1367-2630/8/8/135

M Ziese: *Study of the micromagnetic structure of a La$_{0.7}$Sr$_{0.3}$MnO$_3$ film*, Phys. Stat. Sol. B **243**, 1383 (2006), doi:10.1002/pssb.200541447

M. Ziese, A. Bollero, I. Panagiotopoulos, N. Moutis: *Magnetoresistance switch-effect in a multiferroic Fe$_3$O$_4$/BaTiO$_3$ bilayer*, Appl. Phys. Lett. **88**, 212502 (2006), doi:10.1063/1.2206121

Books

P. Esquinazi, R. Höhne, K.-H. Han, D. Spemann, A. Setzer, M. Diaconu, H. Schmidt, T. Butz: *Induced Magnetic Order by Ion Irradiation of Carbon-based Structures*, in: *Carbon-based Magnetism*, ed. by T. Makarova, F. Palacio (Elsevier, Amsterdam 2006).

Talks

P. Esquinazi: *Magnetic order in carbon structures*, Int. Conf. Nanoelectron. 2006, Lancaster, UK, 08.–11. January 2006

P. Esquinazi: *Magnetic order in carbon structures*, Real Sociedad Expañola de Física, Alicante, Spain, 01.–03. February 2006

P. Esquinazi: *Magnetic order in carbon structures*, Univ. Autonoma de Madrid, Spain, 01.–04. March 2006

P. Esquinazi: *Proton-induced magnetic ordering in carbon structures*, Int. Conf. Atomic Collision Solids ICACS 2006, Berlin, 22.–24. July 2006

P. Esquinazi: *Magnetic Carbon*, British Carbon Group, London, UK, 14. December 2006

M. Ziese: *Current-induced variation of the magnetoresistance of magnetite and manganite based heterostructures*, III. Joint Eur. Magn. Symp., San Sebastian, Spain, 26.–30. June 2006

M. Ziese: *Spin dependent properties of magnetic oxide films and heterostructures*, Nanyang Technological University, Singapore, 12. January 2006

M. Ziese: *Spin dependent properties of magnetic oxide films and heterostructures*, Data Storage Institute, Singapore, 13. January 2006

8.11 Graduations

Diploma

- Roland Salzer
  Magnetische Eigenschaften von d- und f-Elektronen freien Substanzen
  March 2006

- Norman Leps
  Rauschmessungen an hochorientiertem pyrolytischem Graphit
  June 2006

Bachelor

- Katharina Fritsch
  Resistivity of dual-beam produced palladium wires
  April 2006

8.12 Guests

- Prof. Dr. Yakov Kopelevich, Mercator Visiting Professorship
  State University of Campinas, Brazil
  30. September 2005 – 28. February 2006

- Yimeng Lu
  University of Shanghai, PR China
  01. July 2006 – 31. August 2006

- Cagri Karahan
  Technical University Ankara, Turkey
  10. July 2006 – 25. August 2006

- Dr. E.H. Brandt
  MPI für Metallforschung, Stuttgart
  10./11. August 2006

- Dr. G.P. Mikitik
  Verkin Institute for Low Temperature Physics, Kharkov, Ukraine
  10./11. August 2006

III

Institute for Theoretical Physics

9

Computational Quantum Field Theory

9.1 Introduction

The Computational Physics Group performs basic research into classical and quantum statistical physics with special emphasis on phase transitions and critical phenomena. In the centre of interest are currently the physics of spin glasses, diluted magnets and other materials with quenched, random disorder, soft condensed matter physics with focus on fluctuating paths and interfaces, and biologically motivated problems such as protein folding, aggregation and adhesion as well as related properties of semiflexible polymers. Investigations of a geometrical approach to the statistical physics of topological defects with applications to superconductors and superfluids and research into fluctuating geometries with applications to quantum gravity (e.g., dynamical triangulations) are conducted within the EC-RTN Network "ENRAGE": *Random Geometry and Random Matrices: From Quantum Gravity to Econophysics*. The statistical mechanics of complex networks is studied within the frame of an Institute Partnership with the Jagellonian University in Krakow, Poland, supported by the Alexander-von-Humboldt Foundation. And with the help of a Development Host grant of the European Commission, also research into the physics of anisotropic quantum magnets has been established.

The methodology is a combination of analytical and numerical techniques. The numerical tools are currently mainly Monte Carlo computer simulations and high-temperature series expansions. The computational approach to theoretical physics is expected to gain more and more importance with the future advances of computer technology, and will probably become the third basis of physics besides experiment and analytical theory. Already now it can help to bridge the gap between experiments and the often necessarily approximate calculations of analytical work. To achieve the desired high efficiency of the numerical studies we develop new algorithms, and to guarantee the flexibility required by basic research all computer codes are implemented by ourselves. The technical tools are Fortran, C, and C++ programs running under Unix or Linux operating systems and computer algebra using Maple or Mathematica. The software is developed and tested at the Institute on a cluster of PCs and workstations, where also most of the numerical analyses are performed. Large-scale simulations requiring vast amounts of computer time are car-

ried out at the Institute on a Beowulf cluster with 40 Athlon MP1800+ CPUs and an Opteron cluster with 18 processors of 64-bit architecture, at the parallel computers of the University computing center, and upon grant application at the national supercomputing centres in Jülich and München on IBM and Hitachi parallel supercomputers. This combination of various platforms gives good training opportunities for the students and offers promising job perspectives in many different fields for their future career.

Within the University, our research activities are tightly bound to the Centre for Theoretical Sciences (NTZ) of the Centre for Advanced Study (ZHS) and the recently established priority research areas ("Profilbildende Forschungsbereiche (PbF)") and Research Academy Leipzig (RAL), providing in particular the organizational frame for our cooperations with research groups in experimental physics and biochemistry. On a wider scale, they are embedded in a wide net of national and international collaborations funded by network grants of the European Commission and the European Science Foundation (ESF), and by binational research grants with scientists in Sweden, China and Poland funded by the German Academic Exchange Service (DAAD) and the Alexander-von-Humboldt Foundation. Further close contacts and collaborations are also established with research groups in Armenia, Austria, France, Great Britain, Israel, Italy, Russia, Spain, Taiwan, Turkey, Ukraine, and the United States.

Wolfhard Janke

9.2   Free-Energy Landscapes and Barriers of Spin Glasses

A. Nußbaumer, E. Bittner, W. Janke

Spin glasses are characterized by random, competing interactions leading to "frustration" effects, i.e., no unique spin configuration is favoured by all interactions [1]. This is the reason for a rugged free energy landscape in such systems which, in Monte Carlo computer simulations, is reflected by an extremly slow (pseudo-) dynamics. To some extent this problem can be overcome by our recently proposed multi-overlap algorithm [2]. Using this algorithm in a large-scale study of the three-dimensional (3D) short-range Edwards-Anderson Ising (EAI) $\pm J$ model, we were able to determine the scaling behaviour of the barrier heights [3] and the tails of the overlap-parameter distribution [4]. In particular the barrier-height distribution was found not to agree with mean-field predictions.

This prompted us to generalize our method to long-range models [5]. By this means we investigated the finite-size scaling behaviour of free-energy barriers in the Sherrington-Kirkpatrick (SK) model. With N denoting the number of spins, here we found for the barrier-height scaling a power law N^α with $\alpha = 1/3$ [5], in perfect agreement with the theoretical prediction.

Since the analysis tools were precisely the same as in the previous EAI study, the central question thus is: Does the barrier-height scaling show a qualitative difference between short- and long-range models, or did we simply not yet reach the truly asymptotic region in the previous study? The latter possibility is quite conceivable because due to the technical difficulties the simulations had to be performed quite close to the freezing transition. To answer this question, we therefore further improved our multi-overlap method by combining it with parallel tempering in temperature [6]. As a result this allows us to perform meaningful simulations at much lower temperatures than before where the asymptotic limit should be reached already for much smaller lattice sizes. Still, these simulations are very demanding and require many years of CPU time on parallel supercomputers such as JUMP at Forschungszentrum Jülich. The data production is running at full pace and to date we have already completed a few hundred disorder realizations for various lattice sizes. A few more are still needed, however, before a meaningful quenched average and the final data analysis can be performed.

Along another line of this project we are investigating also the random orthogonal model (ROM), which is a generic representative for 1-step replica symmetry breaking (1SRB). Here, however, the simulations turned out to be even more intricate than in the other two models and the data production is correspondingly severely hampered.

One possible reason for the still very slow dynamics are "hidden" barriers which are not directly visible in the commonly considered quantities such as the energy, magnetization or overlap. This conjecture is born out by analogous observations for the simpler Ising model at low temperatures [7]. To underscore this possibility we have performed extensive simulations of this simpler model and studied in great detail the "hidden" barriers associated with both, the droplet-strip [8] and the evaporation/condensation [9, 10] transition [11]. Once these barriers are fully understood in the simpler Ising model, the hope is that similar ideas can be transferred to spin glasses as well.

[1] K.H. Fischer, J.A. Hertz: *Spin Glasses* (Cambridge University Press, Cambridge 1991)
[2] B.A. Berg, W. Janke: Phys. Rev. Lett. **80**, 4771 (1998)
[3] B.A. Berg et al.: Phys. Rev. B **61**, 12 143 (2000); Physica A **321**, 49 (2003)
[4] B.A. Berg et al.: Phys. Rev. E **65**, 045 102(R) (2002); *ibid.* **66**, 046 122 (2002)
[5] E. Bittner, W. Janke: Europhys. Lett. **74**, 195 (2006)
[6] A. Nußbaumer, E. Bittner, W. Janke: in preparation.
[7] T. Neuhaus, J.S. Hager: Stat. Phys. **113**, 47 (2003)
[8] K. Leung, R.K.P. Zia: J. Phys. A Math. Gen. **23**, 4593 (1990)
[9] M. Biskup et al.: Europhys. Lett. **60**, 21 (2002)
[10] K. Binder: Physica A **319**, 99 (2003)
[11] A. Nußbaumer et al.: Europhys. Lett. **75**, 716 (2006); in: *Computer Simulation Studies in Condensed-Matter Physics XX*, ed. by D.P. Landau et al. (Springer, Berlin 2007), in print

9.3   High-Temperature Series Expansions for Potts Models: Disordered Magnets and Percolation

M. Hellmund[*], W. Janke

[*]*Fakultät für Mathematik und Informatik*

Systematic series expansions for statistical physics models defined on a lattice are a well-known alternative to large-scale numerical simulations for the study of phase transitions and critical phenomena [1]. For quenched disordered systems the extension of this method [2] requires especially adapted graph theoretical and algebraic algorithms. In this project we developed a computer package based on the "star-graph" method [2, 3] which allows the generation of high-temperature series expansions for the free energy and susceptibility. We consider the class of disordered q-state Potts models on d-dimensional hypercubic lattices $\mathbb{Z}^d$ with bimodal probability distributions of quenched couplings parametrized by $P(J_{ij}) = p\delta(J_{ij} - J_0) + (1 - p)\delta(J_{ij} - RJ_0)$, which includes spin glasses, diluted ferromagnets, random-bond models and transitions between them. The limiting case $p = 1$ describes the pure ferromagnetic ($J_0 > 0$) models. Even though the method is highly optimized for the problem at hand, it is extremely demanding since the number of contributing graphs grows exponentially with the order of the series and all intermediate calculations have to be performed by means of symbolic computer algebra, which we implemented ourselves in C++ since the available standard software products such as `Mathematica` or `Maple` are too slow and require far too much memory.

In a first step we considered the bond-diluted Ising model ($q = 2$) for which we used our computer package to generate high-temperature series up to order 21 in $d = 3$ dimensions [4, 5] and up to order 19 in $d = 4, 5$ [5]. Applying various analysis tools we determined the phase diagrams in the temperature-dilution plane and estimated the critical exponent γ, parametrizing the singularity of the susceptibility at criticality, $\chi \sim (T - T_c)^{-\gamma}$. Depending on the dimension, our results can be compared with field-theoretic predictions and estimates from our Monte Carlo simulations performed in another project [6]. We established the irrelevance of disorder above the critical dimension $d = 4$ and the existence of unusual logarithmic corrections at the critical dimension.

We also obtained and analysed series for the pure q-state Potts model with arbitrary parameter q [7]. The series are generated up to order 21 in $d = 3$ dimensions, order 19 in $d = 4, 5$, and order 17 for *arbitrary* dimensions, that is with d as a symbolic parameter. This allowed a throughout analysis of bond percolation (described by the $q \to 1$ limit of the Potts model) on hypercubic lattices giving new estimates of the percolation thresholds and the critical exponent of the mean cluster size.

[1] C. Domb, M.S. Green (Eds.): *Phase Transitions and Critical Phenomena*, Vol. 3 (Academic Press, New York 1974)
[2] R.R.P. Singh, S. Chakravarty: Phys. Rev. B **36**, 546 (1987)
[3] M. Hellmund, W. Janke: Cond. Matter Phys. **8**, 59 (2005)
[4] M. Hellmund, W. Janke: Comp. Phys. Comm. **147**, 435 (2002)
[5] M. Hellmund, W. Janke, Phys. Rev. B **74**, 144201 (2006)
[6] W. Janke et al.: invited plenary talk, PoS **LAT2005**, 018 (2005)
[7] M. Hellmund, W. Janke: Phys. Rev. E **74**, 051 113 (2006)

9.4 Self-Avoiding Walks on Percolation Clusters

V. Blavatska, Y. Holovatch[*], W. Janke

[*]Institute for Condensed Matter Physics, National Academy of Sciences, Lviv, Ukraine

In close analogy to scaling laws at second-order phase transitions, the behaviour of long fexible polymer chains in a good solvent can be described by power laws in the number of monomers N. It is well established that these scaling properties are perfectly described within a model of a self-avoiding walk (SAW) on a regular lattice [1]. In particular, for the average squared end-to-end distance R and the number Z_N of SAWs with N steps, one finds in the asymptotic limit $N \to \infty$:

$$\langle R^2 \rangle \propto N^{2\nu}, \quad Z_N \propto z^N N^{\gamma-1} , \tag{9.1}$$

where ν and γ are universal critical exponents and z is the effective coordination number of the considered lattice. By exact enumerations, Monte Carlo simulations, or mapping this problem onto the $n \to 0$ limit of O(n) symmetric field theory and applying the renormalization-group approach (e.g. ϵ-expansions), the values of these exponents are very precisely known in physical dimension $D = 3$.

A question of great current interest is the influence of structural disorder on the universal properties of a SAW, namely: does the scaling law holds with new exponents ν_p and γ_p when a SAW resides on a structurally disordered (diluted) lattice? The question of how linear polymers behave in disordered media is not only of academic interest, rather it is also of relevance for understanding transport properties of polymer chains in porous media, such as enhanced oil recovery, gel electrophoresis, gel permeation chromatography, etc. [2].

Currently, the behaviour of SAWs in disordered media is still a subject where many principal questions are unsettled. In this project, we focus on the special case where the disordered lattice is taken as a percolation cluster exactly at threshold. Both, SAWs and percolation clusters are among the most frequently encountered examples of fractals in condensed matter physics. As it has become clear by now, higher-order correlations of a fractal object living on another fractal lead to multifractality, so that a SAW on a percolation cluster is thus a good candidate for observing multifractal behaviour.

Flory like theories predict that [3]

$$\nu_p = \frac{3}{2 + d_f} , \tag{9.2}$$

where d_f is the fractal dimension of the percolation cluster, leading in three dimensions to $\nu_p = 0.662$, in fairly good agreement with Monte Carlo simulations [3], while recent ϵ-expansions yield $\nu_p = 0.678$ [4]. In higher dimensions, up to the so-called upper critical dimension $d_u = 6$ (where mean-field behaviour sets in), much less is known. In our ongoing numerical study we employ chain growth methods with population control, in particular the Pruned-Enriched Rosenbluth-Rosenbluth Method (PERM) [5], relying on our experience with similar simulations of lattice proteins [6].

[1] J. des Cloizeaux, G. Jannink: *Polymers in Solution* (Clarendon Press, Oxford 1990); P.-G. de Gennes: *Scaling Concepts in Polymer Physics* (Cornell University Press, Ithaca and London 1979)

[2] K. Barat, B.K. Chakrabarti: Phys. Rep. **258**, 378 (1995)

[3] K. Kremer: Z. Phys. B **45**, 149 (1981)

[4] V. Blavatska et al.: Phys. Rev. E **70**, 035 104(R) (2004)

[5] P. Grassberger: Phys. Rev. E **56**, 3682 (1997); H.-P. Hsu et al.: J. Chem. Phys. **118**, 444 (2003)

[6] M. Bachmann, W. Janke: Phys. Rev. Lett. **91**, 208 105 (2003); J. Chem. Phys. **120**, 6779 (2004)

9.5 Percolation of Vortex Networks in the $U(1)$ Lattice Higgs Model

S. Wenzel, E. Bittner, W. Janke, A.M.J. Schakel[*]

[*]Institut für Theoretische Physik, Freie Universität Berlin

Simple field theories in three dimensions like the complex ϕ^4 theory coupled to an electromagnetic field (gauge field) play an important role as effective theories describing phase transitions in the field of superconductivity and QCD. These transitions occur upon a change of (coupling) parameters like the self-coupling λ of the ϕ field and the parameter κ which couples the ϕ and gauge field.

Recently, we analysed the compact lattice version of such a field theory, the $U(1)$ lattice Higgs model, via Monte Carlo simulations [1] and argued that despite the non-existence of an ordinary phase transition the phase diagram is clearly separated into two phases which can be identified by the existence of monopoles or vortex lines. The latter are objects much like the vortex lines found in superconducting liquids. Our central thesis [2] was therefore, that the phase separation line can be interpreted as a Kertész line [3] on which a vanishing line tension leads to a proliferation of vortices. Although no divergences (phase transition) in the (free) energy can be seen we should find weak singularities in so-called cluster or droplet observables as a consequence. One such quantity is for instance the size of clusters formed by vortices. Our most recent simulations focused on these cluster quantities directly and give strong support for our previous findings. Figure 9.1 shows that we find the expected scaling behaviour of the maximal cluster size. As a second result we find that the critical exponents describing this phenomena are just the ordinary percolation exponents [4].

[1] S. Wenzel: Master Thesis, Universität Leipzig 2004

[2] S. Wenzel et al.: Phys. Rev. Lett. **95**, 051 601 (2005)

[3] J. Kertesz: Physica A **161**, 58 (1989)

[4] D. Stauffer, A. Aharony: *Introduction to Percolation Theory* (Taylor and Francis, London 1994)
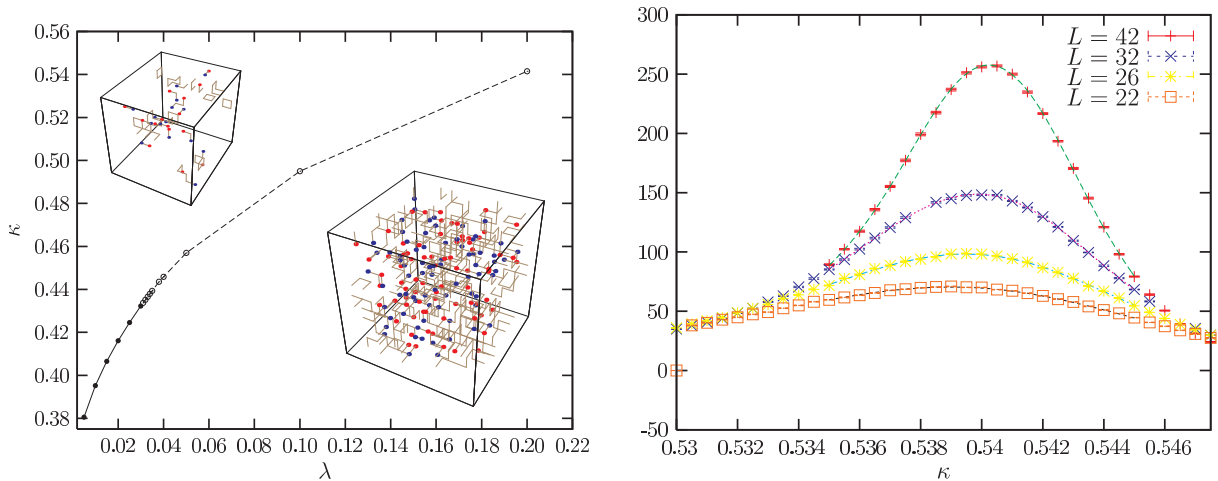
Figure 9.1: *Left:* Phase diagram of the $U(1)$ lattice Higgs model in dependence on two coupling constants. While for small λ the type of the transition line is of first order (*black dots*), the line continues as a Kertész line (*open dots*) with no thermal phase transition. The *insets* show typical configurations of the vortex network in the two phases. *Right:* Diverging susceptibility of the maximal cluster size at the Kertész line $\lambda = 0.20$.

9.6 Geometric and Stochastic Clusters: Fractal Dimensions and Critical Exponents in Regular and Gravitating Potts Models

W. Janke, A.M.J. Schakel[*], M. Weigel[†]

[*]Institut für Theoretische Physik, Freie Universität Berlin
[†]School of Mathematical and Computer Sciences, Heriot-Watt University, Edinburgh, UK

The relation between the percolation problem and thermal phase transitions of lattice spin systems has been a question of intense research for at least three decades. Clusters of even spins are natural objects occurring in the analysis of phase ordering processes and nucleation [1], and a theory of critical phenomena in terms of purely geometrical objects appears appealing. In this context, it had long been surmised that a continuous phase transition of a spin system might be accompanied (or, in fact, caused) by a percolation transition of the clusters of like spins (*geometric clusters*), the appearance of a percolating cluster sustaining the onset of a non-zero magnetisation. While for the special case of the Potts model in two dimensions it turned out that, indeed, the thermal phase transition point coincides with the percolation transition of the spin clusters, this behaviour is not generic and does not occur in three-dimensional systems [2]. Also, the critical exponents associated to the percolation of geometric clusters are not directly related to the thermal exponents of the spin model. However, a close relation between the percolation and thermal phase transitions can be established by considering *stochastically* defined clusters (or droplets) as they occur in the Fortuin–Kasteleyn (FK) representation of the Potts model, and it can be shown that, in fact, the Potts model is equivalent to a site-bond correlated percolation problem [3] such that the corresponding critical exponents agree. This

identification of the proper cluster objects (*FK clusters*) percolating at the thermal phase transition subsequently also allowed for the design of *cluster algorithms* for the efficient simulation of Potts models in the vicinity of the ordering transition [4], beating the observed critical slowing down of local update algorithms. Similarly, relations of continuous-spin models to percolation problems could be established and corresponding cluster algorithms formulated [5], such that the continuous phase transitions of many standard models of statistical mechanics are by now understood in terms of the percolation properties of some suitably defined ensemble of stochastic clusters.

Although not sharing the critical exponents of the thermal phase transition, the clusters of like spins or geometric clusters still undergo a percolation transition in the course of thermal phase ordering. This transition is in general not equivalent to ordinary (site or bond) percolation and it remains an interesting open question to determine the general critical behaviour of clusters of aligned spins. For the case of the two-dimensional Ising model, it has been conjectured and numerically verified that the geometric clusters are described by the $q = 1$ tricritical Potts model; this correspondence can be understood from a direct construction starting from the dilute Potts model [6] and the fact that both models are characterized by the same central charge c. Subsequently, analogous conjectures for the $2 < q \leq 4$ Potts models were made and some of them substantiated by numerical simulations [7]. Analytical calculations concerning clusters occurring in systems of statistical physics and their boundaries, traditionally based on methods of conformal field theory and the Coulomb gas [8], have recently seen major advances from the insight that fractal random curves can be described in a framework dubbed *stochastic Loewner evolution* (SLE) [9]. Collecting these observations, a more systematic analysis of the relation between the critical and tricritical branches of the Potts model and their connection to the FK and geometric clusters has been performed, resulting in the identification of exact values for the different cluster fractal dimensions and their numerical verification [10, 11].

Recently we considered the fractal dimensions of critical clusters occurring in configurations of a q-state Potts model coupled to the planar random graphs of the dynamical triangulations formulation of Euclidean quantum gravity in two dimensions which, from a statistical mechanics point of view, may be regarded as a particular type of annealed connectivity disorder. We applied the KPZ formalism [12] to derive exact theoretical predictions for the fractal dimensions of both FK and geometric clusters in the case of Potts models and employed numerical simulation methods to succesfully confirm them for the Ising case $q = 2$ [13].

[1] K. Binder et al.: Phys. Rev. B **12**, 5261 (1976); A.J. Bray: Adv. Phys. **43**, 357 (1994)

[2] A. Coniglio et al.: J. Phys. A **10**, 205 (1977)

[3] C.M. Fortuin, P.W. Kasteleyn: Physica **57**, 536 (1972); A. Coniglio, W. Klein: J. Phys. A **13**, 2775 (1980)

[4] R.H. Swendsen, J.-S. Wang: Phys. Rev. Lett. **58**, 86 (1987); U. Wolff: Phys. Rev. Lett. **62**, 361 (1989)

[5] P. Blanchard et al.: J. Phys. A **33**, 8603 (2000)

[6] C. Vanderzande, A.L. Stella: J. Phys. A **22**, L445 (1989); A.L. Stella, C. Vanderzande: Phys. Rev. Lett. **62**, 1067 (1989)

 [7] B. Duplantier, H. Saleur: Phys. Rev. Lett. **63**, 2536 (1989); C. Vanderzande: J. Phys. A **25**, L75 (1992)
 [8] B. Duplantier: J. Stat. Phys. **110**, 691 (2003)
 [9] O. Schramm: Israel J. Math. **118**, 221 (2000); M. Bauer, D. Bernard: arXiv:math-ph/0602049
[10] Y.J. Deng et al.: Phys. Rev. E **69**, 026 114 (2004)
[11] W. Janke, A.M.J. Schakel: Nucl. Phys. B **700**, 385 (2004); Phys. Rev. E **71**, 036 703 (2005); Braz. J. Phys. **36**, 708 (2006)
[12] V.G. Knizhnik et al.: Mod. Phys. Lett. A **3**, 819 (1988)
[13] W. Janke, M. Weigel: Phys. Lett. B **639**, 373 (2006)

9.7 Statistical Mechanics of Complex Networks

B. Wacław, L. Bogacz[*], Z. Burda[†], W. Janke

[*]Jagellonian University, Krakow, Poland (since October 2006)
[†]Jagellonian University, Krakow, Poland

Complex networks are present in many systems, having either natural or artificial origin [1]. For example, the Internet is built up of computers linked by various physical or wireless links. The World Wide Web is a large complex of webpages connected by hyperlinks. The living cell can be described as a set of chemicals and appropriate chemical reactions. Also the social contacts between people form a network with high level of complexity, which allows for spreading ideas as well as diseases. The above systems are only a few examples of a rapidly developing interdisciplinary field of research often called the "science of complex networks", joining many different areas of human activity. The subject of interest of biologists, chemists, sociologists, computer scientists and others is to find general laws governing the creation and growth of complex networks. Despite an enormous variety of networks and big differences in their physical structure it is possible to form such general laws. This situation still motivates researchers to study basic mechanisms underlying many properties of observed networks.

The main objective of this project is to investigate the influence of coupled matter fields on the geometry and topology of complex networks. Similar problems have been addressed in the context of quantum simplicial gravity or string theory but have not yet been thoroughly studied in the context of complex networks. Only the opposite problem has been investigated so far, namely how geometrical and topological properties of the underlying network influence the behaviour of matter fields. In a broad sense, one can understand by matter field any set of dynamical degrees of freedom living on the nodes or links of a network. This type of questions plays an important role in studies of complex systems whose architecture is represented by a network resulting from the interactions of entities forming the system. In our investigations we try to adapt methods of statistical mechanics developed earlier in the different applications mentioned above, employing both numerical Monte Carlo simulations as well as analytic calculations.

More specifically, we consider so-called zero-range processes [2], where particles move through the sites of a network according to some ultra-local rules. The main objective is to understand how geometrical and topological properties of networks and the dynamics of the particles are interrelated [3]. This is an example of interaction between "matter" and "geometry".

Similar problems appear in the dynamical triangulation approach to quantum gravity [4, 5], where one studies an ensemble of graphs of a special kind, preserving Lorenzian or Euclidean symmetry. There one tries to understand how the space-time geometry represented by those graphs changes when it interacts with matter fields [6]. For example the Ising model on dynamical triangulation corresponds to a fermionic field coupled to two-dimensional quantum gravity [7]. At the critical point, the appearance of long-range correlations of the Ising spins strongly influences the geometrical properties of the dynamical triangulations on which the "matter" model is defined. This is a clear signal of the back-reaction of geometry to the changes in the matter sector.

Part of the project is devoted to studies of non-equilibrium processes. In particular, the zero-range process mentioned above, when studied on a network can be used as a model for the dynamics of backgammon or "balls-in-boxes" condensation [8]. The statistical properties of this condensation have already been well established, but the issue of how the equilibrium of the condensate is reached, has not yet been studied thoroughly. The condensation of backgammon-type is a state of the system represented by a distribution of balls on the nodes such that one of the nodes collects a finite fraction of balls proportional to the total number in the system, similar to Bose-Einstein condensation, but here in real space. One can think of the links of the network as channels along which balls can flow between the nodes. The question of interest for non-equilibrium physics is how the condensate is produced in time and how much time it takes to produce it [9].

This type of problem can be a prototype for a wide class of problems concentrating on the back-reaction of the architecture of a complex system on internal matter flows and distributions and can be of interest for transportation, telecommunication, sociology and biology, where the systems automatically adjust to the changing situation.

[1] R. Albert, A.-L. Barabási: Rev. Mod. Phys. **74**, 47 (2002)
[2] C. Godreche, J.M. Luck, J. Phys. A **38**, 7215 (2005)
[3] L. Bogacz et al.: arXiv:cond-mat/0701553, Chaos (in print)
[4] J. Ambjorn et al.: Phys. Rev. D **72**, 064 014 (2005)
[5] J. Ambjorn et al.: Phys. Rev. D **48**, 3695 (1993)
[6] W. Janke et al.: Cond. Matter Phys. **9**, 263 (2006)
[7] D.V. Boulatov, V.A. Kazakov: Phys. Lett. B **186**, 379 (1987)
[8] P. Bialas et al.: Nucl. Phys. B **493**, 505 (1997)
[9] B. Wacław et al.: arXiv:cond-mat/0703243, submitted to Phys. Rev. E.

9.8 Microcanonical Analyses of Peptide Aggregation Processes

C. Junghans, M. Bachmann[*], W. Janke

[*]Universität Leipzig and Lunds Universitet, Lund, Sweden

Thermodynamic phase transitions in macroscopic, infinitely large systems are typically analysed in the thermodynamic limit of a canonical ensemble, i.e., the temperature is treated as an intensive external control parameter adjusted by a heat bath, and the total system energy is distributed according to the Boltzmann-Gibbs statistics. Since the microcanonical entropy is typically a concave function of energy, the microcanonical specific heat is positive. The specific heat can only become negative in an energetic regime, where the entropy is convex. In this region, the caloric temperature, i.e., the temperature as a function of energy, bends back, i.e., the system becomes colder with increasing total energy and the temperature is no appropriate control parameter [1]. It is a surprising fact that the backbending effect is indeed observed in transitions with phase separation. Although this phenomenon has already been known for a long time from astrophysical systems [2], it has been widely ignored since then as somehow "exotic" effect. Recently, however, experimental evidence was also found from melting studies of sodium clusters [3], nuclei fragmentation [4], spin models [5], and a large number of other isolated finite model systems for evaporation and melting effects [6].

We could show that the aggregation transition of peptides (small proteins) is also a phase separation process, where the loss of entropy due to the existence of the phase boundary results in negative specific heat [7, 8]. This effect is guided by changes of the interfacial entropy as a result of surface effects. Since peptides and proteins, like the exemplified model heteropolymers used in our study, are *necessarily* systems of *finite* length, a thermodynamic limit cannot be defined and, therefore, the effect does not vanish. For this reason, standard canonical formalisms are not suitable for the interpretation of conformational pseudophase transitions with phase separation, as the temperature is not a unique control parameter and the total system energy is not an extensive, separable quantity. In such cases, microcanonical thermodynamics with the energy itself as the external control parameter provides a more favorable basis for the study of first-order-like transitions. The interesting phenomenon of the negativity of the microcanonical specific heat in peptide aggregation should motivate an experimental verification which is still pending.

[1] D.H.E. Gross: *Microcanonical Thermodynamics* (World Scientific, Singapore 2001)
[2] W. Thirring: Z. Physik **235**, 339 (1970)
[3] M. Schmidt et al.: Phys. Rev. Lett. **86**, 1191 (2001)
[4] O. Lopez et al.: Phys. Rev. Lett. **95**, 242 701 (2005)
[5] W. Janke: Nucl. Phys. B Proc. Suppl. **63A-C**, 631 (1998); H. Behringer, M. Pleimling: Phys. Rev. E **74**, 011 108 (2006)
[6] S. Hilbert, J. Dunkel: Phys. Rev. E **74**, 011 120 (2006)
[7] C. Junghans et al.: Phys. Rev. Lett. **97**, 218 103 (2006)
[8] C. Junghans, M. Bachmann, W. Janke: Mainz/Lund/Leipzig preprint (2007)

9.9   Structural Cooperativity in Collapse, Crystallization, and Folding Transitions of Polymers and Proteins

T. Vogel, S. Schnabel, M. Bachmann[*], W. Janke

[*]Universität Leipzig and Lunds Universitet, Lund, Sweden

In general, phase transitions of many-particle systems are due to a complex interplay between a large number of system constituents, called cooperativity. In single-molecule systems, structure formation results from competing covalent and noncovalent interactions between atoms or, on a coarse-grained level, between mesoscopic parts of the molecule. For flexible homopolymers, which are in the focus of our interest, the situation *seems* to be plausible. At the critical temperature, a polymer of infinite length collapses from random-coil to globular conformations. This transition is expected to be continuous. But, as the upper critical dimension is $d = 3$, field theory predicts logarithmic corrections to the scaling – which have, however, neither been confirmed in experiments nor in computer simulations over more than three decades. In our chain-growth studies of lattice polymers with up to 32000 monomers [1], we also find rather mean-field-like behaviour which might be reasoned by the chain lengths which are still too short. A second transition homopolymers experience, is the crystallization transition, where globular ("fluid") conformations go over into metastable, glass-like structures. In a recent study of a specially parametrized bond-fluctuation model, it was shown that in the thermodynamic limit, collapse and crystallization can happen at the same temperature [2]. We have found that this is not a universal, model-independent phenomenon as there are strong indications in our lattice studies that both transitions will remain separated in the thermodynamic limit.

Conformational transitions are also of essential importance in biological systems, mainly for stabilizing the functional network of biomolecules keeping cells alive. A major fraction of these functional molecules are proteins, and the unraveling of their folding characteristics into stable "native" conformations is one of the major keys to the understanding of the biophysical mechanisms behind a large number of epidemic diseases, such as Alzheimer's disease or bovine spongiform encephalopathy (BSE). Due to the large number of possible amino acid sequences building up proteins and the evolutional factor which is hardly understood, systematic experimental or computational analyses of the relations between sequence, native fold, and folding characteristics are extremely difficult. Employing a simple mesoscopic hydrophobic-polar protein model [3], we could show that typical tertiary protein folding processes such as two-state folding, folding through weakly stable intermediate structures, as well as folding into metastable structures do not necessarily depend of atomic details as it is widely believed. Figure 9.2 shows folding channels and free-energy landscapes of three different hydrophobic-polar sequences with the same content of hydrophobic and polar residues: Fig. 9.2a two-state folding with a single free-energy barrier that separates folded (N) from unfolded, denatured (D) states; Fig. 9.2b an example with two barriers, i.e., the folding pathway involves an intermediate macrostate (I); Fig. 9.2c bifurcation of the folding channel into two separate degenerate, metastable macrostates (M_1 and M_2) [4, 5]. These results shed new light on an old story: Tertiary protein folding depends
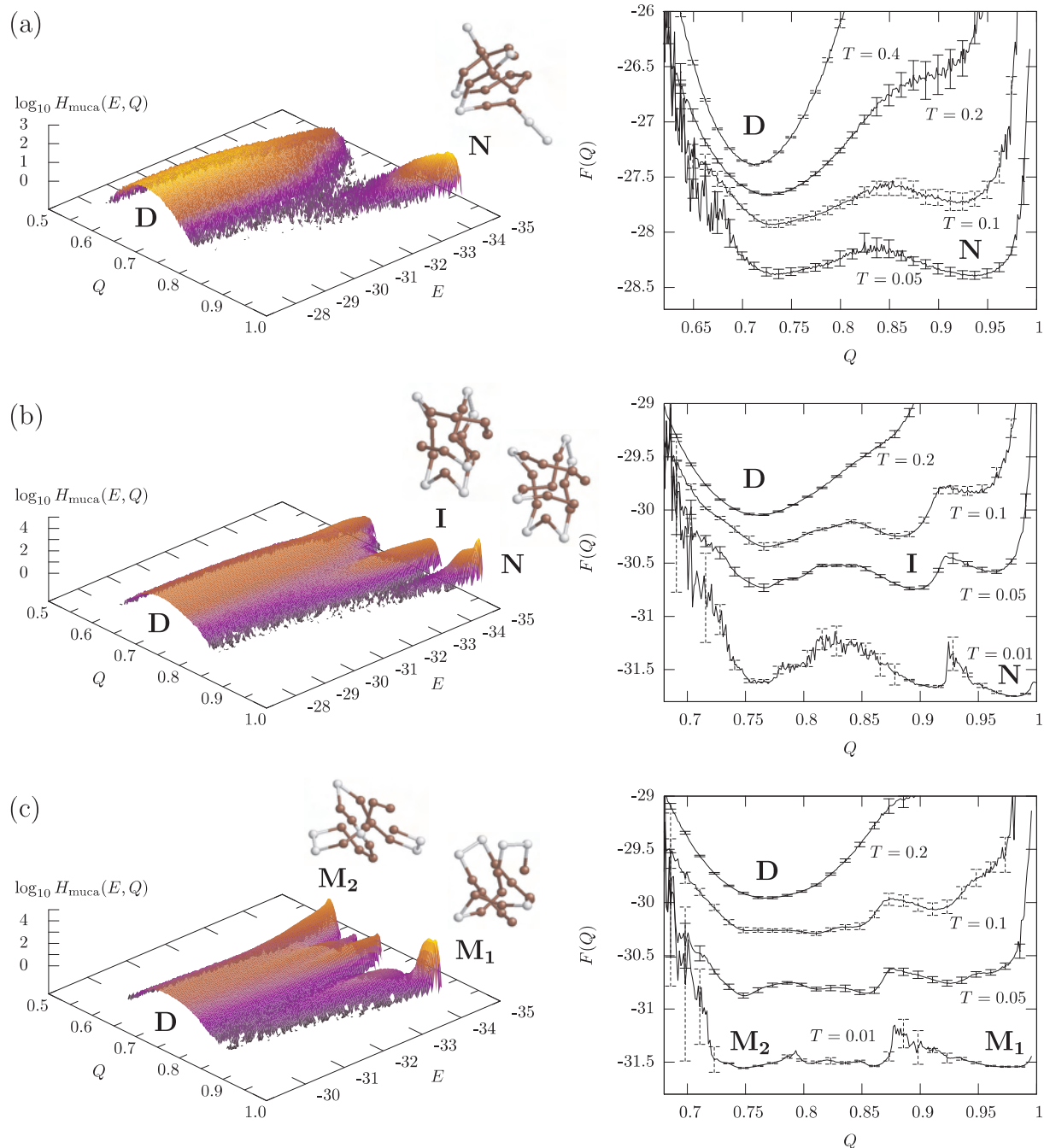
Figure 9.2: Folding channels (*left*) and free energies as a function of a suitable order parameter, parametrized by temperature (*right*) for three different protein-like hydrophobic-polar heteropolymers with different sequences.

on *general intrinsic* properties of polymeric objects at a mesoscopic scale in combination with the nonnegligible hydrophobic interaction, and these intrinsic properties are probably responsible for the "native" folds to be the only possible thermodynamically stable geometries.

[1] T. Vogel, M. Bachmann, W. Janke: Leipzig/Lund preprint (2007)

[2] F. Rampf et al.: Europhys. Lett. **70**, 628 (2005)

[3] F.H. Stillinger et al.: Phys. Rev. E **48**, 1469 (1993); F.H. Stillinger, T. Head-Gordon: Phys. Rev. E **52**, 2872 (1995)

[4] S. Schnabel et al.: Phys. Rev. Lett. **98**, 048 103 (2007)

[5] S. Schnabel et al.: J. Chem. Phys. **126**, 105 102 (2007)

9.10 Adsorption and Solution Behaviour of Semiconductor-Binding Synthetic Peptides

M. Bachmann[*], W. Janke, K. Goede[†], M. Grundmann[†], A. Irbäck[‡], S. Mitternacht[‡], G. Gökoğlu[§], T. Çelik[§]

[*]Universität Leipzig and Lunds Universitet, Lund, Sweden

[†]Semiconductor Physics Group, Institute for Experimental Physics II

[‡]Lunds Universitet, Lund, Sweden

[§]Hacettepe Üniversitesi, Ankara, Turkey

In recent experimental and theoretical works [1–4], it could be shown that peptide binding to solid substrates, in particular, semiconductor surfaces, is specific to crystallographic (e.g., atomic pattern of the surface net plane) and physicochemical properties (e.g., hydrophobicity) of the substrate and solvent (pH value, temperature). The understanding of these adsorption processes is not only of particular importance for biosensory and nanoelectronic applications, but it is also a great theoretical challenge as a computationally tractable realistic hybrid model for the interaction between soft *and* solid matter is still simply lacking.

For this reason, we have first performed computer simulations to analyze solvent properties (without substrate) of four synthetic peptides used in the experiments. In these experiments [1], three of these sequences exhibited good binding properties to (100) GaAs and poor adhesion to (100) Si surfaces, whereas the (100) Si binding strength of the fourth sequence was comparatively quite good. We employed two different implicit-solvent models, one being based on the ECEPP forcefield with all atomic details [5], the other one with a reduced set of atomic parameters and simplified energetic contributions [6]. The big advantage of the latter model is that it is capable to predict realistic transition temperatures [7]. The shortness of the peptide sequences with 12 residues each is responsible for the expected behaviour that under physiological conditions the peptides are widely unstructured in solution. This result confirms the experimental observation from analyzing corresponding CD spectra [1]. Nonetheless, decreasing the temperature, the computer simulations revealed the remarkable result displayed in Fig. 9.3: Three peptides showed tendency to fold into α helical conformations, whereas the fourth formed a β sheet. The latter sequence was exactly the one with the improved Si binding properties. A first analysis showed that the position of proline, one of the amino acids in all sequences, is responsible for the different folding behaviour. To what extent this will be the reason for the different adsorption qualities is still unclear and is subject of ongoing computational studies of the hybrid system.
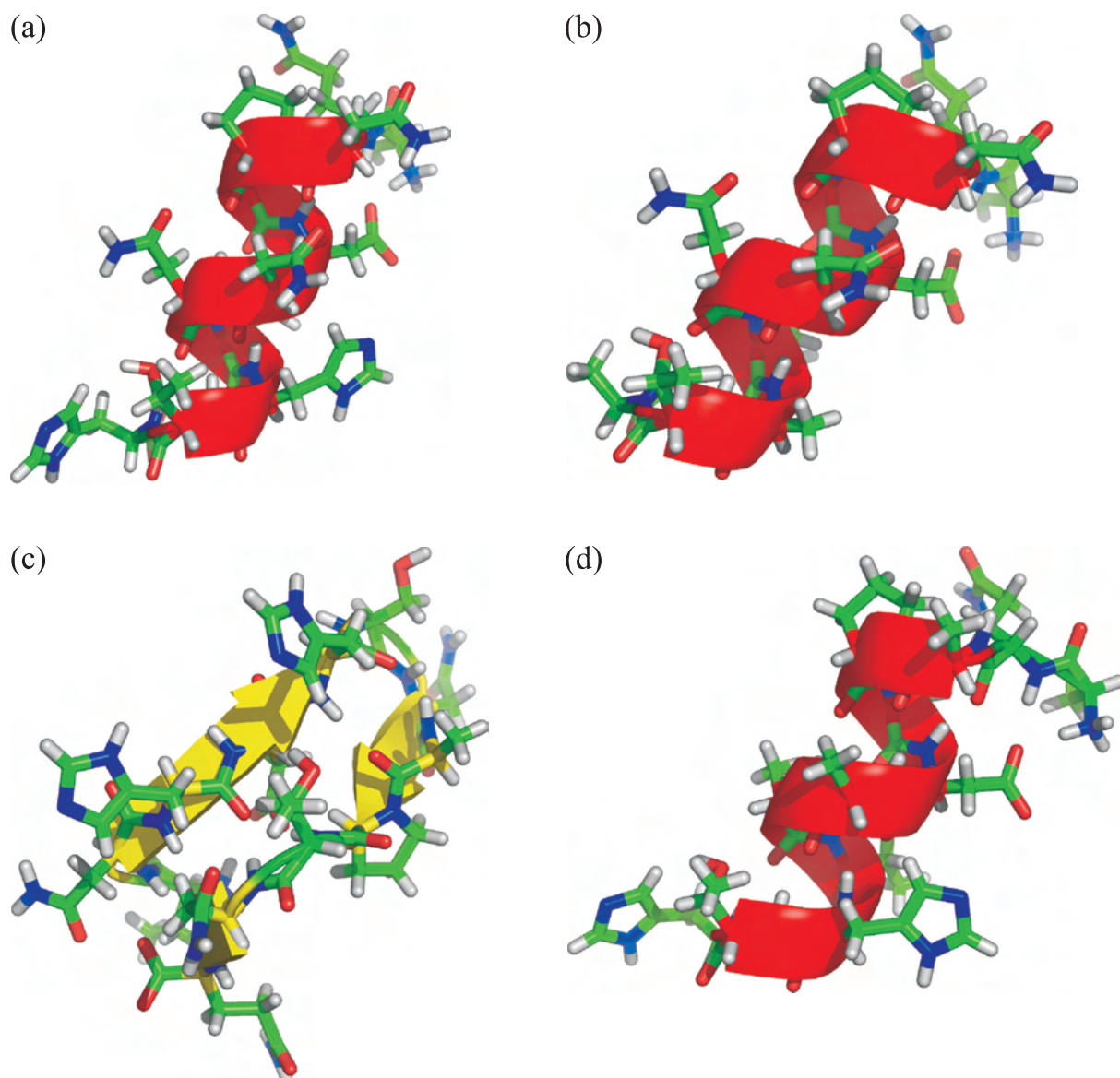
Figure 9.3: Typical low-energy conformations for the peptide sequences (**a**) AQNPSDNNTHTH, (**b**) AQNPSDNNTATA, (**c**) TNHDHSNAPTNQ, and (**d**) AQAPSDAATHTH, where (**b**) is a double His → Ala mutant of (**a**), (**c**) a random permutation of (**a**), and (**d**) a triple Asn → Ala mutant of (**a**). These structures had the lowest energy in ten simulated annealing runs for each sequence, starting from random conformations. The three sequences (**a**), (**b**), and (**d**) exhibit α helical conformations, whereas sequence (**c**) forms a β sheet.

[1] K. Goede et al.: Langmuir **22**, 8104 (2006)

[2] K. Goede et al.: *Specific Adhesion of Peptides on Semiconductor Surfaces in Experiment and Simulation*, to appear in: Proc. 28th Int. Conf. Physics of Semiconductors, Vienna, 24.–28. July 2006

[3] M. Bachmann, W. Janke: Phys. Rev. E **73**, 020 901(R) (2006)

[4] M. Bachmann, W. Janke: Phys. Rev. E **73**, 041 802 (2006)

[5] G. Gökoğlu et al.: Phys. Rev. E **74**, 041 802 (2006)

[6] S. Mitternacht et al.: J. Phys. Chem. B **111**, 4355 (2007)

[7] A. Irbäck et al.: Biophys. J. **85**, 1466 (2003)

9.11 Quantum Critical Phenomena: Dimerized Spin Systems and (Heisenberg) Spin Chains

S. Wenzel, R. Bischof, L. Bogacz[*], D. Ihle[†], W. Janke,

[*]Jagellonian University, Kraków, Poland (since October 2006)
[†]Theory of Condensed Matter group

Understanding quantum critical phenomena in low-dimensional quantum spin systems becomes ever more important since experimentalists succeed more and more in fabricating such materials in laboratories. One example are the well known cuprate-superconductors which are well described by quantum anti-ferromagnets. In our work we are thus interested in such systems which can be effectively described by a quantum Heisenberg model.

Our focus in the first subproject lies on studying the phase transitions that non-equivalent nearest neighbour couplings can trigger there. Changing the ratio J_1/J_2 of those couplings can drive the system from an ordered (Néel) state to disorder. Figure 9.4 (left) shows an example of this model class. Since analytical quantum many-body calculations pose an extreme challenge we use Quantum Monte Carlo methods to characterize the phase transition. Such methods have recently seen a surge of improvements. Among these is the so called Stochastic Series Expansion (SSE) [1, 2] which we have implemented and customized for our needs. Using this method we are able to determine the quantum critical point of the model in Fig. 9.4 by looking at quantities like the spin stiffness or correlation lengths. These quantities have (close to) universal features and curves at different system sizes meet in the quantum critical point. Taking into account finite-size corrections we can give the quantum critical point to be $J_1/J_2 = 2.521(1)$
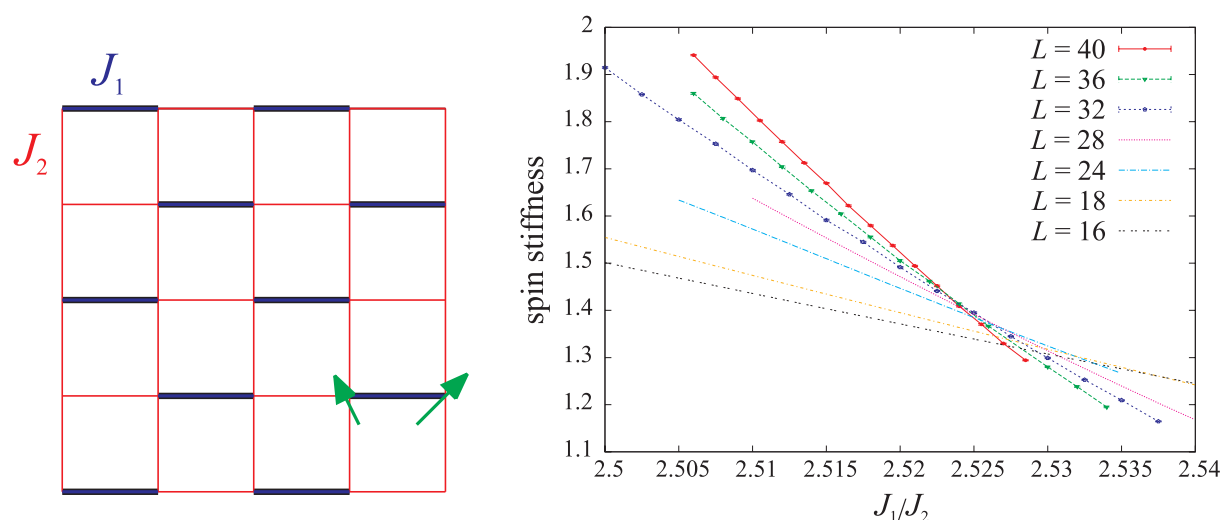
Figure 9.4: *Left:* An example for the class of models we consider here. The green quantum spins ($S = 1/2$) live on a square lattice with different nearest-neighbour couplings (*red* and *blue*). *Right:* The spin stiffness allows extraction of the quantum critical value for J_1/J_2. Note that there are large corrections which can be accounted for by finite-size scaling.

which is a considerable improvement to best previously known values. Secondly, we can show that the phase transition lies in the 3D Heisenberg universality class.

In the second subproject we have investigated quantum chains of mixed spins [3, 4]. The low temperature properties of quantum spin chains (1D Heisenberg model) depend significantly on the size of spins involved. Uniform chains of half-odd integer spins have no energy gap between ground state and first excited states (i.e. they are quantum critical), whereas chains with integer spins do show this gap [5]. However, even integer spin chains can be driven to quantum criticality by tuning the bond alternation of the coupling strength.

By means of quantum Monte Carlo simulations (continuous imaginary time loop-cluster algorithm) at low temperatures, the quantum phase transitions in antiferromagnetic Heisenberg spin chains consisting of two different kinds of spin, S_a and S_b, that appear alternatingly in pairs, have been studied for the cases $S_a = 1/2$ and $S_b = 1$, $S_a = 1/2$ and $S_b = 3/2$ as well as $S_a = 1$ and $S_b = 3/2$. In particular, the so-called twist order parameter as well as spatial and imaginary temporal correlation lengths have been measured in order to analyse quantum critical points that separate regions with qualitatively different ground states (quantum phases).

The twist order parameter showed a temperture dependent formation of a plateau, which could be directly linked to the width of the quantum critical region at non-zero temperatures. This feature will be, among certain extensions of the model, subject of future studies.

[1] A.W. Sandvik, J. Kurkijärvi: Phys. Rev. B **43**, 5950 (1991)
[2] O.F. Syljuasen, A.W. Sandvik: Phys. Rev. E **66**, 046 701 (2002)
[3] K. Takano: Phys. Rev. Lett. **82**, 5124 (1999); Phys. Rev. B **61**, 8863 (2000)
[4] Z. Xu et al.: Phys. Rev. B **67**, 214 426 (2003)
[5] F.D.M. Haldane: Phys. Rev. Lett **50**, 1153 (1983)

9.12   Interface Tension of the Square Lattice Ising Model with Next-Nearest-Neighbour Interactions

A. Nußbaumer, E. Bittner, W. Janke

In a recent letter [1], Zandvliet presented a simple derivation of an analytical expression for the interface free energy in the (10) direction of the Ising model on a square lattice with nearest- *and* next-nearest-neighbour couplings having a Hamiltonian of the form

$$\mathcal{H} = -J_x \sum_{\langle i,j \rangle} \sigma_i \sigma_j - J_y \sum_{\langle i,j \rangle} \sigma_i \sigma_j - J_d \sum_{(i,j)} \sigma_i \sigma_j \,, \tag{9.3}$$

where J_x, J_y are the nearest-neighbour couplings, J_d the next-nearest-neighbour couplings and $\sigma_i = \pm 1$ classical Ising spins. For the special case of only nearest-neighbour

interactions ($J_d = 0$) Zandvliet's expression reproduces the famous exact Onsager formula [2]

$$\sigma_0 = 2J_y + k_B T \ln \tanh \left(J_x / k_B T \right) , \tag{9.4}$$

where σ_0 is the interface free energy. By comparing the resulting transition temperatures, determined as the point where the interface tension vanishes ($\sigma_0 = 0$), with previous numerical results in the literature, support for the validity of the new analytical formula in the general case was claimed. Guided by the fact that Zandvliet's simple, but rather heuristic derivation neglects overhang configurations and bubble excitations completely, we show that his approach is equivalent to the classic solid-on-solid (SOS) approximation [3] which is known [4] to reproduce accidentally the exact interface tension along one of the two main axes in the case of only nearest-neighbour interactions [5]. In the limiting situation where only next-nearest-neighbour interactions are considered ($J_x = J_y = 0$), we prove analytically that such a coincidence no longer holds.

To assess the accuracy of Zandvliet's formula for the general model we have performed a careful computer simulation study using multicanonical Monte Carlo techniques combined with finite-size scaling analyses. Figure 9.5 shows a typical scaling plot of the maximum-to-minimum ratio of the magnetisation distribution at a temperature close to the critical temperature. The extrapolation of the fit gives an estimate of the interface tension of the infinite system ($L \to \infty$) which is clearly off the value predicted by Zandvliet.

Our results for the hitherto unknown interface tension and the transition temperatures show that the analytical formula yields fairly good approximations but, in general, is not exact.
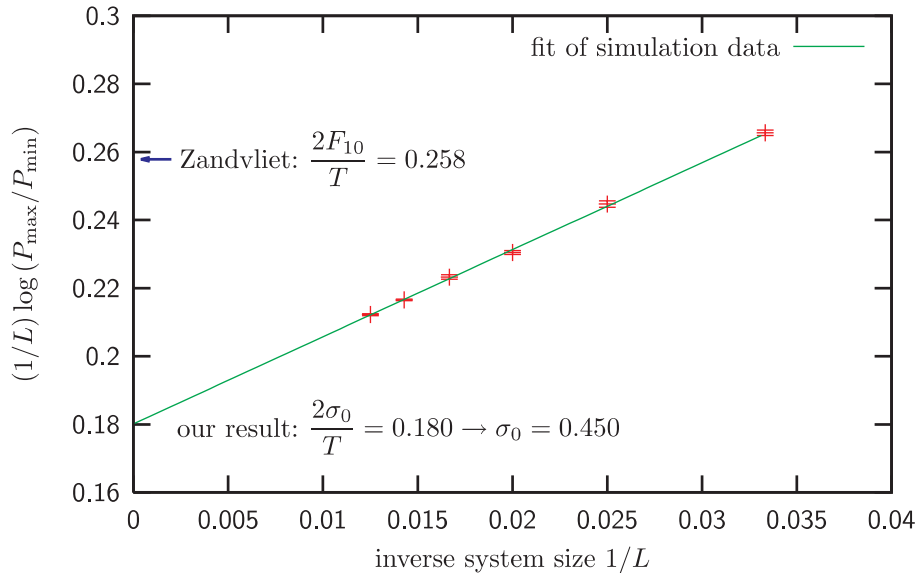
Figure 9.5: Scaling of the interface-tension estimates from the histogram method for $J_x = J_y = J_d = 1.0$, temperature $T = 5.0$ and system sizes $L = 30, 40, 50, 60, 70,$ and 80. The straight line shows the fit of the ratio $\ln(P_{max}^{(L)} / P_{min}^{(L)})$ with goodness-of-fit parameter $Q = 0.42$, yielding an interface tension estimate of $\sigma_0 = 0.4504 \pm 0.0014$. The *arrow* on the y axis points to the analytical result of Zandvliet [1].

[1] H.J.W. Zandvliet: Europhys. Lett. **73**, 747 (2006)
[2] L. Onsager: Phys. Rev. **65**, 117 (1944)
[3] W.K. Burton et al.: Phil. Trans. Roy. Soc. (London) A **243**, 299 (1951)
[4] F. Calheiros et al.: J. Phys. A **20**, 5991 (1987)
[5] A. Nußbaumer et al.: Europhys. Lett. **78**, 16 004 (2007)

9.13   Football Fever: Goal Distributions and Non-Gaussian Statistics

E. Bittner, A. Nußbaumer, W. Janke, M. Weigel[*]

[*]School of Mathematical and Computer Sciences, Heriot-Watt University, Edinburgh, UK

In recent years, the generic properties of socially interacting systems have followed economic and biological systems in exciting the interest of statistical physicists [1]. In this context, it is hoped that the experience with simplification and model building gathered from the investigation of interacting physical systems might add a new perspective to the much more detailed investigations performed in the social sciences and humanities on the same subjects.

In this context, we investigated motivation and demotivation effects occurring in ball sports such as football, reflected in the probability distributions of the total number of goals scored by a team in a single match [2, 3]. It is assumed that, considering averages over the matches played in a league season or cup, scoring is a random process where, however, the scoring probability might depend on parameters that can change in the course of a match. Previous studies [4–6] have effectively considered goals scored as statistically independent events, leading to descriptions with Poissonian, negative binomial or extremal value distributions. Although satisfactory descriptions of the score data for a number of football leagues can be obtained in this way, each of these distributions seems to describe at most a certain number of cases while failing in others. What is more, there appear to be no plausible microscopic stochastic processes explaining the occurrence of these distributions. We argue that the crucial ingredient missed in these descriptions are the *correlations* between subsequent scoring events, leading to a feedback effect where each goal motivates or enables a team to score more likely subsequently. This leads to simple feedback models involving an initial scoring probability and a motivation parameter describing the "football fever", which can be solved exactly from a Pascal type recurrence relation, and precise closed-form approximations are derived from a saddle-point calculation [3]. The corresponding increase of the average scoring probability over the course of a match has been explicitly observed previously [7].

We consider football score data from many European leagues and, in particular, the premier leagues of the East and West in the divided Germany as well as the subsequently united league, the German women's premier league, and the qualification stage of the FIFA World Cup series. We find that at least one of the considered feedback
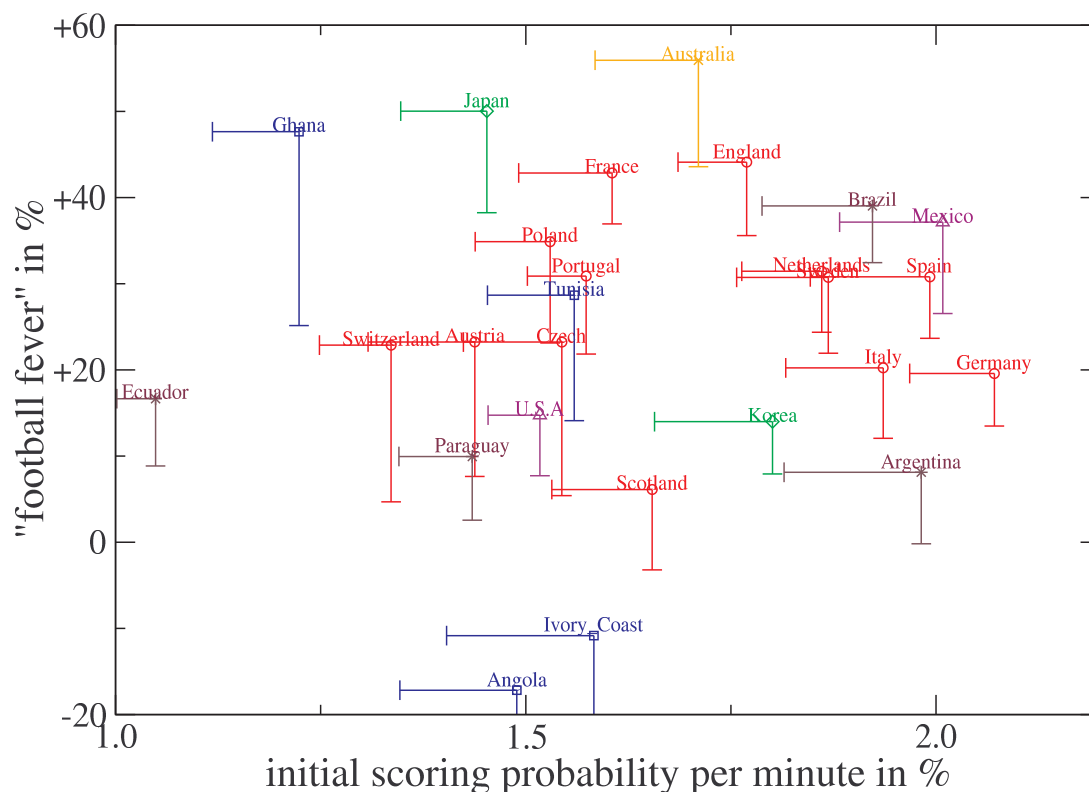
Figure 9.6: Initial scoring probability and self-affirmation parameter ("football fever") of the national teams as estimated from the past world cup qualifications.

models describes *all* of the considered data well, providing a unified description of the problem of scoring in football with a plausible model of microscopical correlations. In terms of the self-affirmation parameter of the model, we find some significant differences between the considered data sets, with the less professionalized women's and East German men's premier leagues apparently being more seriously infected with the football fever. A team-specific analysis of the world cup data allows to extract estimates for the self-affirmation parameters of the nations participating in the qualification as depicted in Fig. 9.6, to be compared with everyone's favorite prejudices about national characteristics in the football world.

[1] D. Stauffer: Physica A **336**, 1 (2004)
[2] E. Bittner et al.: *Self-affirmation model for football goal distributions*, Eur. Phys. Lett. (in print)
[3] E. Bittner et al.: arXiv:physics/0606016
[4] M.J. Moroney: *Facts from Figures*, 3rd Ed. (Penguin, London 1956)
[5] C. Reep et al.: J. Roy. Stat. Soc. A **134**, 623 (1971)
[6] J. Greenhough et al.: Physica A **316**, 615 (2002)
[7] M.J. Dixon, M.E. Robinson: Statistician **47**, 523 (1998)

9.14 Wang–Landau/Multibondic Cluster Algorithm for Simulations of Second-Order Phase Transitions

B.A. Berg[*], W. Janke

[*]Department of Physics, Florida State University, Tallahassee, USA

Equilibrium properties of statistical physics systems are often estimated by Markov chain Monte Carlo (MCMC) simulations [1]. In many cases one is interested in calculating expectation values for a range of temperatures with respect to the Gibbs canonical ensemble. It has turned out that instead of performing simulations of the canonical ensemble at distinct temperatures it is often advantageous to combine them into one simulation of a "generalized" ensemble [2–5]; for reviews see [6–8].

While the power of generalized ensembles is well documented for first-order phase transitions and complex systems such as spin glasses and peptides (small proteins), this is not the case for second-order phase transitions. In the latter case the critical energy range of interest is often larger than the energy range covered by a canonical Monte Carlo simulation close to the critical temperature. Such an extended energy range can, in principle, be covered by performing a Wang–Landau recursion [5] for the spectral density followed by a multicanonical simulation [3] with fixed weights. However, in the conventional approach one loses the advantage of cluster algorithms [9], which can reduce critical slowing down dramatically. The goal of this project was therefore to develop a cluster version of the Wang–Landau recursion and to combine it with a subsequent multibondic simulation [10]. Our present implementation of this idea improves for 2D and 3D Ising models the efficiency of the conventional Wang–Landau/multicanonical approach by power laws in the lattice size [11]. In our simulations real gains in CPU time reach two orders of magnitude.

[1] J. Gubernatis (Ed.): *The Monte Carlo Method in Physical Sciences*, AIP Conf. Proc., Vol. 690 (AIP, Melville 2003)
[2] G.M. Torrie, J.P. Valleau: J. Comp. Phys. **23**, 187 (1977)
[3] B.A. Berg, T. Neuhaus: Phys. Rev. Lett. **68**, 9 (1992)
[4] A.P. Lyubartsev et al.: J. Chem. Phys. **96**, 1776 (1992); E. Marinari, G. Parisi: Europhys. Lett. **19**, 451 (1992)
[5] F. Wang, D.P. Landau: Phys. Rev. Lett. **86**, 2050 (2001)
[6] U.H. Hansmann, Y. Okamoto: Ann. Rev. Comp. Phys. **6**, 120 (1999)
[7] B.A. Berg: *Markov Chain Monte Carlo Simulations and Their Statistical Analysis* (World Scientific, Singapore 2004)
[8] W. Janke: in *Computer Simulations of Surfaces and Interfaces*, NATO Science Series, II. Mathematics, Physics and Chemistry – Vol. **114**, ed. by B. Dünweg et al. (Kluwer, Dordrecht 2003) p 137
[9] R.H. Swendsen, J.-S. Wang: Phys. Rev. Lett. **58**, 86 (1987); U. Wolff: Phys. Rev. Lett. **62**, 361 (1989)
[10] W. Janke, S. Kappler: Phys. Rev. Lett. **74**, 212 (1995); M.S. Carroll, W. Janke, S. Kappler: J. Stat. Phys. **90**, 1277 (1998)
[11] B.A. Berg, W. Janke: Phys. Rev. Lett. **98**, 040 602 (2007)

9.15   Scaling Relations for Logarithmic Corrections at Second-Order Phase Transitions

R. Kenna[*], D.A. Johnston[†], W. Janke

[*]School of Mathematical and Information Sciences, Coventry University, UK
[†]School of Mathematical and Computer Sciences, Heriot-Watt University, Edinburgh, UK

The conventional leading scaling behaviour at a second-order phase transition are power-laws in the reduced temperature $t = 1 - T/T_c$ and field h. With $h = 0$, the correlation length, specific heat and susceptibility behave as $\xi_\infty(t) \sim |t|^{-\nu}$, $C_\infty(t) \sim |t|^{-\alpha}$ and $\chi_\infty(t) \sim |t|^{-\gamma}$, while the magnetization in the broken phase has $m_\infty(t) \sim |t|^\beta$. Here the subscript indicates the assumed infinite extent of the system. At $t = 0$ the magnetization scales as $m_\infty(h) \sim h^{1/\delta}$ while the anomalous dimension η characterizes the correlation function at criticality. In the 1960's, it was shown that these six critical exponents are related via four scaling relations, which are now firmly established and fundamentally important in the theory of critical phenomena [1].

Multiplicative logarithmic corrections to scaling are frequently encountered in the critical behaviour of certain statistical-mechanical systems, e.g., at their upper critical dimension d_u from which on mean-field behaviour (which is independent of d) prevails [2]. In our work [3], a Lee–Yang zero approach is used to systematically analyse the exponents of such logarithms and to propose new scaling relations between them.

In a second step [4], by considering also Fisher zeros, the theory has been extended to account for circumstances which often occur when the leading specific-heat critical exponent vanishes such as, e.g., for the two-dimensional Ising model. Furthermore the theory could be widened to encompass also the correlation function.

These proposed scaling relations among the exponents of logarithmic corrections were then successfully confronted with a variety of results from the literature and some new predictions for logarithmic corrections in certain models could be made which are still subject to numerical or experimental verification.

[1] M.E. Fisher: Rev. Mod. Phys. **70**, 653 (1998); D.A. Lavis, G.M. Bell: *Statistical Mechanics of Lattice Systems 2* (Springer, Berlin 1999)
[2] F.J. Wegner: in *Phase Transitions and Critical Phenomena VI*, ed. by C. Domb, M.S. Green (Academic Press, London 1976) p 8
[3] R. Kenna et al.: Phys. Rev. Lett. **96**, 115 701 (2006)
[4] R. Kenna et al.: Phys. Rev. Lett. **97**, 155 702 (2006)

9.16   Funding

9.17 Organizational Duties

E. Bittner

- Scientific Secretary of the Workshop *CompPhys06 – 7. NTZ-Workshop on Computational Physics*, ITP, Universität Leipzig, 30. November – 02. December 2006

W. Janke

- Director of the Naturwissenschaftlich-Theoretisches Zentrum (NTZ) at the Zentrum für Höhere Studien (ZHS), Universität Leipzig
- Chairperson of the Programme Committee "Scientific Computing" of Forschungszentrum Jülich
- Member of the Scientific-Technical-Council of the Supervisory Board ("Aufsichtsrat") of the Forschungszentrum Jülich GmbH
- Editor: "Computational Physics", Central European Journal of Physics
- Member of Editorial Board: Cond. Matter Phys.
- Permanent Member of "International Advisory Board" of the *Conference of the Middle European Cooperation in Statistical Physics (MECO)*
- Member of the "Advisory Committee" of the International Workshop *COVLAT06 – 16. Workshop on Lattice Field Theory*, Coventry, England, UK, 29. June – 01. July 2006
- Member of the "Local Organizing Committee" of the International Conference *MG11 – 11th Marcel Grossmann Meeting*, FU Berlin, 23. – 29. July 2006
- Member of the "International Program Committee" of the International Conference *Mathematical Modeling and Computational Physics 2006*, High Tatra Mountains, Slovakia, 28. August – 01. September 2006
- Organizer of the Workshop *CompPhys06 – 7. NTZ-Workshop on Computational Physics*, ITP, Universität Leipzig, 30. November – 02. December 2006
- Organizer of the Symposium *Finite-Size Effects at Phase Transitions* within the German Physics Spring Meeting ("Physiker-Tagung") 2007, Universität Regensburg, 27. – 28. March 2007 (with Prof. Dr. Walter Selke, RWTH Aachen)
- Organizer of the 9th International Conference *Path Integrals – New Trends and Perspectives*, Max Planck-Institut für Physik komplexer Systeme (MPI-PKS), Dresden, 23. – 28. September 2007 (with PD Dr. Axel Pelster, Universität Duisburg-Essen)
- Organizer of the Workshop *Statistical Mechanics of Complex Networks*, Jagellonian University, Krakow, Poland, 11. – 13. October 2007 (with Prof. Dr. Zdzisław Burda, Jagellonian University, Krakow, Poland)
- Editor of *Rugged Free Energy Landscapes: Common Computational Approaches in Spin Glasses, Structural Glasses and Biological Macromolecules*, Proceedings of CECAM Workshop, to appear in Lecture Notes in Physics (Springer, Berlin 2007) (in print)
- External Reviewer: Humboldt-Stiftung; Studienstiftung des deutschen Volkes; "Jeffress Memorial Trust", Bank of America, Virginia, USA; "Fond zur Förderung der wissenschaftlichen Forschung (FWF)", Österreich; "The Royal Society", UK; "Engineering and Physical Sciences Research Council (EPSRC)", UK; The University of Warwick, UK; Coventry University, UK; CECAM, Lyon, France
- Referee: Phys. Rev. Lett., Phys. Rev. B, Phys. Rev. E, J. Chem. Phys., Europhys. Lett.,

Phys. Lett. A, Phys. Lett. B, Eur. Phys. J. B, Physica A, Proc. Royal Phys. Soc., J. Phys. A, Comp. Phys. Comm., J. Stat. Mech.-Theory E., New J. Phys., Int. J. Mod. Phys. C

9.18 External Cooperations

Academic

- EU RTN-Network "ENRAGE" – *Random Geometry and Random Matrices: From Quantum Gravity to Econophysics*
  research collaboration with 13 teams throughout Europe

- Department of Physics, Florida State University, Tallahassee, USA
  Prof. Dr. Bernd A. Berg

- CEA/Saclay, Service de Physique Théorique, France
  Dr. Alain Billoire

- Laboratoire de Physique des Matériaux (UMR CNRS No 7556), Université Henri Poincaré, Nancy, France
  Prof. Dr. Bertrand Berche, Dr. Christophe Chatelain

- Groupe de Physique des Matériaux (UMR CNRS No 6634), Université de Rouen, France
  Dr. Pierre-Emmanuel Berche

- School of Mathematical and Computer Sciences, Heriot-Watt University, Edinburgh, UK
  Prof. Dr. Desmond A. Johnston, Dr. Martin Weigel

- School of Mathematical and Information Sciences, Coventry University, UK
  Dr. Ralph Kenna

- Department of Physics, Hacettepe University, Ankara, Turkey
  Prof. Dr. Tarik Çelik, Dr. Handan Arkin, Gökhan Gökoğlu

- Institute for Condensed Matter Physics, National Academy of Sciences, Lviv, Ukraine
  Prof. Dr. Yurij Holovatch

- Complex Systems Division, Department of Theoretical Physics, Lund University, Sweden
  Prof. Dr. Anders Irbäck, Simon Mitternacht

- NIC, Forschungszentrum Jülich
  Prof. Dr. Ulrich Hansmann, Prof. Dr. Peter Grassberger, PD Dr. Thomas Neuhaus

- Institut für Physik, Universität Mainz
  Prof. Dr. Kurt Binder, Dr. Hsiao-Ping Hsu

- Atominstitut, TU Wien, Austria
  Prof. Dr. Harald Markum, Dr. Rainer Pullirsch

- Brunel University of West London, UK
  Dr. Gernot Akemann

- Institut für Theoretische Physik, FU Berlin
  Prof. Dr. Hagen Kleinert, Dr. Adriaan M.J. Schakel

- IAC-1, Universität Stuttgart
  PD Dr. Rudolf Hilfer

- Institut für Theoretische Physik, Universität Bielefeld
  PD Dr. Thomas Neuhaus

- Institute of Physics, Jagellonian University, Kraków, Poland
  Prof. Dr. Zdzisław Burda

- Landau Institute for Theoretical Physics, Chernogolovka, Russia
  Prof. Dr. Lev N. Shchur

- Yerevan Physics Institute, Yerevan, Armenia
  Prof. Dr. David B. Saakian

- University of Sri Jayewardenepura, Sri Lanka
  Dr. Ranasinghe P.K.C. Malmini

- Department of Physics, Sri Venkateswara College, University of Delhi, New Delhi, India
  Dr. Bibudhananda Biswal

- Department of Mechanical Engineering and Intelligent Systems, Tokyo University of Electro-communications, Chofu, Tokyo, Japan
  Prof. Dr. Hans-Georg Mattutis

- Zhejiang Institute of Modern Physics, Zhejiang University, Hangzhou, PR China
  Prof. Dr. He-Ping Ying, Prof. Dr. Bo Zheng

9.19   Publications

Journals

M. Bachmann, W. Janke: *Substrate Adhesion of a Nongrafted Polymer in a Cavity*, Phys. Rev. E **73**, 041 802 (2006)

M. Bachmann, W. Janke: *Substrate Specificity of Peptide Adsorption: A Model Study*, Phys. Rev. E **73**, 020 901(R) (2006)

B.A. Berg, W. Janke: *Wang–Landau Multibondic Cluster Simulations for Second-Order Phase Transitions*, Phys. Rev. Lett. **98**, 040 602 (2007)

E. Bittner, W. Janke: *Free-Energy Barriers in the Sherrington-Kirkpatrick Model*, Europhys. Lett. **74**, 195 (2006)

G. Gökoğlu, M. Bachmann, T. Çelik, W. Janke: *Structural Properties of Small Semiconductor-Binding Synthetic Peptides*, Phys. Rev. E **74**, 041 802 (2006)

M. Hellmund, W. Janke: *High-Temperature Series Expansions for the q-State Potts Model on a Hypercubic Lattice and Critical Properties of Percolation*, Phys. Rev. E **74**, 051 113 (2006)

M. Hellmund, W. Janke: *High-Temperature Series for the Bond-Diluted Ising Model in 3, 4 and 5 Dimensions*, Phys. Rev. B **74**, 144 201 (2006)

W. Janke: *Der Faktor Zeit – Theoretische Physiker interessieren sich für alternde Materialien*, Universität Leipzig Journal **4/2006**, 25 (2006)

W. Janke, D.A. Johnston, R. Kenna: *Properties of Higher-Order Phase Transitions*, Nucl. Phys. B **736**, 319 (2006)

W. Janke, D.A. Johnston, M. Weigel: *Two-Dimensional Quantum Gravity – A Laboratory for Fluctuating Graphs and Quenched Connectivity Disorder*, Cond. Matter Phys. **9**, 263 (2006)

W. Janke, A.M.J. Schakel: *Two-Dimensional Critical Potts and its Tricritical Shadow*, Braz. J. Phys. **36**, 708 (2006)

W. Janke, M. Weigel: *Geometric and Stochastic Clusters of Gravitating Potts Models*, Phys. Lett. B **639**, 373 (2006)

C. Junghans, M. Bachmann, W. Janke: *Microcanonical Analyses of Peptide Aggregation Processes*, Phys. Rev. Lett. **97**, 218 103 (2006)

R. Kenna, D.A. Johnston, W. Janke: *Scaling Relations for Logarithmic Corrections*, Phys. Rev. Lett. **96**, 115 701 (2006)

R. Kenna, D.A. Johnston, W. Janke: *Self-Consistent Scaling Theory for Logarithmic Correction Exponents*, Phys. Rev. Lett. **97**, 155 702 (2006)

E. Lorenz, W. Janke: *Numerical Tests of Local Scale Invariance in Ageing q-State Potts Models*, Europhys. Lett. **77**, 10 003 (2007)

S. Mitternacht, S. Schnabel, M. Bachmann, W. Janke, A. Irbäck: *Differences in Solution Behavior Between Four Semiconductor-Binding Peptides*, J. Phys. Chem. B **111**, 4355 (2007)

A. Nußbaumer, E. Bittner, W. Janke: *Interface Tension of the Square Lattice Ising Model with Next-Nearest-Neighbour Interactions*, Europhys. Lett. **78**, 16 004 (2007)

A. Nußbaumer, E. Bittner, T. Neuhaus, W. Janke: *Monte Carlo Study of the Evaporation/Condensation Transition of Ising Droplets*, Europhys. Lett. **75**, 716 (2006)

S. Schnabel, M. Bachmann, W. Janke: *Identification of Characteristic Protein Folding Channels in a Coarse-Grained Hydrophobic-Polar Peptide Model*, J. Chem. Phys. **126**, 105 102 (2007)

S. Schnabel, M. Bachmann, W. Janke: *Two-State Folding, Folding Through Intermediates, and Metastability in a Minimalistic Hydrophobic-Polar Model for Proteins*, Phys. Rev. Lett. **98**, 048 103 (2007)

Books

M. Bachmann, W. Janke: *Adsorption Phenomena at Organic-Inorganic Interfaces*, in: *From Computational Biophysics to Systems Biology 2006*, Proc. NIC Workshop, Jülich, 06. – 09. June 2006, ed. by U.H.E. Hansmann, J. Meinke, S. Mohanty, O. Zimmermann, NIC Series, Vol. **34** (John von Neumann Institute for Computing, Jülich 2006) p 95

M. Bachmann, W. Janke: *Chain-Growth Simulations of Lattice-Peptide Adsorption to Attractive Substrates*, in: *NIC Symposium 2006 Proceedings*, ed. by G. Münster, D. Wolf, M. Kremer, NIC Series, Vol. **32**, (John von Neumann Institute for Computing, Jülich 2006) p 245

M. Bachmann, W. Janke: *Reduction to the Simplest – The Complexity of Minimalistic Heteropolymer Models*, in: *From Computational Biophysics to Systems Biology 2006*, Proc. NIC Workshop, Jülich, 06.–09. June 2006, ed. by U.H.E. Hansmann, J. Meinke, S. Mohanty, O. Zimmermann, NIC Series, Vol. **34** (John von Neumann Institute for Computing, Jülich 2006) p 59

W. Janke: *Introduction to Simulation Techniques* in: *Ageing and the Glass Transition*, ed. by M. Henkel, M. Pleimling, R. Sanctuary, Lecture Notes in Physics **716** (Springer, Berlin 2007) p 207

W. Janke (Ed.): *Rugged Free Energy Landscapes: Common Computational Approaches in Spin Glasses, Structural Glasses and Biological Macromolecules*, Lecture Notes in Physics (Springer, Berlin 2007) in press

W. Janke, E. Bittner: *Phase Transitions in a Generalized $|\psi|^4$ Model*, in: *Proc. 8th Int. Conf. Path Integrals from Quantum Information to Cosmology*, Prague, Czech Republic, 06.–10. June 2005, ed. by Č. Burdik, O. Navrátil, S. Pošta (JINR Press, Dubna 2006) p 1 [electronically available at www.jinr.ru/publish/Proceedings/Burdik-2005/index.html]

in press

M. Bachmann, W. Janke: *Minimalistic Hybrid Models for the Adsorption of Polymers and Peptides to Substrates*, Proc. Conf. Mathematical Modeling and Computational Physics 2006, High Tatra Mountains, Slovakia, 28. August–1. September, 2006

M. Bachmann, W. Janke: *Thermodynamics of Protein Folding from Coarse-Grained Models' Perspectives*, in: *Rugged Free Energy Landscapes: Common Computational Approaches in Spin Glasses, Structural Glasses and Biological Macromolecules*, ed. by W. Janke, Lecture Notes in Physics (Springer, Berlin 2007)

E. Bittner, A. Nußbaumer, W. Janke, M. Weigel: *Self-Affirmation Model for Football Goal Distributions*, Europhys. Lett.

L. Bogacz, Z. Burda, W. Janke, B. Wacław: *Balls-in-Boxes Condensation on Networks*, Chaos

K. Goede, M. Bachmann, W. Janke, M. Grundmann: *Specific Adhesion of Peptides on Semiconductor Surfaces in Experiment and Simulation*, Proc. 28th Int. Conf. Physics of Semiconductors (ICPS-28)

W. Janke, A.M.J. Schakel: *Spacetime Approach to Phase Transitions*, in: *Order, Disorder and Criticality: Advanced Problems of Phase Transition Theory*, Vol. 2, ed. by Y. Holovatch (World Scientific, Singapore 2007)

Talks

M. Bachmann: *Adsorption Phenomena at Hybrid Organic-Inorganic Interfaces*, Workshop *Statistical Physics and Low-Dimensional Systems*, Nancy, France, 17. – 19. May

M. Bachmann: *Adsorption Phenomena at Hybrid Organic-Inorganic Interfaces*, Workshop *Self-Assembly of Complex Nanostructures*, Leipzig, 25. – 26. September

M. Bachmann: *Complex Conformational-Phase Diagrams of Simple Hybrid Polymer–Substrate Models*, Workshop *Recognition and Adsorption Processes of Biomolecules*, Bielefeld, 06. – 07. March

M. Bachmann: *Complex Conformational-Phase Diagrams of Simple Hybrid Polymer–Substrate Models*, 31th Conf. of the Middle European Cooperation in Statistical Physics MECO31, Primošten, Croatia, 23. – 26. April

M. Bachmann: *Folding and Aggregation of Protein-Like Heteropolymers at Mesoscopic Scales*, Seminar talk, Computational Biology & Biological Physics Group, Lunds Universitet, Lund, Sweden, 30. October

M. Bachmann: *Mesoscopic Modeling of Protein Folding and Aggregation*, 7th NTZ Workshop Computational Physics, Leipzig, 30. November – 02. December

M. Bachmann: *Minimalistic Hybrid Models for the Adsorption of Polymers and Peptides to Solid Substrates*, Conf. Mathematical Modeling and Computational Physics (MMCP 2006), High Tatra Mountains, Štrba (Slovakia), 28. August – 01. September

M. Bachmann: *Minimalistic Models for Polymer and Peptide Adhesion to Solid Substrates*, Seminar talk, Institut für Physik, Johannes Gutenberg-Universität Mainz, 17. January

M. Bachmann: *Molekulare Strukturbildung bei Faltungs-, Aggregations- und Adsorptionsprozessen von weicher Materie*, Colloquium talk, Universität Dortmund, 18. December

M. Bachmann: *Polymer and Peptide Adsorption to Attractive Substrates*, Spring Meeting of the German Physical Society, Dresden, 27. – 31. March

M. Bachmann: *Proteinfaltung – Interdisziplinäre Herausforderung für die Physik*, Colloquium talk, Technische Universität Ilmenau, 18. April

M. Bachmann: *Reduction to the Simplest – The Complexity of Minimal Heteropolymer Models*, Workshop "From Computational Biophysics to Systems Biology", Jülich, 06. – 09. June

E. Bittner: *Droplet Condensation/Evaporation Transition*, *Workshop on Computational Physics* CompPhys06, Leipzig, 30. November – 02. December

E. Bittner: *Free-Energy Barriers in a Mean-Field Spin*, Spring Meeting of the German Physical Society, Dresden, 27. – 31. March

E. Bittner: *Free-Energy Barriers in the Sherrington-Kirkpatrick Model*, Les Houches Meeting 2006, Les Houches, France, 20. – 24. February

E. Bittner: *Football Fever: Goal Distributions and Non-Gaussian Statistics*, invited talk, *16. Workshop on Lattice Field Theory and Statistical Physics* COVLAT06, Coventry, UK, 29. June – 01. July

E. Bittner: *On the Overlap Probability Distribution in the Sherrington-Kirkpatrick Model*, ENRAGE Network Conf., Edinburgh, 03. – 07. April

E. Bittner: *The Evaporation/Condensation Transition of Ising Droplets*, invited talk, Workshop *Statistical Physics and Low-Dimensional Systems*, Nancy, France, 17. – 19. May

L. Bogacz, Z. Burda, W. Janke, B. Wacław: *A Program Generating Homogeneous Random Graphs with Given Weights*, Spring Meeting of the German Physical Society, Dresden, 27. – 31. March

W. Janke: *Adsorption Phenomena at Hybrid Organic-Inorganic Interfaces*, NIC Workshop CBSB06, Jülich, 06. – 09. June

W. Janke: *Adsorption Phenomena at Hybrid Organic-Inorganic Interfaces*, invited talk, Sitzung des Wissenschaftlichen Rates des NIC, DESY Zeuthen, 21. June

W. Janke: *Adsorption Phenomena at Hybrid Organic-Inorganic Interfaces*, invited talk, 16. Workshop on Lattice Field Theory and Statistical Physics – COVLAT06, Coventry University, UK 29. June – 01. July

W. Janke: *Diluted Magnets – Simulations vs Series Expansions*, invited talk, 3rd Int. Workshop Hangzhou 2006 on *Simulational Physics*, Zhejiang University, Hangzhou, China, 16. – 18. November

W. Janke: *First-Order Phase Transitions*, two invited lectures, Block Course on *Phase Transitions in Statistical Physics and Field Theory* of the Int. Graduate School *Quantum Fields and Strongly Interacting Matter*, Universität Bielefeld, 04. – 09. October

W. Janke: *Fortuin-Kasteleyn Versus Geometrical Clusters*, joint DPG-und ESF-Frühjahrstagung, TU Dresden, 27. – 31. March

W. Janke: *Fortuin-Kasteleyn Versus Geometrical Clusters – Fractal Dimensions and Critical Exponents*, invited talk, Workshop Programme *Stochastic Geometry and Field Theory: From Growth Phenomena to Disordered Systems*, Kavli Institute for Theoretical Physics, University of California Santa Barbara, USA, 06. September

W. Janke: *Geometrical Description of Critical Behaviour*, Seminar zur Theorie der kondensierten Materie, Institut für Theoretische Physik, RWTH Aachen, 31. January

W. Janke: *Geometrical Picture of Phase Transitions*, 31th Conf. Middle European Cooperation in Statistical Physics MECO31, Primošten, Croatia, 23. – 26. April

W. Janke: *Geometrical Picture of Phase Transitions*, invited talk, Atelier Nancy *Statistical Physics and Low Dimensional Systems*, Nancy, France, 17. – 19. May

W. Janke: *Monte Carlo Methods in Classical Statistical Physics*, two invited lectures, Heraeus Summerschool *Computational Many Particle Physics*, Universität Greifswald, 18. – 29. September

W. Janke: *Multi-Scale Modelling and Simulation of Protein Folding*, PAP$_3$A Workshop, Schloß Oppurg, 13. – 14. January

W. Janke: *Picturing Phase Transitions Geometrically*, ENRAGE Network Conf., Edinburgh, UK, 03. – 07. April

W. Janke: *Quenched Connectivity Disorder: Spin Models on Random Lattices and Graphs*, invited talk, Int. Workshop *The World a Jigsaw: Tessellations in the Sciences*, Lorentz Center, Leiden University, The Netherlands, 06. – 10. March

A. Nußbaumer: *Football Fever: goal distributions and non-Gaussian statistics*, CompPhys06 *Workshop on Computational Physics*, Leipzig, 30. November – 02. December

A. Nußbaumer: *Numerical Results for the 3D Edwards-Anderson-Ising Model*, Spring Meeting of the German Physical Society, Dresden, 27. – 31. March

T. Vogel, M. Bachmann, W. Janke: *Polymer Chain Growth on Lattice*, Department of Theoretical Physics, Lund University, Sweden, 06. February

Posters

E. Bittner, W. Janke: *Tails of the Sherrington-Kirkpatrick Model*, 31th Conf. Middle European Cooperation in Statistical Physics MECO31, Primošten, Croatia, 23. – 26. April

K. Goede, M. Bachmann, W. Janke, M. Grundmann: *Specific Adhesion of Peptides on Semiconductor Surfaces in Experiment and Simulation*, 28th Conf. Physics of Semiconductors, Vienna, Austria, 24. – 28. July

G. Gökoğlu, M. Bachmann, C. Çelik, W. Janke: *Conformational Properties of Semiconductor–Binding Synthetic Peptides*, Spring Meeting of the German Physical Society, Dresden, 27. – 31. March

M. Hellmund, W. Janke: *Series Expansions for Percolation and Bond-Diluted Ising Models on Z^D*, Spring Meeting of the German Physical Society, Dresden, 27. – 31. March

C. Junghans, M. Bachmann, W. Janke: *Microcanonical analysis of polymer aggregation*, CompPhys06 *Workshop on Computational Physics*, Leipzig, 30. November – 02. December

C. Junghans, U.H.E. Hansmann: *Cross-Check Methods in Protein Simulations*, From Computational Biophysics to Systems Biology 2006, FZ Jülich, 06. – 09. June

C. Junghans, U.H.E. Hansmann: *Modern Methods in Protein Simulations*, Spring Meeting of the German Physical Society, Dresden, 27. – 31. March

A. Kallias, W. Janke, M. Bachmann: *Thermodynamics and Folding Kinetics of Coarse-Grained Protein Models*, Spring Meeting of the German Physical Society, Dresden, 27. – 31. March

E. Lorenz, W. Janke: *Phase-Ordering and Ageing Phenomena in q-State Potts Models with q = 3 and 8*, Spring Meeting of the German Physical Society, Dresden, 27.–31. March

S. Mitternacht, S. Schnabel, A. Irbäck, M. Bachmann, W. Janke: *Solution Behavior of Semiconductor-Binding Peptides*, CompPhys06 *Workshop on Computational Physics*, Leipzig, 30. November–02. December

J. Schluttig, M. Bachmann, W. Janke: *Comparing Thermodynamics of the AB Protein Model in Monte Carlo and Molecular Dynamics Simulations*, Spring Meeting of the German Physical Society, Dresden, 27.–31. March

S. Schnabel, M. Bachmann, W. Janke: *Folding Channels for Coarse-Grained Heteropolymer Models*, Spring Meeting of the German Physical Society, Dresden, 27.–31. March

T. Vogel, M. Bachmann, W. Janke: *Application of New Chain Growth Algorithms for Lattice Polymers*, Spring Meeting of the German Physical Society, Dresden, 27.–31. March

T. Vogel, M. Bachmann, W. Janke: *Collapse and Freezing Transitions of Polymers on Regular Lattices*, CompPhys06 *Workshop on Computational Physics*, Leipzig, 30. November– 02. December

S. Wenzel, L. Bogacz, W. Janke: *Quantum Monte Carlo Simulations of Dimerized Heisenberg Models*, Spring Meeting of the German Physical Society, Dresden, 27.–31. March

S. Wenzel, L. Bogacz, W. Janke: *Quantum Monte Carlo Simulations of Dimerized Heisenberg Models*, 31th Conf. Middle European Cooperation in Statisitical Physics MECO31, Primošten, Croatia, 23.–26. April

S. Wenzel, A.M.J. Schakel, W. Janke: *Percolation of Vortex Networks in the U(1) Lattice Higgs Model*, 3rd Int. Workshop on Simulational Physics, Hangzhou, China, 16.–18. November

S. Wenzel, A.M.J. Schakel, W. Janke: *Percolation of Vortex Networks in the U(1) Lattice Higgs Model*, CompPhys06 *Workshop on Computational Physics*, Leipzig, 30. November– 02. December

9.20   Graduations

Diploma

- Thomas Haase
  2D/3D Crossover beim Isingmodell – Optimierung des Spin-1 Modells
  October 2006

- Christoph Junghans
  Aggregation of Mesoscopic Protein-Like Heteropolymers
  October 2006

9.21 Guests

- PD Dr. Thomas Neuhaus
  NIC Jülich
  NTZ-Kolloquium/TKM-Seminar, 11. April 2006: *Global Radius of Curvature and its Applications in Polymer Physics*, 11.–12. April 2006

- Dr. Thorsten Pöschel
  Charité Berlin
  NTZ-Kolloquium, 11. May 2006: *Instabilities in Driven Granular Gases*, 11.–12. May 2006

- Dr. Tommaso Roscilde
  MPI für Quantenoptik, Garching
  NTZ-Kolloquium, 22. May 2006: *Exploring New Quantum Phases of Correlated Matter via Lattice Disorder: The Route of Quantum Spin Systems*, 22.–23. May 2006

- Dr. Alain Billoire
  DSM/SphT CE Saclay, Gif-sur-Yvette, France
  NTZ-Kolloqium, 22. June 2006: *Finite-Size Effects in the Sherrington-Kirkpatrick Model*, 22.–23. June 2006

- Prof. Dr. Lawrence S. Schulman
  Clarkson University, Potsdam, USA
  NTZ/Department-Kolloquium, 27. June 2006: *Imaging Dynamics: Phase transitions, Clusters, and Geometry*, 27.–28. June 2006

- Prof. Dr. Karl Heinz Hoffmann
  TU Chemnitz
  NTZ-Kolloquium, 06. July 2006: *Dynamics on Energy Landscapes*, 06.–07. July 2006

- Prof. Dr. Friederike Schmid
  Universität Bielefeld
  NTZ/Department-Kolloquium, 18. July 2006: *Statistical Physics of Molecular Recognition: Some Insights from Simple Model Systems*, 18.–19. July 2006

- Prof. Dr. Frank Steiner
  Universität Ulm
  NTZ-Kolloquium, 09. November 2006: *Die kosmische Mikrowellenhintergrundstrahlung als Fenster zum frühen Universum*, 09.–10. November 2006

- Prof. Dr. Volker Dohm
  RWTH Aachen
  NTZ/Department-Kolloquium, 30. November 2006: *Universality and Diversity of Critical Phenomena*, 29. November–01. December 2006

10

Molecular Dynamics / Computer Simulation

10.1   Introduction

Using methods of statistical physics and computer simulations we investigate classical many-particle systems interacting with interfaces. One aim of the research in our group is to built up a bridge between theoretical and experimental physics. By means of analytical theories of statistical physics and computer simulations (Molecular dynamics, Monte Carlo procedures, percolation theories) using modern workstations and supercomputers we examine subjects for which high interest exists in basic research and industry as well. The examinations involve transport properties (diffusion of guest molecules) in zeolites and the structural and phase behaviour of complex fluids on bulk conditions and in molecular confinements. Especially we are interested to understand

- the diffusion behaviour of guest molecules in zeolites in dependence on thermodynamic parameters, steric conditions, intermolecular potentials and the concentration of the guest molecules,
- structure and phase equilibria of complex (aqueous) fluids in interfacial systems (e.g. pores, thin films, model membranes) in dependence on geometric and thermodynamic conditions,
- and the migration of molecules in (random) porous media by the use of percolation theories.

in microscopic detail and to compare the results with experimental data. The use of a network of PC's and workstations (Unix, Linux, Windows), the preparation and application of programs (Fortran, C, C^{++}), and the interesting objects (zeolites, membranes) give excellent possibilities for future careers of undergraduates, graduate students and postdocs. Our research is part of several national and international programs (DFG - Schwerpunktprogramm 1155, an International Research Graduate Training program (IRTG 1056), a joint research project DFG/TRF-Thailand, a joint research project DAAD/TRF-Thailand and joint research projects with UOIT Oshawa and SHARCNET, Canada) and includes a close collaboration with the Institute of Experimental Physics I (Physics of Interfaces and Biomembranes) of Leipzig University and many institutions in Germany and other countries. Details are given in the list of external cooperations.

Horst-Ludger Vörtler and Siegfried Fritzsche

10.2 Chemical Potentials and Phase Equilibria in Bulk Fluids and Thin Fluid Films

H.L. Vörtler, I. Nezbeda[*], W.R. Smith[†]

[*]Czech. Acad. Sci., Prague
[†]University of Ontario Institute of Technology, Oshawa, Canada

In this long-term project we investigate thermodynamic properties and phase equilibria of several classes of bulk and confined fluids using Monte Carlo Simulation with particle insertion. A summary of recent results concerning the efficient simulation of strongly associating water models with gradual and monomer/dimer particle insertion methods is given in [1].

In 2006 we focussed on a systematic study of the system size influence on chemical potentials and phase coexistence properties in 3-dimensional bulk fluids and 2-dimensional layers by performing series of canonical simulations with different numbers of particles. In agreement with recent findings for Lennard-Jones fluids [2] the chemical potential isotherms show significant finite-size effects in the vapour-liquid transition range (shrinking van der Waals loops). But only small size effects are observed in the stable gas and liquid phase. For bulk square-well fluids the size dependence of chemical potentials and coexistence densities are shown in Fig. 10.1. These results demonstrate that the number dependence of the phase coexistence properties is small and the data approach the best known literature values with increasing particle number [3]. We expect from these investigations general information about the system size required in phase equilibrium simulations. For two-dimensional systems the size dependence of the phase equilibrium properties is found to be significantly larger than in bulk fluids [4]. These systems are currently under further investigation [5]. To reach a more fundamental understanding of structural properties in the critical range cluster distributions are estimated and analyzed by percolation theory.

In general the results may serve as quasi-experimental reference data for an improvement of hierarchic potential models of complex fluids and of thermodynamic
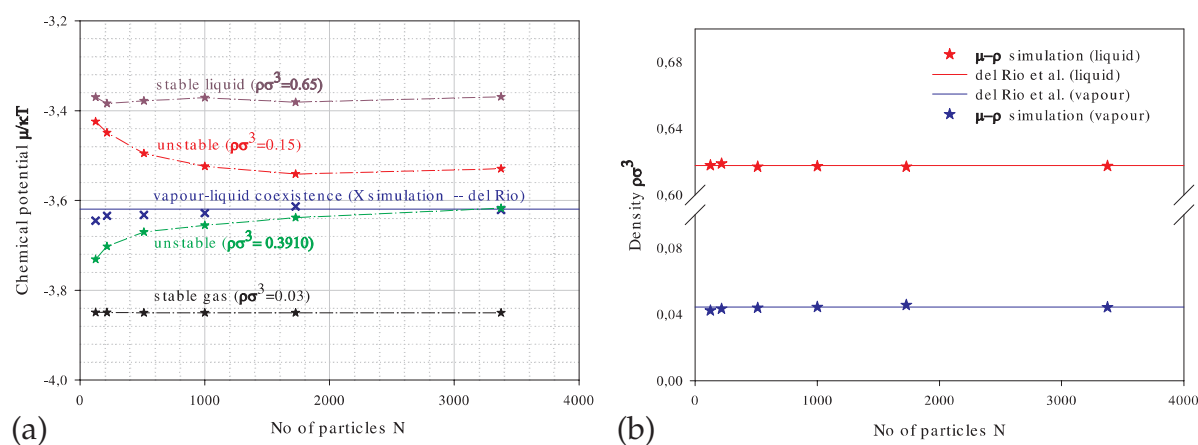
Figure 10.1: Coexistence chemical potential (**a**) and coexistence densities (**b**) (bulk square well $T^\star = 1.05$).

perturbation theories which contribute to a microscopic understanding of solubility and hydration phenomena of associating fluids in molecular confinements, such as porous media and biomembranes.

[1] H.L. Vörtler, M. Kettler: Mol. Phys. **104**, 233 (2006)
[2] L.G. MacDowell et al.: J. Chem. Phys. **120**, 5293 (2004); L.G. MacDowell et al.: J. Chem. Phys. **125**, 034 705 (2006)
[3] H.L. Vörtler et al.: Poster at 7th Liblice Conference on the Statistical Mechanics of Liquids, Lednice, 11.06.–16.06.2006
[4] K. Schaefer: Diploma Thesis, Universität Leipzig 2006
[5] H.L. Vörtler et al.: Talk at 71st Annual Meeting DPG, Regensburg, März 28, 2007

10.3 Molecular Theory of Fluid Phase Equilibria in Confined Systems

H.L. Vörtler, W.R. Smith[*], M. Kettler

[*]University of Ontario Institute of Technology, Oshawa, Canada

This research deals with the molecular structure of hard-core fluids in simple molecular confinements in terms of cavity- and background correlation functions [1, 2]. We study the BGY-like hierarchies between k- and $k + 1$-particle cavity functions. Particularly, we analyze the properties of cavity pair distribution functions obtained by means of novel MC methods which use virtual insertions of particles and cavities. These investigations are crucial for an improvement of closure relations of integral equations for cavity functions.

In general, the results of these studies provide basic structural information for the understanding of phase coexistence in geometrically restricted fluids on a molecular level. For comparison we estimate properties of coexisting fluid phases on the basis of perturbed virial expansions and simulate thermodynamic pressures in coexisting confined phases by means of recently developed virtual parameter variation techniques which permit a direct numerical calculation of the relevant canonical partition function derivatives.

The long-term goals of our research are contributions to a statistical-mechanical theory of phase equilibria of inhomogeneous fluids with applications to nanoporous materials and biointerfaces.

[1] W.R. Smith, H.L. Vörtler: Mol. Phys. **101**, 805 (2003)
[2] S. Fritzsche et al.: in *Molecules in Interaction With Surfaces and Interfaces,* ed. by R. Haberlandt et al. (Springer, Heidelberg 2004) p 1
[3] H.L. Vörtler, W.R. Smith: J. Chem. Phys. **112**, 5168 (2000)

10.4 Analytical Treatment and Computer Simulations of the Influence of the Crystal Surface on the Exchange of Guest Molecules Between Zeolite Nanocrystals and the Surrounding Gas Phase

A. Schüring[*†], J. Gulín-González[*‡], S. Vasenkov[†§], S. Fritzsche[*]

[*]Abteilung MDC, Institut für Theoretische Physik
[†]Abteilung GFP, Institut für Experimentelle Physik I
[‡]University of Informatics Sciences, La Habana, Cuba
[§]University of Florida, Gainesville, USA

Molecular dynamics simulations of tracer-exchange between zeolite crystals and the surrounding gas phase are applied to study the influence of crystal boundaries on the overall diffusional transport of molecules in nanoporous crystals. Boundary effects are expected to be of importance if the crystals are small, i.e. if the ratio of surface to volume is high. This is the case e.g. in catalysis, where relatively small crystals are used, and, furthermore, in currently developed hierarchically ordered porous materials [1] which enable a fast transport of molecules to the active crystals through a mesoporous channel system.

The investigations follow two main lines, where we distinguish between the cases of normal diffusion and single-file diffusion. The shape of intracrystalline concentration profiles in the presence of boundary effects are illustrated in the Figure in comparison to simple diffusion-limited transport. In the case of single-file diffusion, the particles are confined in a one-dimensional channel and, furthermore, they are too large to mutually exchange their positions. Therefore, the order of the particles is conserved as long as they stay in the channel. This restriction leads to anomalous diffusion; in this case, the mean square displacement of the particles grows with the root of the time. In the last year, we could successfully describe the magnitudes of the boundary effects by analytical relations between system parameters [5, 7, 8].

A novel boundary effect, reported in [2, 3] for single-file systems, is verified by MD simulations [4] and has now been quantified by analytical calculations [5]. An example for the observed boundary effect in single-file systems is shown in Fig. 10.2a. The concentration profiles of particles obeying single-file diffusion are flat near the boundaries. Two diffusion mechanisms occuring in parallel were found to be responsible for the boundary effect. On the one hand, the exchange of the particles in the center of the channel is possible only by a collective movement of the whole "chain" of particles (center-of-mass diffusion), because the order of the particles within the channel is conserved. On the other hand, each particle can move within a certain range relative to the center of mass of all particles in the channel. In [5] it has been shown that by separating the two types of movement from each other, that the spatial extent of the deviation of the concentration profile to the Fickian behaviour is given by the limiting average displacement of the particles relative to the center of mass of the chain.

In the second line of the project, the passage of molecules through the crystal margins is studied for the case of normal diffusion. The quantity describing the ability
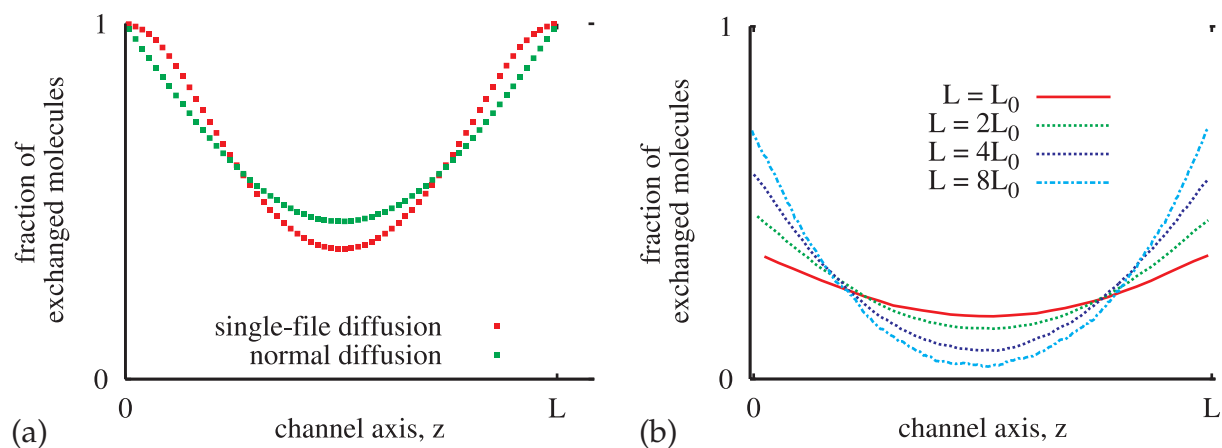
Figure 10.2: Boundary effects occuring im the cases of single-file diffusion (**a**) and normal diffusion (**b**). In the case of single-file diffusion, the concentration profiles have a shape that deviates from those of normal diffusion. In the case of normal diffusion, the influence of the permeability of the surface was studied. Flat concentration profiles indicate a low permeability and limitation of the overall transport by the surface.

of molecules to overcome the boundary region between gas phase and crystal is referred in [6] to as permeability, α, and is defined by specifying the boundary condition for Fick's law,

$$J(t) = \alpha(C_0 - C(t)) \, , \tag{10.1}$$

where it is assumed that the flux, $J(t)$ through the surface is proportional to the difference between the concentration C_0 necessary to maintain equilibrium with the surrounding gas phase and the actual concentration $C(t)$ in the crystal margin. If the ratio $\alpha L/D$ (L is the length of the crystal and D the intracrystalline diffusion coefficient) is low, flat profiles may be observed as can be seen in Fig. 10.2. In this case the transport is limited by the surface.

Analytical investigations have revealed a fundamental dependence of α on the energy difference between the inner part of the crystal and the gas phase [7]. Furthermore, a relation between the entering probability and the intracrystalline self-diffusion coefficient has been worked out in analytical calculations. The validity of the relation has been shown by MD simulations [8].

[1] Y. Tao, H. Kanoh: J. Am. Chem. Soc. **125**, 6044 (2003), doi:10.1021/ja0299405
[2] P.H. Nelson, S.M. Auerbach: J. Chem. Phys. **110**, 9235 (1999), doi:10.1063/1.478847
[3] S. Vasenkov, J. Kärger: Phys. Rev. E **66**, 0 526 011 (2002), doi:10.1103/PhysRevE.66.052601
[4] A. Schüring et al.: J. Phys. Chem. B **109**, 16 711 (2005), doi:10.1021/jp052314k
[5] S. Vasenkov et al.: Langmuir **22**, 5728 (2006)
[6] J. Crank: *The Mathematics of Diffusion* (Claredon Press, Oxford 1956)
[7] J. Gulín-González et al.: Chem. Phys. Lett. **430**, 60 (2006)
[8] A. Schüring: submitted to J. Phys. Chem. C.

10.5 Diffusion of Water in the Zeolite Chabazite

S. Fritzsche, P. Biswas, A. Schüring, P.A. Bopp[*], J. Kärger[†]

[*]Laboratoire de Physico-Chimie Moleculaire, University Bordeaux, France
[†]Abteilung GFP, Institut für Experimentelle Physik I

This is a project in the framework of the International Research Training Group (IRTG) "Diffusion in Porous Materials". Basing on [1] the diffusion of water in the zeolite chabazite is investigated. In opposition to most of the well known systems the diffusion coefficient increases with increasing concentration of guest molecules. This effect is strongly correlated with the presence of extra framwork cations. The diffusion coefficient of water in this system is very small so that special technics like a multiple-time-step algorithm must be used. Nevertheless, each simulation requires about 3 weeks computer time on modern workstations. Even then a reasonable statistics for diffusion coefficients can be obtained only for temperatures above 600 K [2]. In 2006 new simulations and evaluations have been carried out in Bordeaux in order to get deeper insight into the different time scales of local movements of water molecules in the vicinity of one adsorption place (cation) and the rare moves to other adsorption places [2]. These results may form the basis for future theoretical investigations that should finally open the possibility to calculate analytically the diffusion coefficient at room temperature which is to small to be obtained by direct MD simulations.

[1] S. Jost: Ph.D. thesis, University of Leipzig 2004
[2] S. Jost, P. Biswas, A. Schüring, J. Kärger, P.A. Bopp, R. Haberlandt, S. Fritzsche: *Structure and self-diffusion of water molecules in chabazite: A molecular dynamics study*, in preparation

10.6 How Do Guest Molecules Enter Zeolite Pores? Quantum Chemical Calculations and Classical MD Simulations

S. Fritzsche, R. Haberlandt, S. Hannongbua[*], T. Remsungnen[†], O. Saengsawang, S. Thompho

[*]Chulalongkorn University, Bangkok, Thailand
[†]Khon Khaen University, Khon Khaen, Thailand

This is a common project of the German DFG and the NRTC (Thailand Research Fund). Basing on experience with fitting classical potentials [1] from *ab initio* calculations such potentials have been developped by quantum chemical calculations [4, 5]. Using earlier knowledge from dynamical studies [2] they have been used to study the energetics and dynamics of guest molecules and the surface of zeolites by Molecular Dynamics (MD) simulations. The work includes also a cooperation with Prof. Kärger (Institut für Experimentalphysik I, Uni Leipzig). The publications [3–5] appeared.

[1] C. Bussai et al.: Langmuir **21**, 5847 (2005)
[2] S. Fritzsche et al.: Chem. Phys. **289**, 321 (2003)

[3] S. Fritzsche et al.: Chem. Phys. Lett. **411**, 423 (2005)
[4] O. Saengsawang et al.: Stud. Surf. Sci. Catal. **158**, 947 (2005)
[5] O. Saengsawang et al.: J. Phys. Chem B **109**, 5684 (2005)

10.7 Potential Models and the Investigation of the Diffusion of Pentane in Silicalite-1

S. Fritzsche[*], A. Longsinruin[*†], A. Schüring[*], S. Hannongbua[†]

[*]Abteilung MDC, Institut für Theoretische Physik
[†]Chulalongkorn University, Bangkok, Thailand

This is a common project of the German DAAD and the TRF (Thailand Research Fund). Parameters obtained before from quantum chemical calculations (Gaussian, MP2-level) [1] have been used in classical MD simulations to investigate the some structural quantities and the diffusion coefficient of pentane in silicalite-1. The pentane is used in united atom approximation. The bond and angle elasticity and the torsional elasticity are taken into account. In 2006 the comparison with other model potentials (mainly that of [3]) have caused us to reinvestigate the technics and algorithms for potential fitting from quantum calculations. This is a very challenging task because it is connected with finding a minimum of a control function in a multidimensional parameter space. The control function is the square deviation of potential values calculated using the model function from those obtained by quantum calculations. The problem is that the optimizing algorithm will often be trapped in minima that are only local in the parameter space. On the basis of former results [1] a new potential is proposed that yields a resonable diffusion coefficient and a better heat of adsorption for pentane in silicalite than other potentials (e.g. that of [3]). New insights in the technics of such fittings are presented in [2] and will be published in a future paper.

[1] A. Loisruangsin et al.: Chem. Phys. Lett. **390**, 485 (2004)
[2] A. Loisruangsin: Dissertation, Chulalongkorn University, Bangkok 2007
[3] D. Dubbeldam et al.: J. Phys. Chem. B **108**, 12 301 (2004)
[4] A. Loisruangsin, S. Fritzsche, S. Hannongbua: *Potential Calculations and MD Simulations of n-Pentane in Silicalite-1*, in preparation

10.8 Investigation of the Rotation and Diffusion of Pentane in the Zeolite ZK5

S. Fritzsche, O. Saengsawang, A. Schüring, P. Magusin[*] A. Dammers[†]

[*]Eindhoven University, The Netherlands
[†]Delft University, The Netherlands

This is a project in the framework of the International Research Training Group (IRTG) "Diffusion in Porous Materials". After construction the lattice of the H-ZK5 bei Molecular Mechanics the rotation and diffusion of pentane within this zeolite is investigated.

It turns out that the rotation within the smaller one of the different cavities of the ZK5 (γ-cage) which was examined experimentally in [1] is strongly hindered by lack of space and that therefore the rotation depends critically upon lattice vibrations and upon the choice of the interaction parameters. This is now investigated in detail. In cooperation with A. Dammers (Delft University) the challenging mew method of transition path sampling [2] is used to investigate also the diffusion for this system which is to slow to be investigated by MD simulations.

[1] V.E. Zorine et al.: J. Phys. Chem. B **108**, 5600 (2004)
[2] C. Dellago et al.: Adv. Chem. Phys. **123**, 1 (2002)

10.9   Funding

Analytical Treatment and Computer Simulations of the influence of the crystal surface on the exchange of guest molecules between zeolite nanocrystals and the surrounding gas phase
S. Fritzsche, S. Vasenkov, A. Schüring
SPP1155, DFG FR1486/2-2

Diffusion of Water in the Zeolite Chabazite
S. Fritzsche, O. Saengsawang, P. Biswas, A. Schüring
DFG: IRTG 1056

Investigation of the rotation and diffusion of pentane in the zeolite ZK5
S. Fritzsche, O. Saengsawang, A. Schüring
DFG: IRTG 1056

How do guest molecules enter zeolite pores? Quantum Chemical calculations and classical MD simulations
S. Fritzsche, S. Thompho
DFG FR1486/1-4

10.10   Organizational Duties

H.L. Vörtler
- Speaker of the MDC group
- Reviewer: Czech Science Foundation
- Referee: J. Chem. Phys., Chem. Phys. Lett., J. Molec. Liquids, Chem. Phys.

S. Fritzsche
- Project leader of one project in the International Research Training Group, IRTG 1056
- Project leader of one project in the SPP1155, DFG FR1486/2-1
- Project leader of a German/Thai research project, DFG FR1486/1-1, FR1486/1-2, FR1486/1-3
- Referee: Chem. Phys. Lett., Micropor. Mesopor. Mater., J. Molec. Graph. Model.

10.11   External Cooperations

Academic

- Chulalongkorn University, Thailand
  Prof. Dr. S. Hannongbua

- Indian Institute of Science, Bangalore, India
  Prof. Dr. S. Yashonath

- Khon Khaen University, Thailand
  Dr. T. Remsungnen

- University Bordeaux, France
  Prof. Dr. P. A. Bopp

- Eindhoven University, The Netherlands
  Prof. Dr. P. Magusin

- University of California, Irvine, USA
  Prof. M. Wolfsberg

- Charles University and Czech Acad. Sci., Prague, Czech Republic
  Prof. I. Nezbeda, Dr. M. Lisal

- University of Ontario Institute of Technology, Oshawa, Canada
  Prof. W.R. Smith

- Universität Regensburg
  Prof. H. Krienke

10.12   Publications

Journals

J. Gulin-Gonzalez, A. Schüring, S. Fritzsche, J. Kärger, S. Vasenkov: *The influence of the desorption barrier on the transport of molecules through the external surface of nanoporous crystals*, Chem. Phys. Lett. **430**, 60 (2006)

T. Remsungnen, V. Kormilets, A. Loisruangsin, A. Schüring, S. Fritzsche, R. Haberlandt, S. Hannongbua: *Optimal Binding Site of a Methane Molecule on the Silanol Covered (010) Surface of Silicalite-1: ONIOM Calculations*, J. Phys. Chem. B **110**, 11 932 (2006)

S. Vasenkov, A. Schüring, S. Fritzsche: *Single-File Diffusion near Channel Boundaries*, Langmuir **22**, 5728 (2006)

H.L. Vörtler, M. Kettler: *Efficient simulation of chemical potentials and phase equilibria in associating fluids: monomer/dimer insertion versus gradual particle insertion in primitive water models*, Mol. Phys. **104**, 233 (2006)

Talks

S. Fritzsche: *An Entropic Effect in the Diffusion of Dumbbell Molecules and its random treatment*, Indian Institute of Science, Bangalore, India, 07. March 2006

S. Fritzsche: *Statistical Derivation and Application of the Concept of the Local Free Energy*, Indian Institute of Science, Bangalore, India, 08. March 2006,

S. Fritzsche: *Understanding Sructural and Dynamical Effects by the Tool: Local Free Energy Landscape*, Chulalongkorn University, Bangkok, 27. February 2006

H.L. Vörtler: *System size dependence of chemical potentials and phase equilibria of bulk fluids and thin fluid films*, 7th Workshop on Computational Physics CompPhys06, Leipzig, 02. December 2006

Posters

H.L. Vörtler, M. Kettler, K. Schäfer: *Chemical potentials, phase equilibria and critical data of bulk and confined fluids by particle insertion simulation methods*, 7th Liblice Conf. on the Statistical Mechanics of Liquids, Lednice, Czech Republic, 11.–16. June 2006

10.13   Graduations

Diploma

- Katja Schäfer
  Monte Carlo Simulation von Phasengleichgewichten des planaren square-well fluids
  June 2006

10.14   Guests

- Prof. W.R. Smith
  UOIT Oshawa, Canada
  02.–10. June 2006 and 09.–14. October 2006
- Dr. T. Remsungnen
  Khon Khaen University, Thailand
  03.–31. October 2006

11

Quantum Field Theory and Gravity

11.1 Quantum Field Theory under the Influence of External Conditions

M. Bordag

The vacuum of quantum fields shows a response to changes in external conditions with measurable consequences. The most prominent manifestation is the Casimir effect. It belongs to the few number of macroscopic quantum effects and it is of big importance in nanometer sizes systems. At present, the dependence of the Casimir forces on geometry is in the focus of actual research. With a new representation in terms of a functional determinant which is free of ultraviolet divergences it became possible to perform numerical evaluations, for example for a sphere in front of a plane. Also, by an asymptotic expansion for small separations, for the first time an analytic correction to the well known proximity force approximation could be calculated, see [1].

[1] M. Bordag: Phys. Rev. D **73**, 125 018 (2006)

11.2 Higher Order Correlation Corrections to Color Ferromagnetic Vacuum State at Finite Temperature

M. Bordag, V. Skalozub[*]

[*]Physics Faculty, University of Dnepropetrovsk, Russia

Topic of the investigation is the stability of the ground state of QCD with temperature and color magnetic magnetic background field by means of the calculation of the polarization tensor of the gluon field. Special attention was payed to the investigation of the polarization tensor for the neutral charged gluons at finite temperature. A new technique for a parametric representation was found which allowed for an explicit separation of the Debye and the magnetic masses and, for instance, for an easy calculation of the Debye mass's field and temperature dependence [1]. For the magnetic mass mechanism the disappearance of the fictitious pole could be shown in detail.

[1] M. Bordag, V. Skalozub: arXiv:hep-th/0611256

11.3   Casimir Effect and Real Media

M. Bordag, B. Geyer, G.L. Klimchitskaya[*], V.M. Mostepanenko[†]

   [*]Physics Department, University of St. Petersburg, Russia
   [†]Noncommercial partnership "Scientific Instruments", Ministry of Industry, Sciences and
      Technology, Moscow, Russia

The vacuum of quantum fields shows a response to changes in external conditions with measurable consequences. The investigation of the electromagnetic vacuum in the presence of real media is of actual interest in view of current experiments as well as nanoscopic electro-mechanical devices. In recent experiments using atomic force microscopy the Casimir effect had been measured with high accuracy. This required a detailed investigation of the influence of real experimental structures on the corresponding force.

Since the year 2000, the behavior of the thermal correction to the Casimir force between real metals has been hotly debated. As was shown by several research groups, the Lifshitz theory, which provides the theoretical foundation for the calculation of both the van der Waals and Casimir forces, leads to different results depending on the model of metal conductivity used. To resolve these controversies, the theoretical considerations based on the principles of thermodynamics and new experimental tests were invoked. Furthermore, the study has to be extended to the case of dielectrics as well as semiconductors.

- The properties of the Lifshitz formulas for the free energy, entropy and pressure combined with dielectric permittivities of metal, dielectric and semiconductor test bodies possessing *dissipation* have been analysed. Thereby, different kinds of dissipation were considered, namely, dissipation observed in the region around the characteristic frequency of the Casimir effect, $\omega_c = c/(2a)$, and dissipation at very low (quasistatic) frequencies – the latter being connected with the conductivity of dielectric materials at constant current. As a thermodynamic criterion it has been shown [1] that the van der Waals and Casimir forces are not related to the actual conductivity properties of material bodies at frequencies much less than the characteristic frequency and the first Matsubara frequency, $\xi_1 = 2\pi k_B T/\hbar$, where k_B is the Boltzmann constant. For so low frequencies not the actual low-frequency behavior should be substituted into the Lifshitz formula but, instead, the extrapolation to low frequencies of the dielectric response in the region of frequencies $\sim \xi_1, \omega_c$. The formulated criterion is illustrated by the examples of metal-dielectric and metal-semiconductor plates. If this criterion is not followed, a violation of the third law of thermodynamics occurs. The same happens in the case of two metal plates [2]. The obtained results were presented in the review paper [3].

- In addition, we have investigated the thermal Casimir force in the configuration of one metallic and one dielectric plate made of *real materials* and developed a perturbation theory in some small parameter being proportional to the product of the separation between the plates and the temperature and we derived analytic asymptotic expressions at low temperatures for the Casimir free energy, pressure and entropy. The obtained analytic results were compared with numerical computations for Au and Si plates, and very good agreement has been found. These results prove that the Lifshitz theory in the configuration of metal-dielectric is in

agreement with thermodynamics. We have also proved that if the static dielectric permittivity of a dielectric plate is infinitely large due to the account of dc conductivity, the Casimir entropy takes a positive value when the temperature vanishes, i.e., the Nernst heat theorem is violated. This important result is in agreement with our earlier result, obtained for two dielectric plates and with the above criterion that the low-frequency behavior in the Lifshitz formula should be obtained by the extrapolation from the region of the characteristic frequency and the first Matsubara frequency. The obtained results are presented in [4, 5].

- The above described fundamental results were applied in nanotechnology by studying special *carbon nanostructures*: Carbon nanotubes are of high promise for the problem of hydrogen storage. Most of theoretical work on the interaction of hydrogen atoms with carbon nanotubes was made using the density functional theory permitting only numerical computations. In 2004 we pioneered an application of the fundamental Lifshitz theory to multi-wall carbon nanotubes. In this case it is possible to describe wall material using the dielectric permittivity of graphite. However, the case of single-wall nanotubes, important for the problem of hydrogen storage, remained uncovered in the framework of the Lifshitz theory. In our recent work we have used the description of graphene in terms of a two-dimensional free electron gas in order to extend the Lifshitz theory of the van der Waals and Casimir interaction to the case of carbon nanosystems. We have obtained Lifshitz-type formulas describing the interaction of graphene with metal or semiconductor walls (Au or Si, respectively) and the interaction of H atoms or molecules with graphene. We have also obtained the analytic formulas describing the interaction of single-wall carbon nanotubes with metal or dielectric plates. The computations using the obtained formulas were performed demonstrating that the developed formalism is of high promise for the problem of H storage in carbon nanostructures. The obtained collaborative results are presented in [1].

[1] G.L. Klimchitskaya et al.: J. Phys. A: Math. Gen. **39**, 6495 (2006)
[2] V.M. Mostepanenko et al.: J. Phys. A: Math. Gen. **39**, 6589 (2006)
[3] B. Geyer et al.: Int. J. Mod. Phys. A **21**, 5007 (2006)
[4] B. Geyer et al.: submitted to Phys. Rev. A
[5] G.L. Klimchitskaya, B. Geyer: Proc. XIth Marcel Grossmann Meeting on General Relativity, Berlin, 2006, submitted
[6] M. Bordag et al.: Phys. Rev. B **74**, 205 431 (2006)

11.4 Quantum Field Theory of Light-Cone Dominated Hadronic Processes

B. Geyer, J. Blümlein[*], D. Robaschik[†], O. Witzel[‡]

[*]Institut für Hochenergiephysik, Zeuthen
[†]Institute for Theoretical Physics, Brandenburg Technical University, Cottbus
[‡]Institute for Physics, Humboldt-Universität Berlin

Light-cone dominated, polarized hadronic processes at large momentum transfer factorize into process-dependent hard scattering amplitudes and process-independent

non-perturbative generalized distribution amplitudes. Growing experimental accuracy requires the entanglement of various twist as well as (target) mass contributions and radiative corrections. Their quantum field theoretic prescription is based on the nonlocal light-cone expansion [1] and the group theoretical procedure of decomposing *nonlocal, tensor-valued* QCD operators into tensorial harmonic operators with well-defined geometric twist (τ = dimension − spin) developed in our previous work [2, 3].

Continuing these studies the following results were obtained and applied to generic hadronic processes:

- Starting from the rigorous determination of the twist-2 part of the Compton amplitude including all target mass corrections [4] which led to a closed expressions for the Compton amplitude in terms of iterated generalized parton distribution amplitudes (GPD) and allowed the the derivation of generalized Wandzura-Wilczek and extended Callan-Gross relations we applied these results to *diffractive Compton scattering*.

  We presented a quantum field theoretic treatment of inclusive deep-inelastic diffractive scattering. That process can be described in the general framework of non-forward scattering processes using the light-cone expansion in the generalized Bjorken region. Target mass and inite t corrections of the diffractive hadronic tensor are derived at the level of the twist–2 contributions both for the unpolarized and the polarized case. They modify the expressions contributing in the limit $t, M^2 \to 0$ for larger values of β or/and t in the region of low Q^2. The different diffractive structure are expressed through integrals over the relative momentum of non-perturbative t-dependend 2-particle distribution functions. In the limit $t, M^2 \to 0$ these distribution functions are the diffractive parton distribution. Relations between the different diffractive structure functions are derived.

- The fundamental results [5] on the complete twist decomposition of generic non-local tensor operators for hadronic processes have been applied to *B-meson physics* [6]. Two- and three-particle distribution amplitudes of heavy pseudoscalar mesons of well-defined geometric twist are introduced. They are obtained from appropriately parametrized vacuum-to-meson matrix elements by applying those twist projectors which determine the enclosed light-cone operators of definite geometric twist and, in addition, observing the heavy quark constraint. Comparing these distribution amplitudes with the conventional ones of dynamical twist we derive relations between them, partially being of Wandzura–Wilczek type; also sum rules of Burkhardt–Cottingham type are derived. The derivation is performed for the (double) Mellin moments and then re-summed to the non-local distribution amplitudes. Furthermore, a parametrization of vacuum-to-meson matrix elements for non-local operators off the light-cone in terms of distribution amplitudes accompanying independent kinematical structures is derived.

  These results have been extended to derive the operator relations resulting from the quark equations of motion as well as from the relations between Dirac structures. We determined the first derivative of the two-particle off-cone dispersion amplitudes of definite (geometric) twist which are required for these relations

and restricted them to the light-cone. Then, local as well as non-local relations between two- and three-particle light-cone dispersion amplitudes are derived. The extension of the obtained results to the off-cone dispersion amplitudes is under study.

[1] S.A. Anikin, O.I. Zavialov: Ann. Phys. (N.Y.) **116**, 135 (1978); D. Müller et al.: Fortschr. Phys. **42**, 101 (1994)
[2] B. Geyer et al.: Nucl. Phys. B **559**, 339 (1999); Nucl. Phys. B **618**, 99 (2001); B. Geyer, M. Lazar, Nucl. Phys. B **581**, 341 (2000); Phys. Rev. D **63**, 094 003 (2001); J. Eilers, B. Geyer: Phys. Lett. B **546**, 78 (2002)
[3] J. Eilers et al.: Phys. Rev. D **69**, 034 015 (2004)
[4] B. Geyer et al.: Nucl. Phys. B **704**, 279 (2005)
[5] J. Eilers: arXiv:hep-th/0608173
[6] B. Geyer, O. Witzel: Phys. Rev. D **72**, 034 023 (2005)

11.5 Long Time Behavior of Black Holes

D. Grumiller, R. Meyer, D.V. Vassilevich

The project "Long time behavior of black holes" was originally envisaged for two years, but it lasted less than eigth months because another project had been granted in Spring 2006 and started in Summer 2006. The full project report was sent to DFG in Autumn 2006 [1]. Here is just a very brief summary.

The main goal of this project had been a mathematical description and a physical understanding of the long time behavior of black holes (or black hole analogues in condensed matter systems) which evaporate due to the Hawking process. This is pivotal not only for a deeper understanding of the dynamics of black holes beyond the semi-classical approximation, but also for an explanation / a resolution of the information loss problem.

Since the main insight to be gained by such a study is of conceptual nature, it is useful to simplify the theory technically as much as reasonably achievable. In this context particularly dilaton gravity in two dimensions has provided an attractive set of models, including the Schwarzschild, Reissner–Nordström, Witten and exact string black holes, as well as the Jackiw–Teitelboim model.

Our main result [2] was the observation that physical degrees of freedom existing on a generic boundary are converted into gauge degrees of freedom if the boundary happens to be a black hole horizon, concurrent with a conjecture by 't Hooft [3].

[1] D. Grumiller: Project Report on GR-3157/1
[2] L. Bergamin et al.: Class. Quant. Grav. **23**, 3075 (2006); L. Bergamin, D. Grumiller: arXiv:gr-qc/0605148, to be published in Int. J. Mod. Phys. D
[3] G. 't Hooft: arXiv:gr-qc/0401027

11.6   Structure of the Gauge Orbit Space and Study of Gauge Theoretical Models

G. Rudolph, S. Charzynski, A. Hertsch, J. Huebschmann, P. Jarvis[*], J. Kijowski[†], M. Schmidt, I.P. Volobuev[‡]

[*]School of Physics, University of Tasmania, Hobart, Australia
[†]Faculty of Physics, Uinversity of Warsaw, Poland
[‡]Skobeltsyn Insitute for Nuclear Physics, Moscow State University, Russia

The investigation of gauge theories in the Hamiltonian approach on finite lattices with emphasis on the role of nongeneric strata was continued, including

- singular Marsden-Weinstein reduction of specific models [1],
- structure of the reduced configuration and phase spaces [1, 2],
- stratified Kähler quantization for gauge group SU(2) [3].

The second problem was studied in collaboration with S. Charzynski as a part of the DFG project RU692/3-2. The third problem was studied in collaboration with J. Huebschmann in the framework of a Mercator visiting professorship funded by DFG (project Le758/22-1). In addition, J. Huebschmann proved a Peter-Weyl theorem for the Hilbert space of holomorphic sections obtained by Kähler quantization on the cotangent bundle of a compact Lie group [4].

Based on [5], the investigations of specific models of quantum lattice gauge theory in terms of gauge invariant quantities concerning the structure of the algebra of observables and its representations were continued, too.

A. Hertsch worked on the classification of the orbit types of the action of the group of local gauge transformations on the space of connections for arbitrary compact gauge group.

[1] E. Fischer et al.: J. Geom. Phys. **57**, 1193 (2007)
[2] S. Charzyński et al.: arXiv:hep-th/0512129
[3] J. Huebschmann et al.: arXiv:hep-th/0702017
[4] J. Huebschmann: arXiv:math.DG/0610613
[5] J. Kijowski et al.: Ann. H. Poincaré **4**, 1137 (2003); J. Kijowski, G. Rudolph: J. Math. Phys. **46**, 032 303 (2005); Rep. Math. Phys. **55**, 199 (2005); P. Jarvis et al.: J. Phys. A **38**, 5359 (2005)

11.7   Noncommutative Geometry

G. Rudolph, P. Hajac[*], R. Matthes[*], W. Szymanski[†]

[*]Faculty of Physics, University of Warsaw, Poland
[†]Faculty of Science and Information Technology, University of Newcastle, UK

The study of quantum principal bundles was continued. Two papers about examples of generalized locally trivial Hopf bundles have appeared. In [2], both Hopf-Galois

and C^*-algebraic aspects (including K-theory) of the locally trivial $U(1)$-Hopf bundle introduced in [1] are analyzed. The note [3] announces results for the $U(1)$-Hopf bundles over quantum two-spheres arising from a gluing of two quantum discs with (mirror-type quantum sphere) or without (Podleś sphere) an extra twist. Also, non-commutative analogues of lense spaces (as bundles over the mirror sphere) are considered, and it is proved that the corresponding C^*-algebras are not isomorphic to crossed products.

In the preprint [4] (collaboration with P.F. Baum), the notions of principal and associated bundle are reconsidered from the point of view of noncommutative geometry. The main points of this article are a completely proven C^*-algebraic characterization of free and proper actions, a description of sectons of associated bundles as algebraic cotensor products, an algebraic characterization of connections in principal bundles, and a computation of the pairing between the K_0-class of line bundles associated to the $U(1)$-Hopf bundle with the cyclic cocycle of integration over the two-sphere. Also, examples of proper and free actions that do not give rise to locally trivial principal bundles are given.

The investigation of topological invariants (K-theory) of observable algebras has been continued. This concerns observable algebras determined by Kijowski and Rudolph [5] for several models of gauge field theory. The hope is to identify superselection sectors of quantum field theory as invariants of K-theory and to relate them to other notions of noncommutative geometry. In the case of spinorial electrodynamics, the computation of the K-groups can be carried out easily. The group K_1 vanishes, whereas K_0 is a direct sum of copies of $\mathbb{Z}$, with two generators for each lattice point. For scalar electrodynamics, one has to compute K-theory for a quotient of a group C^*-algebra by an ideal generated by elements affiliated to that algebra. A publication concerning these matters is under preparation.

[1] D. Calow, R. Matthes: J. Geom. Phys. **41**, 114 (2002)
[2] P.M. Hajac et al.: C. R. Acad. Sci. Paris **343**, 731 (2006)
[3] P.M. Hajac et al.: Algebr. Represent. Th. **9**, 121 (2006)
[4] P. Baum et al.: *Noncommutative geometry approach to principal and associated bundles*, Preprint IHES M/06/65
[5] J. Kijowski, G. Rudolph: J. Math. Phys. **46**, 032 303 (2005); Rep. Math. Phys. **55**, 199 (2005)

11.8 Contributions to Quantum Informatics

A. Uhlmann, P. Alberti, B. Crell, J. Dittmann

The following problems were studied: representation and properties of the fidelity of density operators and related quantities [1, 2], differential geometry of monotonous metrics on the space of states, in particular, of Bures' metric, properties of purifying lifts, transport of states, and geometrical phases [3], refinements of Bures' metric (partial fidelities, decomposition of pairs of states), operators and mappings related to Einstein-Podolski-Rosen channels and quantum teleportation [4]. Furthermore, characteristic parameters (entropy, channel capacity) for quantum channels of length two

were calculated [5]. The use of anti-linearity in quantum information and possible connections with k-positivity were discussed. One aim is the algebraic formulation of some basic concepts of quantum information theory.

[1] P. Alberti, A. Uhlmann: Acta Appl. Math. **60**, 1 (2000)
[2] A. Uhlmann: arXiv:quant-ph/9909060; arXiv:quant-ph/9912114
[3] J. Dittmann, A. Uhlmann: J. Math. Phys. **40**, 3246 (1999)
[4] A. Uhlmann: in: *Fin De Siecle*, ed. by A. Borowiec et al., Lecture Notes in Physics 539 (Springer, Berlin 2000) p 93; in: *Trends in Quantum Mechanics* (World Scientific, River Edge 2000) p 138
[5] A. Uhlmann: Open Sys. Inf. Dyn. **12**, 93 (2005)

11.9 Aspects of Noncommutative and Supersymmetric Field Theories and Black Holes

D.V. Vassilevich, D. Grumiller, L. Bergamin[*], R. Fresneda[†], D. Gitman[†], W. Kummer[‡], P. van Nieuwenhuizen[§]

[*]European Space Agency, ESTEC, Noordwijk, The Netherlands
[†]Departamento de fisico nuclear, Universidade de Sao Paulo, Brazil
[‡]Institut für Theoretische Physik, Technische Universität Wien, Austria
[§]Institute for Theoretical Physics,State University of New York at Stony Brook, USA

Space-time noncommutative theories contain an infinite number a time derivatives which makes applications of standard canonical Hamiltonian methods a very hard task. However, one can define a Poisson structure which makes it possible to analyze gauge symmetries by looking at the algebra of first-class constraints [1], precisely as in the commutative case. This procedure was used in [2] to analyze possible deformations of the noncommutative Jackiw-Teitelboim model, and it was demonstrated that no such deformations exist. This result implies that very few two-dimensional gravity models have their noncommutative counterparts if one is restricted to the standard gauge principle. This no-go result motivated us to look for alternative gauge principles, and a twisted version of noncommutative gauge symmetries was found in [3]. A similar result was obtained independently a little bit later in [4].

The one-loop counterterms and quantum anomalies can be defined through the heat kernel expansion. Such an expansion on noncommutative torus was constructed in [5]. It depends crucially on the number theoretic properties of the noncommutativity parameter.

Some applications, like calculations of the back hole entropy, require the analysis of the algebra of boundary constraints. We perform such an analysis in generic two-dimensional models [6] and found that on the horizon a part of physical degrees of freedom is converted to gauge degrees of freedom thus confirming a conjecture by 't Hooft. Important boundary symmetries are local supersymmetry transformations. An approach to analyzing these symmetries was formulated in [7].

[1] D.V. Vassilevich: Theor. Math. Phys. **148**, 928 (2006) [Teor. Mat. Fiz. **148**, 64 (2006)]
[2] D.V. Vassilevich et al.: Eur. Phys. J. C **47**, 235 (2006)
[3] D.V. Vassilevich: Mod. Phys. Lett. A **21**, 1279 (2006)
[4] P. Aschieri et al.: Lett. Math. Phys. **78**, 61 (2006)
[5] V. Gayral et al.: arXiv:hep-th/0607078, to be published in Commun. Math. Phys.
[6] L. Bergamin et al.: Class. Quant. Grav. **23**, 3075 (2006)
[7] P. van Nieuwenhuizen et al.: Int. J. Mod. Phys. D **15**, 1643 (2006)

11.10 Quantum Field Theory on Non-Commutative Geometries, Quantum Energy Inequalities, Generally Covariant Quantum Field Theory

R. Verch, P. Marecki, M. Borris, C.J. Fewster[*], M. Paschke[†], J. Schlemmer

[*]Department of Mathematics, University of York, UK
[†]Max Planck Institute for Mathematics in the Sciences, Leipzig

One of the questions of recent interest is if there is a general framework for quantum field theory on non-commutative spacetimes. This question is analysed in collaboration with M. Paschke and M. Borris. On one hand, an approach to Lorentzian non-commutative geometry in the spirit of spectral geometry is being established. On the other hand, the quatization of such structures is shown to lead to simple examples of quantum field theories on non-commutative spacetimes for concrete non-commutative spacetime models. The research on these topics is in progress.

Another line of research is devoted to an extension of the framework of local general covariant quantum field theories to the case of a relation between quantum field theories on several, different dimensions. This connects to the question of how to distinguish theories of Kaluza-Klein type at the quantized level. The research work on these matters is carried out in collaboration with C.J. Fewster.

The definition and analysis of states which can be viewed as local thermal equilibrium states in quantum field theory will be extended to quantum fields in curved spacetime, with a view on application in cosmological situations. Current research work with J. Schlemmer points at a close connection between local thermal equilibrium states and quantum energy inequalities which is being further analyzed.

A standing problem is the concept of quantum field theories on non-globally hyperbolic spacetimes. A special class of such spacetimes are certain types of rotating spacetimes. Several issues in setting up quantum field theories on such spacetimes are being studied by P. Marecki.

11.11 Funding

Structure of the gluon polarization tensor in a color magnetic field background at finite temperature
PD Dr. M. Bordag
DFG 436 UKR 17/25/06

Spectral Zeta Functions and Heat Kernel Technique in Quantum Field Theory with Nonstandard Boundary Condition
PD Dr. M. Bordag, Dr. D. Vassilevich
Heisenberg-Landau programme

Parallel nano assembling directed by short-range field forces
PD Dr. M. Bordag
PARNASS: Specific targeted research project within the 6th Framework Programme of EU, NMP4-CT-2005-017071

Improved study of the Casimir force between real metals and its application to constraints for testing extra-dimensional physics
Prof. Dr. B. Geyer
DFG 436 RUS 113/789/0-2

The long time behavior of Black Holes and Black Hole analogues
D. Grumiller
DFG GR-3157/1-1 (01.01.06–15.08.06)

Quantum Theory of Lattice Gauge models
A. Hertsch
IMPRS fellowship

Mercator professorship Sept 1, 2005–August 31, 2006
Prof. Dr. J. Huebschmann
DFG Le 758/22-1

Untersuchungen zur physikalischen Bedeutung der Stratifizierung des Eichorbitraumes
Prof. Dr. G. Rudolph
DFG RU 692/3-2

Local thermodynamic equilibrium in cosmological spacetimes
J. Schlemmer
IMPRS fellowship

11.12   Organizational Duties

M. Bordag
• Referee: J. Phys. A, Phys. Rev. D, J. Math. Phys.

B. Geyer
• Member of electing board Latin America-South of DAAD
• Vertrauensdozent of Gesellschaft Dt. Naturforscher und Ärzte
• Referee: DFG, DAAD, Humboldt Foundation

D. Grumiller
- Co-editor: December 2005 Special Issue of Int. J. Mod. Phys. D
- Referee: Class. Quant. Grav., Int. J. Mod. Phys. D, Mod. Phys. Lett. A, Phys. Lett. B
- Member of Editorial Board of FAKT-webpage www.teilchen.at (FAKT="Fachaus-schuß Kern- und Teilchenphysik" of the Austrian Physical Society)

J. Huebschmann
- Coeditor: J. Pure and Applied Algebra; Homology, Homotopy, and its Applications; Proc. A. Razmadze Mathi. Inst. (Tiflis/Georgien); Journal of Homotopy and Related Structures; Travaux Mathématiques (Luxembourg)
- Referee: Acta Math. Hung., Annali dell'Universita' di Ferrara, sez. VII, Scienze Matematiche, J. Symb. Comp., Diff. Geom. Appl.

G. Rudolph
- Director of the Institute for Theoretical Physics
- Referee: Class. Quant. Grav., J. Math. Phys., J. Geom. Phys., J. Phys. A, Rep. Math. Phys.

M. Schmidt
- Referee: J. Phys. A, Int. J. Mod. Phys. A

A. Uhlmann
- Board member: Rep. Math. Phys., Open Syst. Inf. Dyn.

D.V. Vassilevich
- Referee: Class. Quant. Grav., J. Phys. A, Nucl. Phys. B, Mod. Phys. Lett. A, J. High Energy Phys., Nuovo Ciment. B, London Math. Soc.
- Program Committee, Fock School on Advances in Physics (St. Petersburg)

R. Verch
- Vice chairman of the board for the Theoretical and Mathematical Physics Section, Deutsche Physikalische Gesellschaft (DPG)
- Referee for the 'Fonds zur Förderung der wissenschaftlichen Forschung in Österreich' (FWF)
- Referee: Commun. Math. Phys., J High Energy Phys., J. Math. Phys., Rev. Math. Phys.
- Reviewer for Mathematical Reviews

11.13   External Cooperations

Academic

- Max-Planck Institute for Mathematics in the Sciences (MPI MIS), Leipzig
  Dr. C. Fleischhack, Dr. M. Paschke

- Institute for Physics/Computational Physics, Humboldt University, Berlin
  DP Oliver Witzel

- DESY-Institute of High Energy Physics, Zeuthen
  Dr. Johannes Blümlein

- Institute for Theoretical Physics, Brandenburg Technical University, Cottbus
  Prof. Dr. Dieter Robaschik

- Inst. f. Mathematical Physics, TU Braunschweig
  Prof. Dr. R.F. Werner

- Institute for Theoretical Physics, Universität Regensburg
  Prof. Dr. J. Siewert

- Charles University Prague, Czech Republic
  Dr. Alfredo Iorio

- Institute for Theoretical Physics, Universität Wien, Austria
  Prof. Dr. H. Narnhofer

- Technische Universität Wien, Austria
  Dr. Herbert Balasin, Prof. Wolfgang Kummer, Prof. Dr. A. Rebhan

- Center for Theoretical Physics, Polish Academy of Sciences Warsaw, Poland
  Prof. Dr. J. Kijowski

- Mathematics Institute, Polish Academy of Sciences and University of Warsaw, Poland
  Prof. Dr. P. Hajac, Dr. R. Matthes

- Dept. of Physics, North-West Polytechnical University St. Petersburg, Russia
  Prof. Dr. G.L. Klimchitskaya

- St. Petersburg University, Russia
  Prof. Y.V. Novozhilov, Y. Grebenjuk

- Skobeltsyn Institute of Nuclear Physics, Lomonosov Moscow State University, Russia
  Dr. I.P. Volobuev

- Noncommercial Partnership "Scientific Instruments" of Ministry of Industry, Sciences and Technologies, Moscow, Russia
  Prof. Dr. V.M. Mostepanenko

- Joint Institute for Nuclear Research, Dubna, Russia
  Prof. D. Fursaev

- National University, Dnepropetrovsk, Russia
  Prof. V. Skalozub

- Université des Sciences et Technologies de Lille, France
  Prof. Dr. J. Huebschmann

- Department of Mathematics, University of York, UK
  Dr. C.J. Fewster

- European Space Agency, ESTEC, Noordwijk, The Netherlands
  Dr. Luzi Bergamin

- Dipartimento di Matematica, Universita di Trento, Trento, Italy
  Prof. Dr. V. Moretti

- Pamukkale University, Turkey
  Prof. Muzaffer Adak

- State University of New York at Stony Brook, USA
  Prof. P. van Nieuwenhuizen

- Massachusetts Institute of Technology, Cambridge, USA
  Prof. Roman Jackiw

- Department of Mathematics, Central Connecticut State University, New Britain, USA
  Prof. Dr. T. Roman

- Department of Physics, University of South Carolina, Columbia, USA
  Prof. Dr. P. Mazur

- University of North Carolina at Chapel Hill, USA
  Prof. em. Dr. J.D. Stasheff

- University of Oregon, Eugene, USA
  Prof. P.B. Gilkey

- Department of Mathematics, University of Florida, Gainesville, USA
  Prof. Dr. S.J. Summers

- University of Tasmania, Hobart, Australia
  Prof. Dr. P. Jarvis

- University of Newcastle, Australia
  Prof. Dr. W. Szymanski

- Canterbury University, UK
  Prof. D. Ahluwalia-Khalilova

- Universidade de São Paulo, Brazil
  Prof. D. Gitman

11.14 Publications

Journals

L. Bergamin, D. Grumiller, W. Kummer, D.V. Vassilevich: *Physics-to-gauge conversion at black hole horizons*, Class. Quant. Grav. **23**, 3075 (2006)

V.B. Bezerra, R.S. Decca, E. Fischbach, B. Geyer, G.L. Klimchitskaya, D.E. Krause, D. López, V.M. Mostepanenko, C. Romero: *Comment on 'On the temperature dependence of the Casimir effect'*, Phys. Rev. E **73**, 028 101-1-5 (2006)

J. Blümlein, B. Geyer, D. Robaschik: *Target mass and finite momentum transfer corrections to unpolarized and polarized diffractive scattering*, Nucl. Phys. B **755**, 112 (2006)

M. Bordag: *The Casimir effect for a sphere and a cylinder in front of plane and corrections to the proximity force theorem*, Phys. Rev. D **73**, 125 018 (2006)

M. Bordag, B. Geyer, G.L. Klimchitskaya, V.M. Mostepanenko: *Lifshitz-type formulas for graphene and single-wall carbon nanotubes: van der Waals and Casimir interactions*, Phys. Rev. B **74**, 205 431 (2006)

M. Bordag, Y.O. Grebenyuk, V.V. Skalozub: *Nontransversality of the gluon polarization tensor in a chromomagnetic background field*, Theor. Math. Phys. **148**, 910 (2006)

B. Geyer, G.L. Klimchitskaya, V.M. Mostepanenko: *Recent results on thermal Casimir force between dielectrics and related problems*, Int. J. Mod. Phys. A **21**, 5007 (2006)

D. Grumiller: *The volume of 2D black holes*, J. Phys. Conf. Ser. **33**, 361 (2006)

D. Grumiller, R. Meyer: *Ramifications of lineland* Turk. J. Phys. **30**, 349 (2006)

D. Grumiller, R. Meyer: *Quantum dilaton gravity in two dimensions with fermionic matter*, Class. Quant. Grav. **23**, 6435 (2006)

J. Huebschmann: *Kähler quantization and reduction*, J. Reine Angew. Math. **591**, 75 (2006)

G.L. Klimchitskaya, B. Geyer, V.M. Mostepanenko: *Universal behavior of dispersion forces between two dielectric plates in the low-temperature limit*, J. Phys. A **39**, 6495 (2006)

V.M. Mostepanenko, V.B. Bezerra, R.S. Decca, B. Geyer, E. Fischbach, G.L. Klimchitskaya, D.E. Krause, D. López, C. Romero: *Present status of controversies regarding the thermal Casimir force*, J. Phys. A **39**, 6589 (2006)

A. Uhlmann: *On Concurrence and Entanglement of Rank Two Channels*, Open Sys. Inf. Dyn. **12**, 93 (2005)

P. van Nieuwenhuizen, A. Rebhan, D.V. Vassilevich, R. Wimmer: *Boundary terms in supergravity and supersymmetry*, Int. J. Mod. Phys. D **15**, 1643 (2006)

D.V. Vassilevich: *Constraints, gauge symmetries, and noncommutative gravity in two dimensions*, Theor. Math. Phys. **148**, 928 (2006)

D.V. Vassilevich: *Twist to close*, Mod. Phys. Lett. A **21**, 1279 (2006)

D.V. Vassilevich, R. Fresneda, D.M. Gitman: *Stability of a noncommutative Jackiw-Teitelboim gravity*, Eur. Phys. J. C **47**, 235 (2006)

Books

J. Huebschmann: *Quantization in the presence of singularities*, in: *Quantum Theory and Symmetries*, Vol. IV, ed. by V.K. Dobrev (Heron Press, Sofia 2006) p 51

D. Mülsch, B. Geyer: *An Abelian cohomological gauge theory*, in: *Proc. of the 10th Marcel Grossmann Meeting on General Relativity*, Part C, ed. by M. Novello, S.P. Bergliaffa, R. Ruffini (World Scientific, Singapore 2006) p 2375

G. Rudolph: *On the observable algebra and its representations for lattice QCD*, in: *Quantum Theory and Symmetries*, Vol. I, ed. by V.K. Dobrev (Heron Press, Sofia 2006) p 429

M. Schmidt: *On the structure of the reduced configuration space of classical lattice chromodynamics*, in: *Quantum Theory and Symmetries*, Vol. I, ed. by V.K. Dobrev (Heron Press, Sofia 2006) p 441

in press

L. Bergamin, D. Grumiller: *Killing horizons kill horizon degrees*, arXiv:gr-qc/0605148, to be published in Int. J. Mod. Phys. D

E. Fischer, G. Rudolph, M. Schmidt: *A Lattice Gauge Model of Singular Marsden-Weinstein Reduction. Part I. Kinematics*, J. Geom. Phys. **57**, 1193 (2007)

V. Gayral, B. Iochum, D.V. Vassilevich: *Heat kernel and number theory on NC-torus*, arXiv:hep-th/0607078, to be published in Commun. Math. Phys.

D. Grumiller, R. Jackiw: *Kaluza-Klein reduction of conformally flat spaces*, arXiv:math-ph/0609025, to be published in Int. J. Mod. Phys. D

J. Huebschmann: *Singular Poisson-Kähler geometry of certain adjoint quotients*, in: *Proceedings, The mathematical legacy of C. Ehresmann*, Bedlewo, 2005, to be published in 2007

Talks

L. Bergamin, D. Grumiller: *Universal black hole thermodynamics from horizon symmetries*, XIth Marcel Grossmann meeting, Berlin, Germany, July 2006

D. Grumiller: *(Super-)gravity in 2D: An Overview*, 5th Workshop on quantization, dualities and integrable systems in Denizli, Turkey, January 2006

D. Grumiller: *Phase space reduction through horizon constraints*, DPG Tagung in Munich, March 2006

D. Grumiller: *Phase space reduction through horizon constraints*, XIth Marcel Grossmann meeting, Berlin, July 2006

J. Huebschmann: *Singular Poisson-Kähler geometry of stratified Kähler spaces*, Workshop *Sophus Lie*, Darmstadt, 05. January 2006

J. Huebschmann: *Singular Poisson-Kähler geometry of stratified Kähler spaces*, University of Jena, 17. January 2006

J. Huebschmann: *Singular Poisson-Kähler geometry of stratified Kähler spaces*, University of Münster, 25. April 2006

J. Huebschmann: *Singular Poisson-Kähler geometry of stratified Kähler spaces*, University of Freiburg, 28. April 2006

J. Huebschmann: *Poisson-Kähler geometry of stratified Kähler spaces*, Banach Center, Warsaw, Poland, 10. May 2006

J. Huebschmann: *Algebra and geometry of Maurer-Cartan algebras*, Department of Physics, Polish Academy of Sciences, Warsaw, Poland, 11. May 2006

J. Huebschmann: *Singular Poisson-Kähler geometry of stratified Kähler spaces*, SFB 647, Humboldt University, Berlin, 16. May 2006

J. Huebschmann: *Singular Poisson-Kähler geometry of stratified Kähler spaces*, University of Paderborn, 26. June 2006

J. Huebschmann: *Kan group and lattice gauge theory*, University of Jena, 29. June 2006

G.L. Klimchitskaya, B. Geyer: *Theory of the Casimir effect between dielectric and semiconductor plates*, XIth Marcel Grossmann Meeting on General Relativity, Berlin, 23.–29. July 2006

R. Meyer: *Quantum Dilaton Gravity with Fermions*, DPG Tagung in Munich, Germany, March 2006

G. Rudolph: *The geometry of gauge fields*, 4 lectures at the IMPRS of MPI MIS, Leipzig, April–May, 2006

M. Schmidt: *Classical reduction of lattice gauge theory*, NTZ Leipzig, 28. February 2006

M. Schmidt: *Quantization on stratified spaces*, Miniworkshop Fokoop Clausthal-Leipzig-Sofia, Clausthal-Zellerfeld, 11. November 2006

11.15   Graduations

Diploma

- Frank Bauer
  Kommutatorrelationen und erzeugte C^*-Algebren
  October 2006

- Friederike Danneil
  On the topological structure of the reduced phase space and reduced configuration space of lattice chromodynamics
  September 2006

- Stefan Funkner
  Die Geometrie der Ashtekar-Variablen
  January 2006

- Diana Kaminski
  A theory of self-adjoint extensions for positive and symmetric operators on Hilbert space
  January 2006

- Michael Kath
  Noncommutative worlds and Feynman's proof of Maxwell equations
  September 2006

- René Meyer
  Classical and quantum dilaton gravity in two dimensions with fermions
  May 2006

- Gilbert Spiegel
  Zur Dynamik der starken Wechselwirkung in der klassischen Gittereichtheorie
  August 2006

Bachelor

- Sebastian Sturm
  Visible effects of special relativity
  September 2006

11.16 Guests

- Prof. Muzaffer Adak
  Pamukkale University, Turkey
  June 2006

- Dr. Luzi Bergamin
  European Space Agency, ESTEC, Noordwijk, The Netherlands
  February 2006

- J. Huebschmann
  Université des Sciences et Technologies de Lille, France
  23. – 27. October 2006; 18. – 20 December 2006

- Prof. M. Ioffe
  State University St. Petersburg, Russia
  06. – 16 June 2006

- Prof. Dr. J. Kijowski
  Center for Theoretical Physics, Polish Academy of Sciences, Warsaw, Poland
  September 2006

- Prof. V. Nesterenko
  JINR Dubna, Russia
  24. February – 16. March 2006

- Prof. Dr. H. Römer
  University of Freiburg
  10. – 11. January 2006

- Prof. V. Skalozub
  Dnepropetrovsk National University, Ukraine
  7. January – 5. February 2006; 11. – 31. August, 2006

12

Statistical Physics

12.1 Introduction

We work on the connections of statistical mechanics to quantum field theory, on the mathematical and physical aspects of renormalization group (RG) theory and on its applications to high–energy and condensed matter physics, and on quantum kinetic theory. Our methods range from mathematical proofs to computational techniques.

The RG method applied here is an exact functional transformation of the action of the system, which leads to an infinite hierarchy of equations for the Green functions. Truncations of this hierarchy are used in applications. In a number of nontrivial cases, this truncation can be justified rigorously, so that the method lends itself to mathematical studies. These mathematical aspects are also under investigation.

Another topic we study is the long–time dynamics of large quantum systems, with a view of understanding how dissipative dynamics on the macroscopic scale arises from the microscopically reversible dynamics in interesting scaling limits.

We have ongoing collaborations with the Max–Planck Institute for Solid State Research in Stuttgart, the University of British Columbia, Vancouver, the University of Munich, the University of Würzburg, the University of Mainz, and Harvard University.

Manfred Salmhofer

12.2 Asymptotic Safety in Quantum Einstein Gravity: Nonperturbative Renormalizability and Fractal Spacetime Structure

O. Lauscher, M. Reuter[*]

[*]Institut für Physik, Universität Mainz

Recent results obtained within the framework of the renormalization group and its nonperturbative applications indicate that four-dimensional Quantum Einstein Gravity (QEG), the quantum field theory of the spacetime metric, is likely to be an asymptotically safe theory which is applicable at arbitrarily small distance scales. On sub-

Planckian distances it predicts that spacetime is a fractal with an effective dimensionality of 2. The original argument leading to this result was based upon the anomalous dimension η of Newton's constant. In [1, 2] we show that also the spectral dimension $\mathcal{D}_s$ of asymptotically safe QEG (if it indeed exists) equals 2 microscopically, while it is equal to 4 on macroscopic scales. In fact, these results for $\mathcal{D}_s$ coincide with those which were recently obtained by Monte Carlo simulations of the causal dynamical triangulation model. While until recently it has been difficult to compare the continuum theory to this discrete approach, the new results suggest that they might be closely related.

It is also quite remarkable that the equality of the microscopic values for $d + \eta$ (i.e. the effective dimensionality associated to η) and $\mathcal{D}_s$ is a special feature of $d = 4$ classical dimensions. While we obtain $d + \eta = 2$ for any d the spectral dimension is found to be d-dependent: $\mathcal{D}_s = d/2$. These two values coincide if, and only if, $d = 4$. This result is an exact consequence of asymptotic safety and does not rely on any truncation.

[1] O. Lauscher, M. Reuter: J. High Energy Phys. **10**, 050 (2005), arXiv:hep-th/0508202

[2] O. Lauscher, M. Reuter: in *Quantum Gravity: Mathematical Models and Experimental Bounds*, ed. by B. Fauser et al. (Birkhäuser, Basel 2007) p 293, arXiv:hep-th/0511260

12.3   Quantum Diffusion

L. Erdös[*], M. Salmhofer, H.-T. Yau[†]

[*]Mathematisches Institut, Universität München
[†]Mathematics Department, Harvard University, Cambridge, USA

We study the long-time limit of the time evolution of the Anderson model (quantum Lorentz gas). We prove that, for a weakly coupled system with coupling strength g, the time evolution on timescale t of order g^{-2-a}, $a > 0$, is given by a diffusion equation. This is the first time that a proof about the behaviour of these systems on time scales bigger than g^{-2} is given. It shows how diffusive behaviour emerges from a microscopically reversible dynamics. The essential complication is that the number of collisions that happen on such timescales diverges as an inverse power of g. In [1, 2] we have treated the continuum case. The detailed proof for the lattice case is in [3]. This proof requires new bounds for the decay of the Fourier transform of surfaces with vanishing Gauss curvature, proven in [4].

[1] L. Erdös et al.: arXiv:math-ph/0512014, submitted to Acta Math.
[2] L. Erdös et al.: arXiv:math-ph/0512015, Comm. Math. Phys. (2007), in press
[3] L. Erdös et al.: Ann. Henri Poincare, in press
[4] L. Erdös, M. Salmhofer: arXiv:math-ph/0604039, Math. Z., in press

12.4   Determinant Bounds and the Ultraviolet Problem of Fermionic Field Theories

W. Pedra, M. Salmhofer

It is known that perturbation theory converges in fermionic field theory at weak coupling if the interaction and the covariance are summable and if certain determinants arising in the expansion can be bounded efficiently, e.g. if the covariance admits a Gram representation with a finite Gram constant. The covariances of the standard many–fermion systems do not fall into this class due to the slow decay of the covariance at large Matsubara frequency, giving rise to a UV problem in the integration over degrees of freedom with Matsubara frequencies larger than some Ω (usually the first step in a multiscale analysis). We show that these covariances do not have Gram representations on any separable Hilbert space. We then prove a general bound for determinants associated to chronological products which is stronger than the usual Gram bound and which applies to the many–fermion case. This allows us to prove convergence of the first integration step in a rather easy way, for a short–range interaction which can be arbitrarily strong, provided Ω is chosen large enough. Moreover, we give – for the first time – nonperturbative bounds on all scales for the case of scale decompositions of the propagator which do not impose cutoffs on the Matsubara frequency.

[1] W. Pedra, M. Salmhofer: *Determinant Bounds and the Matsubara UV Problem of Many-Fermion Systems*, to appear

12.5   Competing Ordering Tendencies and the RG

C. Honerkamp[*], C. Husemann, O. Lauscher, W. Metzner[†], M. Salmhofer

[*]Institut für Theoretische Physik und Astrophysik, University Würzburg
[†]Abteilung Theorie, Max-Planck-Institut für Festkörperforschung, Stuttgart

The flow to strong coupling observed in many RG studies of interacting fermion systems [1, 2] indicates the occurrence of symmetry breaking. It is also a major technical problem for the attempt to give a more detailed description of the symmetry-broken phases of such models. We have developed a method to continue the fermionic renormalization group flow into phases with broken global symmetry [3]. For the reduced BCS model, we have shown how a small initial gap amplitude flows to the value given by the exact solution of the model [3]. In a more general situation with phonons, we have shown how to derive the Eliashberg equations by renormalization group methods [4].

The study of competing ordering tendencies necessitates flows in very high-dimensional spaces. We are working on efficient parametrizations of the action to obtain good approximations by fewer parameters. To this end we have constructed projectors on a subspace spanned by d-wave superconductivity, antiferromagnetism, d-density-wave, forward- and exchange scattering. The form we consider is taylored for doing

Hubbard–Stratonovich-transformations which we use to study the competition of ordering tendencies when the order parameter fields are well-developed.

[1] C. Halboth, W. Metzner: Phys. Rev. B **61**, 7364 (2000); Phys. Rev. Lett. **85**, 5162 (2000)
[2] C. Honerkamp et al.: Phys. Rev. B **63**, 035 109 (2001)
[3] M. Salmhofer et al.: Prog. Theor. Phys. **112**, 943 (2004)
[4] C. Honerkamp, M. Salmhofer: Prog. Theor. Phys. **113**, 1145 (2005)
[5] C. Honerkamp, M. Salmhofer: Phys. Rev. Lett. **87**, 187 004 (2001); Phys. Rev. B **64**, 184 516 (2001)

12.6   Mathematical Theory of Singular Fermi Surfaces

J. Feldman[*], M. Salmhofer

[*]Mathematics Department, University of British Columbia, Vancouver, Canada

We study the regularity properties of the fermionic self–energy for the case where the Fermi surface of the interacting system has singular points because the gradient of the dispersion relation vanishes (van Hove points). We prove regularity properties to all orders in perturbation theory using RG methods. We find a striking asymmetry in the derivatives of the self–energy and interpret it physically. We also investigate if there is an analogue of the inversion theorem proven in [1] for regular Fermi surfaces, also in this singular case, and its physical consequences [2, 3].

[1] J. Feldman et al.: Comm. Pure Appl. Math. **53**, 1350 (2000)
[2] J. Feldman, M. Salmhofer: *Singular Fermi Surfaces I. General power counting and higher–dimensional cases*, to appear
[3] J. Feldman, M. Salmhofer: *Singular Fermi Surfaces II. The Two–Dimensional Case*, to appear

12.7   Funding

12.8   Organizational Duties

M. Salmhofer
- Member of the advisory board of the *Andrejewski–Stiftung*.
  Organization of the Andrejewski lectures in Leipzig.
- Referee for Comm. Math. Phys., Phys. Rev. Lett., Phys. Rev. B
- grant review for NSERC of Canada, ANR (France)
- Associate editor: J. Math. Phys., since September 2006

12.9   External Cooperations

Academic

- MPI für Festkörperforschung Stuttgart
  W. Metzner

- Universität Würzburg
  C. Honerkamp

- University of British Columbia
  J. Feldman

- Universität München
  L. Erdös

- Harvard University
  H–T. Yau

- Universität Mainz
  M. Reuter

12.10   Publications

Journals

M. Salmhofer: *Dynamical Adjustment of Propagators in Renormalization Group Flows*, Ann. Phys. (Leipzig) **16**, 171 (2007)

in press

L. Erdös, M. Salmhofer, H.-T. Yau: *Quantum diffusion of the random Schrödinger evolution in the scaling limit II. The recollision diagrams*, arXiv:math-ph/0512015, Comm. Math. Phys.

L. Erdös, M. Salmhofer, H.-T. Yau: *Quantum diffusion for the Anderson model in the scaling limit*, Ann. Henri Poincare

L. Erdös, M. Salmhofer: *Decay of the Fourier Transform of Surfaces with Vanishing Curvature*, arXiv:math-ph/0604039, Math. Z.

Books

L. Erdös, M. Salmhofer, H.-T. Yau: *Towards the Quantum Brownian Motion*, in *Mathematical Physics of Quantum Mechanics, Selected and Refereed Lectures from QMath9*, Springer Lecture Notes in Physics **690**, ed. by J. Asch, A. Joye (Springer, Berlin 2006) p 233

M. Salmhofer: *Renormalization: Statistical Mechanics and Condensed Matter*, in *Encyclopedia of Mathematical Physics*, Vol. 4, ed. by J.-P. Francoise, G.L. Naber, S.T. Tsou (Elsevier, Oxford 2006) p 407

Talks

W. Pedra: *Zur mathematischen Theorie der Fermiflüssigkeiten bei positiven Temperaturen*, 18th Workshop on Foundations and Constructive Aspects of Quantum Field Theory, Hamburg, 12. May 2006

M. Salmhofer: *Diffusive Scale in the Random Schrödinger Time Evolution*, Mathematics Department, University of Toronto, Canada, 01. June 2006

M. Salmhofer: *Fermi surfaces, their renormalization group flows, and Fermi liquid theory in two dimensions*, University of California at Davis, USA, 18. May 2006

M. Salmhofer: *Renormalization Group for Correlated Fermions*, 3rd Int. Conf. Exact Renormalization Group, Lefkada, Greece, 19. September 2006

12.11   Graduations

Diploma

- Kay–Uwe Giering
  Renormalization Group Differential Equations: An application to the Ginsburg–Landau–Wilson functional
  March 2006

12.12   Guests

- C. Villani
  ENS Lyon, France
  7. – 8. December 2006

13

Theory of Condensed Matter

13.1   Introduction

Major research topics in our group include nonequilibrium phenomena and pattern formation in systems of various nature, e.g. in soft condensed matter and in biological systems. In our investigations the use of modern analytic methods of statistical physics and computer simulations complement and stimulate each other. Cooperations with mathematicians, theoretical and experimental physicists, biologists and medical researchers are well established. We collaborate with colleagues in France, Germany, Italy, Ireland, UK, and USA. More specifically we are interested in the following problems.

Noise induced phenomena (Behn). Noise induced non-equilibrium phase transitions are studied in coupled arrays of stochastically driven nonlinear systems. Furthermore, stability and statistical characteristics of stochastic nonlinear systems with time delay are investigated.

Mathematical modeling of the immune system (Behn). Using methods of nonlinear dynamics and statistical physics, we study the architecture and the random evolution of the idiotypic network of the B-cell subsystem and describe the regulation of balance of Th1/Th2-cell subsystems, its relation to allergy and the hyposensitization therapy (Cooperation with the Institute for Clinical Immunology).

Non-equilibrium dynamics in soft-condensed-matter systems (Kroy). The latter range from desert dunes spontaneously developing as a generic consequence of aeolian sand transport, through non-equilibrium gels of adhesive colloids and proteins, the viscoelastic mechanics of the cytoskeleton, to the non-equilibrium dynamics of single DNA molecules under strong external fields. (Related experimental work is currently in progress at Institute for Experimental Physics I: PWM & PAF work groups.) A common feature is the presence of strong fluctuations and stochastic dynamics on the micro-scale. The emergence of macroscopic structure and (non-linear) deterministic macroscopic dynamics is to be understood. The applied methods range from analytical studies of stochastic integro-differential equations through liquid-state theories, mode-coupling theory, effective hydrodynamic equations, phenomenological modeling, to numerical simulations.

13.2 Noise Induced Phenomena in Nonlinear Systems

U. Behn, F. Senf, C. Brettschneider, S. Gütter, P. Altrock

Non-equilibrium phase transitions [1] in arrays of spatially coupled nonlinear dynamical systems driven by multiplicative Gaussian white noise show close analogies to phase transitions in equilibrium. We have previously determined the phase diagram, the order of the transitions, and the critical behaviour for both global coupling and nearest neighbour coupling on simple cubic lattices comparing analytical results and numerical simulations [2].

The H-theorem [3] for a system of N globally coupled Stratonovich models is found and the convergence to the stationary solution independent of the initial distribution is shown. Performing a sectorization of the state space we are able to show that in the large time limit a stochastic trajectory will be trapped in one of those sectors which have their boundary flows pointing inward, only. In these sectors, the Kullback entropy can be identified as a Lyapunov functional which guarantees the convergence toward a steady state for long times. This result holds for finite N so that phase transistions associated with the breaking of ergodicity occur already in the finite system. New analytical results for the critical exponents are given in some limit cases [4].

We also investigate the universal behaviour of systems driven by independent additive and multiplicative noise. Furthermore we study the continuum limes of our system in the case of nearest neighbour coupling and the relation to growth models formulated as stochastic partial differential equations.

Stability and statistical characteristics of first return times of stochastic systems with delayed time argument driven by Gaussian white noise are studied analytically and by computer simulations [5].

[1] J. Garcia-Ojalvo, J.M. Sancho: *Noise in Spatially Extended Systems* (Springer, New York 1999)
[2] T. Birner et al.: Phys. Rev. E **65**, 046 110 (2002)
[3] T.D. Frank: *Nonlinear Fokker-Planck Equations* (Springer, Berlin 2005)
[4] F. Senf: Diplomarbeit, Universität Leipzig 2006; F. Senf, U. Behn: in preparation
[5] C. Brettschneider: Diplomarbeit, Universität Leipzig 2006

13.3 Randomly Evolving Idiotypic Networks

U. Behn, H. Schmidtchen

The paradigm of idiotypic networks was conceived about 30 years ago by Niels Jerne [1]. In the last few years it experiences a renewed interest mainly from the side of system biology and from clinical research, for a recent review see [2].

B-cells express on their surface receptors (antibodies) of a given specificity (idiotype). Crosslinking these receptors by complementary structures (antigen or antibodies) stimulates the lymphocyte to proliferate. Thus even without antigen there is a large functional network of interacting lymphocytes, the idiotypic network.
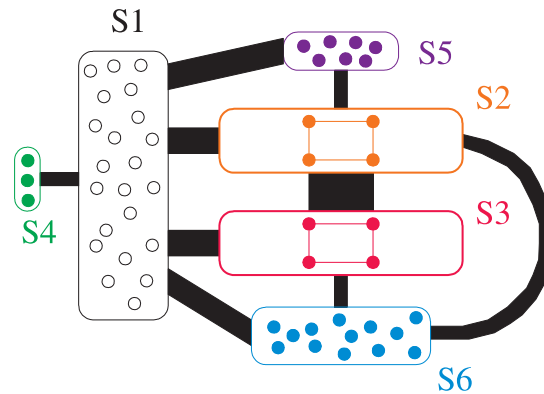
Figure 13.1: Visualization of the six-group structure, cf. [3, 5]. The size of the *boxes* corresponds to the group size. The *lines* show possible links between vertices of the groups and their thickness is a measure of the number of links

We developed a minimalistic model [3] where the idiotypes are caricatured by bit-strings. The dynamics of the idiotypic network is driven by the influx of new idiotypes randomly produced in the bone marrow and by the population dynamics of the lymphocytes themself. An idiotype survives only if it receives enough but not too much stimulation by complementary structures. The random evolution of the network leads to a highly organized dynamical architecture.

The nodes of the network can be classified into different groups (see Fig. 13.1), which are clearly distinguished by their statistical properties. They include densely connected core groups and peripheral groups of isolated vertices, resembling central and peripheral part of the biological network. We found the building principles of the architecture which allows to compute analytically size and connectivity of the idiotype groups [4–6], previously found by computational methods [3]. Based on this architecture we developed a mean field approach to calculate mean occupation of the groups and the mean life time of occupied vertices.

[1] N.K. Jerne: Ann. Inst. Pasteur Immunol. **125C**, 373 (1974)
[2] U. Behn: Immunol. Rev. **216**, 142 (2007)
[3] M. Brede, U. Behn: Phys. Rev. E **67**, 031 920 (2003)
[4] H. Schmidtchen: Diplomarbeit, Universität Leipzig 2006
[5] H. Schmidtchen, U. Behn: in: *Artificial Immune Systems*, ed. by H. Bersini, J. Carneiro, LNCS **4163** (Springer, Berlin 2006) p 81
[6] H. Schmidtchen, U. Behn: in *Mathematical Modeling of Biological Systems*, Vol. II, ed. by A. Deutsch et al. (Birkhäuser, Boston 2007) p 163

13.4   Th1–Th2 Regulation and Allergy

U. Behn, R. Vogel

T-helper lymphocytes have subtypes which differ in their spectrum of secreted cytokines. These cytokines have autocrine effects on the own subtype and cross-suppressive effects on the other subtype and regulate the type of immunoglobulines secreted by
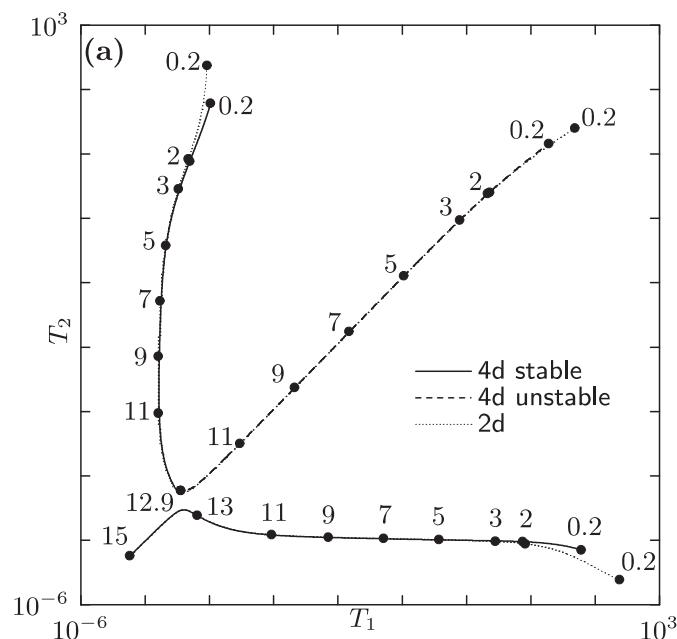
Figure 13.2: The manifold of stable (*solid line*) and unstable (*dashed line*) fixed points of the stroboscopic map. The curves are parametrized by the period of injections. The dotted lines show results of a simplified two-variable model which differ from the complete model only for small periods. The dynamical separatrix (*dashed line*) is crossed during a successful therapy from left to right. From [5]

B-lymphocytes. The balance of Th1- and Th2-cells is perturbed in several diseases [1]. For example, in allergy the response to allergen is Th2-dominated. A widespread and successful therapy consists in the injection of increasing doses of allergen following empirically justified protocols of administration.

In collaboration with Prof. G. Metzner (Institute for Clinical Immunology) we have developed a mathematical model [2, 3] based on a simplified scheme of Th1–Th2 regulation mediated by the cytokine network. The model provides a theoretical explanation of the switch from a Th2 dominated response to a Th1 dominated response to allergen in allergic individuals as a result of a hyposensitization therapy.

The therapeutic injections of allergen drive the system across a dynamical separatrix towards new attractors, where the response is Th1-dominated as for healthy individuals. The dynamical separatrix is formed by the set of unstable fixed points of a stroboscopic map describing periodic injections of the allergen (see Fig. 13.2). The maintenance phase of the therapy holds the system near the stable fixed point of the stroboscobic map.

We have shown that our model can account for essential features of hyposensitization therapy and are able to explain the structure of the empirical protocols. Different protocols can be tested in computer simulations.

[1] S. Romagnani (ed.): *Th1 and Th2 cells in health and disease*, Chem. Immunol. **63** (Karger, Basel 1996)
[2] U. Behn et al.: in *Dynamical Modeling in Biotechnologies*, ed. by F. Bagnoli et al. (World Scientific, Singapore 2001) p 227
[3] J. Richter et al.: J. Theor. Med. **4**, 119 (2002)

[4] R. Vogel: Diplomarbeit, Universität Leipzig 2006
[5] R. Vogel, U. Behn: in *Mathematical Modeling of Biological Systems*, Vol. II, ed. by A. Deutsch et al. (Birkhäuser, Boston 2007) p 151

13.5   Biopolymers

B. Obermayer, J. Glaser, K. Kroy

Many important biopolymers are accurately described by the wormlike chain model. With this model, the dynamic structure factor for a single chain is being studied reveiling information about the thermal fluctuations of the polymer in a solvent. Hydrodynamic interactions needed to be taken into account in order to obtain consistent results. Another investigation resulted in a unified picture of the effects of a stretching force applied at the ends of such an inextensible chain. A concise explanation of the dominant relaxation mechanisms has been given and a full characterization of the dynamic longitudinal response of stiff polymers and stretched (semi)flexible filaments has been developed: (i) a straight initial configuration due to strong stretching is not equivalent to an initial low-temperature environment (quenching); (ii) monitoring eigenvalues of the gyration tensor is not equivalent to measuring the actual end-to-end distance, see Fig. 13.3.
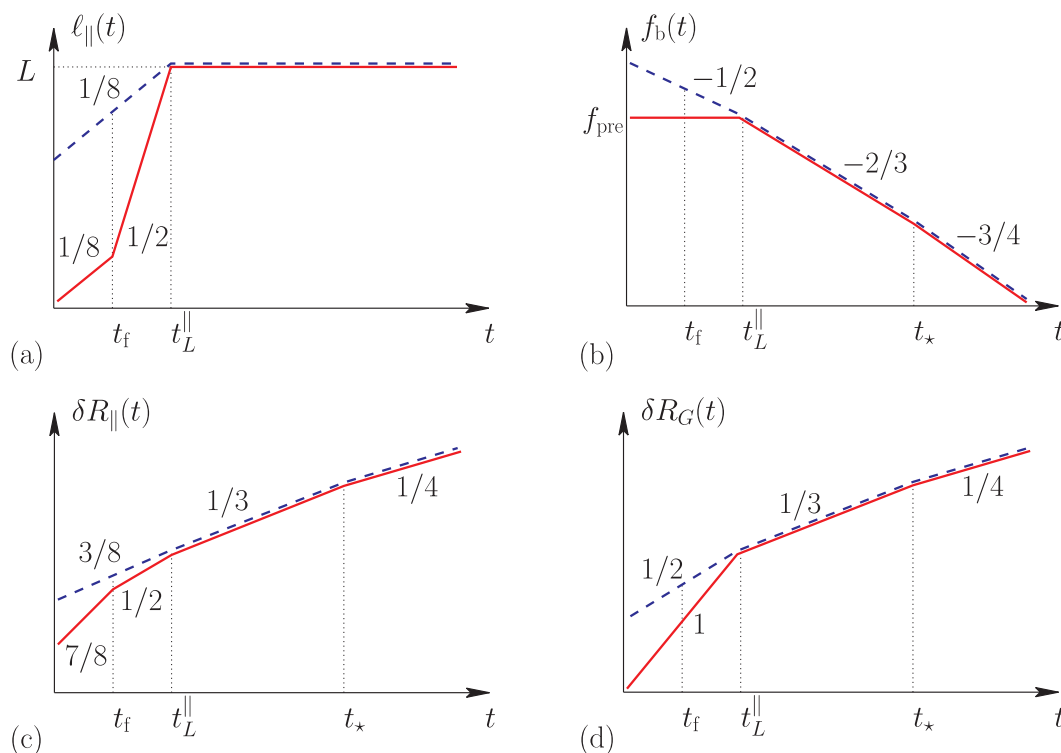
Figure 13.3: Stretching (*solid*) vs. quenching (*dashed*). Asymptotic scaling laws for the boundary layer size $l_{\parallel}(t)$ (**a**), for the bulk tension $f_b(t)$ (**b**), for the change in end-to-end distance $\delta R_{\parallel}(t)$ (**c**), and for the change in the gyration tensor's eigenvalue $\delta R_G(t)$ (**d**) vs. time t (*log-log scale*). The stretching force f_{pre} has been related to the quenching strength $r = l_p^< / l_p^>$ via $f_{\text{pre}} = r^4 \kappa (l_p^> / L^2)^2$.

13.6   Cell Mechanics

P. Fernandez, K. Kroy

Unlike the concrete and steel of buildings and bridges, most mechanical elements of biological cells are soft, in that their shape is subject to significant thermal fluctuations. The cytoskeleton provides mechanical stability and integrity of biological cells, see Figs. 13.4 and 13.5. In close cooperation with experimentalist Andreas Bausch, the biological complexity has been reviewed from a physicist's perspective.
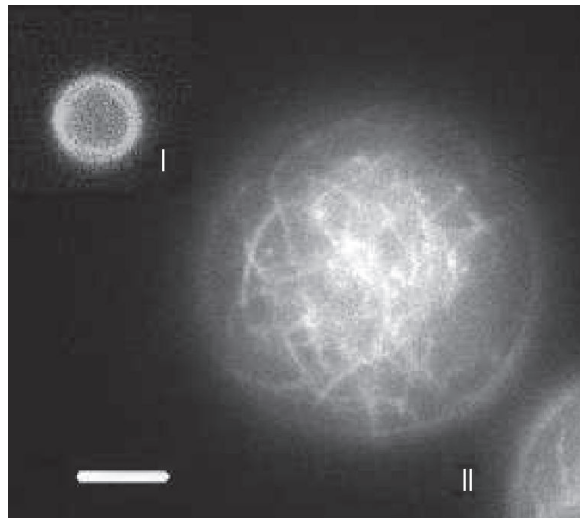
Figure 13.4: Fluorescent micrographs of emulsion droplets containing rhodamine phalloidin-labelled actin filaments. In small droplets (D < 12 microns), the actin is organized in a cortex close to the droplet surface (*I*), whereas it is more homogeneously distributed in large droplets (*II*). The scale bar is 10 μm. In general, actin solutions encapsulated in sufficiently small emulsion droplets are locally more heterogeneous and more elastic than bulk solutions.
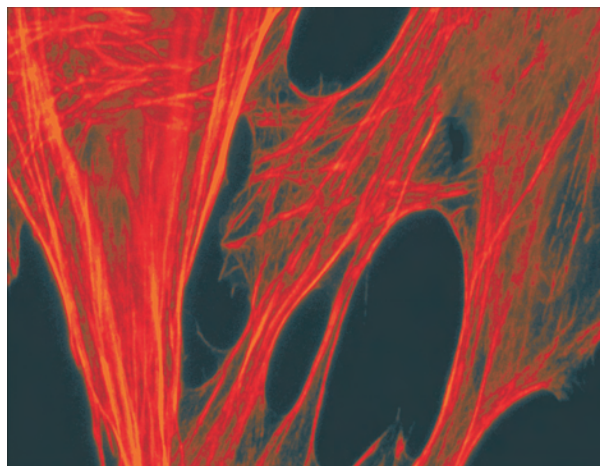
Figure 13.5: Microscopic image of a cell's (dyed) cytoskeleton. Filament bundles are clearly recognized as well as interconnecting crossings.

13.7 Colloidal Aggregation

D. Rings, K. Kroy

Describing particle coagulation is of great interest in various branches of research from medicine to engineering. Shear-induced gelation, i.e. the transition from sol to gel, is accompanied by a sharp increase in viscosity which may pose considerable problems both in technological as well as life sciences.

Our numerical study of a two-dimensional toy model for the phenomenon of shear-driven aggregation and gelation in suspensions of adhesive colloids has two objectives:

- to develop an efficient simulation algorithm,

- to analyze the most salient features of shear-driven aggregation that distinguish it from other common kinetic models such as diffusion- or reaction-limited cluster aggregation, as well as the crossover to universal percolation behavior at gelation (Fig. 13.6).

$\phi = 0.1$

$\phi = 0.2$ $\phi = 0.4$
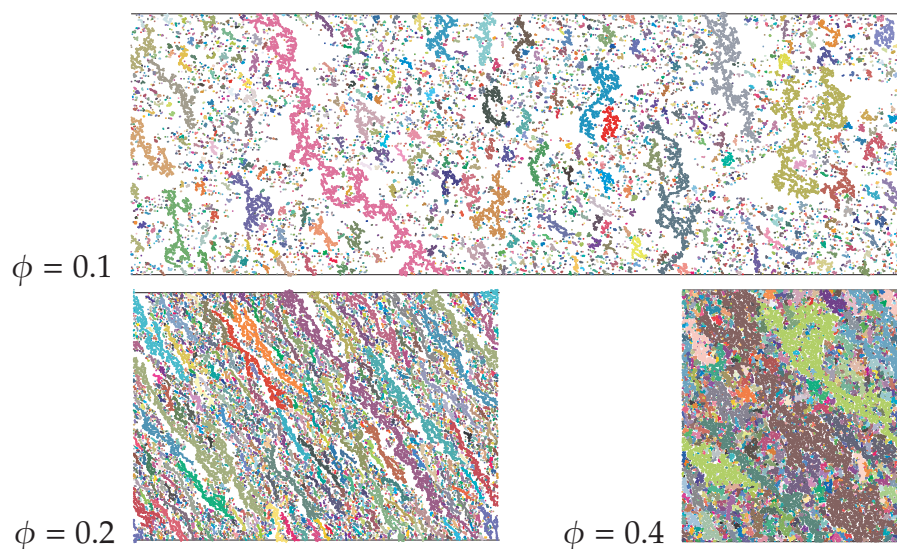
Figure 13.6: Snapshots of spanning clusters in the final state of simulations at different area fractions. At low densities the clusters have rather isotropic shapes, and their orientation is not clear. Around $\phi = 0.2$, a stringy shape is most pronounced and orientational alignment is strong, while at high ϕ it weakens again, and clusters become "fatter".

13.8 Sand Dunes

S. Fischer, K. Kroy

In collaboration with H. Herrmann of the University of Stuttgart a minimal model has been formulated which elucidates the basic physical mechanisms underlying dune formation and migration. It allows us to analyze the effect of environmental conditions uncontrollable in the field on the characteristic shapes of dunes systematically. While the previously studied stationary solutions obtained under periodic boundary
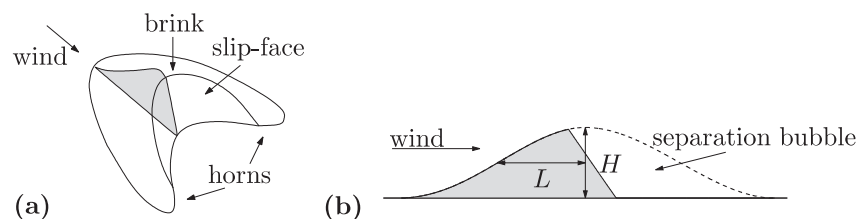
Figure 13.7: (**a**) Sketch of a barchan dune. (**b**) Central slice of a barchan dune. Beyond the brink, inside of the so-called separation bubble the air flow near the ground is stagnant or even reverse. As a consequence, there is no wind erosion on the slip face. The height profile can be parameterized by height H and windward length L at half height of the common envelope of the dune profile and its separation bubble.
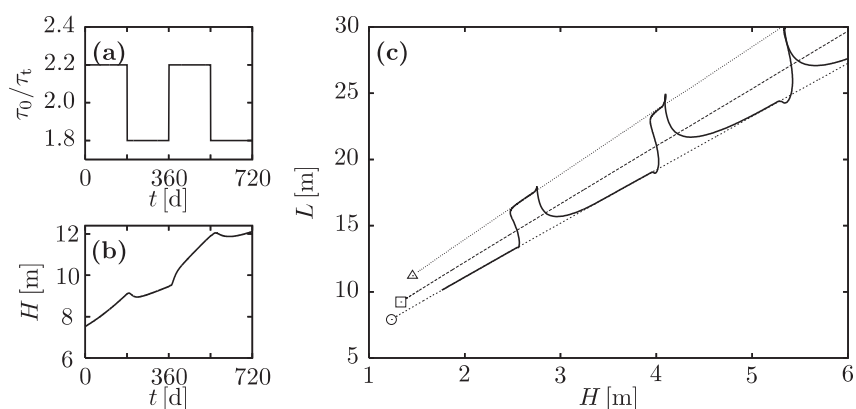
Figure 13.8: Evolution of a growing dune subject to periodically changing wind strength. (**a**) Shear stress protocol. (**b**) Evolution of the height H. (**c**) Reduced phase space trajectory of a growing heap recorded for three cycles (*solid line*). As long as the dune volume is small, the trajectory switches rapidly between the unstable manifolds with $\tau_0/\tau_t = 1.8$ (*triangle*) and $\tau_0/\tau_t = 2.2$ (*circle*).

conditions are "unphysical" in the sense that they correspond to unstable fixed points of the equations, the solutions for open boundary conditions are shown to be strongly constrained by the unstable manifolds of these fixed points. (Figs. 13.7 and 13.8.)

13.9 Organizational Duties

U. Behn
- Speaker Condensed Matter Theory group
- Vertrauensdozent für die Nobelpreisträgertagungen in Lindau
- Referee: J. Theor. Biol., Phys. Biol., Physica D, Phys. Rev. E, Springer Lecture Notes in Computational Sciences

K. Kroy
- Vice director of the ITP
- Member of the Graduiertenkommission of the University of Leipzig
- Referee: Phys. Rev. Lett., Phys. Rev. E, J. Theor. Biol., Soft Matter

13.10   External Cooperations

Academic

- Universität Bayreuth
  Dr. P. Fernandez

- TU München
  Prof. Dr. A. Bausch, S. Fischer

- Edinburgh University, UK
  Prof. Dr. M.E. Cates

- Institut für Klinische Immunologie, Universität Leipzig
  Prof. Dr. G. Metzner

- Department of Mathematical Physics, University College Dublin, Ireland
  Prof. Dr. J. Pulé

- Institut für Theoretische Physik, Otto-von-Guericke-Universität Magdeburg
  Prof. Dr. J. Richter

- Center for Complex Systems Science, CSIRO, Canberra, Australia
  Dr. M. Brede

- Cyprus Institute of Neurology and Genetics, Nicosia, Cyprus
  Dr. J. Richter

- Harvard University, Program for Evolutionary Dynamics, USA
  Dr. A. Traulsen

- Centre de Physique Theorique, CNRS, Marseille, France
  Prof. Dr. V. Zagrebnov

13.11   Publications

Journals

A.R. Bausch, K. Kroy: *A bottom-up approach to cell mechanics*, Nature Phys. **2**, 231 (2006)

M.M.A.E. Claessens, R. Tharmann, K. Kroy, A.R. Bausch: *Microstructure and viscoelasticity of confined semiflexible polymer networks*, Nature Phys. **2**, 186 (2006)

K. Kroy: *Elasticity, dynamics and relaxation in biopolymer networks*, Curr. Opin. Colloid. Interface Sci. **11**, 56 (2006)

J. Liu, M.L. Gardel, K. Kroy, E. Frey, B.D. Hoffman, J.C. Crocker, A.R. Bausch, D.A. Weitz: *Microrheology Probes Length Scale Dependent Rheology*, Phys. Rev. Lett. **96**, 118 104 (2006)

M. Salomo, K. Kroy, K. Kegler, C. Gutsche, M. Struhalla, J. Reinmuth, W. Skokov, C. Immisch, U. Hahn, F. Kremer: *Binding of TmHU to single dsDNA as observed by optical tweezers*, J. Mol. Biol. **359**, 769 (2006)

D. Schmalfuß, R. Darradi, J. Richter, J. Schulenburg, D. Ihle: *The quantum J1-J2 anti-ferromagnet on the stacked square lattice: Influence of the interlayer coupling on the ground-state magnetic ordering*, Phys. Rev. Lett. **97**, 157 201 (2006)

Books

H. Schmidtchen, U. Behn: *Randomly Evolving Idiotypic Networks: Analysis of Building Principles*, in: *Artificial Immune Systems*, ed. by H. Bersini, J. Carneiro, Lecture Notes in Computational Sciences **4163** (Springer, Berlin 2006) p 81, doi:10.1007/11823940

in press

U. Behn: *Idiotypic networks: toward a renaissance?*, Immunol. Rev. **216**, 142 (2007)

S. Fischer, K. Kroy: *Dynamics of Aeolian Sand Heaps and Dunes: The Influence of the Wind Strength*, in *Traffic and Granular Flow 05*, ed. by A. Schadschneider et al. (Springer, Heidelberg 2007)

H. Schmidtchen, U. Behn: *Architecture of Randomly Evolving Idiotypic Networks*, in: *Mathematical Modeling of Biological Systems*, Vol. II, ed. by A. Deutsch et al. (Birkhäuser, Boston 2007) p 163

R. Vogel, U. Behn: *Th1–Th2 Regulation and Allergy: Bifurcation Analysis of the Non-autonomous System*, in: *Mathematical Modeling of Biological Systems*, Vol. II, ed. by A. Deutsch et al. (Birkhäuser, Boston 2007) p 151

Talks

U. Behn: *Noise induced non-equilibrium phase transitions in extended systems*, Invited Talk, Workshop Stochastic Processes, Fluctuations and Noise, PHYSBIO 06, St. Etienne de Tineé, France, 29. September 2006

U. Behn: *Randomly evolving idiotypic networks*, Invited Lecture, PHYSBIO 06, St. Etienne de Tineé, France, 27. September 2006

U. Behn, H. Schmidtchen: *Architecture of randomly evolving idiotypic networks*, 6th Symp. Understanding Complex Systems, University of Illinois at Urbana-Champaign, Urbana, USA, 16. May 2006

U. Behn, H. Schmidtchen: *Randomly evolving idiotypic networks: Analysis of building principles*, 5th Int. Conf. on Artificial Immune Systems, Oeiras, Portugal, 04. September 2006

J. Glaser: *Hydrodynamic interactions for stiff polymers*, DPG Frühjahrstagung, Dresden, 27. – 31. March 2006

K. Kroy: *On Growth and Form of Desert Dunes*, Invited Talk, Otto von Guericke Universität, Magdeburg, 26. June 2006

K. Kroy: *Tension Dynamics in Stiff Polymers*, Invited Talk, Martin-Luther-Universität Halle-Wittenberg, 06. June 2006

K. Kroy: *Warum ist die Wüste nicht flach? Und warum ist das mathematisch so schwer zu beweisen?*, Leipziger Buchmesse, 17. March 2006

B. Obermayer: *Dynamics of single semiflexible polymers under force*, DPG Frühjahrstagung, Dresden, 27.–31. March 2006

H. Schmidtchen, U. Behn: *Architecture of randomly evolving idiotypic networks*, DPG Frühjahrstagung, Dresden, 27.–31. March 2006

H. Schmidtchen, U. Behn: *Architecture of randomly evolving idiotypic networks*, CompPhys06, 7th NTZ-Workshop on Computational Physics, Universität Leipzig, 30. November–02. December 2006

R. Vogel: *Th1-Th2 Regulation and Allergy: Bifurcation Analysis of the Non-autonomous System*, Seminar Mathematische Modellierung Biologischer Systeme, MPI für Mathematik in den Naturwissenschaften, Leipzig, 24. May 2006

Posters

D. Rings: *Shear-driven gelation in two dimensions*, DPG Frühjahrstagung, Dresden, 27.–31. March 2006

D. Rings: *Simulation of shear-driven aggregation*, CompPhys06, 7th NTZ-Workshop on Computational Physics, Universität Leipzig, 30. November–02. December 2006

F. Senf, U. Behn: *H-Theorem for interacting systems driven by multiplicative noise*, DPG Frühjahrstagung, Dresden, 27.–31. March 2006

13.12 Graduations

Diploma

- Jens Glaser
  Dynamic Light Scattering of Stiff Polymers
  February 2006

- Fabian Senf
  Rauschgetriebene Phasenübergänge im Nichtgleichgewicht: Asymptotische Eigenschaften gekoppelter Stratonovich-Modelle
  February 2006

- Reinhard Vogel
  Th1–Th2-Regulation und Allergie: Bifurkationsanalyse des nichtautonomen Systems
  March 2006

- Holger Schmidtchen
  Architecture of randomly evolving idiotypic networks
  April 2006

- Daniel Rings
  Shear-driven Aggregation: An Event-Driven Simulation Approach
  August 2006

- Christian Brettschneider
  Statistische Eigenschaften marginal stabiler stochastischer Systeme mit zeitlicher Verzögerung
  October 2006

13.13 Guests

- Dr. Pablo Fernandez
  Universität Bayreuth, Lehrstuhl Experimentalphysik I
  October – December 2006

14

Theory of Elementary Particles

14.1 Introduction

The Particle Physics Group performs basic research in the quantum field theoretic description of elementary particles and in phenomenology. Topics of current interest are conformal symmetry and its breaking in the context of supersymmetric theories, the formulation of models which realize noncommutative geometry, renormalization problems, electroweak matter at finite temperature, the lattice formulation of gauge theories, the derivation of Regge behaviour of scattering amplitudes from Quantum Chromodynamics and the related study of integrable models with and without supersymmetry. Perturbative and non-perturbative methods are applied to answer the respective questions. In perturbation theory the work is essentially analytic using computers only as a helpful tool. Lattice Monte Carlo calculations as one important non-perturbative approach however are based on computers as an indispensable instrument. Correspondingly the respective working groups are organized: in analytical work usually very few people collaborate, in the lattice community rather big collaborations are the rule. Our group is involved in many cooperations on the national and international level (DESY, Munich; France, Russia, Armenia, USA, Japan). Since elementary particles are very tiny (of the order of 10^{-15} m) and for the study of their interactions large accelerators producing enormously high energy are needed, it is clear that results in this direction of research do not have applications in daily life immediately. To clarify the structure of matter is first of all an aim in its own and is not pursued for other reasons. But particle theory has nevertheless a very noticeable impact on many other branches of physics by its power of providing new methodological insight. Similarly for the student specializing in this field the main benefit is her/his training in analysing complex situations and in applying tools which are appropriate for the respective problem. As a rule there will be no standard procedures which have to be learned and then followed, but the student has to develop her/his own skill according to the need that arises. This may be a mathematical topic or a tool in computer application. Jobs which plainly continue these studies are to be found at universities and research institutes only. But the basic knowledge which one acquires in pursuing such a subject opens the way to many fields where analytical thinking is to be combined with application of advanced mathematics. Nowadays this seems to be the case in banks, insurance companies and consulting business.

Klaus Sibold

14.2 The Moyal Product in Quantum Field Theory

K. Sibold

At very short distances the structure of spacetime has to undergo presumably a drastic change. Qualitative arguments show that a horizon builds up which prohibits the interpretation of coordinates as on large distances. This points to a possible solution: consider the coordinates as selfadjoint operators on a Hilbert space and understand their eigenvalues as the replacement for the original coordinates. If these operators do not commute one has uncertainty relations which then permit to avoid the aforementioned clash. Implementing this idea in conventional field theories one is naturally led to the socalled Moyal product of field operators. The usual interactions become nonlocal and thus create all sorts of difficulties when deriving Feynman rules. Some of them have been overcome in earlier papers but the construction of higher orders is still a problem due to subtleties of the respective integrals. Work on this is in progress.

[1] S. Doplicher et al.: Commun. Math. Phys. **172**, 187 (1995)
[2] Y. Liao, K. Sibold: Eur. Phys. J. C **25**, 469 (2002)
[3] Y. Liao, K. Sibold: Eur. Phys. J. C **25**, 479 (2002)
[4] D. Bahns et al.: Phys. Lett. B **533**, 178 (2002)
[5] T. Reichenbach: Diploma Thesis, Leipzig University 2004
[6] P. Heslop, K. Sibold: Eur. Phys. J. C **41**, 545 (2005)

14.3 3D Abelian Higgs Model with Singly and Doubly-Charged Matter Fields

A. Schiller

In this project we continue to study properties of coupled gauge-Higgs models in three dimensions using Monte Carlo methods.

In [1, 2] we started to study a three dimensional Abelian Higgs model containing singly- and doubly-charged scalar fields coupled to a compact Abelian gauge field in the London limit. The model attracts interest because of its relevance to high-T_c superconductors with charge 1 holon and charge 2 spinon-pair fields. Its action is defined as

$$S_{\text{A2HM}} = -\beta \sum_P \cos \theta_P - \sum_{i=h,s} \kappa_i \sum_l \cos(\text{d}\varphi_i + q_i \theta)_l \,, \tag{14.1}$$

where θ_P is the standard lattice plaquette, φ_h the phase of the singly-charged holon field and and φ_s the phase of the doubly-charged spinon-pair field. The sums run over plaquettes P and links l, respectively. The model contains two types of vortices carrying magnetic flux and one type of instanton-like monopoles.

We investigate [3, 4] non-perturbative features that model. It is pretending to describe various planar systems of strongly correlated electrons such as high-T_c superconductivity in the overdoped regime and exotic materials possessing excitations with
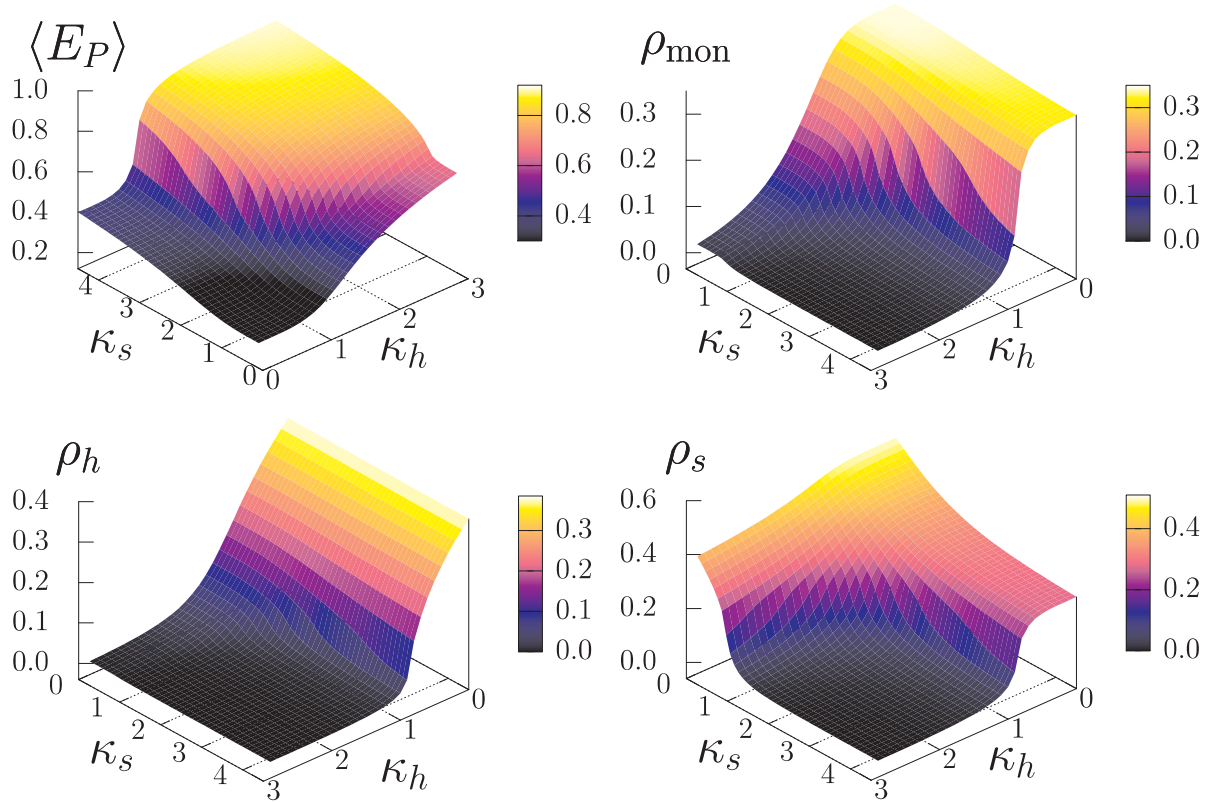
Figure 14.1: Expectation value of the gauge plaquette and the densities of the topological defects (monopoles, holon vortices and spinon vortices) at $\beta = 0.5$ on a 16^3 lattice.

fractionalized quantum numbers. The complicated phase structure of the model is studied thoroughly using numerical tools and analytical arguments. In the tree-dimensional space of coupling parameters we identify the Fermi liquid, the spin gap, the superconductor and the strange metallic phases. The behavior of three kinds of topological defects – holon and spinon vortices and monopoles – is explored in various phases. We also observe a new effect, the strong enhancement of the phase transition strength reflected in decreasing the order of the transition: at sufficiently strong gauge coupling the two second order phase transitions – corresponding to spinon-pair and holon condensation lines – join partially in the phase diagram and become, unexpectedly, a first order phase transition in that region. The last observation may have an analogue in Quantum Chromodynamics at non-zero temperature and finite baryon density. We argue that at sufficiently large baryon density the finite-temperature transition between the (3-flavor paired) color superconducting phase and the quark-gluon plasma phases should be much stronger compared with the transition between 2-flavor paired and 3-flavor paired superconducting phases. Typical measurements for thermodynamic and topological variables are shown in the (κ_h, κ_s)-plane signaling the phase transition.

[1] M.N. Chernodub et al.: PoS **LAT2005** (2005) 295, arXiv:hep-lat/0509088
[2] M.N. Chernodub et al.: Phys. Rev. B **73**, 100 506 (2006), arXiv:cond-mat/0512111

[3] M. Bock et al.: *An Abelian two-Higgs model of strongly correlated electrons: phase structure, strengthening of phase transition and QCD at finite density*, in preparation

[4] M. Bock: Master Thesis, Leipzig University 2006, submitted

14.4 Lattice Perturbation Theory and Renormalisation

H. Perlt, A. Schiller

To obtain continuum results from lattice calculations of hadron matrix elements (three-point correlation functions), the underlying operators have to be renormalised. A perturbative calculation of the corresponding renormalisation constants is always the first step.

During the last years our team in close collaboration with Zeuthen, Regensburg and other members of the QCDSF collaboration has computed lattice renormalisation constants of local bilinear quark operators for overlap fermions and improved gauge actions. Among the actions we have considered are the Symanzik, Lüscher-Weisz, Iwasaki and DBW2 gauge actions by considering local bilinear quark operators. The calculation have been extended to one-link quark operators and to stout smeared SU(3) links in the fermionic action.

Among others we have considered in this year the renormalisation of lattice QCD operators with one and two covariant derivatives related to the first and second moments of generalised parton distributions and meson distribution amplitudes. Employing the clover fermion action [1] we have calculated their non-forward quark matrix elements in one-loop lattice perturbation theory. For some representations of the hypercubic group commonly used in simulations we determined the sets of all possible mixing operators and compute the matrices of renormalisation factors in one-loop approximation. We describe how tadpole improvement is applied to the results. Using overlap fermions [2] we have presented the resulting matrices of mixing and renormalisation factors. For overlap fermions we explicitly checked the absence of mixing with lower-dimensional operators of different chirality in particular representations of the hypercubic group. This feature favours the use of chiral fermions.

First results have been presented [3] for Wilson coefficients of operators up to first order in the covariant derivatives for the case of Wilson fermions. They are derived from the off-shell Compton scattering amplitude $\mathcal{W}_{\mu\nu}(a, p, q)$ of massless quarks with momentum p. The Wilson coefficients are classified according to the transformation of the corresponding operators under the hypercubic group H(4). We give selected examples for a special choice of the momentum transfer q. All Wilson coefficients are given in closed analytic form and in an expansion in powers of a up to first corrections.

[1] M. Göckeler et al.: Eur. Phys. J. C **48**, 523 (2006), arXiv:hep-lat/0605002

[2] M. Göckeler et al.: PoS **LAT2006**, 161 (2006), arXiv:hep-lat/0610060

[3] M. Göckeler et al.: PoS **LAT2006**, 119 (2006), arXiv:hep-lat/0610064

14.5 Integrable Quantum Systems and Gauge Field Theories

R. Kirschner

Integrable quantum systems are applied successfully to the study of the high-energy asymptotics and of the renormalization of composite operators in gauge theories [1–4]. These application stimulated the development of the methods of quantum systems.

We have dveloped appropriate methods of solving the Yang-Baxter relation and applied them to cases of one dimenesional conformal symmetry and its supersymmetric extensions and algebraic deformations. We have discovered a factorization structure in the Yang-Baxter operators providing essential advantages [5]. In 2006 we solved the Yang-Baxter relation with elliptically deformed $sl(2)$ symmetry extending our approach from the undeformed to the deformed cases [6].

Also the application of our approach to higher rank symmetries $sl(n)$ has been shown and worked out explicitly for the $sl(3)$ case [7].

[1] L.N. Lipatov: Padova preprint DFPD-93-TH-70B; and J. Exp. Theor. Phys. Lett. B **342**, 596 (1994)
[2] L.D. Faddeev, G.P. Korchemsky: Phys. Lett. B **342**, 311 (1995), arXiv:hep-th/9404173
[3] V.M. Braun et al.: Phys. Rev. Lett. **81**, 2020 (1998), arXiv:hep-ph/9805225
[4] N. Beisert: Phys. Rept. **407**, 1 (2004)
[5] S. Derkachov et al.: Nucl. Phys. B **738**, 368 (2006), arXiv:hep-th/0511024
[6] S. Derkachov et al.: arXiv:hep-th/0703076
[7] P. Valinevich: Diploma thesis, in preparation

14.6 Factorization in Semi-Hard Scattering Processes

R. Kirschner

Factorization is an essential step in all applications of Quantum chromodynamics to high-energy scattering, separating the part of the dynamics explicitly described in terms of quarks and gluons from the one related to the hadron structure. Only in some cases the factorization relies on general proofs. In last decade the methods for treating exclusive particle production processes have been developed essentially.

In 2006 we have started a project intending to study the issue by comparing different factorization schemes in overlapping regions of applicability, trying to answer open questions of earlier studies [1]. The exclusive production of two vector mesons in electron-positron interaction is a standard example of interest both for the theoretical question of factorization as well as for the analysis of ongoing experiments and project studies for the International Linear Collider. The work relies on recent results in the Regge factorization [2] and the hard factorization [3] schemes.

We have also prepared the theoretical formulation to be supplemented by a numerical study of diffractive central production relying on the Regge asymptotics factorization intending comparison with planned Large Hadron Collider experiments. This continues earlier work [4].

Support of the visit of D.Y. Ivanov (Novosibirsk) by DFG and NTZ; support of the visit of O. Teryaev (Dubna) by SMWK; support of a visit of R. Kirschner in Liege by Universite de Liege.

[1] A. Ivanov, R. Kirschner: Eur. Phys. J. C **29**, 353 (2003), arXiv:hep-ph/0301182
[2] D.Y. Ivanov, A. Papa: Nucl. Phys. B **732**, 183 (2006), arXiv:hep-ph/0508162
[3] M. Segond et al.: arXiv:hep-ph/0703166
[4] P. Hagler et al.: Phys. Rev. D **62**, 071 502 (2000), arXiv:hep-ph/0002077

14.7 Organizational Duties

K. Sibold
- Associated member of the Graduiertenkolleg: Analysis, Geometrie und die Naturwissenschaften
- Coorganizer of the "Mitteldeutsche Physik-Combo"(joint graduate lecture courses with universities Jena and Halle)
- Member of the "Beirat" of the Fachverband "Mathematische und Theoretische Grundlagen der Physik" (German Physical Society)

A. Schiller
- Referee: Phys. Rev. D

R. Kirschner
- Referee: Phys. Rev. D, Phys. Letters A and B.
- Member of the PhD graduation commission of the faculty

14.8 External Cooperations

Academic

- ITEP, Moscow, Russia
  Dr. M.N. Chernodub

- Humboldt University, Berlin
  Dr. E.-M. Ilgenfritz, Prof. M. Müller-Preussker

- Regensburg University
  Dr. M. Göckeler, Prof. A. Schäfer, Prof. V. Braun

- Edinburgh University, UK
  Dr. R. Horsley

- Department of Mathematics, Liverpool University, UK
  Dr. P.E.L. Rakow

- NIC, Zeuthen & DESY, Hamburg
  Prof. G. Schierholz

- Nuclear Physics Institute, St. Petersburg, Russia
  Prof. L.N. Lipatov

- Steklov Mathematical Institute, St. Petersburg, Russia
  Dr. S.E. Derkachov

- Theory Department, Yerevan Physics Institute, Armenia
  Prof. A. Sedrakyan

- Soltan Institut of Nuclear Studies, Warsaw, Poland and Universiy Liege, Belgium
  Dr. L. Szymanowski

- Sobolev Institut of Mathematics, Novosibirsk, Russia
  Dr. D.Y. Ivanov

- Institut für Theoretische Physik, University Hamburg & DESY
  Prof. J. Bartels

- Ecole Polytechnique, Paris-Palaiseau, France
  Prof. B. Pire

14.9 Publications

Journals

V.M. Braun, M. Göckeler, R. Horsley, H. Perlt, D. Pleiter, P.E.L. Rakow, G. Schierholz, A. Schiller, W. Schroers, H. Stüben, J.M. Zanotti: *Moments of pseudoscalar meson distribution amplitudes from the lattice*, Phys. Rev. D **74**, 074 501 (2006), arXiv:hep-lat/0606012

M.N. Chernodub, E.-M. Ilgenfritz, A. Schiller: *Phase structure of an Abelian two-Higgs model and high temperature superconductors*, Phys. Rev. B **73**, 100 506 (2006), arXiv:cond-mat/0512111

S.E. Derkachov, D. Karakhanyan, R. Kirschner: *Baxter Q-operators of the XXZ chain and R-matrix factorization*, Nucl. Phys. B **738**, 368 (2006), arXiv:hep-th/0511024

M. Göckeler, R. Horsley, H. Perlt, P.E.L. Rakow, A. Schäfer, G. Schierholz, A. Schiller: *Perturbative Renormalisation for Low Moments of Generalised Parton Distributions with Clover Fermions*, Nucl. Phys. B Proc. Suppl. **153**, 269 (2006), arXiv:hep-lat/0511041

M. Göckeler, R. Horsley, H. Perlt, P.E.L. Rakow, A. Schäfer, G. Schierholz, A. Schiller: *Renormalisation of composite operators in lattice perturbation theory with clover fermions: Non-forward matrix elements*, Eur. Phys. J. C **48**, 523 (2006), arXiv:hep-lat/0605002

A. Sternbeck, E.-M. Ilgenfritz, M. Müller-Preussker, A. Schiller: *Landau gauge ghost and gluon propagators and the Faddeev-Popov operator spectrum*, Nucl. Phys. B Proc. Suppl. **153**, 185 (2006), arXiv:hep-lat/0511053

Books

E.-M. Ilgenfritz, M. Müller-Preussker, A. Sternbeck, A. Schiller, *Gauge-variant propagators and the running coupling from lattice QCD*, in: *Sense of Beauty in Physics*, ed. by M. D'Elia, K. Konishi, E. Meggiolaro, P. Rossi (Pisa University Press 2006) p 359, arXiv:hep-lat/0601027

Talks

V.M. Braun, M. Göckeler, R. Horsley, H. Perlt, D. Pleiter, P.E.L. Rakow, G. Schierholz, A. Schiller, W. Schroers, H. Stüben, J.M. Zanotti: *Distribution Amplitudes of Pseudoscalar Mesons*, PoS **LAT2006**, 122 (2006), arXiv:hep-lat/0610055

M. Göckeler, R. Horsley, H. Perlt, P.E.L. Rakow, G. Schierholz, A. Schiller: *One-loop Renormalisation of Lattice QCD Operators for Non-forward Matrix Elements: From Clover to Overlap Fermions*, PoS **LAT2006**, 161 (2006), arXiv:hep-lat/0610060

M. Göckeler, R. Horsley, H. Perlt, P.E.L. Rakow, G. Schierholz, A. Schiller: *Operator product expansion on the lattice: analytic Wilson coefficients*, PoS **LAT2006**, 119 (2006), arXiv:hep-lat/0610064

E.-M. Ilgenfritz, M. Müller-Preussker, A. Sternbeck, A. Schiller, I.L. Bogolubsky: *Landau gauge gluon and ghost propagators from lattice QCD*, Workshop IRQCD '06, Rio de Janeiro, Brazil, June 2006, arXiv:hep-lat/0609043

A. Sternbeck, E.-M. Ilgenfritz, M. Müller-Preussker, A. Schiller, I.L. Bogolubsky: *Lattice study of the infrared behavior of QCD Green's functions in Landau gauge*, PoS **LAT2006**, 076 (2006), arXiv:hep-lat/0610053

Author Index

Jörg Kärger
Leipzig, Einstein, Diffusion

with contributions by   *mit Beiträgen von*
Jean Philibert, Helmut Rechenberg & Gerald Wiemers, Gero Vogl,
Douglas M. Ruthven, Shlomo Havlin, Ilpo Vattulainen

Paintings by   *Aquarelle von*
Taro Ito

Leipziger Universitätsverlag

Tilman Butz
Fourier Transformation for Pedestrians

Springer

Tilman Butz
Fouriertransformation für Fußgänger

5. Auflage

Teubner